No d’ordre: 42563

Université Lille 1 – Sciences et Technologies

Ecole Doctorale 104 – Sciences de la Matiére, du Rayonnement, et de l’Environment

Thése de Doctorat

par

Volodymyr KOVERGA

pour l’obtention du titre de

Docteur de l’Université Lille 1

Discipline: Physique-Chimie

Organisation de la structure locale de mélanges liquide ionique/solvant moléculaire: une étude théorique basée sur la dynamique moléculaire

Soutenue le 19 décembre 2017 devant le jury:

Pál	**JEDLOVSZKY** *Professeur, Université Eszterhazy Karoly (Hongrie)*	**Rapporteur**
Michael	**KISELEV** *Professeur, Institut de la chimie de solutions (Russie)*	**Rapporteur**
Abdenacer	**IDRISSI** *Professeur, Université Lille 1*	**Directeur de thése**
Oleg	**KALUGIN** *Professeur, Université nationale de Kharkiv V. N. KARAZINE (UKRAINE)*	**Co-directeur de thése**
Sylvain	**CRISTOL** *Professeur, Université Lille 1*	**Président**
Ari	**SEITSONEN** *Professeur, Université de Zurich (Suisse)*	**Examinateur**
Frederic	**AFFOUARD** *Professeur, Université Lille 1*	**Examinateur**

No of order: 42563

Lille 1 University – Science and Technology

Doctoral School 104 – Science of the Matter, of the Radiation, and of the Environment

Doctoral Thesis

by

Volodymyr KOVERGA

to obtain the degree of

Doctor of Lille 1 University

Discipline: Physical Chemistry

Local Structure Organization in Ionic Liquids and Molecular Solvents Mixtures: A Molecular Dynamics Simulation

Defended on 19 december 2017 in front of the jury:

Pál	**JEDLOVSZKY** *Professor, Eszterhazy Karoly University (Hungary)*	**Referee**
Michael	**KISELEV** *Professor, Institute of Solution Chemistry (Russia)*	**Referee**
Abdenacer	**IDRISSI** *Professor, Lille 1 University*	**Supervisor**
Oleg	**KALUGIN** *Professor, V.N. Karazin Kharkiv National University (UKRAINE)*	**Co-supervisor**
Sylvain	**CRISTOL** *Professor, Lille 1 University*	**President**
Ari	**SEITSONEN** *Professor, University of Zurich (Switzerland)*	**Examiner**
Frederic	**AFFOUARD** *Professor, Lille 1 University*	**Examiner**

ACKNOWLEDGEMENTS

This work was done in the framework of co-tutorial agreement between Lille 1 University – Science and Technologies and V. N. Karazin Kharkiv National University under co-supervision of Prof. Abdenacer IDRISSI and Prof. Oleg KALUGIN and I hereby express my sincere gratitude to both of them for the wise and consistent guidance as well as for all the experience and knowledge they shared during my PhD. Their motivation and strong support have been vital for my successful defense.

Also, I would like to thank to Ukrainian government for the basic scholarships as well as "Erasmus Mundus IANUS II" and "Eiffel excellence scholarship" research mobility grants for the given opportunity to perform my research work here in Lille.

The referees of this thesis, Profs. Pal JEDLOVSZKY and Michael KISELEV, are gratefully acknowledged for their time and efforts to examine my thesis.

A special gratitude to my colleagues in Kharkiv University, namely Dr. Yaroslav KOLESNIK, Oleksandr KORSUN, Igor VOVCHYNSKYI, Anastasiia RYABCHUNOVA, and in LASIR – Dr. Bogdan MAREKHA, Dr. Konstantin SMIRNOV, Dr. François-Alexandre MIANNAY, Yulia Ashina and others, for the extremely interesting discussions and for the friendly, almost family-like atmosphere throughout last two years.

Finally, my deepest gratitude is given to my family for all their love and strength.

RESUME

Ce travail est motivé par l'utilisation dans de nombreux dispositifs électrochimiques des mélanges de liquides ioniques (LIs) à base du cation 1-butyl-3-méthylimidazolium (C_4mim^+) couplés à des anions perfluorés (BF_4^-, PF_6^-, TFO^-, $TFSI^-$), avec d'autre part des solvants aprotiques polaires tels que l'acétonitrile (AN), la γ-butyrolactone (GBL), le carbonate de propylène (PC). Nous avons réalisé des simulations de dynamique moléculaire afin de caractériser la structure locale de ces mélanges. Les variations de la structure microscopique en fonction de la composition du mélange ont été calculées via l'utilisation d'un arsenal de fonctions statistiques avancées, basé sur la structure locale. Celle-ci est largement déterminée par la distribution radiale et orientationelle des plus proches voisins à un ion ou une molécule de référence.

Dans un premier temps, la structure locale dans les LIs purs et dans les solvants moléculaires a été analysée. Pour l'ensemble des LIs, il a été établi que les interactions de liaison H de type C−H···X impliquant les atomes d'hydrogène $H^{2,4-5}$ du cycle imidazolium et les atomes électronégatifs de l'anion sont faibles et peuvent être classés dans l'ordre suivant BF_4^-, PF_6^-, TFO^-, $TFSI^-$. Pour le solvant pur, nos résultats montrent que les interactions dipôle-dipôle jouent un rôle important dans la structure locale des solvants étudiés, alors que les interactions liaison H dans le PC et le GBL sont faibles.

Les résultats montrent que dans tous les mélanges LI/solvant moléculaire étudiés, la distribution de l'anion autour du cation n'est pas fortement affectée lorsque la fraction molaire du LI, x_{IL}, varie entre 0.30 et 1.00. Mais pour les valeurs de x_{IL} inférieures à 0.30 les interactions entre cation et anion sont fortement diminuées. Ces résultats corroborent les données publiées sur le comportement du déplacement chimique du proton ^2H en fonction de x_{IL}. Nos résultats soulignent aussi l'importance des interactions anion-solvant dans la description de la structure locale des mélanges LI/solvant moléculaire.

Mots clés: liquides ioniques, solvants dipolaires aprotiques, interactions de liaison hydrogène, facteur de Kirkwood, les plus proches voisins approche, orientation mutuelle.

RESUME

Mixtures of imidazolium ionic liquids (ILs) with perfluorinated anions and dipolar aprotic solvent are promising candidates for electrolytic components used in different electrochemical applications. Current state of technologies requires detailed information on the influence of the mixture composition on the physical and chemical properties of the mixture.

This thesis presents a molecular dynamics simulation analysis of the local structure organization of the mixtures of 1-butyl-3-methylimidazolium (C_4mim^+) ILs with perfluorinated anions (BF_4^-, PF_6^-, TFO^-, $TFSI^-$) and dipolar aprotic solvents such as acetonitrile (AN), γ-butyrolactone (GBL) and propylene carbonate (PC).

As a first step, the local structure in the neat ILs and molecular solvents has been analyzed. For the set of ILs it was established that H-bonding interactions at the H^2 site is strongly enhanced compared to the H^{4-5} sites in the case of asymmetric and/or strongly basic anions like TFO^- or $TFSI^-$. The cation-cation contacts via the aggregation of the butyl chains is much stronger and less anion-dependent than the $\pi^+–\pi^+$ stacking of the imidazolium rings.

For the pure solvent our results show that although the dominant dipole-dipole orientation between a reference molecule and first neighbor is the antiparallel one, while for the subsequent neighbors the antiparallel orientation is gradually weakened in favor of the parallel one. More distant neighbors tend to be parallel to the reference molecule. A deep analysis of the local structure made it possible to identify the presence of weak hydrogen bonds in the selected dipolar solvents.

For the mixtures of imidazolium-based ILs the results show that in all the studied IL/molecular solvent mixtures, the distribution of the anion around the cation is not drastically affected in the range of x_{IL} between 1.00 and 0.30 and for further decrease of x_{IL} noticeable changes in the distance characteristics describing the cation and anion hydrogen bonding interactions, occur. These changes are associated with the expected weakening of the cation and anion interactions. These results are in good agreement with the behavior of the ^2H chemical shift as a function of x_{IL}. Furthermore, our results point out to the importance of the anion-solvent interactions in describing the locale structure in these mixture.

Keywords: ionic liquids, dipolar aprotic solvents, H-bonding interactions, Kirkwood factor, nearest neighbors approach, mutual orientation.

TABLE OF CONTENTS

LIST OF ABBREVIATIONS

AN	acetonitrile
GBL	γ-butyrolactone
PC	propylene carbonate
IL	ionic liquid
C_4mim^+	1-*n*-butyl-3-methylimidazolium
TFO^-	trfluoromethylsulfonate, triflate, $CF_3SO_3^-$
$TFSI^-$	bis(trifluoromethanesulfonyl)imide, triflimide, $(CF_3SO_2)_2N^-$
IR	infrared
AIMD	*ab initio* molecular dynamics
PBC	periodic boundary conditions
PME	Particle-Mesh-Evald
LJ	Lennard-Jonnes
GAFF	generalized AMBER force field
DFT	density functional theory
PES	potential energy surface
MD	molecular dynamics
ADF	angular distribution function
CDF	combined distribution function
SDF	spatial distribution function

Chapter 1. General Introduction

Ionic liquids (ILs) constitute a large class of substances, which present a considerable scientific interest due to their number of advantageous properties. In many applications ILs are used in mixtures with molecular solvents of different nature. It still remains to be an unresolved task of creating a comprehensive microscopic picture on the structure in such systems as a function of mixture composition and nature of the constituents.

This chapter gives a brief introduction to ILs, as well as an overview of the problem and possible strategies to study mixtures of ILs with molecular solvents.

During the last decade ionic liquids (ILs), the class of low-temperature molten salts, have turned from promising functional materials into objects that are used across many areas of scientific and engineering research.[1-5] ILs successfully used as alternative solvents for carrying out organic reactions, and their still increasing popularity goes beyond simply solvating molecules, *i.e.*, they have a growing potential on the application in almost every single branch of physical sciences, ranging from catalysis;[6,7] separation science, such as liquid-liquid extraction[8,9] and extraction of metals[10] and hazardous waste;[11] liquid mirror telescopes,[12] molecular gas capture, such as H_2, CO and CO_2;[13,14] active pharmaceutical ingredients;[15,16] and alternative energy devices, such as metal-ion batteries,[17] fuel,[18] thermoelectrochemical[19] and solar cells.[20] Such progress in the scale and in the range of applications of ILs is determined by the unique set of properties of these materials (negligibly low vapor pressure, wide range of liquid state, thermal and electrochemical stability, high dissolving capability towards both organic and inorganic matter *etc*.) and also by enormous number of possible counterion combinations[7,21] which allow one to select an IL fitting almost any requested set of properties.

ILs are usually composed of large (organic or inorganic) ions, where the ionic head groups (ammonium, imidazolium, sulfate, sulfonate etc.) are attached to non-polar (mostly alkyl) side chains. The charge is usually not centered at one particular atom, with the exception of halide anions, but rather delocalized over several atoms of a molecular ion. Asymmetry is also essential for ILs, and either the cations or the anions size and their shape are very different or the attached side chains vary in length. Molecular structures of commonly employed cations and anions of ILs are shown in Figure 1.1. Among the cations, it is the family of dialkylimidazolium-based ILs, which is the most investigated, particularly the ILs containing 1-alkyl-3-methylimidazolium cations. The selection of anion depends more on the field of application, *e.g.*, OAc^- are popular for cellulose dissolution, while perfluorinated anions like BF_4^-, PF_6^- and $(CF_3SO_2)_2N^-$ are common for electrochemical applications and catalytic reactions.

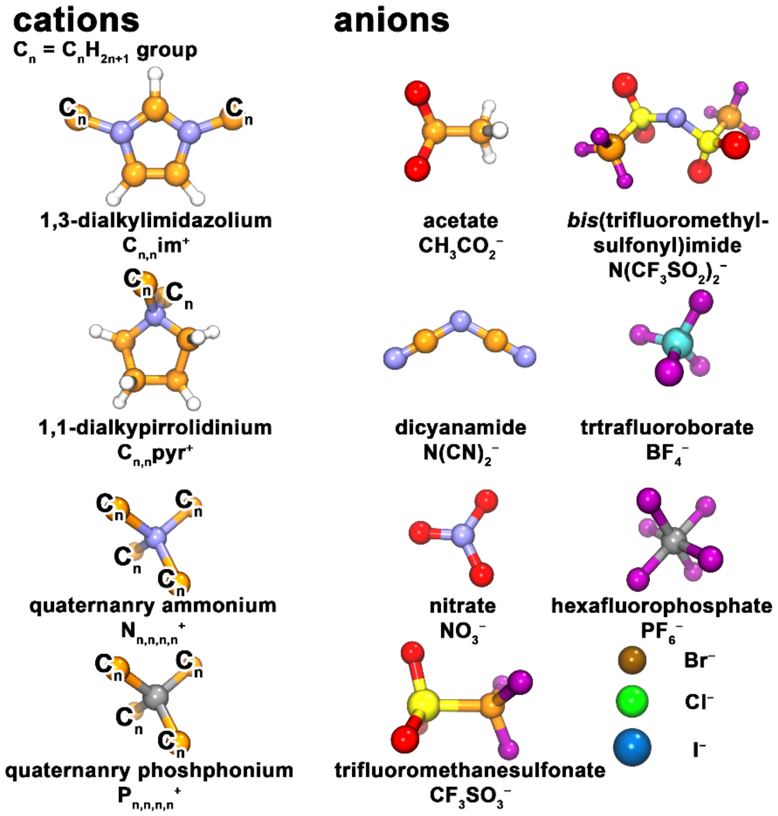

Figure 1.1. Chemical structures of typical cations and anions composing ILs.

However, the effective usage of ILs is partly hindered by several disadvantages, where the very high viscosity is the primary one, while difficulties in purification and rather high cost should also be mentioned. In particular, in the field of electrochemical applications the family of 1-alkyl-3-methylimdazolium (C_nmim^+) ILs with perfluorinated anions (PF_6^-, BF_4^-, $CF_3SO_3^-$, $(CF_3SO_2)_2N^-$) has proven to be good candidates for conducting components of various electrochemical devices such as supercapacitors or electrochemical actuators.[22-28] Among the key factors which determine successful performance of these ILs in electrochemical devices, it is the mobility of ions which is limited by the inherent high viscosity of ILs stemming from strong long range Coulomb interactions between the ions.[29]

Temperature variations (*ca.* by less than 50 K) would only lead to reduction in viscosity by less than one order of magnitude.[30] However, this point can be overcome by combining the ILs with low-weight molecular solvents, which leads to an exponential decay of the viscosity as a function of molar fraction,[31-33] whereby the increasing the electrical conductivity of the resulting ion-molecular mixture.

In this regard, dipolar aprotic solvents, such as acetonitrile (AN) and cyclic organic esters and carbonates, *e.g.*, γ-butyrolactone (GBL) and propylene carbonate (PC), seem to be a good choice for admixing to ILs. In particular, in the field of electrochemical applications,[34-36] unlike the aqueous solutions, they have a number of attractive properties like wide electrochemical window, relatively high dielectric constant and low viscosity making them easily dissolve electrolyte salts and fully miscible with ILs. Moreover, for the family of cyclic organic esters and carbonates, like GBL and PC, peculiar the wide temperature range of the liquid state, nontoxicity along with environmental friendliness that particularly appreciated in electrolytes media for the various electrochemical devices.

For a broad selection of mixtures of imidazolium-based ILs with polar dipolar aprotic solvents it was found that electrical conductivity has a maximum at IL mole fraction, x_{IL}, between 0.1 and 0.2.[37-39] This phenomenon is traditionally explained by the interplay between concentration and ionic association effects from one side and viscosity variation from the other.[40] The former determine the effective number of charge carriers while the latter influences their mobility.[40]

Indeed, admixing molecular solvent to IL should, in general, influence not only the viscosity but modulate the overall microscopic structure as a result of concentration modulation of the interactions between the components. Depending on the propensity of each neat component to give up its inherent interaction pattern (*i.e.*, ion-ion interactions giving rise to network structure in ILs and dipole-dipole interactions in dipolar aprotic solvents leading to their self-association) in favor of solvation one could anticipate different concentration regimes over the entire range of compositions.[41] Thus, the prediction of the practically important macroscopic properties of the ion-molecular systems based on the detailed description of the influence of the nature of individual constituents as well as of the concentration on the local organization of the mixtures of ILs with molecular solvents at the microscopic level is an actual task

In context of the binary mixtures the ILs with molecular solvents can be considered as electrolyte solutions for which their structure and properties from one side are determined by the balance of such types of interactions as interionic (mainly by hydrogen bonds) and intermolecular (dipole-dipole) interactions but also by more complex interactions as ion-molecular (cation···solvent and anion···solvent) from the other side. Thus, one of the most prominent feature of binary systems based on ILs is that the composing ions are multiatomic and, in general, asymmetric, as a result, the mentioned above interactions should be regarded as anisotropic ones, having preferential localization around some molecular fragment (interaction center or site). Another feature of these systems, in comparison with conventional electrolyte solutions, is the full miscibility of ILs with many molecular solvents that allows obtaining mixtures corresponding to either a solution of IL in molecular solvent or a solution of molecular solvent in IL.

Interactions in mixtures of two liquids of different nature at different compositions of these mixtures can be represented as a gradual transition from one pure liquid through solution of the second liquid in the first one, then through solution of the first liquid in the second one, and to pure second liquid. In this type of representation the problem converges to the following question: which composition ranges correspond to the mentioned above regions and which type interactions are the dominant ones.

In pure dipolar aprotic liquids the main structure motif is the dipole-dipole interactions which are considered to be the key ones. However, the issue of the dipolar orientation of molecules, parallel ("head-to-tail") or antiparallel, is still controversial. Additionally, for some solvents the presence of hydrogen bonds between the solvent molecules is also the subject of hottest discussions.

Along with the complex structures and diverse properties, the ILs remains rather complex systems. The interactions between anions and cations range from weak van der Waals, solvophobic, dispersion forces to strong Coulomb and anisotropic hydrogen bonding, halogen bonding, dipole-dipole, magnetic dipole, electron pair donor/acceptor interactions, which leads to their obviously different properties. Particularly, for the imidazolium-based ILs. Particularly, for the imidazolium-based ILs it is widely considered that the local structure in neat ILs defined by the strong Coulombic attraction formally determining the association of the counterions that existed prior to the interaction and remain unchanged in the interaction.[42,43] A significant contribution is also supposed to arise from other strong secondary interactions between the ions, in particular directional hydrogen bonds between the cations and anions. Furthermore, Dupont[44-46] postulated that ILs form a clustered supramolecular structure to maintain a 3D H-bond network. The strength and structure of these clusters are determined by the nature (polarizability, polarizing action, size *etc.*) of anion. Triolo and his colleagues have established a substantial degree of microheterogeneity in various ILs by means of a set of scattering techniques complemented with simulations.[47-50] The effect is more pronounced for ILs with longer alkyl chains and it is attributed to the microscopic segregation of the polar (ionic) and nonpolar (alkyl chain) domains.

The mentioned above considerations on the structure of pure components suggest for the corresponding mixtures two main phenomena, in which redistribution of the balance between possible interionic, intermolecular and ion-molecular interactions upon the composition change can be manifested. They are ionic association/aggregation and ionic solvation. Going from pure IL to pure solvent, these phenomena can be understood as a gradual destruction of large ionic aggregates into smaller ones up to ion pairs.[51]

Experimental information about the local structure in the binary mixtures of ILs with molecular solvent, particularly the change of character of interionic interactions (loose and contact ion pairs, and higher aggregates), upon the change in mixture composition can be extracted directly by conductivity measurements. Furthermore, the information about the relative speed of motion of different molecules and ions along with idea of which supramolecular entities are composed of which particles can be a sufficient basis to build a model of determinative interactions and the corresponding microstructure.

Vibrational and NMR spectroscopies are fundamental tools to characterize the phenomena of ionic association and solvation in the mixtures of ILs with molecular solvents at the microscopic level. The vibrational spectroscopy techniques of infrared (IR) and Raman can provide deep insights on the nature of ionic interactions, the role played by interionic hydrogen bonds, molecular conformations, and their modifications as pressure and temperature is varied in the normal liquid phase, during phase transition to crystalline or amorphous (glassy) solid phases, after vaporization, etc. From another side, NMR measurements are valuable supplement to the IR/Raman, since such measurements allow bring out information on the change of the electronic microenvironment of every chemically non-equivalent nucleus and on the relative arrangement for some nuclei. In a broad perspective, NMR spectroscopy is more advantageous since it suffers from spectral overlaps and signal assignment much less than vibrational spectroscopy

The two phenomena being considered (association and solvation) are also reflected in “statistical” microstructure of such binary mixtures, especially in the microstructure of ionic subsystem. Thus, a certain ordering of mutual distribution of counterions at low distances can be expected in case of pronounced ionic association as well as a certain ordering of distribution of the solvent molecules relative to ions in case of specific solvation. Nowadays experimental evidence on “statistical” microstructure at different temporal and dimensional scales can only be provided by diffraction techniques (various methods of diffraction of X-rays and neutrons). These methods are rather expensive and not easily accessible, as well as complicated in terms of raw data treatment. At the same time they are the only ‘direct’ methods of investigation of microstructure of condensed matter. Most of the studies in this field deal with a single representative system IL-molecular solvent,[52-54] so the generalized and systematic picture is still to be established.

Despite the broad set of experimental approaches targeted at the discovery of peculiarities of intermolecular interactions in binary systems of ILs with molecular solvents, as mentioned above, most of them are indirect methods which are typically challenging in interpretation. Modern methods of molecular modeling can help to solve these problems and they also can be a valuable complement and sometimes even an alternative to otherwise unfeasible experiments with ILs and IL-based system. In view of the phenomena, effects and objects of interest, methods that would be definitely complementary to the proposed experimental techniques are quantum chemical calculations as well as the methods of molecular dynamics simulation.[55,56]

Quantum chemical electronic structure calculations have been routinely used to study various properties of the IL-based systems, to help with the analysis of experimental results and to design new potentially better performing ILs. One should always be cautious when trying to connect the results obtained from calculations on model systems of the size of tens of atoms, often performed in the gas phase, to subtle properties of the macroscopic samples. At present, quantum chemical calculations of small model systems are affordable for the routine use in order to reveal the electronic properties of ILs in detail. The limitations of static quantum chemical calculations are external conditions (usually zero point temperature and without consideration of any effects of medium) as well as the size of a system that can be investigated.

The modeling of a liquid phase, the analysis of the links between its macroscopic properties and their nature at a molecular level is a problem that can be effectively explored within the framework of statistical mechanics. In this context, molecular dynamics (MD) simulations have been used as either predictive or interpretative tools to establish relations between the complex structure and interactions of ionic liquids and their fascinating properties. Over the last few years, the use of MD simulations as a powerful tool to discuss experimental results at a molecular level has successfully been applied to different sources of IL data as diverse as gas solubility/absorption and fluid-phase equilibria, X-ray and neutron diffraction, FTIR/Raman/NMR spectroscopy, TE/AF microscopy, transport properties and rheology, or physical and chemical adsorption.

Despite the fact, that the classical MD simulations can provide reliable information on the structure and dynamics unfortunately, the problem of the force-field development for classical MD simulation of ILs remains an open issue and a subject to discussion. In this regard the methods of ab initio molecular dynamics (AIMD) can be additionally applied. Since AIMD is based on the explicit treatment of the electronic structure on-the-fly during the MD simulations of a larger assembly of molecules with periodic boundary conditions, it provides reliable structural information in a statistical ensemble. Therefore, it can be used to validate, for example, structures from classical MD simulations.

1.1. Organization of the thesis

In this thesis a classical MD simulation have been used to investigate the local structure organization of the binary mixtures of imidazolium-based ILs with dipolar aprotic solvents, relevant for the various electrochemical applications. The discussion of the obtained results organized as follows.

Chapter 2 presents the computational details used in the study and brief review on the available potential models for ILs and molecular solvents. A special emphasis made to the description of the methodology on the developing new potential models for the set of molecular solvents.

The analysis of the local structure organization of the neat individual constituents, neat ILs and dipolar solvents, discussed in details in Chapter 3 and 4. The hydrogen bonding, stacking and dipole-dipole interactions as well as the mutual orientation aspects of the cation···anion, cation···cation and solvent···solvent are established within the nearest neighbors approach.

Chapter 5 is devoted to study role of the solvent and the behavior of ILs with the same cation and the different counterions in the binary mixtures by following the evolution of hydrogen bonding, stacking and dipole-dipole interactions depending from the mixture compositions. Particular attention is paid to the cation···solvent and anion···solvent complexes.

The influence of the charge distribution model depending from the mixture compositions on the structure organization in binary mixtures of ILs with molecular solvents are set forth in Chapter 6.

Finally, conclusions, summarizing the key findings of the work, and future perspectives are outlined.

1.2. References for Chapter 1

(1) Hallett, J. P.; Welton, T. Room-Temperature Ionic Liquids: Solvents for Synthesis and Catalysis. 2. *Chem. Rev.* **2011**, *111*, 3508-3576.
(2) Torimoto, T.; Tsuda, T.; Okazaki, K. I.; Kuwabata, S. New Frontiers in Materials Science Opened by Ionic Liquids. *Adv. Mater.* **2010**, *22*, 1196-1221.
(3) Olivier-Bourbigou, H.; Magna, L.; Morvan, D. Ionic liquids and catalysis: recent progress from knowledge to applications. *Appl. Catal., A* **2010**, *373*, 1-56.
(4) Giernoth, R. Task-Specific Ionic Liquids. *Angew. Chem., Int. Ed.* **2010**, *49*, 2834-2839.
(5) Patel, D. D.; Lee, J.-M. Applications of Ionic Liquids. *Chem. Rec.* **2012**, *12*, 329-355.
(6) Sheldon, R. Catalytic reactions in ionic liquids. *Chem. Commun.* **2001**, 2399-2407.
(7) Plechkova, N. V.; Seddon, K. R. Applications of ionic liquids in the chemical industry. *Chem. Soc. Rev.* **2008**, *37*, 123-150.
(8) Zhao, H.; Xia, S.; Ma, P. Use of ionic liquids as ‘green’ solvents for extractions. *Journal of Chemical Technology & Biotechnology* **2005**, *80*, 1089-1096.
(9) Poole, C. F.; Poole, S. K. Extraction of organic compounds with room temperature ionic liquids. *J. Chromatogr. A* **2010**, *1217*, 2268-2286.
(10) Abbott, A. P.; Frisch, G.; Hartley, J.; Ryder, K. S. Processing of metals and metal oxides using ionic liquids. *Green Chemistry* **2011**, *13*, 471-481.
(11) Visser, A. E.; Swatloski, R. P.; Reichert, W. M.; Mayton, R.; Sheff, S.; Wierzbicki, A.; Davis, J. H.; Rogers, R. D. Task-Specific Ionic Liquids Incorporating Novel Cations for the Coordination and Extraction of Hg2+ and Cd2+: Synthesis, Characterization, and Extraction Studies. *Environmental Science & Technology* **2002**, *36*, 2523-2529.
(12) Borra, E. F.; Seddiki, O.; Angel, R.; Eisenstein, D.; Hickson, P.; Seddon, K. R.; Worden, S. P. Deposition of metal films on an ionic liquid as a basis for a lunar telescope. *Nature* **2007**, *447*, 979.
(13) Vijayraghavan, R.; Pas, S. J.; Izgorodina, E. I.; MacFarlane, D. R. Diamino protic ionic liquids for CO2 capture. *PCCP* **2013**, *15*, 19994-19999.
(14) MacDowell, N.; Florin, N.; Buchard, A.; Hallett, J.; Galindo, A.; Jackson, G.; Adjiman, C. S.; Williams, C. K.; Shah, N.; Fennell, P. An overview of CO2 capture technologies. *Energy & Environmental Science* **2010**, *3*, 1645-1669.
(15) Hough, W. L.; Smiglak, M.; Rodriguez, H.; Swatloski, R. P.; Spear, S. K.; Daly, D. T.; Pernak, J.; Grisel, J. E.; Carliss, R. D.; Soutullo, M. D.; Davis, J. J. H.; Rogers, R. D. The third evolution of ionic liquids: active pharmaceutical ingredients. *New J. Chem.* **2007**, *31*, 1429-1436.
(16) Petkovic, M.; Seddon, K. R.; Rebelo, L. P. N.; Silva Pereira, C. Ionic liquids: a pathway to environmental acceptability. *Chem. Soc. Rev.* **2011**, *40*, 1383-1403.
(17) Scrosati, B.; Garche, J. Lithium batteries: Status, prospects and future. *J. Power Sources* **2010**, *195*, 2419-2430.
(18) Noda, A.; Susan, M. A. B. H.; Kudo, K.; Mitsushima, S.; Hayamizu, K.; Watanabe, M. Brønsted Acid−Base Ionic Liquids as Proton-Conducting Nonaqueous Electrolytes. *J. Phys. Chem. B* **2003**, *107*, 4024-4033.
(19) Abraham, T. J.; MacFarlane, D. R.; Pringle, J. M. Seebeck coefficients in ionic liquids - prospects for thermo-electrochemical cells. *Chem. Commun.* **2011**, *47*, 6260-6262.
(20) Grätzel, M. Conversion of sunlight to electric power by nanocrystalline dye-sensitized solar cells. *Journal of Photochemistry and Photobiology A: Chemistry* **2004**, *164*, 3-14.
(21) Rogers, R. D.; Seddon, K. R. Ionic Liquids--Solvents of the Future? *Science* **2003**, *302*, 792-793.
(22) MacFarlane, D. R.; Forsyth, M.; Howlett, P. C.; Pringle, J. M.; Sun, J.; Annat, G.; Neil, W.; Izgorodina, E. I. Ioinc Liquids in Electrochemical Devices and Processes: Managing Interfacial Electrochemistry. *Acc. Chem. Res.* **2007**, *40*, 1165-1173.

(23) MacFarlane, D. R.; Tachikawa, N.; Forsyth, M.; Pringle, J. M.; Howlett, P. C.; Elliott, G. D.; Davis, J. H.; Watanabe, M.; Simon, P.; Angell, C. A. Energy applications of ionic liquids. *Energy & Environmental Science* **2014**, *7*, 232-250.

(24) Lu, W.; Qu, L.; Henry, K.; Dai, L. High performance electrochemical capacitors from aligned carbon nanotube electrodes and ionic liquid electrolytes. *J. Power Sources* **2009**, *189*, 1270-1277.

(25) Fedorov, M. V.; Kornyshev, A. A. Ionic Liquids at Electrified Interfaces. *Chem. Rev.* **2014**, *114*, 2978-3036.

(26) Merlet, C.; Rotenberg, B.; Madden, P. A.; Taberna, P.-L.; Simon, P.; Gogotsi, Y.; Salanne, M. On the molecular origin of supercapacitance in nanoporous carbon electrodes. *Nat. Mater.* **2012**, *11*, 306-310.

(27) Lewandowski, A.; Galiński, M. Carbon–ionic liquid double-layer capacitors. *Journal of Physics and Chemistry of Solids* **2004**, *65*, 281-286.

(28) Liu, S.; Liu, W.; Liu, Y.; Lin, J.-H.; Zhou, X.; Janik, M. J.; Colby, R. H.; Zhang, Q. Influence of imidazolium-based ionic liquids on the performance of ionic polymer conductor network composite actuators. *Polymer International* **2010**, *59*, 321-328.

(29) Fumino, K.; Wulf, A.; Ludwig, R. Strong, Localized, and Directional Hydrogen Bonds Fluidize Ionic Liquids. *Angew. Chem., Int. Ed.* **2008**, *47*, 8731-8734.

(30) Tokuda, H.; Hayamizu, K.; Ishii, K.; Susan, M. A. B. H.; Watanabe, M. Physicochemical Properties and Structures of Room Temperature Ionic Liquids. 1. Variation of Anionic Species. *J. Phys. Chem. B* **2004**, *108*, 16593-16600.

(31) Canongia Lopes, J. N.; Costa Gomes, M. F.; Husson, P.; Pádua, A. l. A. H.; Rebelo, L. P. N.; Sarraute, S.; Tariq, M. Polarity, Viscosity, and Ionic Conductivity of Liquid Mixtures Containing [C_4C_1im][Ntf_2] and a Molecular Component. *J. Phys. Chem. B* **2011**, *115*, 6088-6099.

(32) Li, W.; Zhang, Z.; Han, B.; Hu, S.; Xie, Y.; Yang, G. Effect of water and organic solvents on the ionic dissociation of ionic liquids. *J. Phys. Chem. B* **2007**, *111*, 6452-6456.

(33) Wang, J.; Tian, Y.; Zhao, Y.; Zhuo, K. A volumetric and viscosity study for the mixtures of 1-n-butyl-3-methylimidazolium tetrafluoroborate ionic liquid with acetonitrile, dichloromethane, 2-butanone and N, N - dimethylformamide. *Green Chem.* **2003**, *5*, 618-622.

(34) Rizzuto, A. M.; Pennington, R. L.; Sienerth, K. D. Study of the BMIM-PF6: Acetonitrile binary mixture as a solvent for electrochemical studies involving CO2. *Electrochim. Acta* **2011**, *56*, 5003-5009.

(35) Trivedi, S.; Sarkar, A.; Pandey, S. Solvatochromic absorbance probe behavior within 1-butyl-3-methylimidazolium hexafluorophosphate + propylene carbonate: preferential solvation or solvent–solvent interaction? *Chem. Eng. J.* **2009**, *147*, 36-42.

(36) Chagnes, A.; Diaw, M.; Carré, B.; Willmann, P.; Lemordant, D. Imidazolium-Organic Solvent Mixtures as Electrolytes for Lithium Batteries. *J. Power Sources* **2005**, *145*, 82-88.

(37) Stoppa, A.; Hunger, J.; Buchner, R. Conductivities of Binary Mixtures of Ionic Liquids with Polar Solvents. *J. Chem. Eng. Data* **2009**, *54*, 472-479.

(38) Nishida, T.; Tashiro, Y.; Yamamoto, M. Physical and electrochemical properties of 1-alkyl-3-methylimidazolium tetrafluoroborate for electrolyte. *J. Fluorine Chem.* **2003**, *120*, 135-141.

(39) Kalugin, O. N.; Voroshylova, I. V.; Riabchunova, A. V.; Lukinova, E. V.; Chaban, V. V. Conductometric study of binary systems based on ionic liquids and acetonitrile in a wide concentration range. *Electrochim. Acta* **2013**, *105*, 188-199.

(40) Marcus, Y.; Hefter, G. Ion Pairing. *Chem. Rev.* **2006**, *106*, 4585-4621.

(41) Dupont, J. On the solid, liquid and solution structural organization of imidazolium ionic liquids. *J. Braz. Chem. Soc.* **2004**, *15*, 341-350.

(42) Angenendt, K.; Johansson, P. Ionic liquid structures from large density functional theory calculations using mindless configurations. *J. Phys. Chem. C* **2010**, *114*, 20577-20582.

(43) Tokuda, H.; Tsuzuki, S.; Susan, M. A. B. H.; Hayamizu, K.; Watanabe, M. How Ionic Are Room-Temperature Ionic Liquids? An Indicator of the Physicochemical Properties. *J. Phys. Chem. B* **2006**, *110*, 19593-19600.
(44) Avent, A. G.; Chaloner, P. A.; Day, M. P.; Seddon, K. R.; Welton, T. Evidence for hydrogen bonding in solutions of 1-ethyl-3-methylimidazolium halides, and its implications for room-temperature halogenoaluminate(III) ionic liquids. *J. Chem. Soc., Dalton Trans.* **1994**, 3405-3413.
(45) Bonhôte, P.; Dias, A.-P.; Papageorgiou, N.; Kalyanasundaram, K.; Grätzel, M. Hydrophobic, Highly Conductive Ambient-Temperature Molten Salts. *Inorg. Chem.* **1996**, *35*, 1168-1178.
(46) Consorti, C. S.; Suarez, P. A. Z.; de Souza, R. F.; Burrow, R. A.; Farrar, D. H.; Lough, A. J.; Loh, W.; da Silva, L. H. M.; Dupont, J. Identification of 1,3-dialkylimidazolium salt supramolecular aggregates in solution. *J. Phys. Chem. B* **2005**, *109*, 4341-4349.
(47) Russina, O.; Lo Celso, F.; Di Michiel, M.; Passerini, S.; Appetecchi, G. B.; Castiglione, F.; Mele, A.; Caminiti, R.; Triolo, A. Mesoscopic structural organization in triphilic room temperature ionic liquids. *Faraday Discuss.* **2013**, *167*, 499-513.
(48) Fazio, B.; Triolo, A.; Di Marco, G. Local organization of water and its effect on the structural heterogeneities in room-temperature ionic liquid/H_2O mixtures. *J. Raman. Spectrosc.* **2008**, *39*, 233-237.
(49) Macchiagodena, M.; Gontrani, L.; Ramondo, F.; Triolo, A.; Caminiti, R. Liquid structure of 1-alkyl-3-methylimidazolium-hexafluorophosphates by wide angle x-ray and neutron scattering and molecular dynamics. *J. Chem. Phys.* **2011**, *134*, 114521.
(50) Zheng, W.; Mohammed, A.; Hines, L. G.; Xiao, D.; Martinez, O. J.; Bartsch, R. A.; Simon, S. L.; Russina, O.; Triolo, A.; Quitevis, E. L. Effect of Cation Symmetry on the Morphology and Physicochemical Properties of Imidazolium Ionic Liquids. *J. Phys. Chem. B* **2011**, *115*, 6572-6584.
(51) Stassen, H. K.; Ludwig, R.; Wulf, A.; Dupont, J. Imidazolium Salt Ion Pairs in Solution. *Chemistry – A European Journal* **2015**, *21*, 8324-8335.
(52) Russina, O.; Sferrazza, A.; Caminiti, R.; Triolo, A. Amphiphile Meets Amphiphile: Beyond the Polar–Apolar Dualism in Ionic Liquid/Alcohol Mixtures. *J. Phys. Chem. Lett.* **2014**, *5*, 1738-1742.
(53) Takamuku, T.; Honda, Y.; Fujii, K.; Kittaka, S. Aggregation of imidazolium ionic liquids in molecular liquids studied by small-angle neutron scattering and NMR. *Anal. Sci.* **2008**, *24*, 1285-1290.
(54) Shimomura, T.; Takamuku, T.; Yamaguchi, T. Clusters of Imidazolium-Based Ionic Liquid in Benzene Solutions. *J. Phys. Chem. B* **2011**, *115*, 8518-8527.
(55) Kirchner, B.: Ionic liquids from theoretical investigations. In *Ionic Liquids*; Kirchner, B., Ed.; Topics in Current Chemistry; Springer-Verlag: Berlin/Heidelberg, 2010; Vol. 290; pp 213-262.
(56) Zahn, S.; Brehm, M.; Brüssel, M.; Hollóczki, O.; Kohagen, M.; Lehmann, S.; Malberg, F.; Pensado, A. S.; Schöppke, M.; Weber, H.; Kirchner, B. Understanding ionic liquids from theoretical methods. *J. Mol. Liq.* **2014**, *192*, 71-76.

Chapter 2. Methodology and computational details

2.1. Introduction

In the framework of MD simulation, investigation of the microstructure of the binary mixtures of ILs with molecular solvent allows to obtain the wide range of different properties, which not only well corroborate with experimental observations but also significantly complements them. For accurate prediction of properties of neat ILs and their mixtures by means of MD simulation, a reliable and transferrable potential model is required.

Certain potential models are quite system specific, whereas other have been developed and successfully applied to broad set of cation and anion. The most widely applicable potential of IL has been developed by Lopes and Padua.[1] This all-atom fully flexible potential model was parametrized by means of *ab initio* calculations on the dihedral energy profiles and further compared with experimental densities. The resulting model reproduces experimental density within 3% for the most of investigated ILs, as well as the cell parameters in the crystalline phase. On the other hand, the computed transport properties, particularly self-diffusion coefficient, shear viscosity and ionic conductivity, are fail to reproduce the experimental measurements.

Another universal potential model developed by Maginn *et al.*[2-5] has been validated against experimental heat capacities, self-diffusion coefficients, viscosities and melting points. While for a number of ILs it was yielded satisfactory agreement with the experimental data, there remains a group of the alkylpyridinium-based ILs for which the simulated dynamic properties are about an order of magnitude lower compared with experimental ones.

Borodin[6] have introduced new polarizable potential model for a wide set of ILs. The validation procedure included comparison of the resulting dynamic and thermodynamics properties to the corresponding experimental values. In most cases the agreement between simulated and experimental results is obtained. Nevertheless, for some ILs the deviations up to 50% were noted, often in the case of the pyridinium- and piperidinium-based ILs. Borodin suggests that this may be caused by unreliability of the experimental data, which are still scarce for certain types of ILs. Further, using *ab initio* parametrization Yethiraj at al.[7] developed a polarizable potential model for $C_n$mim-based ILs that predict the experimental density, enthalpy of vaporization, self-diffusion coefficient and conductivity.

Thus, in order to achieve an accurate dynamic, one needs to incorporate electronic polarizability effect in the potential models. The inclusion of the polarizability does not come without a significant computational effort. Additionally, ILs require very long simulation times in order to ensure an adequate sampling of phase trajectory. The inclusion of polarizability amplifies computation cost by 4–10 times. This is especially true if ionic conductivities and shear viscosities, that are of primary interest.

Voth *et al.*[8] showed that ionic clusters of ILs tend to form stable cells which remain neutral for long time and slow down the overall dynamics of the simulated system. When electrostatic charge fluctuations are considered, an additional mechanism operates charge screening, which increases the dynamics of the simulated system, turning it more realistic.

A few attempts have been made to obtain a realistic dynamics in ILs without including polarizability. Thus, Bhargava and Balasubramanian[9] proposed a refined potential model for C_4mimPF_6 in which partial charges on the cation and anion were allowed. The physical justification for this approach were ab initio calculations showing a significant charge transfer between the ions of ILs. According to these calculations, C_4mim^+ has a total charge of +0.904 *e*, and PF_6^-, consequently, –0.904 *e*, instead of ± 1 *e*. Reducing the partial charges on the ions improves self-diffusion by an order of magnitude, making them closer to the experimental values. Later, the similar methodology was used to develop the set of Lennard-Jones parameters and charge distribution for other potential models of imidazolium ILs.[10,11] The derived set of parameters well reproduce basic experimental thermodynamic and transport properties, namely density, enthalpy of vaporization, self-diffusion coefficient, shear viscosity *etc*.

Another way to improve the correctness of the simulated dynamic properties is the adjusting of Lennard-Jones parameters. Koedderman *et al.*[12] changed the Lennard-Jones parameters on some selected centers of $C_n$mimTFSI to get correct dynamic and thermodynamic properties of this particular ILs. Micaelo *et al.* optimized F–F and O–O Lennard-Jones parameters for PF_6^- and NO_3^- to achieve proper matches for $C_n$mim-based ILs. Values of ε for P in PF_6^- and O in NO_3^- were set 0.001-0.01 kJ mol^{-1}. Although reproducing density and transport properties very well, this potential model underestimates the enthalpy of vaporization.

Considering the available potential models for the dipolar aprotic solvents one can see the significant similarities in approaches for the developing or calibrating of the potential models for ILs and solvents. The most prominent example is the case of potential model for acetonitrile. At present, numerous potential models for acetonitrile have been designed to reproduce various experimental properties. Their degree of detail commonly ranges from models with six interaction sites (all atom models),[13-22] to the more simplified three-site models (united atoms models)[23-29] where hydrogen atoms of the CH_3 group are not considered explicitly to reduce the computational cost and to allow for simulations of larger systems over longer time scales.

Most of the recent computational studies devoted to neat acetonitrile are directly connected to calibration of parameters for all-atom models. Rather successful potential models of acetonitrile were implemented in terms of OPLS/AA[21] and AMBER[17] force fields. The thermodynamic and structural properties derived with these models show reasonable agreement with experimental measurements. However, their further usage undergone considerable revisions. Thus, Wu *et al.*[30] by calibration of the Lennard-Jones parameters has introduced a potential model able to reproduce an experimental value of diffusion coefficient, while the density was noticeably underestimated. Similar effort on the calculations of thermodynamic properties was reported in the study of Nikitin and Lyubartsev.[18] Despite the several advantages, a common drawback of these potential models is that some intramolecular parameters significantly different depending from the force field. Typically, such parameters are defined from the quantum-chemical calculations. Nevertheless, based on DREIDING[31] force field Orhan has presented another approach that combines empirical tuning of both intra- and intramolecular parameters and leads to the good agreement of the studied dynamic and dielectric properties.[20]

2.2. General aspects

All the molecular dynamics simulation were carried out using GROMACS 4.5.5 simulation package.[32] Initial systems containing 864 particles (molecules, ion pairs and/or their combinations), generated by Packmol[33] and placed randomly in a cubic simulation box with periodic boundary conditions (PBC) applied. A Velocity-rescaling thermostat maintained the temperature and Parrinello-Rahman barostat set the pressure at 1 bar throughout the simulation with relaxation times of 0.1 and 0.5 ps, respectively. Equations of motion were integrated using Verlet leap-frog algorithm with a time-step of 0.5 fs. The electrostatic long-range interactions were accounted by the computationally efficient Particle-Mesh-Ewald (PME) algorithm. The 12-6 Lennard-Jones (LJ) interactions are treated by the conventional shifted force technique. Cross interactions between different atom types were derived using standard Lorentz-Berthelot combination rule. The structure properties presented here was analyzed using TRAVIS-1.14.0 code.[34]

For the simulation of pure molecular solvents, firstly, the derived set of the potential model parameters were tested with respect to their ability to reproduce the basic experimental thermodynamics and dynamics properties, namely density, enthalpy of vaporization, self-diffusion coefficient and shear viscosity, at the room temperature. For each temperature, the system was equilibrated in isothermal-isobaric (NPT) ensemble during 500 ps. This step was followed by 1000 ps performed in canonical (NVT) that was used to obtain reliable values for the self-diffusion coefficient and shear viscosity. The structure properties were derived from 500 ps trajectory in NVT ensemble. The electrostatic long-range interactions equal to 1.2 nm and similar to cut-off distance for real-space component. The 12-6 LJ interactions are treated with a switch region between 1.0 and 1.1 nm.

Due to the slow internal dynamics of ILs the initial relaxation is carried out at 400 K for 5000 ps in NVT ensemble to achieve ergodicity. Next, the generated systems are cooled down to the room temperature at NPT ensemble during 15000 ps. The transport properties are derived from 50000 ps trajectories for each system in NVT ensemble. The structure properties were than derived from the last 1000 ps trajectory. The electrostatic long-range interactions equal to 1.5 nm and similar to cut-off distance for real-space component. The 12-6 LJ interactions are treated with a switch region between 1.3 and 1.4 nm. For the mixtures of ILs with molecular solvents with mole fraction of ILs, x_{IL}, 0.05; 0.10; 0.15; 0.20; 0.30; 0.40; 0.50; 0.60; 0.70; 0.80 the same set of parameters was used during the simulation.

2.3. Force field development

As was mentioned above the selection of proper potential parameters may affect not only on the physicochemical properties of individual compounds but also on properties of the resulting mixtures. Considering the uncertainty in the empirical approaches of parameterization of acetonitrile as well as other solvents under study one can deduce about the demand for such potential model that is able *i*) to reproduce correctly the intramolecular vibrations along with considering the effects polarization in condensed phase; *ii*) to reproduce the greatest possible set of properties at the room temperature. For the studied set ILs (see Figure 2.1) these requirements are well satisfied by the recently developed potential model of Mondal and Balasubramanian.[10] For the dipolar aprotic solvents the new set of potential parameters was derived and adopted in order to reproduce the basic physicochemical properties such as density, enthalpy of vaporization, self-diffusion coefficient and shear viscosity.

In the case of mixture of IL with molecular solvent, the concern of making the results of simulations as close as possible to the experimental ones, especially on diffusion, conductivity and viscosity, the above discussed scaled charge scheme was used by changing the scaling factor, f_{mix}, as function of the composition of a binary mixture of IL with molecular solvent. Indeed, one can expect that the value of the scaling factor of the mixture, f_{mix}, will increase starting from f_{IL} in the neat IL, and going to 1 for the infinitely diluted solution of IL in a molecular solvent.[11] This composition dependent scaling factor is defined as follow:

$$f_{\text{mix}} = \sqrt{(1 - f_{\text{IL}}^2)(1 - x_{\text{IL}}) + f_{\text{IL}}^2} \tag{2.1}$$

where f_{IL} is a scaling factor for the pure IL, and x_{IL} the IL mole fraction in the mixture. The authors justified this functional form by the fact that the interionic and ion-molecular interactions are linearly depend on x_{IL}. The effect of the scaling was addressed by studying the structure (i.e., radial distribution function) properties of C_4mimPF_6/AN mixture.

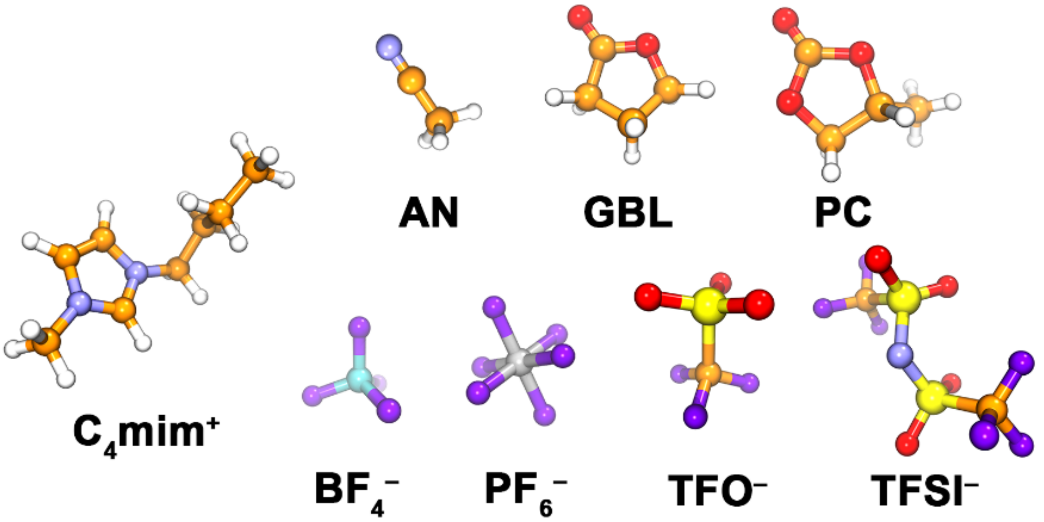

Figure 2.1. Molecular structure of the ions composing four employed ILs C_4mimBF_4, C_4mimPF_6, $C_4mimTFO$, $C_4mimTFSI$ and the three molecular solvents used in this study AN, GBL and PC.

Another questionable issue is which atoms of cation and anion should be involved in the variation of the effective charges. The most sensitive atoms of the imidazolium cation to the anion presence in it vicinity are the ring hydrogens of the C_4mim^+ and of the CH_2 and CH_3 groups connected directly to the nitrogen atoms of the ring. Thus, it would be logical to consider the partial charges of all the atoms of the imidazolium ring and C and H atoms of the CH_2 and CH_3 groups directly connected to the N of the ring (C^2, C^4, C^5, N, H^2, H^4, H^5, C^1 and H^1 atoms, see Figure 2.2a) as variable values, *i.e.*, as a function of the mixture composition. For the anion the respective partial charges of all the atoms should be also rescaled at each composition. Figure 2.2b demonstrates the variation of the partial charges on the C_4mim^+ atoms mentioned above as a function of the mixture composition. In this regard, here we consider both schemes of charge distribution of the studied ILs, namely "constant" and "variable" ones. The former one then will be discussed in Chapter 5, while the comparison of the charge distribution effect on the local structure of the binary mixtures of ILs with molecular solvents will be discussed in detail in Chapter 6.

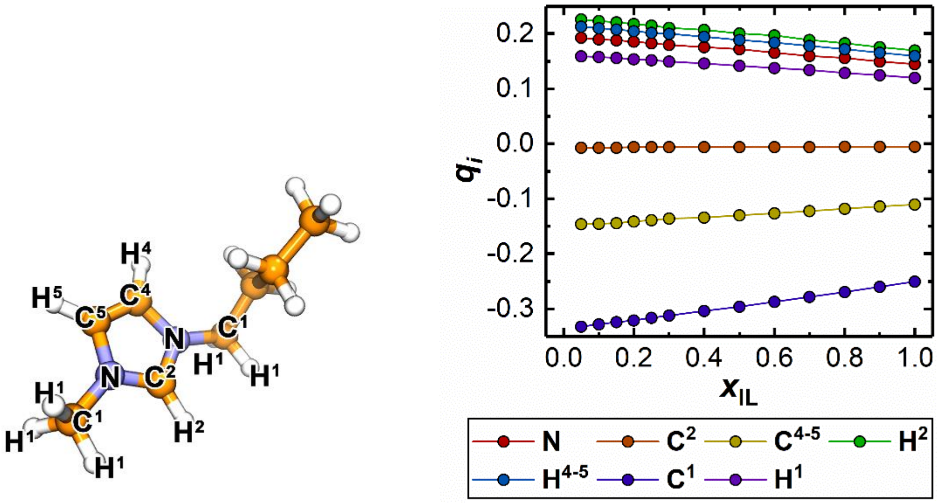

a) b)

Figure 2.2. The numbering scheme of the atoms of the C_4mim^+ cation (a) and variation of partial charges, q_i, on the C_4mim^+ atoms as a function of the mixture composition (b).

2.3.1 Intramolecular force field

A reliable representation of molecular geometry is important in terms of adequate parameterization of the intramolecular potentials, which in turn is essential for reproducing the vibrational spectra of the considered solvents. Toward this purpose, the quantum-chemical calculations of one AN, GBL and PC molecules were carried out followed by harmonic vibrational analysis. The latter were carried out using GAUSSIAN 09W program suite.[35]

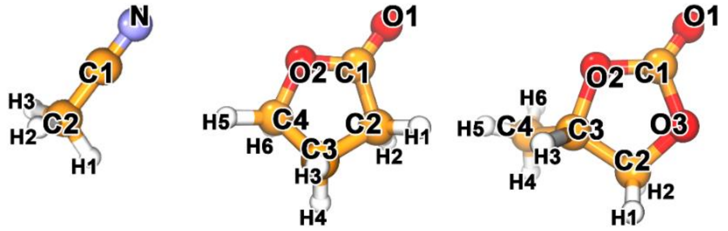

Figure 2.3. Molecular structure of acetonitrile (AN), γ-butyrolactone (GBL) and propylene carbonate (PC) with atomic labeling used for parametrization procedure.

In order to evaluate the reliability of the level of theory for our calculations we performed a benchmark study on small linear AN molecule in gas phase. For this purpose a series of calculations were carried out by using the second-order Møller-Plesset perturbation theory (MP2)[36] together hybrid meta-GGA exchange-correlated functional from Truhlar's group (M06-2X)[37] with six different basis sets (6-31++G(d,p), 6-31++G(2d,2p), 6-311++G(d,p), 6-311++G(2d,2p), aug-cc-pVDZ and aug-cc-pVTZ). The optimal geometry was obtained under very tight optimization convergence criteria as implemented in the software and tested to be true minima by the absence of imaginary frequencies in the corresponding vibration spectra.

Calculated geometry parameters and vibrational frequencies together with literature data[38] are listed in the Table 2.1 and Table 2.2. The geometry parameters obtained by both methods are comparable to each other and are in good agreement with experimental data. Nevertheless, comparing C≡N bond length calculated M06-2X and MP2[39] slightly overestimates this value, making it closer to the value in liquid phase.[40] On another hand, M06-2X significantly blue-shifts the C≡N-stretching band (146-159 cm^{-1}), which is reflected in the energy profiles (See Figure 2.3).

Table 2.1. Optimized geometry of acetonitrile at MP2 and M06-2X with different basis sets along with experimental values.

Methods	Basis set	C^1–C^2 / nm	C^2–H^{1-3} / nm	C^1–N / nm	C^1–C^2–H^{1-3} / deg
MP2	6-31++G(d,p)	0.1463	0.1088	0.1181	109.9
	6-31++G(2d,2p)	0.1464	0.1088	0.1176	110.0
	6-311++G(d,p)	0.1457	0.1095	0.1164	110.4
	6-311++G(2d,2p)	0.1461	0.1085	0.1169	110.0
	aug-cc-pVDZ	0.1471	0.1099	0.1185	109.8
	aug-cc-pVTZ	0.1457	0.1087	0.1170	109.9
M06-2X	6-31++G(d,p)	0.1463	0.1091	0.1155	109.8
	6-31++G(2d,2p)	0.1461	0.1089	0.1151	109.8
	6-311++G(d,p)	0.1459	0.1090	0.1148	109.8
	6-311++G(2d,2p)	0.1460	0.1087	0.1145	109.8
	aug-cc-pVDZ	0.1463	0.1095	0.1155	109.6
	aug-cc-pVTZ	0.1457	0.1088	0.1145	109.8
Experiment	[40]	0.1460	0.1087	0.1170	109.8
	[41,42]	0.1458	0.1104	0.1157	109.5

Table 2.2. Comparison the vibrational frequencies represented as standard deviations (%) obtained at MP2 and M06-2X with different basis sets (where A is 6-31++G(d,p), B - 6-31++G(2d,2p), C - 6-311++G(d,p), D - 6-311++G(2d,2p), E - aug-cc-pVDZ, F - aug-cc-pVTZ) along with experimental values.

Normal mode	Experiment[43]	MP2						M06-2X					
		A	B	C	D	E	F	A	B	C	D	E	F
CCN bend	362	−7.57	−0.47	−1.91	+0.14	−2.90	−0.97	+5.63	+6.27	+6.33	+5.69	+2.76	+6.57
CCN bend	362	−7.57	−0.47	−1.91	+0.14	−2.90	−0.97	+5.72	+6.35	+6.38	+5.74	+2.79	+6.66
CC stretch	920	+2.09	+0.85	+1.49	+0.40	+1.14	+1.58	+1.56	+2.49	+2.28	+1.62	+2.77	+2.19
CH_3 rocking	1041	+3.88	+3.08	+2.77	+3.57	+0.69	+2.49	+1.74	+1.28	+1.87	+1.97	−0.52	+1.78
CH_3 rocking	1041	+3.88	+3.08	+2.77	+3.57	+0.69	+2.49	+1.74	+1.30	+1.88	+1.99	−0.50	+1.79
CH_3 *s* bend	1385	+5.07	+3.49	+2.87	+3.88	+0.40	+2.53	+1.86	+1.33	+1.65	+1.89	−0.83	+1.47
CH_3 *as* bend	1448	+5.03	+4.08	+3.56	+4.18	+1.27	+3.53	+2.29	+2.10	+2.22	+2.50	−0.41	+2.10
CH_3 *as* bend	1448	+5.03	+4.08	+3.56	+4.18	+1.27	+3.54	+2.29	+2.10	+2.22	+2.50	−0.41	+2.10
CN stretch	2267	−2.19	−2.68	−2.53	−3.02	−3.83	−2.54	+7.04	+6.82	+6.86	+6.45	+6.44	+6.76
CH *s* stretch	2954	+6.37	+5.11	+4.93	+5.18	+4.570	+4.79	+4.52	+4.37	+3.98	+4.18	+4.23	+4.06
CH *s* stretch	3009	+7.80	+6.40	+6.14	+6.22	+5.99	+5.98	+5.54	+5.43	+4.83	+4.87	+5.34	+4.81
CH *s* stretch	3009	+7.80	+6.41	+6.14	+6.22	+5.99	+5.98	+5.55	+5.44	+4.83	+4.88	+5.34	+4.81

Starting from the optimized structure the determination of the force constants, associated with the bond lengths and bond angles, in a framework of relaxed potential energy surface (rPES) scanning concept. The rPES scans were performed for all internal coordinates simultaneously optimizing all the unconstrained degrees of freedom, so that the minimum total energy is obtained along the chosen internal coordinate. For each coordinates 18 scans configurations have been computed with a step of 0.0002 nm and 0.3 deg for bonds and angles, respectively. Fitting these curves to suitable polynomials reveals good description by second-order polynomial, i.e. in terms of a simple harmonic approximation. The following functional form has been used for the intramolecular potential, which is the typical expansion in terms of valence coordinates

$$U(r,\theta)=U_{\text{bond}}+U_{\text{angle}}=\sum_{\text{bond}}\frac{k_r}{2}(r-r_0)^2+\sum_{\text{angle}}\frac{k_\theta}{2}(\theta-\theta_0)^2 \qquad (2.2)$$

where $U(r, \theta)$ is a sum over the internal terms as a function of atomic coordinates represented by bond distances (r) and angles (θ). The parameters k_r and k_θ are the respective force constants and the variables with the subscript “0” are the corresponding equilibrium values.

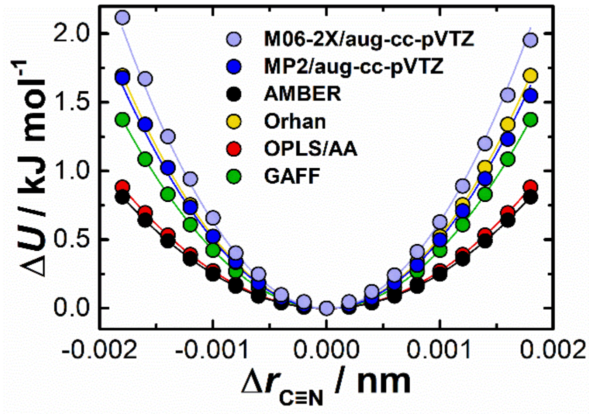

Figure 2.4. Examples of rPES profiles for C≡N stretching from the gas phase *ab initio* calculations and plotted from the literature data: M06-2X/aug-cc-pVTZ, MP2/aug-cc-pVTZ, AMBER based models,[17,18] Orhan,[20] OPLS/AA and GAFF adopted by Caleman et al.[44] Lines represents the harmonic approximation function.

The computed stretching force constants (Table 2.3) are in a relatively good agreement with implemented in earlier force fields. Exceptions are the values for C≡N bond used in OPLS/AA and AMBER based models,[17,18] which are found two times lower than those obtained with rPES scans. An opposite pattern is observed for the C–C≡N bending constants that are significantly overestimated.

Table 2.3. Intramolecular force field parameters for AN obtained with MP2/aug-cc-pVTZ level of theory and from the literature

	MP2/aug-cc-pVTZ		Literature			
Bond	r_0 / nm	k_θ / kJ mol^{-1} nm^{-2}				
			OPLS/AA[44]	GAFF[44]	AMBER[17,18]	Orhan[20]
C^1–C^2	0.1457	318487	326352	308190	334400	293076
C^1–N	0.1170	1002430	543920	848930	501600	1046700
C^2–H	0.1087	333460	284512	282250	284240	278422
Angle	θ_0 / deg	k_θ / kJ mol^{-1} rad^{-2}				
C^1–C^2–H^i	109.9	464.6	292.9	404.2	292.6	418.7
H^i–C^2–H^i	109.0	409.5	276.4	329.7	292.6	268.0
C^2–C^1–N^i	180.0	188.1	1255.2	487.9	668.8	205.1

2.3.2 Intermolecular force field

2.3.2.1 Atomic charges derivation

In order to estimate the effective partial charges on the atoms of AN molecule in the liquid state an *ab initio* molecular dynamics (MD) simulations were performed on the systems consisted of 32 deuterated acetonitrile (AN-d_3) molecules placed in the cubic super-cell. Substitution of the H-atoms by D-atoms allowed one to increase essentially the MD time step and to eliminate quantum effects for the proton dynamics. The lattice constant equals to 1.41027 nm was chosen taking into account AN-d_3 experimental density at the 298.15 K and high-precision atomic masses values.[45-47] The periodic boundary conditions (PBC) have been applied. Initial configuration of the simulated system was generated through the classical MD simulation using AN model developed by Nikitin and Lyubartsev.[18]

Ab initio MD simulation in Car-Parrinello (CP) version and subsequent static quantum-chemical calculations were carried out using CPMD program package.[48]

The CPMD code is based on the pseudo-potential Density Functional Theory and converged plane-wave basis set.[49] For modelling the gradient-corrected B-LYP exchange-correlational functional and the norm-conserving Troullier-Martins (TM) pseudo-potentials were applied.[50-52] The plane-wave kinetic energy cutoff was fixed at 90 Ry. Recently the efficiency of the B-LYP&TM/90 Ry level of theory for the periodic *ab initio* simulations of molecular systems has been shown.[53-55]

To calculate atomic charges of the AN molecule the following procedure was chosen. At the first stage the single point density optimization of the initial atomic configuration has been done. Then a time step of 0.175 fs for the CP simulation has been used, and by variation of the fictitious electron mass it was identified that the stable CP dynamics in microcanonical ensemble is possible if the variable value equals to 1200 a.u. or higher. The value of the fictitious electron mass was increase by 50 a.u. and was used in the equilibration and production CP runs.

Within a second stage in the canonical ensemble at 298.15 K the two equilibration runs of 1.05 ps time length have been carried out: without, B-LYP&TM/90 Ry, and with the vdW-corrections by Grimme (D2) for all simulated atoms, B-LYP&TM+vdW/90 Ry.[56] In both cases the Nosé-Hoover chain thermostat for the nuclei with 2263.1 cm^{-1} frequency has been applied.[57,58] Used frequency corresponds to the maximal vibrational mode in the liquid AN-d_3.[59]

During the third stage, after a preliminary single point density optimization, two production trajectories of 3.15 ps duration time each were generated. For the given runs Nosé-Hoover chain thermostat for the so-called fictitious electron dynamics was also included to the invariable parameters of canonical ensemble. The target kinetic energy on the basis of equilibration runs and frequency of the new thermostat equals to 0.05 a.u. and 7500 cm^{-1} correspondingly were used.

At the final stage the atomic charges were evaluated by analysing 100 uniformly distributed nuclear configurations for the both production trajectories. For each configuration the single point density optimization with subsequent computation of the atomic charges derived from electrostatic potential have been done.[60] Calculated charges for all atomic species were statistically handled along the both trajectories. The obtained values of atomic charges with their standard errors are listed in the Table 2.4 along with the literature data.

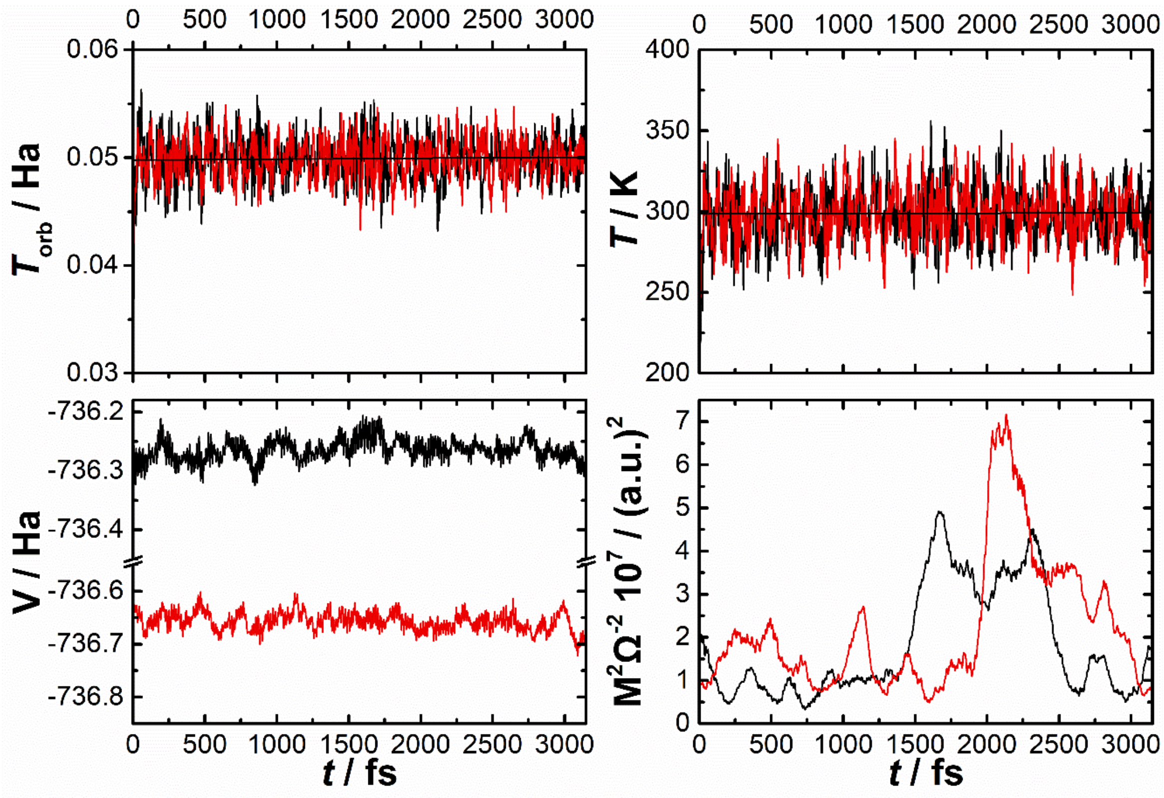

Figure 2.5. Time evolution of the fictitious orbital kinetic energy, T_{orb}, nuclear temperature, T, total potential, V, and suare of total dipole moment per volume unit, $\mathbf{M}^2\Omega^{-2}$, during production Car-Parrinello MD simulations of the system consisted of 32 AN-d_3 molecules at 298.15 K. The black and red lines correspond to the MD simulation without (B-LYP&TM/90 Ry) and with vdW-corrections by Grimme (B-LYP&TM+vdW/90 Ry), respectively.

Comparison of the Table 2.4 data computed with and without vdW-corrections indicates that partial charges are exactly the same for the nitrile group atoms and slightly differ for the methyl group atoms. The main point to stress is that both levels of theory results in small charges negative values on hydrogen atoms. We also point out that the polarity of the C–H bonds is essentially inversed compared to all the others force fields and the CH_3 group then is sufficiently more polar. In the present paper, the atomic charges from B-LYP&TM+vdW/90 Ry level of theory have been implemented in our new model.

Table 2.4. Atomic charges (q) in the liquid AN evaluated from the Car-Parrinello MD trajectories with subsequent static quantum-chemical calculations and from the literature. MD trajectories were generated without B-LYP&TM/90 Ry, and with vdW-corrections by Grimme, B-LYP&TM+vdW/90 Ry, the difference expressed as a standard deviation Δq.

	New model			Literature			
Atom	B-LYP&TM/ 90 Ry	B-LYP&TM +vdW/90 Ry	Δq / e	OPLS/AA[44]	GAFF[44]	Nikitin[18]	Orhan[16,20]
	q / e	q / e		q / e	q / e	q / e	q / e
N	−0.475	−0.475	0.001	−0.56	−0.5168	−0.5126	−0.493
C^1	+0.305	+0.305	0.002	+0.46	+0.4484	+0.4917	+0.475
C^2	+0.185	+0.182	0.002	−0.08	−0.4008	−0.5503	−0.552
H^{1-3}	−0.005	−0.004	0.000	+0.06	+0.1564	+0.1904	+0.190

2.3.2.2 Lennard-Jones parameters

Careful tuning of Lennard-Jones (LJ) parameters (σ, ε) is extremely important for an accurate reproduction of the thermodynamic and the dynamic properties and several attempts were undertaken on this direction. For example, Nikitin and Lyubartsev[18] modified mainly the values of the LJ parameters of nitrogen and nitrile carbon (C^1) of the different force fields to reproduce density and enthalpy of vaporization. A better agreement of thermodynamic properties with the experimental data was found while the self-diffusion coefficient is 20% less the corresponding experimental one. In another study reported by Orhan[20] only the value of the nitrogen LJ values were modified in order to obtain reasonable agreement with the experimental dynamic and dielectric properties. To get an adequate value of the self-diffusion coefficient of pure AN Wu *et al.*[30] inserted a reduced separation distance (σ) of hydrogen to the model developed by Grabuleda *et al.*[17] Thus, the empirical approach to obtain the LJ parameters is fully justifiable.

As the density, ρ, as well as the enthalpy of vaporization, $\Delta_{\mathrm{vap}}H_T$, are sensitive to the used force field model, the refined set of potential parameters was used along with LJ parameters for nitrogen and hydrogen taken from literature (see Table 2.5 for details). The $\Delta_{\mathrm{vap}}H_T$ values can be computed from the equation

$$\Delta_{\mathrm{vap}}H_T = H_{T,\mathrm{gas}} - H_{T,\mathrm{liq}} \equiv U_{T,\mathrm{gas}} - U_{T,\mathrm{liq}} + RT \qquad (2.3)$$

where U_T is the ensemble-averaged potential energy in either the gas or liquid (liq) phase at the temperature T.

Quantitative estimation of translational dynamics can be implemented by means of the self-diffusion coefficient of the center of mass of a molecule i which is obtained from the well-known Einstein relation

$$D_i = \frac{1}{6}\lim_{t\to\infty}\frac{d}{dt}\left\langle \left|\mathbf{r}_i(t)-\mathbf{r}_i(0)\right|^2\right\rangle \tag{2.4}$$

where $\left\langle \left|\mathbf{r}_i(t)-\mathbf{r}_i(0)\right|^2\right\rangle$ is the ensemble-averaged mean-square displacement (MSD) of molecule i.

Additionally the β coefficient was calculated using equation:

$$\beta(t) = \frac{d\log \mathrm{MSD}(t)}{d\log t} \tag{2.5}$$

where the MSD(t) is the mean square displacement of the molecule and is given by:

$$\mathrm{MSD}(t) = \frac{1}{N}\sum_{i=1}^{N}\left\langle \left|\mathbf{r}_i(t)-\mathbf{r}_i(0)\right|^2\right\rangle \tag{2.6}$$

The range time where β coefficient is equal 1,[10] evidences that the system has reached the diffusive regime during the simulation and β follows from the Einstein relation.

The shear viscosity of the system was estimated through the fitting of the transverse current autocorrelation functions (TCAFs) for plane waves based on momentum fluctuations[61,62] realized within the "g_tcaf" tool of GROMACS package. The dependence of the viscosity on the plane wave vector, k, is extrapolated to k = 0 to obtain the share viscosity. This achieved using the expansion

$$\eta(k) = \eta(0)(1-ak^2)+O(k^4) \tag{2.7}$$

Table 2.5. The fine-tuning procedure of Lennard-Jones parameters, σ and ε, for the new AN model and obtained with the substitution of this parameters on H and N thermodynamic and dynamic properties in comparison with experimental data.

Parameters	σ / nm		ϵ / kJ mol^{-1}		ρ g cm^{-3}	ΔH_{vap} kJ mol^{-1}	D 10^5 cm^2 s^{-1}	η mPa s
	N	H	N	H				
Initial[18]	0.3011	0.2649	0.55726	0.06563	0.7707	33.4211	3.0028	0.3625
σ_{N}[63]	0.3189	0.2649	0.55726	0.06563	0.7410	32.5873	3.6021	0.3345
σ_{N}[44]	0.3200	0.2649	0.55726	0.06563	0.7175	31.9182	3.6312	0.3191
σ_{N}, σ_{H}[63]	0.3189	0.2388	0.55726	0.06563	0.7945	34.0327	2.9749	0.3878
σ_{N}, σ_{H}[44]	0.3200	0.2500	0.55726	0.06563	0.7714	33.4400	3.0111	0.3697
σ_{N},[63] σ_{H}[44]	0.3189	0.2500	0.55726	0.06563	0.7748	33.5276	3.1173	0.3617
σ, ε[63]	0.3189	0.2388	0.75312	0.10042	0.8180	38.0642	1.9507	0.5033
σ, ε[44]	0.3200	0.2500	0.71128	0.06276	0.7815	34.9530	3.1927	0.3594
Final	0.3100	0.2530	0.55726	0.02000	0.7763	32.8823	4.0300	0.3228
Experiments					0.7761[64] 0.7766[65] 0.7778[66]	32.94[67] 33.50[68] 34.48[69]	4.04[70] 4.31[71] 4.37[72] 4.34[73] 4.85[74] 5.10[75]	0.344[76] 0.345[77] 0.341[78]

In the first step of the process of refinement of the LJ parameters values, those of Nikitin model[18] were considered; to evaluate their ability to the produce both the thermodynamic (density and enthalpy of evaporation) and the dynamic (self-diffusion coefficient and shear viscosity) properties of AN. The analysis of this model shows satisfactory results for density (~0.7-0.9% of deviation) and enthalpy of vaporization (~1.5-3.0% of deviation) compared to the available experimental data, however the dynamic properties significantly differ from the experimental ones. In a second step, the σ_{N} value were increased within the parameters taken from OPLS/AA[44] and CGenFF[63]. In the frame of these changes the self-diffusion coefficient takes the values ~20% higher than those obtained using parameters, while the shear viscosity, the density and enthalpy of vaporization undergo certain losses. Furthermore, decreasing the values of σ_{H} and σ_{N} using the CGenFF parameters results in a better agreement for the density (~0.6-

0.8%). Finally, the interaction energy parameter ϵ_{H} was tuned to reach the experimental values of diffusion and viscosity. This was achieved with minor changes of CGenFF nitrogen and OPLS/AA hydrogen separation distance (σ_{N} and σ_{H}).

Since the success of the refinement procedure of the potential model in general determined by the tuning of LJ parameters, for GBL and PC potential models the partial atomic charges were obtained by fitting the electrostatic potential energy surface according to the Merz-Singh-Kollman scheme. This approach to obtain the partial charges is less resource-intensive compared with AIMD calculations and successfully reproduce the total molecular dipole moment as well. Preliminary, the optimal geometry of each single molecules were carried out in gas phase followed by determination of the force constants using rPES scanning concept, similarly to refinement procedure for AN. All the calculations was conducted in MP2/6-311++G(d,p). The selection of this level of theory was dictated by rather successful results on parameterization of GBL, able to reproduce correctly the intramolecular vibrations along with considering the effects polarization in condensed phase.

Optimal geometry was tested to be true minima by the absence of imaginary frequencies in the corresponding vibration spectra. Starting from the optimized structures rPES scans were performed for all internal coordinates simultaneously optimizing all the unconstrained degrees of freedom, so that the minimum total energy is obtained along the chosen internal coordinate. For each coordinates 18 scans configurations have been computed with a step of 0.0002 nm for bonds, 0.5 and 0.8 deg for angles and proper/improper dihedrals, respectively. Similar to AN, fitting these curves to suitable polynomials in terms of a simple harmonic approximation with addition of dihedral constituent. In this case for GBL and PC the Equation 2.1 could be rewritten in following way

$$\begin{aligned}U\left(r,\theta,\phi,\zeta\right)&=U_{\text{bond}}+U_{\text{angle}}+U_{\text{dihedral}}+U_{\text{improper}}=\sum_{\text{bond}}\frac{k_r}{2}\left(r-r_0\right)^2+\sum_{\text{angle}}\frac{k_\theta}{2}\left(\theta-\theta_0\right)^2+\\&+\sum_{\text{dihedral}}\frac{k_\phi}{2}\left(\phi-\phi_0\right)^2+\sum_{\text{improper}}\frac{k_\xi}{2}\left(\xi-\xi_0\right)^2\end{aligned}\tag{2.8}$$

where $U\left(r,\theta,\phi,\xi\right)$ is a sum over the internal terms as a function of atomic coordinates represented by bond distances (r), angles (θ), dihedrals (ϕ) and improper dihedrals (ξ). The parameters k_i are the respective force constants and the variables with the subscript “0” are the corresponding equilibrium values.

Since our equilibrium values for GBL molecule are similar to those derived by Masia and Rey, we refitted force constants for bond and angles within harmonic approximation, while proper dihedrals were replaced into the harmonic ones. Such approach also allows reproducing reliably intramolecular frequencies whose values are rather close to the experimental measurements. Similarly to GBL parameterization procedure, for PC the C–H distances and the related force constants were averaged; despite the fact that all distances are similar to GBL, the calculated force constants are slightly differ for both molecules.

Based on the optimized geometries and calculated charge distributions for GBL and PC, obtained dipole moment is slightly overestimated for both molecules compared with experimental ones (4.708 and 5.600 D versus the experimental values of 4.270 and 4.900 for GBL and PC, respectively). The initial Lennard-Jones parameters (σ, ε) for GBL and PC were taken from OPLS/AA force field and fitted to reach experimental values of both the thermodynamic and the transport properties according to procedure described for AN. Thus, the values of the interaction energy parameter ε_{H} were set equal to 0.02 kJ mol^{-1} in both force models, while σ_{H} have the values of 0.226 and 0.180 nm for GBL and PC, respectively. This allows increasing significantly the transport properties, while the density and enthalpy of vaporization values are decreasing dramatically. The latter, in turn, were improved by the reducing of ε_0 on the carbonyl oxygen to 0.4786 and 0.2756 kJ mol^{-1} for GBL and PC.

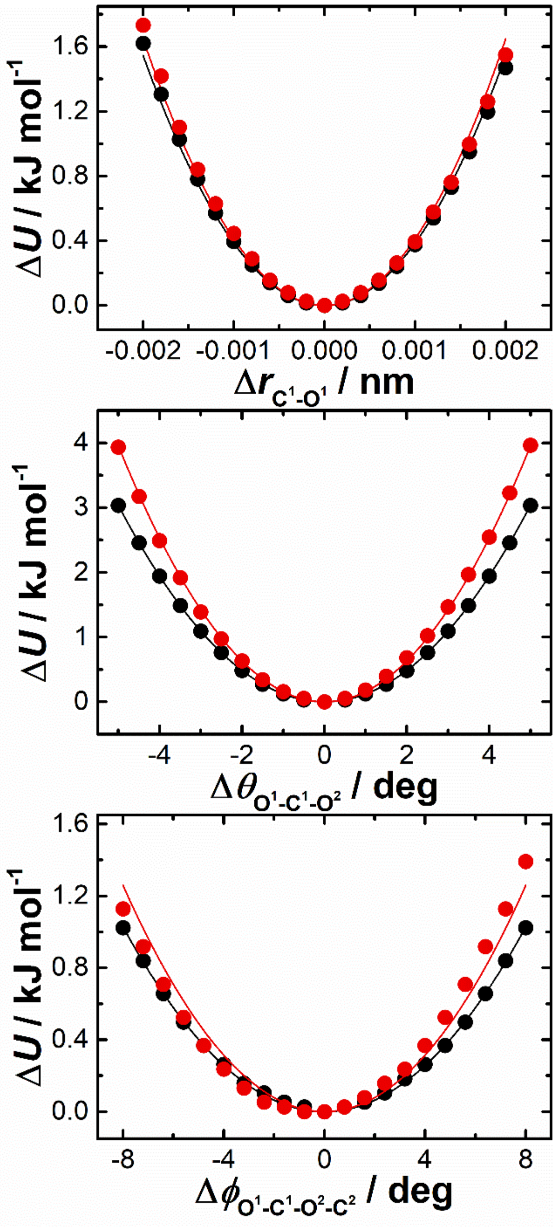

Figure 2.6. Examples of rPES profiles for GBL (*black*) and PC (*red*) from the gas phase ab initio calculations at MP2/6-311++G(d,p) level of theory.

Table 2.6. Charge distribution, q, Lennard-Jones parameters, σ and ε, intramolecular parameters, k_i, for GBL and PC.

	GBL		PC	
Charge	q / e		q / e	
O^1	–0.5336		–0.5407	
O^2	–0.4234		–0.4627	
O^3			–0.4925	
C^1	0.7273		0.9242	
C^2	–0.1623		0.1176	
C^3	–0.0674		0.3841	
C^4	0.1018		–0.5138	
H^1	0.0632		0.0677	
H^2	0.0734		0.0553	
H^3	0.0360		0.0256	
H^4	0.0623		0.1528	
H^5	0.0547		0.1064	
H^6	0.0679		0.1758	
Atom	σ / nm	ε / kJ mol^{-1}	σ / nm	ε / kJ mol^{-1}
O^1	0.302	0.4786	0.302	0.2756
$O^{2–3}$	0.300	0.7113	0.300	0.7113
C^1	0.385	0.4393	0.385	0.4393
$C^{2–4}$	0.350	0.2761	0.350	0.2761
$H^{1–6}$	0.226	0.0200	0.180	0.0200
Bond	r_0 / nm	k_r / kJ mol^{-1} nm^{-2}	r_0 / nm	k_r / kJ mol^{-1} nm^{-2}
C^1–O^1	0.1203	774749.2	0.1183	823856.5
C^1–C^2	0.1523	224180.3		
C^1–O^2	0.1368	278933.4	0.1352	307731.7
C^1–O^3			0.1352	307731.7
C^2–C^3	0.1526	248158.7	0.1519	266275.8
C^2–O^2			0.1429	273422.3
C^3–C^4	0.1529	231992.1	0.1519	266275.8
C^3–O^3			0.1429	273422.3
C^4–O^2	0.1442	241006.1		
C^2–$H^{1–2}$	0.1093	334290.3	0.1092	324276.7
C^3–H^3			0.1092	324276.7
C^4–$H^{3–4}$	0.1093	334290.3		
C^4–$H^{4–6}$			0.1092	324276.7
C^4–$H^{5–6}$	0.1093	334290.3		
Angle	θ_0 / deg	k_θ / kJ mol^{-1} rad^{-2}	θ_0 / deg	k_θ / kJ mol^{-1} rad^{-2}
O^1–C^1–C^2	128.5	376.4		
O^1–C^1–O^2	122.5	797.2	125.0	1033.5
O^1–C^1–O^3			125.0	1033.5
C^1–C^2–C^3	102.9	771.2		
C^1–O^2–C^2			109.5	1415.4
C^1–O^3–C^3			109.5	1415.4
O^2–C^1–O^3			110.1	2011.2
C^2–C^3–C^4	100.9	774.1	115.2	688.1
C^2–C^3–O^3			102.3	1247.8
C^3–C^2–O^2			102.3	1247.8
C^3–C^4–O^2	105.2	840.7		
C^4–C^3–O^3			102.3	1247.8
C^4–O^2–C^1	109.9	594.1		

Table 2.6 continued

O^2–C^1–C^2	109.0	845.3		
C^1–C^2–H^{1-2}	108.9	400.7		
C^3–C^2–H^{1-2}	113.7	400.7	111.1	469.1
C^2–C^3–H^{3-4}	112.3	400.7		
C^2–C^3–H^3			111.1	469.1
C^4–C^3–H^{3-4}	111.1	400.7		
C^4–C^3–H^3			111.1	469.1
C^3–C^4–H^{5-6}	112.9	400.7		
C^3–C^4–H^{4-6}			111.1	469.1
O^2–C^4–H^{5-6}	107.9	545.1		
O^2–C^2–H^{1-2}			108.4	612.0
O^3–C^3–H^3			108.4	612.0
H^{1-2}–C^2–H^{1-2}	108.4	347.1	108.7	430.6
H^{3-4}–C^3–H^{3-4}	109.0	347.1		
H^{5-6}–C^4–H^{5-6}	109.6	347.1		
H^{4-6}–C^4–H^{4-6}			108.7	430.6
Dihedral	ϕ_0 / deg	k_ϕ / kJ mol^{-1} rad^{-2}	ϕ_0 / deg	k_ϕ / kJ mol^{-1} rad^{-2}
O^1–C^1–C^2–C^3	−161.5	107.3		
O^1–C^1–O^2–C^2			171.3	130.5
O^1–C^1–O^3–C^3			171.3	130.5
O^1–C^1–O^2–C^4	−176.5	105.5		
C^1–C^2–C^3–C^4	−31.1	197.8		
C^1–O^2–C^4–C^3	−24.1	130.3		
C^1–O^2–C^2–C^3			20.9	144.2
C^1–O^3–C^3–C^2			20.9	144.2
C^1–O^3–C^3–C^2			143.4	104.1
C^2–C^3–C4–O^2	34.1	184.5		
C^2–C^1–O^2–C^4	3.3	110.2		
C^3–C^2–C^1–O^2	18.7	137.0		
C^4–C^3–C^2–O^2			−143.6	130.2
O^2–C^1–O^3–C^3			−8.7	133.8
O^3–C^1–O^2–C^3			−8.7	133.8
O^2–C^2–C^3–O^3			−24.5	150.8
Improper	ξ_0 / deg	k_ξ / kJ mol^{-1} rad^{-2}	ξ_0 / deg	k_ξ / kJ mol^{-1} rad^{-2}
C^1–O^2–C^2–O^1	0.0	159.1		
C^1–O^2–O^3–O^1			0.0	238.4

2.4. Validation

2.4.1 Individual compounds

As was mentioned above the aim of the parameterization procedure for the solvents potential models is to reproduce as accurate as possible the thermodynamic and transport properties, namely density (ρ), enthalpy of vaporization (ΔH_{vap}), self-diffusion coefficient (D) and shear viscosity (η) at room temperature. The details of calculation these physicochemical properties are given above. Apart the available experimental data, the previously developed models for the studied solvents was used for the comparison of the ability to reproduce the same set of experimental thermodynamic and dynamic properties at the room temperature. The results of comparison of the calculated properties at room temperature are summarized in Table together with experimental data.

For the selected set of ILs it is evident that the results obtained from the simulation for density and enthalpy of vaporization show satisfactory agreement with those reported in literature as well as with experimental ones (see Table 2.7). The small deviations of the calculated quantities could be explained by the sensitivity of the derived inter- and intramolecular parameters to the applied algorithms maintaining constant temperature and pressure.

Similar observations also concerns the calculated transport properties. According to the beta coefficient all the ILs achieve the diffusive regime after 400-500 ps of simulation and the resulted values of *D* are within 20% of experimental results in many systems. Moreover, the values reported in Table is physically correct, since the cations diffuse faster than anions that also agreed with the observations for other imidazolium-based ILs. For the calculated viscosities the observed trend follow the sequence C_4mimPF_6 > C_4mimBF_4 > $C_4mimTFO$ > $C_4mimTFSI$ which is in good agreement with experiment. Such behavior of viscosity was attributed to the difference in the shape and simmetry of anion, where the ILs with highly symmetric, nearly spherical anions found to be more viscous. This order for different anions could be also depend from the strength of the H-bonding interactions between cation and anion as well as to their electrostatic interaction.

Table 2.7. Observed density, ρ, enthalpy of vaporization, ΔH_{vap}, self-diffusion coefficient, D, and share viscosity, η, calculated at 298.15 K for C_4mimBF$_4$, C_4mimPF$_6$, C_4mimTFO and C_4mimTFSI models in comparison with the literature data and experimental measurements.

	this work	Literature[10]	experimental
		ρ / g cm^{-3}	
C_4mimBF$_4$	1.2130	1.2060	1.2020[79]
C_4mimPF$_6$	1.4085	1.3880	1.3680[79]
C_4mimTFO	1.3312	1.3170	1.2980[79]
C_4mimTFSI	1.4972	1.4460	1.4370[79]
		ΔH_{vap} / kJ mol^{-1}	
C_4mimBF$_4$	32.12	31.90	33.78[80]
C_4mimPF$_6$	32.84	33.00	37.00[81]
C_4mimTFO	33.48	32.94	33.22[82]
C_4mimTFSI	31.33	31.23	32.17[83]
		D 10^5 / cm^2 s^{-1}	
C_4mim$^+$ / BF$_4^-$	0.0261 / 0.0210	0.0230 / 0.0183	0.0180 / 0.0170[79]
			0.017 / –[84]
			0.016 / 0.015[85]
			0.0158 / 0.0146[86]
C_4mim$^+$ / PF$_6^-$	0.0142 / 0.0094	0.0105 / 0.0074	0.0089 / 0.0071[79]
			0.0078 / 0.0066[84]
			0.0080 / 0.0059[85]
			0.0071 / 0.0054[86]
C_4mim$^+$ / TFO$^-$	0.0224 / 0.0172	0.0208 / 0.0141	0.0210 / 0.0160[79]
			0.018 / –[84]
			0.019 / 0.014[85]
C_4mim$^+$ / TFSI$^-$	0.0262 / 0.0178	0.0270 / 0.0210	0.0340 / 0.0260[79]
			0.036 / –[84]
			0.0299 / 0.0238[85]
			0.0282 / 0.0216[86]
		η / mPa s	
C_4mimBF$_4$	76.2	71	75.3[79]
			75.4[87]
C_4mimPF$_6$	190.0	185	182.4[79]
			209.1[87]
			209.2[88]
C_4mimTFO	66.3	65	65.4[79]
			63.2[89]
			64.2[90]
C_4mimTFSI	43.3	42	40.0[79]
			40.6[87,91]

Considering dipolar liquids, as follows from the Table 2.8, the computed densities using the selected force fields are in good agreement with each other as well as with experimental data. This may point to the fact that the structural properties in bulk liquids does not depend from the selected force field. The highest deviations observed for the OPLS/AA and GAFF based models are not exceeding 2-5%. For AN the densities obtained with in the frame of new model, Orhan and Nikitin potential models are almost similar and well reproduce the experimental results. Although densities for the refined GBL and PC models are in good agreement with experimental data.

As for enthalpies of vaporization, it is difficult to compare the simulated and experimental values as the values reported using different experimental techniques differ from each other. Thus, a slightly different situation observed for enthalpy of vaporization, where the OPLS/AA model for AN has the highest deviation of 7.6-11.8%. The Nikitin's model provide the best result being in middle of the three available experimental data, while Orhan's and our new model are close to their lowest value. The refined PC has a highest deviation for the enthalpy of vaporization compared with other PC models. The similar observations, however, are also inherent for the previously developed model of Masia for GBL.

The behavior of the transport properties, self-diffusion coefficient and shear viscosity, obtained in canonical ensemble were compared with the available experimental data. The calculation of D was carried out in the range of time between 100 and 850 ps depending on the used force field. In this range of time, the β coefficient is equal to 1, and evidences that the system has reached the diffusive regime. The calculated quantities with the refined models are in excellent agreement with experimental results as well as with some other potential models. Namely, except Nikitin's model, the calculated diffusion coefficients using other models for AN are within the range of the experimental data, while for GBL the experimental values achieved only with OPLS/AA based model. For PC the obtained results with the model of Takeuchi and OPLS/AA are significantly underestimated.

The calculated viscosity for AN is slightly lower for the new model than those obtained with Nikitin's model and compared with experimental data. For

GBL and PC it was found that they fails to reproduce shear viscosity, whereas the opposite situation observed for the previously published models.

Table 2.8. Observed density, ρ, enthalpy of vaporization, ΔH_{vap}, self-diffusion coefficient, D, and share viscosity, η, calculated at 298.15 K for AN, GBL and PC models in comparison with the results obtained through the previously published models and experimental measurements.

	this work	Literature	experimental
ρ / g cm^{-3}			
AN	0.7763	0.7718[18]	0.7761[64]
		0.7713[20]	0.7766[65]
		0.7549[44]	0.7778[66]
		0.8072[44]	
GBL	1.1236	1.1305[92]	1.1212[93]
		1.1313[93]	1.1234[96]
		1.1078[44]	1.1243[97]
PC	1.1997	1.1906[94]	1.1978[98]
		1.2238[95]	1.200[99]
		1.1432[44]	1.1995[96]
			1.1999[100]
ΔH_{vap} / kJ mol^{-1}			
AN	32.88	33.51[18]	32.94[67]
		32.27[20]	33.50[68]
		30.42[44]	34.48[69]
		32.60[44]	
GBL	48.71	62.71[92]	48.0[101]
		57.42[93]	48.9[102]
		49.35[44]	54.4[103]
PC	56.94	57.28[94]	61.5[104]
		67.01[95]	
		60.24[44]	
D 10^5 / cm^2 s^{-1}			
AN	4.04	3.40[18]	4.04[70]
		3.84[20]	4.31[71]
		4.27[44]	4.37[72]
		3.97[44]	4.34[73]
			4.85[74]
			5.10[75]
GBL	0.79	0.64[92]	0.83[84]
		0.52[93]	0.9[105]
		0.80[44]	
PC	0.53	0.10[94]	0.49[106]
		0.31[95]	0.52[107]
PC	0.53	0.25[44]	0.55[108]
			0.57[94]
			0.58[105]
			0.62[84]

Table 2.8 continued.

η / mPa s			
AN	0.32	0.37[18]	0.344[76]
		0.31[20]	0.345[77]
		0.28[44]	0.341[78]
		0.28[44]	
GBL	0.96	1.79[92]	1.72[109]
		1.28[93]	1.73[96,99]
		0.86[44]	1.76[93]
PC	1.08	2.21[94]	2.50[110]
		1.34[95]	2.51[111-113]
		1.28[44]	2.53[96,99]

In general, using the new potential models it is possible to reproduce reasonably both the thermodynamic and the dynamic properties at room temperature compared with the other selected force fields. Moreover, the revision of stretching and bending force constants allows to reproduce the experimental vibration frequencies in pure liquid, while the other models underestimated them significantly.

2.4.2 Binary mixtures of ILs-molecular solvent

To validate the simulated IL-molecular solvent mixtures the basic physicochemical properties were predicted and compared with available experimental data as a function of mixture composition, namely density and self-diffusion coefficient. In this way, we validate suitability of the physical model of the combined force fields for describing the macroscopic properties.

The calculated densities of the IL-solvents mixtures further were compared with several experimental measurements (Figure 2.6). The obtained results are in satisfactory agreement with experimental results at the entire range of mixture compositions. Comparing the behavior of the three different solvents one can see that the great changes are inherent to the binary mixtures with AN and to a less extent for GBL and PC. Indeed, in case of the binary mixtures with AN the respective densities of the mixture decreases only slightly in the concentration range $x_{\mathrm{IL}} > 0.3$, staying almost steady. With further decreasing of x_{IL}, densities decrease exponentially with increasing of solvent content. For the binary mixtures with GBL and PC the respective densities increases with decreasing of x_{IL}, and pass

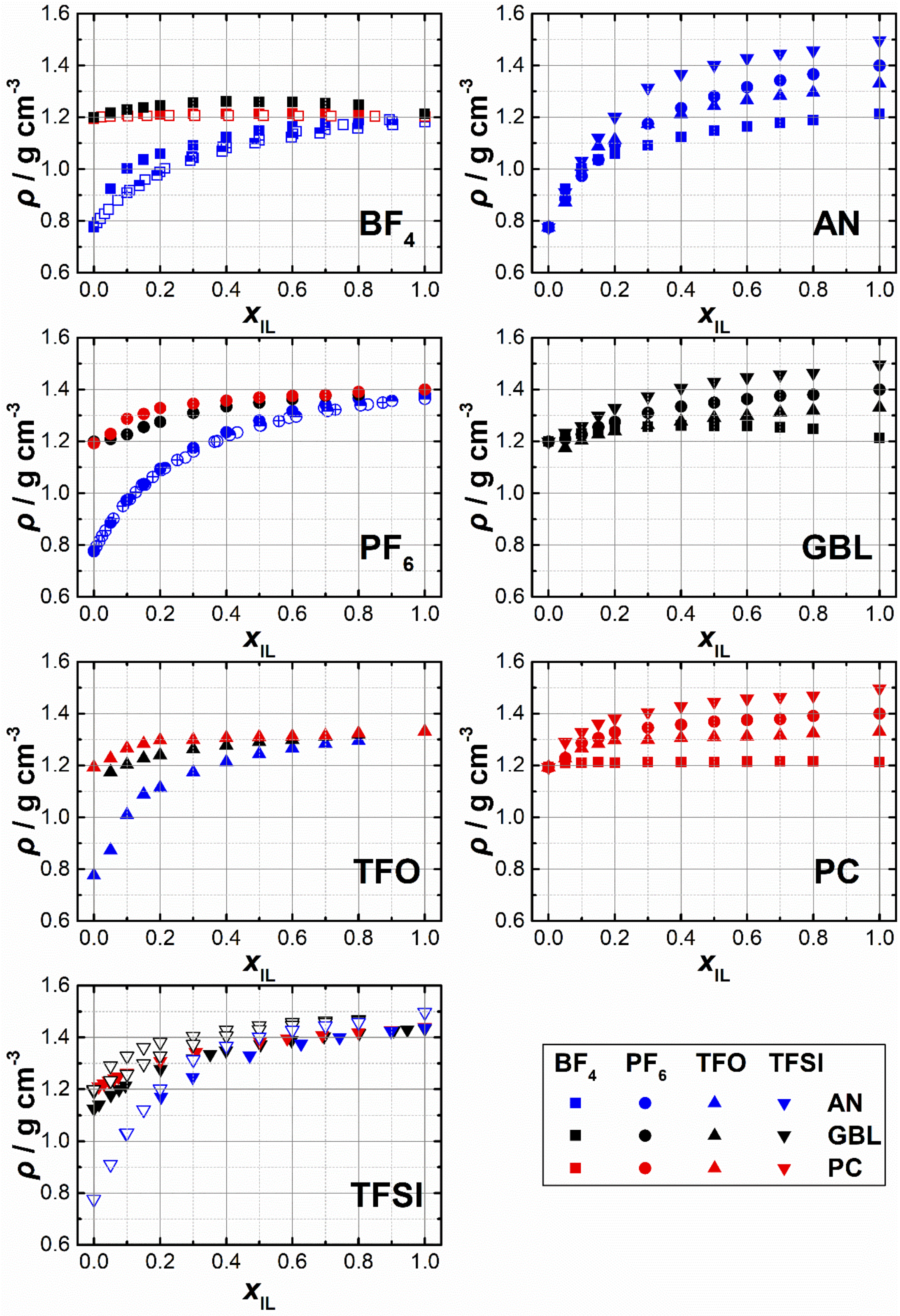

Figure 2.7. Densities calculated for pure ILs and molecular solvents and their mixtures compositions (*solid symbols*) in comparison with experimental measurements (*empty symbols*).

through a maximum at x_{IL} ~ 0.30. With further addition of solvent, the density of the binary mixture gradually decreases. The calculated densities of the mixtures of ILs with GBL and PC are characterized by the minor difference with experimental values, however due to the small spread of the experimental values it is rather difficult to reproduce the same trend, particularly for the binary mixtures with PC.

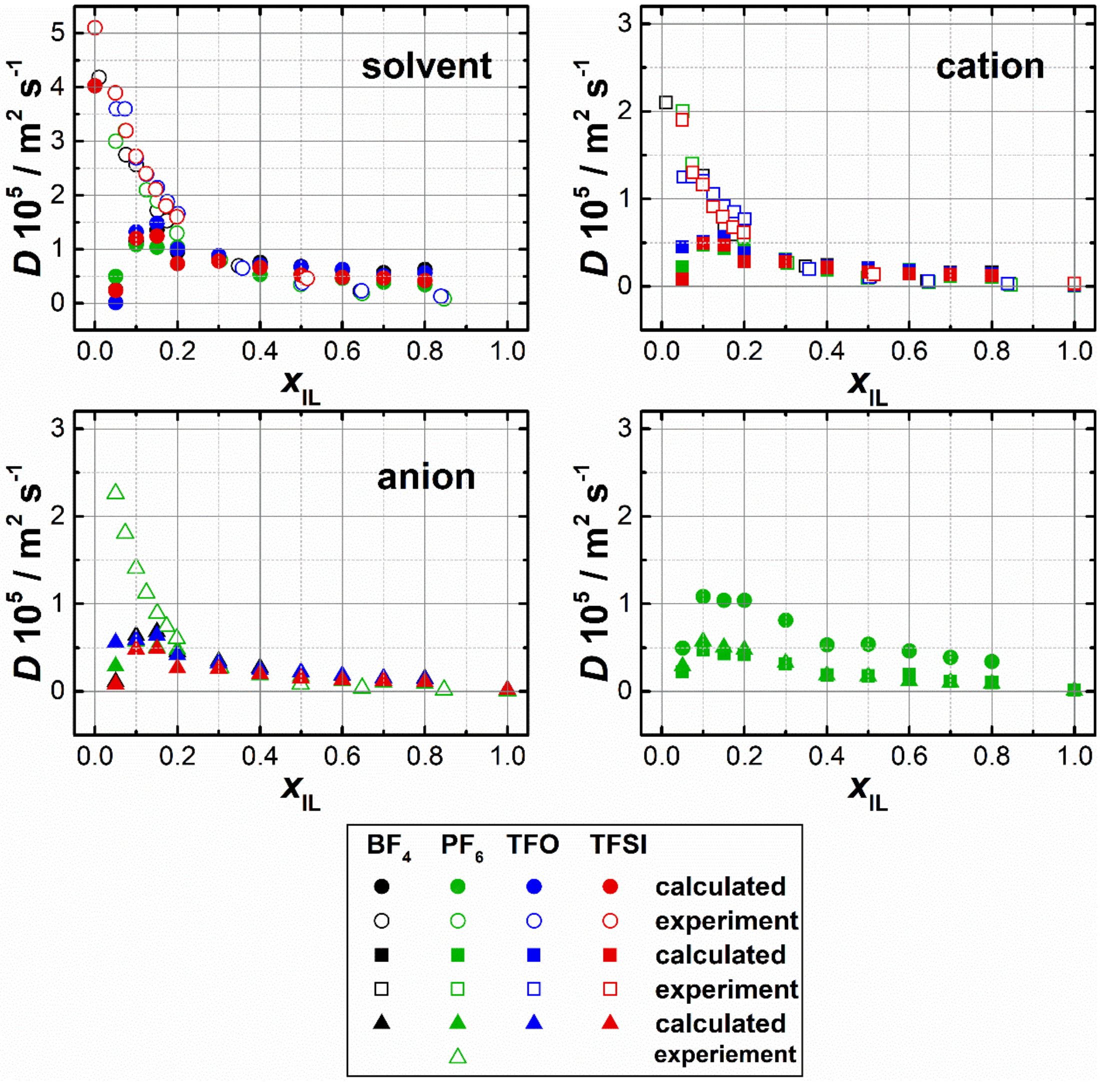

Figure 2.8. Self-diffusion coefficient calculated for pure ILs and AN and their mixtures compositions (*solid symbols*) in comparison with experimental measurements (*empty symbols*).

The results of the calculated self-diffusion coefficients illustrated in Figure 2.8. on the example of IL-AN mixtures. It was found that the solvent molecules diffuse at larger rates than ions in mixtures that well agreed with available experimental measurements. However, it fails to reproduce experimental values at

$x_{\mathrm{IL}} < 0.20$. The respective diffusivities of the cations and anions exponentially increasing with decreasing of x_{IL}, while for the solvent molecules an opposite pattern is observed. The respective diffusivities of the cations and anions exponentially increasing with decreasing of x_{IL}, while for the solvent molecules an opposite pattern observed. At the concentration range of $x_{\mathrm{IL}} > 0.30$, similar to the behavior of density of the ILs-solvent mixtures, the diffusion of ions are relatively stable. However, with further decreasing of x_{IL} it increasing steeply. In this case the cation diffuse faster compared with anion in the whole composition range. The increase of diffusion is most pronounced in AN environment, less significant in GBL and negligible in PC. This may attributed to the rather strong cation solvation in GBL and PC over entire range of compositions.

2.5. Local structure analysis of IL-solvent mixtures

2.5.1 Spatial distribution function

By definition spatial distribution functions (SDFs) depict the three-dimensional density distribution of the studied particle or site at a certain position in space around a fixed reference system of other particles/sites. For setting up a reference frame, three atoms (which must not be located in one line) within the reference molecule have to be chosen: the first one is placed in the origin, the second atom is located on the positive X axis, and the third atom is put into the X–Y plane (with positive Y value) of the reference frame. Every instance of the reference molecule in every time step is transformed into this orientation, which enables averaging of probabilities in the space around the reference molecule. This is only one possibility of setting up a reference frame from 3 points, but as the first reference atom is placed in the center of the frame, this enables direct control over the SDF center.

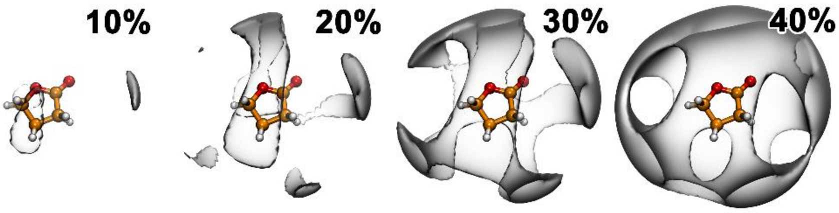

Figure 2.9. Example of spatial distribution function with different extent of the isosurfaces distribution probability of the observed site around the reference molecule.

For the correct presentation it is necessary to reduce the dimensionality to three (or even lower). A common and reasonable method for doing so is to visualize isosurfaces on the data, which can be easily drawn in three-dimensional space. Isosurfaces are surfaces that pass through all areas with the same probability, just like contour lines in topographic maps (but there in one dimension less). In this case it is also necessary to reduce the isosurface area in order to get a physically correct representation of the distribution of the observed site. In most cases, the 30% of the isosurface area is in satisfactory agreement with numerous radial and angular distributions of the systems under study.

2.5.2 Radial distribution function

In order to resolve the radial component of the SDFs the radial distribution function (RDF) may be used. The RDF is an example of a pair correlation function, which describes how, on average, the particles in a system are radially packed around each other. This proves to be a particularly effective way of describing the average structure of disordered molecular systems such as liquids. Another point contributing to the importance of RDFs is the fact that they can not only be computed from simulations but also be calculated from the results of neutron and X-ray diffraction experiments, thus, providing a direct comparison between simulation and experiment. It can also be used in conjunction with the interatomic pair potential function to calculate the internal energy of the system, usually quite accurately.

A RDF provide the probability of finding an observed particle in a certain distance to a reference particle relative to the uniform density of the observed particle. The uniform density is the density one would find if all the observed particles would be uniformly distributed in the simulation cell. RDF values larger than 1 depict that finding an observed particle in this distance to the reference particle is more probable than it should be on average. For large distances, the value of the function should tend toward 1. The RDF determined through the equation, where r_i and r_j denote the position vectors of the i-th and the j-th particle, and δ takes the value 1 in the interval [-w,w) (with w being the bin width), otherwise 0.

$$g_{ab}(r) = \frac{V}{N_a N_b} \sum_{i=1}^{N_a} \sum_{j=i+1}^{N_b} \left\langle \delta\left(r - \left|\vec{r}_i(t) - \vec{r}_j(t)\right|\right) \right\rangle_t \qquad (2.9)$$

The RDF is usually plotted as a function of the interatomic distances r. A typical RDF plot (Figure 2.9) shows a number of important features. Firstly, at short distances the RDF is zero that indicates the effective width of the atoms, since they cannot approach any more closely. Next, a number of peaks and shoulders appear, which indicate that the atoms pack around each other in “shells” (the position of the first minima indicate a border between such shells) of neighbors. The occurrence of peaks at long range indicates a high degree of ordering. At very long range every RDF tends to a value of 1, which happens because the RDF describes the average density at this range.

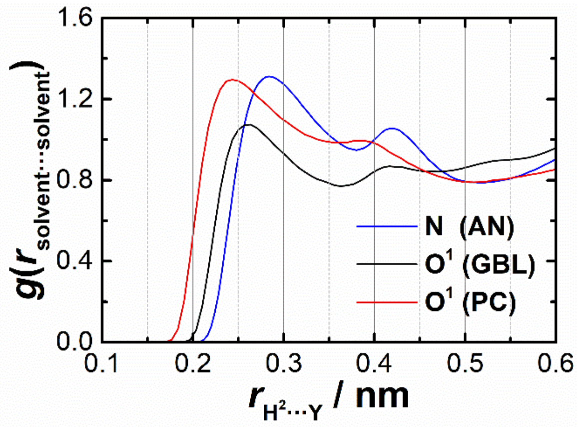

Figure 2.10. Example of the radial distribution function between the reference site H^2 of the one molecule and observed Y of the other.

2.5.3 Angular distribution function

Like RDFs are histograms over a distance development, angular distribution functions (ADFs) are histograms over the development of a certain angle in the system. The term containing sin (α) corrects the uniform angular distribution

$$ADF_{abc}=(\alpha)=\frac{1}{\sin(\alpha)}\frac{1}{N_a N_b N_c}\sum_{i=1}^{N_a}\sum_{j=i+1}^{N_b}\sum_{k=j+1}^{N_c}\left\langle\delta\left(\alpha-\angle\left(\vec{r}_i(t),\vec{r}_j(t),\vec{r}_k(t)\right)\right)\right\rangle_t \quad (2.10)$$

The angle of interest can be defined by specifying two vectors, which may be defined by two points. The base points of the defined vectors may be different, which offers additional flexibility. The points defining the vectors do not necessarily have to be part of the same molecule.

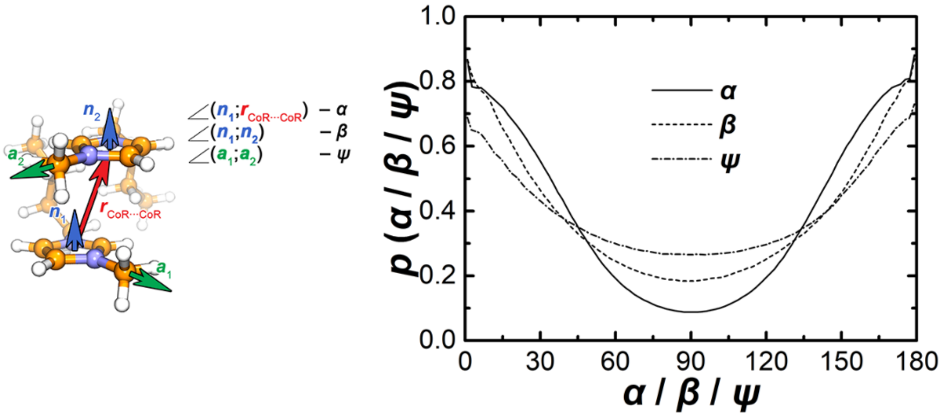

Figure 2.11. Example of angular distribution functions between two C_4mim^+ cations: angle α formed by the normal vector, n_1, of the reference molecule and distance vector, $r_{\mathrm{CoR}\cdots\mathrm{CoR}}$, between the reference and observed C_4mim^+; angle β formed by the two normal vectors, n_1 and n_2 of the reference and observed C_4mim^+; angle ψ formed by the two vectors, a_1 and a_2, along CH_3 group of the reference and observed C_4mim^+.

2.5.4 Combined distribution function

It is also possible to combine several functions, as RDFs and/or ADFs, in order to create histograms of higher dimensionality, which are called combined distribution functions (CDFs). Each different analysis delivering scalar raw data to the CDF is called a channel of the CDF. Because every channel can be chosen to be one out of five two-dimensional analyses, and every of these analyses can be defined in a variety of ways. Since the high-dimensional histograms are hard to handle and to visualize, we will only discuss two-channel CDFs here, resulting in two-dimensional histograms

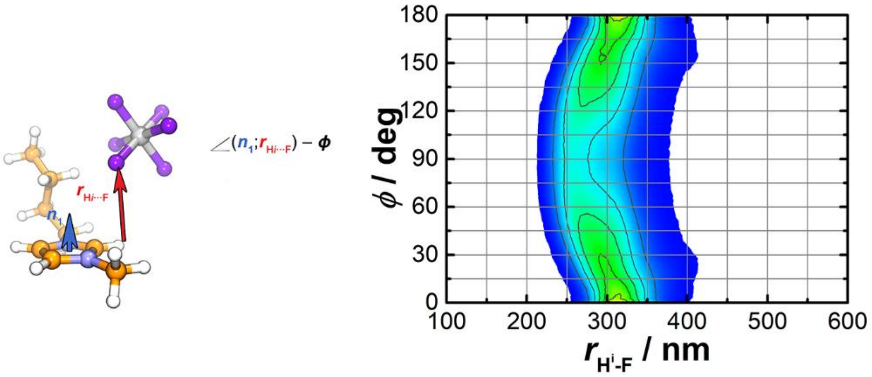

Figure 2.12. Example of combined distribution function containing ADF formed by the normal vector of the reference C_4mim^+ and distance vector between the reference C_4mim^+ and observed PF_6^-, and RDF between the C_4mim^+ and PF_6^-.

2.5.5 Nearest neighbors approach

An additional insight into the local structure may be achieved by using the nearest neighbors approach. According to this approach the neighbors of a central atom are sorted by the distance criterion into the first neighbor, second neighbor etc. Averaging over the ensemble and simulation time separate RDFs may be defined for each set of nearest neighbor atoms *b* (indicated by *n*), and at distance *r* from the central atom *a*. From these distributions the average distance $\langle r_{a\cdots b}(n)\rangle$ between a reference atom *a* and an atom *b* belonging to the *n*-th neighbor class $p_{a\cdots b}(n,r)$ could be calculated, as well as the corresponding standard deviation $\Delta r_{a\cdots b}(n)$ which characterizes the width of the distance distribution between the reference and *n*-th atom. These parameters are defined by the following Equations

$$\langle r_{a\cdots b}(n)\rangle = \int_0^\infty dr' r' p_{a\cdots b}(n,r') \qquad (2.11)$$

$$\langle r^2_{a\cdots b}(n)\rangle = \int_0^\infty dr' r^{2'} p_{a\cdots b}(n,r') \qquad (2.12)$$

$$\Delta r_{a\cdots b}(n) = \left(\langle r^2_{a\cdots b}\rangle - \langle r_{a\cdots b}\rangle^2\right)^{\frac{1}{2}} \qquad (2.13)$$

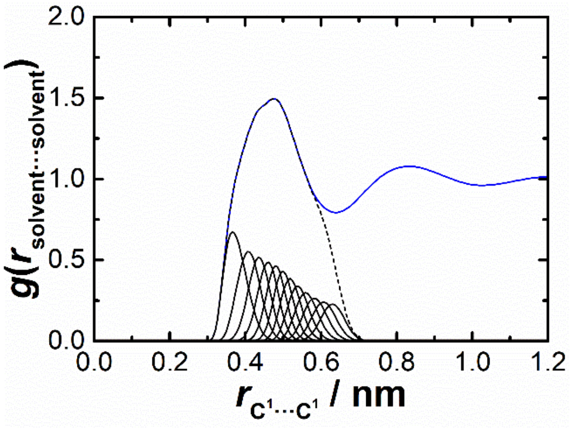

Figure 2.13. Example of the radial distribution function, $g(r)$, (*blue line*), the nearest neighbors radial distributions, $p_{a \cdots b}(n,r)$, for n = 1-12 and the sum of n = 1-12 neighbors, $\sum_{i=1}^{12} p(n,r)$, (*dashed line*) between C^1 of the reference AN molecule and its n nearest neighbors.

2.6. Reference for Chapter 2

(1) Canongia Lopes, J. N.; Deschamps, J.; Pádua, A. A. H. Modeling Ionic Liquids Using a Systematic All-Atom Force Field. *J. Phys. Chem. B* **2004**, *108*, 2038-2047.

(2) Kelkar, M. S.; Maginn, E. J. Effect of Temperature and Water Content on the Shear Viscosity of the Ionic Liquid 1-Ethyl-3-methylimidazolium Bis(trifluoromethanesulfonyl)imide As Studied by Atomistic Simulations. *J. Phys. Chem. B* **2007**, *111*, 4867-4876.

(3) Kelkar, M. S.; Maginn, E. J. Calculating the Enthalpy of Vaporization for Ionic Liquid Clusters. *J. Phys. Chem. B* **2007**, *111*, 9424-9427.

(4) Maginn, E. J. Atomistic Simulation of the Thermodynamic and Transport Properties of Ionic Liquids. *Acc. Chem. Res.* **2007**, *40*, 1200-1207.

(5) Jayaraman, S.; Maginn, E. J. Computing the melting point and thermodynamic stability of the orthorhombic and monoclinic crystalline polymorphs of the ionic liquid 1-n-butyl-3-methylimidazolium chloride. *J. Chem. Phys.* **2007**, *127*, 214504.

(6) Borodin, O. Polarizable Force Field Development and Molecular Dynamics Simulations of Ionic Liquids. *J. Phys. Chem. B* **2009**, *113*, 11463-11478.

(7) McDaniel, J. G.; Choi, E.; Son, C. Y.; Schmidt, J. R.; Yethiraj, A. Ab Initio Force Fields for Imidazolium-Based Ionic Liquids. *J. Phys. Chem. B* **2016**, *120*, 7024-7036.

(8) Yan, T.; Burnham, C. J.; Del Pópolo, M. G.; Voth, G. A. Molecular Dynamics Simulation of Ionic Liquids: The Effect of Electronic Polarizability. *J. Phys. Chem. B* **2004**, *108*, 11877-11881.

(9) Bhargava, B. L.; Balasubramanian, S. Refined potential model for atomistic simulations of ionic liquid [bmim][PF6]. *J. Chem. Phys.* **2007**, *127*, 114510.

(10) Mondal, A.; Balasubramanian, S. Quantitative Prediction of Physical Properties of Imidazolium Based Room Temperature Ionic Liquids through Determination of Condensed Phase Site Charges: A Refined Force Field. *J. Phys. Chem. B* **2014**, *118*, 3409-3422.

(11) Mondal, A.; Balasubramanian, S. A Refined All-Atom Potential for Imidazolium-Based Room Temperature Ionic Liquids: Acetate, Dicyanamide, and Thiocyanate Anions. *J. Phys. Chem. B* **2015**, *119*, 11041-11051.

(12) Köddermann, T.; Paschek, D.; Ludwig, R. Molecular Dynamic Simulations of Ionic Liquids: A Reliable Description of Structure, Thermodynamics and Dynamics. *ChemPhysChem* **2007**, *8*, 2464-2470.

(13) Böhm, H. J.; McDonald, I. R.; Madden, P. A. An effective pair potential for liquid acetonitrile. *Mol. Phys.* **1983**, *49*, 347-360.

(14) Böhm, H. J.; Lynden-Bell, R. M.; Madden, P. A.; McDonald, I. R. Molecular motion in a model of liquid acetonitrile. *Mol. Phys.* **1984**, *51*, 761-777.

(15) Siebers, J. G.; Buck, U.; Beu, T. A. Calculation of structures and vibrational spectra of acetonitrile clusters. *Chem. Phys.* **1998**, *239*, 549-560.

(16) Cabaleiro-Lago, E. M.; RÍOs, M. A. Intermolecular potential for acetonitrile based on ab initio calculations. *Mol. Phys.* **1999**, *96*, 309-321.

(17) Grabuleda, X.; Jaime, C.; Kollman, P. A. Molecular dynamics simulation studies of liquid acetonitrile: New six-site model. *J. Comput. Chem.* **2000**, *21*, 901-908.

(18) Nikitin, A. M.; Lyubartsev, A. P. New six-site acetonitrile model for simulations of liquid acetonitrile and its aqueous mixtures. *J. Comput. Chem.* **2007**, *28*, 2020-2026.

(19) Albertí, M.; Amat, A.; De Angelis, F.; Pirani, F. A Model Potential for Acetonitrile: from Small Clusters to Liquid. *J. Phys. Chem. B* **2013**, *117*, 7065-7076.

(20) Orhan, M. Dielectric and Transport Properties of Acetonitrile at Varying Temperatures: a Molecular Dynamics Study. *Bull. Korean Chem. Soc.* **2014**, *35*, 1469-1478.

(21) Price, M. L. P.; Ostrovsky, D.; Jorgensen, W. L. Gas-phase and liquid-state properties of esters, nitriles, and nitro compounds with the OPLS-AA force field. *J. Comput. Chem.* **2001**, *22*, 1340-1352.

(22) Oldiges, C.; Wittler, K.; Tönsing, T.; Alijah, A. MD Calculated Structural Properties of Clusters in Liquid Acetonitrile/Water Mixtures with Various Contents of Acetonitrile. *J. Phys. Chem. A* **2002**, *106*, 7147-7154.

(23) Edwards, D. M. F.; Madden, P. A. A computer simulation study of the dielectric properties of a model of methyl cyanide. *Mol. Phys.* **1984**, *51*, 1163-1179.

(24) Jorgensen, W. L.; Briggs, J. M. Monte Carlo simulations of liquid acetonitrile with a three-site model. *Mol. Phys.* **1988**, *63*, 547-558.

(25) Guàrdia, E.; Pinzón, R.; Casulleras, J.; Orozco, M.; Luque, F. J. Comparison of Different Three-site Interaction Potentials for Liquid Acetonitrile. *Mol. Simul.* **2001**, *26*, 287-306.

(26) Hirata, Y. Molecular Dynamics Simulation Study of the Rotational and Translational Motions of Liquid Acetonitrile†. *J. Phys. Chem. A* **2002**, *106*, 2187-2191.

(27) Houndonougbo, Y.; Laird, B. B.; Kuczera, K. Transport properties of CO2-expanded acetonitrile from molecular dynamics simulations. *J. Chem. Phys.* **2007**, *126*, 074507.

(28) Deublein, S.; Metzler, P.; Vrabec, J.; Hasse, H. Automated development of force fields for the calculation of thermodynamic properties: acetonitrile as a case study. *Mol. Simul.* **2013**, *39*, 109-118.

(29) Alvarez, H. A.; Suster, C. L.; McCarthy, A. N. Consistent Acetonitrile Molecular Models for both Standart and Computationally Efficient Molecular Dynamics Studies. *Asian J. Comp. Inform. Syst.* **2014**, *2*, 49-62.

(30) Wu, X.; Liu, Z.; Huang, S.; Wang, W. Molecular dynamics simulation of room-temperature ionic liquid mixture of [bmim][BF4] and acetonitrile by a refined force field. *PCCP* **2005**, *7*, 2771-2779.

(31) Mayo, S. L.; Olafson, B. D.; Goddard, W. A. DREIDING: a generic force field for molecular simulations. *The Journal of Physical Chemistry* **1990**, *94*, 8897-8909.

(32) Hess, B.; Kutzner, C.; van der Spoel, D.; Lindahl, E. GROMACS 4: Algorithms for Highly Efficient, Load-Balanced, and Scalable Molecular Simulation. *Journal of Chemical Theory and Computation* **2008**, *4*, 435-447.

(33) Martínez, L.; Andrade, R.; Birgin, E. G.; Martínez, J. M. PACKMOL: A package for building initial configurations for molecular dynamics simulations. *J. Comput. Chem.* **2009**, *30*, 2157-2164.

(34) Brehm, M.; Kirchner, B. TRAVIS - A Free Analyzer and Visualizer for Monte Carlo and Molecular Dynamics Trajectories. *Journal of Chemical Information and Modeling* **2011**, *51*, 2007-2023.

(35) Frisch, M. J.; Trucks, G. W.; Schlegel, H. B.; Scuseria, G. E.; Robb, M. A.; Cheeseman, J. R.; Scalmani, G.; Barone, V.; Mennucci, B.; Petersson, G. A.; Nakatsuji, H.; Caricato, M.; Li, X.; Hratchian, H. P.; Izmaylov, A. F.; Bloino, J.; Zheng, G.; Sonnenberg, J. L.; Hada, M.; Ehara, M.; Toyota, K.; Fukuda, R.; Hasegawa, J.; Ishida, M.; Nakajima, T.; Honda, Y.; Kitao, O.; Nakai, H.; Vreven, T.; Montgomery Jr., J. A.; Peralta, J. E.; Ogliaro, F.; Bearpark, M. J.; Heyd, J.; Brothers, E. N.; Kudin, K. N.; Staroverov, V. N.; Kobayashi, R.; Normand, J.; Raghavachari, K.; Rendell, A. P.; Burant, J. C.; Iyengar, S. S.; Tomasi, J.; Cossi, M.; Rega, N.; Millam, N. J.; Klene, M.; Knox, J. E.; Cross, J. B.; Bakken, V.; Adamo, C.; Jaramillo, J.; Gomperts, R.; Stratmann, R. E.; Yazyev, O.; Austin, A. J.; Cammi, R.; Pomelli, C.; Ochterski, J. W.; Martin, R. L.; Morokuma, K.; Zakrzewski, V. G.; Voth, G. A.; Salvador, P.; Dannenberg, J. J.; Dapprich, S.; Daniels, A. D.; Farkas, Ö.; Foresman, J. B.; Ortiz, J. V.; Cioslowski, J.; Fox, D. J.: Gaussian 09. Gaussian, Inc.: Wallingford, CT, USA, 2009.

(36) Møller, C.; Plesset, M. S. Note on an Approximation Treatment for Many-Electron Systems. *Phys. Rev.* **1934**, *46*, 618-622.

(37) Zhao, Y.; Truhlar, D. G. The M06 suite of density functionals for main group thermochemistry, thermochemical kinetics, noncovalent interactions, excited states, and transition elements: two new functionals and systematic testing of four M06-class functionals and 12 other functionals. *Theor. Chem. Acc.* **2008**, *120*, 215-241.

(38) Alía, J. M.; Edwards, H. G. M. Vibrational Spectroscopic Properties of Hydrogen Bonded Acetonitrile Studied by DFT. *J. Phys. Chem. A* **2005**, *109*, 7977-7987.

(39) Korsun, O. M.; Kalugin, O. M. Quantum chemical modelling of acetonitrile within pseudo-potential and all-electron approaches. *Kh. Univ. Bull.* **2010**, *932*, 150-159.

(40) Bertagnolli, H.; Chieux, P.; Zeidler, M. D. A neutron-diffraction study of liquid acetonitrile. *Mol. Phys.* **1976**, *32*, 1731-1736.

(41) Alston Steiner, P.; Gordy, W. Precision measurement of dipole moments and other spectral constants of normal and deuterated methyl fluoride and methyl cyanide. *J. Mol. Spectrosc.* **1966**, *21*, 291-301.

(42) Costain, C. C. Determination of Molecular Structures from Ground State Rotational Constants. *J. Chem. Phys.* **1958**, *29*, 864-874.

(43) Shimanouchi, T. Tables of molecular vibrational frequencies. Consolidated volume II. *J. Phys. Chem. Ref. Data* **1977**, *6*, 993-1102.

(44) Caleman, C.; van Maaren, P. J.; Hong, M.; Hub, J. S.; Costa, L. T.; van der Spoel, D. Force Field Benchmark of Organic Liquids: Density, Enthalpy of Vaporization, Heat Capacities, Surface Tension, Isothermal Compressibility, Volumetric Expansion Coefficient, and Dielectric Constant. *Journal of Chemical Theory and Computation* **2012**, *8*, 61-74.

(45) Cataliotti, R. S.; Sassi, P.; Morresi, A.; Paliani, G. Mandelstam–Brillouin spectra and hyperacoustic velocities dispersion of trideuteroacetonitrile in the liquid state. *Chemical Physics* **2000**, *255*, 85-93.

(46) Wieser, M. E.; Holden, N.; Coplen, T. B.; Böhlke, J. K.; Berglund, M.; Brand, W. A.; De Bièvre, P.; Gröning, M.; Loss, R. D.; Meija, J.; Hirata, T.; Prohaska, T.; Schoenberg, R.; O'Connor, G.; Walczyk, T.; Yoneda, S.; Zhu, X.-K. Atomic weights of the elements 2011 (IUPAC Technical Report). *Pure and Applied Chemistry* **2013**, *85*, 1047-1078.

(47) Audi, G.; Wapstra, A. H.; Thibault, C. The Ame2003 atomic mass evaluation: (II). Tables, graphs and references. *Nuclear Physics A* **2003**, *729*, 337-676.

(48) CPMD. http://www.cpmd.org/ Copyright IBM Corp 1990-2008, Copyright MPI für Festkörperforschung Stuttgart 1997-2001).

(49) Andreoni, W.; Curioni, A. New advances in chemistry and materials science with CPMD and parallel computing. *Parallel Computing* **2000**, *26*, 819-842.

(50) Becke, A. D. Density-functional exchange-energy approximation with correct asymptotic behavior. *Physical Review A* **1988**, *38*, 3098-3100.

(51) Lee, C.; Yang, W.; Parr, R. G. Development of the Colle-Salvetti correlation-energy formula into a functional of the electron density. *Physical Review B* **1988**, *37*, 785-789.

(52) Troullier, N.; Martins, J. L. Efficient pseudopotentials for plane-wave calculations. *Physical Review B* **1991**, *43*, 1993-2006.

(53) Korsun, O. M.; Kalugin, O. N.; Prezhdo, O. V. Control of Carbon Nanotube Electronic Properties by Lithium Cation Intercalation. *The Journal of Physical Chemistry Letters* **2014**, *5*, 4129-4133.

(54) Korsun, O. M.; Kalugin, O. N. Ab initio molecular dynamics simulation of the first solvent shell of the Li+ in acetonitrile. *Kharkiv University Bulletin* **2010**, *895*, 31-38.

(55) Korsun, O. M.; Kalugin, O. N.; Vasenko, A. S.; Prezhdo, O. V. Electronic Properties of Carbon Nanotubes Intercalated with Li+ and Mg2+: Effects of Ion Charge and Ion Solvation. *The Journal of Physical Chemistry C* **2016**, *120*, 26514-26521.

(56) Grimme, S. Semiempirical GGA-type density functional constructed with a long-range dispersion correction. *Journal of Computational Chemistry* **2006**, *27*, 1787-1799.

(57) Nosé, S. A molecular dynamics method for simulations in the canonical ensemble. *Molecular Physics* **1984**, *52*, 255-268.

(58) Hoover, W. G. Canonical dynamics: Equilibrium phase-space distributions. *Physical Review A* **1985**, *31*, 1695-1697.

(59) Cho, H.-G. Solvation of GaCl3 in deuterated acetonitrile studied by means of vibrational spectroscopy. *Spectrochimica Acta Part A: Molecular and Biomolecular Spectroscopy* **2003**, *59*, 1517-1528.

(60) Singh, U. C.; Kollman, P. A. An approach to computing electrostatic charges for molecules. *Journal of Computational Chemistry* **1984**, *5*, 129-145.

(61) Palmer, B. J. Transverse-current autocorrelation-function calculations of the shear viscosity for molecular liquids. *Phys. Rev. E* **1994**, *49*, 359-366.

(62) Hess, B. Determining the shear viscosity of model liquids from molecular dynamics simulations. *J. Chem. Phys.* **2002**, *116*, 209-217.

(63) Vanommeslaeghe, K.; Hatcher, E.; Acharya, C.; Kundu, S.; Zhong, S.; Shim, J.; Darian, E.; Guvench, O.; Lopes, P.; Vorobyov, I.; Mackerell, A. D. CHARMM general force field: A force field for drug-like molecules compatible with the CHARMM all-atom additive biological force fields. *J. Comput. Chem.* **2010**, *31*, 671-690.

(64) van Meurs, N.; Somsen, G. Excess and apparent molar volumes of mixtures of water and acetonitrile between 0 and 25°C. *J. Solution Chem.* **1993**, *22*, 427-436.

(65) Grande, M. d. C.; Bianchi, H. L.; Marschoff, C. M. On the density of pure acetonitrile. *An. Asoc. Quim. Argent.* **2004**, *92*, 109-114.

(66) Grant-Taylor, D. F.; Macdonald, D. D. Thermal pressure and energy–volume coefficients for the acetonitrile + water system. *Can. J. Chem.* **1976**, *54*, 2813-2819.

(67) Howard, P. B.; Wadsö, I. Enthalpies of Vaporization of Organic Compounds. IV. Alkyl Nitriles. *Acta Chem. Scand.* **1970**, *24*, 145-149.

(68) An, X.-W.; Månsson, M. Enthalpies of combustion and formation of acetonitrile. *The Journal of Chemical Thermodynamics* **1983**, *15*, 287-293.

(69) Baldt, J. H.; Hall, H. K. K. Thermochemistry of strained-ring bridgehead nitriles and esters. *J. Am. Chem. Soc.* **1971**, *93*, 140-145.

(70) Kovacs, H.; Kowalewski, J.; Maliniak, A.; Stilbs, P. Multinuclear relaxation and NMR self-diffusion study of the molecular dynamics in acetonitrile-chloroform liquid mixtures. *The journal of physical chemistry* **1989**, *93*, 962-969.

(71) Hurle, R. L.; Woolf, L. A. Self-diffusion in liquid acetonitrile under pressure. *Journal of the Chemical Society, Faraday Transactions 1: Physical Chemistry in Condensed Phases* **1982**, *78*, 2233-2238.

(72) Holz, M.; Mao, X. a.; Seiferling, D.; Sacco, A. Experimental study of dynamic isotope effects in molecular liquids: Detection of translation-rotation coupling. *The Journal of Chemical Physics* **1996**, *104*, 669-679.

(73) Hawlicka, E.; Grabowski, R. Solvation of Ions in Acetonitrile-Methanol Solutions of Sodium Iodide. *Berichte der Bunsengesellschaft für physikalische Chemie* **1990**, *94*, 486-489.

(74) Liang, M.; Zhang, X. X.; Kaintz, A.; Ernsting, N. P.; Maroncelli, M. Solvation dynamics in a prototypical ionic liquid + dipolar aprotic liquid mixture: 1-butyl-3-methylimidazolium tetrafluoroborate + acetonitrile. *The journal of physical chemistry. B* **2014**, *118*, 1340-1352.

(75) Marekha, B. A.; Kalugin, O. N.; Bria, M.; Buchner, R.; Idrissi, A. Translational diffusion in mixtures of imidazolium ILs with polar aprotic molecular solvents. *The journal of physical chemistry. B* **2014**, *118*, 5509-5517.

(76) Shekaari, H.; Zafarani-Moattar, M. T.; Mirheydari, S. N. Density, Viscosity, Speed of Sound, and Refractive Index of a Ternary Solution of Aspirin, 1-Butyl-3-methylimidazolium Bromide, and Acetonitrile at Different TemperaturesT= (288.15 to 318.15) K. *Journal of Chemical & Engineering Data* **2015**, *60*, 1572-1583.

(77) Saha, N.; Das, B. Viscosities of Some Symmetrical Tetraalkylammonium Salts in Acetonitrile at (288.15, 298.15, 308.15, and 318.15) K. *J Chem Eng Data* **2000**, *45*, 1125-1128.

(78) Dymond, J. H.; Awan, M. A.; Glen, N. F.; Isdale, J. D. Transport properties of nonelectrolyte mixtures. IX. Viscosity coefficients for acetonitrile and for three mixtures of toluene+acetonitrile from 25 to 100°c at pressures up to 500 MPa. *Int J Thermophys* **1991**, *12*, 433-447.

(79) Tokuda, H.; Tsuzuki, S.; Susan, M. A. B. H.; Hayamizu, K.; Watanabe, M. How Ionic Are Room-Temperature Ionic Liquids? An Indicator of the Physicochemical Properties. *J. Phys. Chem. B* **2006**, *110*, 19593-19600.

(80) Xu, W.-G.; Li, L.; Ma, X.-X.; Wei, J.; Duan, W.-B.; Guan, W.; Yang, J.-Z. Density, Surface Tension, and Refractive Index of Ionic Liquids Homologue of 1-Alkyl-3-methylimidazolium Tetrafluoroborate [Cnmim][BF4] (n = 2,3,4,5,6). *J. Chem. Eng. Data* **2012**, *57*, 2177-2184.

(81) Deyko, A.; Hessey, S. G.; Licence, P.; Chernikova, E. A.; Krasovskiy, V. G.; Kustov, L. M.; Jones, R. G. The enthalpies of vaporisation of ionic liquids: new measurements and predictions. *PCCP* **2012**, *14*, 3181-3193.

(82) Deyko, A.; Lovelock, K. R. J.; Corfield, J.-A.; Taylor, A. W.; Gooden, P. N.; Villar-Garcia, I. J.; Licence, P.; Jones, R. G.; Krasovskiy, V. G.; Chernikova, E. A.; Kustov, L. M. Measuring and predicting [capital Delta]vapH298 values of ionic liquids. *PCCP* **2009**, *11*, 8544-8555.

(83) Zaitsau, D. H.; Kabo, G. J.; Strechan, A. A.; Paulechka, Y. U.; Tschersich, A.; Verevkin, S. P.; Heintz, A. Experimental Vapor Pressures of 1-Alkyl-3-methylimidazolium Bis(trifluoromethylsulfonyl)imides and a Correlation Scheme for Estimation of Vaporization Enthalpies of Ionic Liquids. *J. Phys. Chem. A* **2006**, *110*, 7303-7306.

(84) Marekha, B. A.; Kalugin, O. N.; Bria, M.; Buchner, R.; Idrissi, A. Translational Diffusion in Mixtures of Imidazolium ILs with Polar Aprotic Molecular Solvents. *J. Phys. Chem. B* **2014**, *118*, 5509-5517.

(85) Tokuda, H.; Hayamizu, K.; Ishii, K.; Susan, M. A. B. H.; Watanabe, M. Physicochemical Properties and Structures of Room Temperature Ionic Liquids. 1. Variation of Anionic Species. *J. Phys. Chem. B* **2004**, *108*, 16593-16600.

(86) Nama, D.; Kumar, P. G. A.; Pregosin, P. S.; Geldbach, T. J.; Dyson, P. J. 1H, 19F-HOESY and PGSE diffusion studies on ionic liquids: The effect of co-solvent on structure. *Inorg. Chim. Acta* **2006**, *359*, 1907-1911.

(87) Jacquemin, J.; Husson, P.; Padua, A. A. H.; Majer, V. Density and viscosity of several pure and water-saturated ionic liquids. *Green Chemistry* **2006**, *8*, 172-180.

(88) Fan, W.; Zhou, Q.; Sun, J.; Zhang, S. Density, Excess Molar Volume, and Viscosity for the Methyl Methacrylate + 1-Butyl-3-methylimidazolium Hexafluorophosphate Ionic Liquid Binary System at Atmospheric Pressure. *J. Chem. Eng. Data* **2009**, *54*, 2307-2311.

(89) Ge, M.-L.; Zhao, R.-S.; Yi, Y.-F.; Zhang, Q.; Wang, L.-S. Densities and Viscosities of 1-Butyl-3-methylimidazolium Trifluoromethanesulfonate + H2O Binary Mixtures at T = (303.15 to 343.15) K. *J. Chem. Eng. Data* **2008**, *53*, 2408-2411.

(90) Seddon, K. R.; Stark, A.; Torres, M.-J.: Viscosity and Density of 1-Alkyl-3-methylimidazolium Ionic Liquids. In *Clean Solvents*; ACS Symposium Series 819; American Chemical Society, 2002; Vol. 819; pp 34-49.

(91) Katsuta, S.; Shiozawa, Y.; Imai, K.; Kudo, Y.; Takeda, Y. Stability of Ion Pairs of Bis(trifluoromethanesulfonyl)amide-Based Ionic Liquids in Dichloromethane. *J. Chem. Eng. Data* **2010**, *55*, 1588-1593.

(92) Masia, M.; Rey, R. Computational Study of γ-Butyrolactone and Li+/γ-butyrolactone in Gas and Liquid Phases. *J. Phys. Chem. B* **2004**, *108*, 17992-18002.

(93) Aparicio, S.; Alcalde, R. Characterization of two lactones in liquid phase: an experimental and computational approach. *PCCP* **2009**, *11*, 6455-6467.

(94) Takeuchi, M.; Kameda, Y.; Umebayashi, Y.; Ogawa, S.; Sonoda, T.; Ishiguro, S.-i.; Fujita, M.; Sano, M. Ion–ion interactions of LiPF6 and LiBF4 in propylene carbonate solutions. *J. Mol. Liq.* **2009**, *148*, 99-108.

(95) You, X.; Chaudhari, M. I.; Rempe, S. B.; Pratt, L. R. Dielectric Relaxation of Ethylene Carbonate and Propylene Carbonate from Molecular Dynamics Simulations. *J. Phys. Chem. B* **2016**, *120*, 1849-1853.

(96) Salomon, M.; Plichta, E. Conductivities and ion association of 1:1 electrolytes in mixed aprotic solvents. *Electrochim. Acta* **1983**, *28*, 1681-1686.

(97) Barthel, J.; Gores, H.-J.; Schmeer, G.; Wachter, R.: Non-aqueous electrolyte solutions in chemistry and modern technology. In *Physical and Inorganic Chemistry*; Springer Berlin Heidelberg: Berlin, Heidelberg, 1983; pp 33-144.

(98) Moumouzias, G.; Ritzoulis, G. Relative Permittivities and Refractive Indices of Propylene Carbonate + Toluene Mixtures from 283.15 K to 313.15 K. *J. Chem. Eng. Data* **1997**, *42*, 710-713.

(99) Xu, K. Nonaqueous Liquid Electrolytes for Lithium-Based Rechargeable Batteries. *Chem. Rev.* **2004**, *104*, 4303-4418.

(100) Barthel, J.; Feuerlein, F. Dielectric properties of propylene carbonate and propylene carbonate solutions. *J. Solution Chem.* **1984**, *13*, 393-417.

(101) Yevstropov, A. A.; Lebedev, B. V.; Kiparisova, Y. G.; Alekseyev, V. A.; Stashina, G. A. Thermodynamic parameters of transformation of γ-butyrolactone into poly-γ-butyrolactone at normal pressure in the range of 0–400°K. *Polymer Science U.S.S.R.* **1980**, *22*, 2685-2692.

(102) Ramkumar, D. H. S.; Kudchadker, A. P. Phase equilibria of water + γ-butyrolactone system. *Fluid Phase Equilib.* **1990**, *55*, 207-215.

(103) Leitão, M. L. P.; Pilcher, G.; Meng-Yan, Y.; Brown, J. M.; Conn, A. D. Enthalpies of combustion of γ-butyrolactone, γ-valerolactone, and δ-valerolactone. *The Journal of Chemical Thermodynamics* **1990**, *22*, 885-891.

(104) Verevkin, S. P.; Toktonov, A. V.; Chernyak, Y.; Schäffner, B.; Börner, A. Vapour pressure and enthalpy of vaporization of cyclic alkylene carbonates. *Fluid Phase Equilib.* **2008**, *268*, 1-6.

(105) Hayamizu, K.; Aihara, Y.; Arai, S.; Martinez, C. G. Pulse-Gradient Spin-Echo 1H, 7Li, and 19F NMR Diffusion and Ionic Conductivity Measurements of 14 Organic Electrolytes Containing LiN(SO2CF3)2. *J. Phys. Chem. B* **1999**, *103*, 519-524.

(106) Kondo, K.; Sano, M.; Hiwara, A.; Omi, T.; Fujita, M.; Kuwae, A.; Iida, M.; Mogi, K.; Yokoyama, H. Conductivity and Solvation of Li+ Ions of LiPF6 in Propylene Carbonate Solutions. *J. Phys. Chem. B* **2000**, *104*, 5040-5044.

(107) Tsunekawa, H.; Narumi, A.; Sano, M.; Hiwara, A.; Fujita, M.; Yokoyama, H. Solvation and Ion Association Studies of LiBF4−Propylenecarbonate and LiBF4−Propylenecarbonate−Trimethyl Phosphate Solutions. *J. Phys. Chem. B* **2003**, *107*, 10962-10966.

(108) Aihara, Y.; Sugimoto, K.; Price, W. S.; Hayamizu, K. Ionic conduction and self-diffusion near infinitesimal concentration in lithium salt-organic solvent electrolytes. *J. Chem. Phys.* **2000**, *113*, 1981-1991.

(109) Ue, M. Mobility and Ionic Association of Lithium and Quaternary Ammonium Salts in Propylene Carbonate and γ-Butyrolactone. *J. Electrochem. Soc.* **1994**, *141*, 3336-3342.

(110) Srivastava, A. K.; Shankar, S. L. Ionic Conductivity in Binary Solvent Mixtures. 3. Dimethyl Sulfoxide + Propylene Carbonate at 25 °C. *J. Chem. Eng. Data* **1998**, *43*, 25-28.

(111) Barthel, J.; Utz, M.; Groß, K.; Gores, H. J. Temperature and composition dependence of viscosity I. Propylene carbonate-dimethoxyethane mixtures and thermodynamics of fluid flow. *J. Solution Chem.* **1995**, *24*, 1109-1123.

(112) Ue, M. Conductivities and ion association of quaternary ammonium tetrafluoroborates in propylene carbonate. *Electrochim. Acta* **1994**, *39*, 2083-2087.

(113) McDonagh, P. M.; Reardon, J. F. Ionic association and mobility. III. Ionophores in propylene carbonate at 25°C. *J. Solution Chem.* **1996**, *25*, 607-614.

Chapter 3. Local structure in terms of nearest neighbor approach in imidazolium-based ILs

The material presented in this chapter forms the basis of publication

Marekha, B. A.; Koverga, V. A.; Chesneau, E.; Kalugin, O. N.; Takamuku, T.; Jedlovszky, P.; Idrissi, A. Local structure in terms of nearest-neighbor approach in 1-butyl-3-methylimidazolium-based ionic liquids: MD simulation. **J. Phys. Chem. B** 2017, 120 (22), 5029-5041.

Local microscopic structure of the nearest neighboring ions in ionic liquids (ILs) is the key prerequisite in obtaining a comprehensive understanding of the influence of the nature of ions on the properties of ILs. We employed classical molecular dynamics (MD) simulations to study in detail the spatial, radial, and orientational relative distribution of ions in a set of imidazolium ILs based on 1-butyl-3-methylimidazolium (C_4mim^+) cation coupled with acetate tetrafluoroborate (BF_4^-), hexafluorophosphate (PF_6^-), trifluoromethanesulfonate (TFO^-), and bis(trifluoromethanesulfonyl)amide ($TFSI^-$). The main interaction patterns such as cation-anion H-bonding, cation-cation alkyl tail aggregation and ring stacking were considered within the framework of the nearest neighbor approach with respect to each particular interaction site.

It was established that several structural properties are strongly anion-specific while as some can be treated as universally applicable to ILs regardless of the nature of anion. All the anions are tend to occupy positions above/below the plane. Similarly, the H-bond at the H^2 site is particularly enhanced in comparison with the ones at $H^{4/5}$ in the case of asymmetric and/or more basic anions (C_4mimTFO, and C_4mimTFSI) which is accordance with recent spectroscopic and theoretical findings. Other IL-specific details related to the multiple H-bonding and cation stacking issues are also discussed in the paper. The secondary H-bonding of anions with the alkyl hydrogen atoms of cations as well as the cation-cation alkyl chain aggregation turned out to be poorly sensitive to the nature of the anion.

3.1. Introduction

Despite an unprecedentedly detailed description of various structural and dynamical properties that can be accessible from molecular simulations very often the analysis is only based on the radial distribution functions (RDFs) between centers of mass.[1-5] Moreover, many seminal computational studies on ILs have been performed on a single IL or a rather narrow family of systems, *e.g.* chlorides for the sake of computational efficiency, while the results have been presented as universally applicable.[6-8] However, such claims can turn out to be questionable.

Thus, in ILs bearing 1-alkyl-3-methlylimidazolium (C_4mim^+) it is commonly accepted that C-H^2 is the main H-bond donoring site of cation[9-12] and H-bonding at the rear of the imidazolium ring, *i.e.* at H^{4-5}, is often dropped out of discussion. However, as it has been recently highlighted by us for a set of neat C_4mim^+-based ILs and in mixtures with acetonitrile[13,14] and for binary mixtures within a similar set of neat ILs by Matthews *et al.*[5] the relative strength of H-bonding at H^2 and H^{4-5} sites is remarkably anion-dependent.

Another prominent example concerns the potential energy surface describing the position of anion in the vicinity of C_nmim^+ cations. On the basis of model quantum-chemical calculations and molecular dynamics (MD) simulations of C_nmimCl Zahn *et al.* proposed a paradigm of energy landscape relating the mobility of anions with melting points decrease.[15] However, as we shall shown later in this Chapter, the mentioned potential energy profile is strikingly different between ILs bearing Cl^- anion and multiatomic anions with delocalized charge distribution like BF_4^-.[14]

All this highlights the need for detailed and systematic studies of ILs by means of molecular simulations. The former refers to the atomic-level description of the local structure around particularly relevant interaction sites whereas the latter implies a thoughtful selection of systems to be studied so that the eventual conclusions could be of use for the subsequent design of novel better performing ILs.[8,16-18] Despite the fact that even the crudest MD force-fields describe the bulk thermodynamic properties of ILs relatively well[19] it is the description of the local microscopic structure which is of interest for deciphering some spectroscopic findings[13,20-22] or rationalizing their performance in such applications as catalysis[23] or cellulose dissolution[24].

A great deal of systematic MD studies on imidazolium ILs has been devoted to the issue of the alkyl chain length in $C_n mim^+$ cations as this has direct implication on the microscopic heterogeneity, *i.e.* segregation of non-polar alkyl and polar ionic domains.[8,25-28] Regarding the use of molecular simulations in explaining various spectroscopic observations one has to keep in mind that the vast majority of such experimental information reports the local molecular-level environment around specific sites of IL cations, *e.g.* ^1H NMR signals, CH vibrational bands etc.[20,21,29-32] The importance of studying the influence of anion on the microscopic structure around a reference cation is evident in this context.

Several MD works have focused on the influence of anion on the microscopic structure and dynamics in ILs[5,33,34], however, the extent of site-specific information extracted from the simulations is rather limited. Nonetheless, we highlight the works of Kirchner's group [35-37] where both systematic selection of anions and detailed analysis of the microscopic structure have been combined. Namely, they have investigated such aspects as cation-anion H-bonding, relative counterion arrangement and different modes of cation aggregation in such systems as $C_2mimAc/Cl/SCN$ [35], $C_4mimAc/CF_3COO/TFSI/TFO/Br/I$ [37] and their analogues with fluorinated cations, and $C_2mimSCN/N(CN)_2/B(CN)_4$[36].

In this Chapter we present a systematic MD study on the local microscopic structure around cations in six imidazolium-based ILs containing 1-butyl-3-methylimidazolium C_4mim^+ cation coupled with such anions as tetrafluoroborate BF_4^-, hexafluorophosphate PF_6^-, trifluoromethanesulfonate TFO^-, bis(trifluoromethanesulfonyl)imide $TFSI^-$[38] (see Figure 3.1 for the molecular structure). The selected set of ILs are mainly of interest for such applications as electrolytes for batteries and other energy related applications (C_4mimBF_4, C_4mimPF_6, $C_4mimTFO$, $C_4mimTFSI$).[39] We selected the C_4mim^+ cation as the associated ILs are liquids at room temperature. Furthermore, both experimental and theoretical data are available in the literature on their microscopic structure and then makes it possible to compare with our present results. By studying anions of different size, shape, symmetry, charge distribution and basicity we aim to reveal their influence on various fine aspects of the local structure in these systems which is of great importance for fine-tuning the molecular design of novel ILs with better characteristics and for explaining numerous experimental findings.

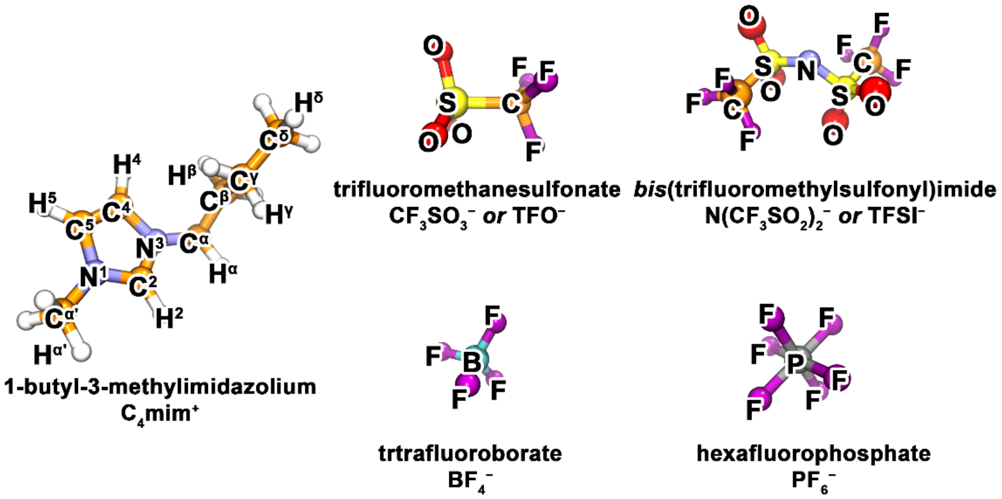

Figure 3.1. Molecular structures of C_4mim^+ cation and four anions constituting the studied ILs with atomic labeling used for the analysis of the structure properties.

3.2. Results and discussion

3.2.1 Cation···anion arrangement

We begin with basic characterization of the relative arrangement of anions around a reference cation. Due to the different shape and symmetry of the studied anions in the present analysis we will describe their position via the corresponding atomic centers of coordinating group X, *i.e.*, B in BF_4^-, P in PF_6^-, S in TFO^- and $TFSI^-$. As most of the positive charge of C_4mim^+ cation is localized at the imidazolium ring a typical approach is to consider the center of ring (CoR)···X radial distribution functions (RDFs) [37]. The resulting RDFs shows the sharpest peaks located at *ca.* 0.47-0.49 nm for C_4mimBF_4, C_4mimPF_6 and $C_4mimTFO$, and less intensive peak for $C_4mimTFSI$ observed at slightly larger distances of 0.53 nm

(Figure 3.2). This behavior indicate the equally strong interactions between the cation and anions in all the studied ILs, however these RDFs show little detail as they sample all the possible orientations of the vector connecting the reference and observed sites.

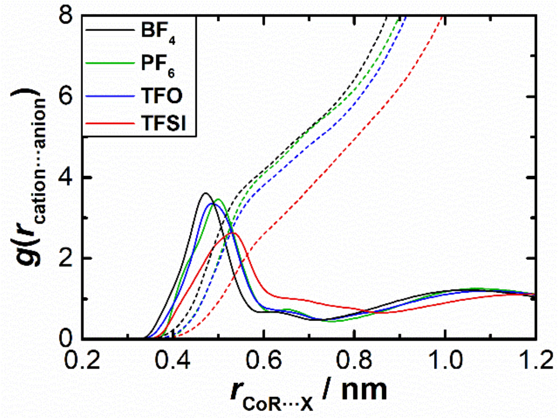

Figure 3.2. Example of the cation···anion radial distribution functions for the pure ILs considered in terms of the distance distributions between the center of imidazolium ring and atomic centers of coordinating group of the anions, CoR···X (B in BF_4^-, P in PF_6^-, S in TFO^- and $TFSI^-$).

A common way to resolve the orientational component of these functions is to study the isosurfaces of so-called spatial distribution functions (SDFs).[4,5,33,40-42] This type of representation, however, suffers from somewhat ambiguous choice of the isovalue and also from the lack of information on the distribution of the observed particle density inside the region enclosed by the isosurface. We overcome these difficulties by using the cross sections of the spatial distribution functions CoR···X with the observed particle density color-mapped on the slicing planes. It is well known from numerous published conventional SDFs[4,33,40-42] that in imidazolium-based ILs anions prefer to occupy three main sites next to the ring CH sites with a higher intensities observed at the C–H^2 group and a minor one next to the C^{α}'H^3 group. It is noteworthy that the latter is often overlooked because of too high SDF isovalue used. In this regard, one of the cutting planes shown in Figure 3.3 is the imidazolium ring plane while the other one is orthogonal to the first one and contains the C–H^2 line.

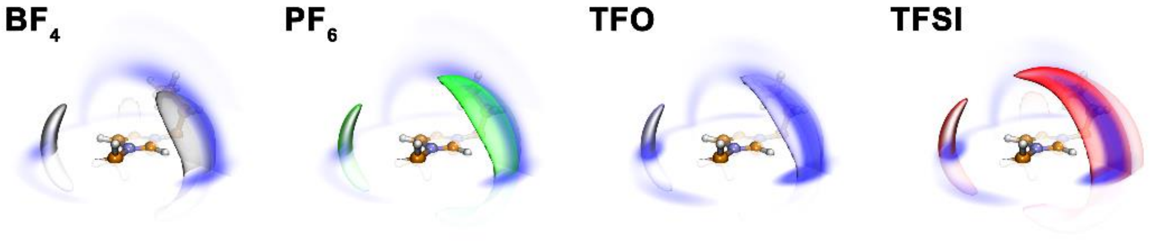

Figure 3.3. Spatial distribution functions (SDFs) along with the cross-sections of the spatial distribution functions corresponding to the probability of finding the central atom of anion's coordinating group (B in BF_4^-, P in PF_6^-, S in TFO^- and $TFSI^-$) around a reference C_4mim^+ cation within 0.75 nm of the imidazolium ring center. One cross-section plane contains the imidazolium ring plane while the other one is orthogonal to it and contains the $C–H^2$ vector. The blue color in cros-sections corresponds to the highest values.

It is readily apparent from the Figure 3.3 that all the aforementioned regions of localization of anions around the reference C_4mim^+ cation (*i.e.*, next the imidazolium ring $C–H^{2/4–5}$ sites and in front of the $C^{\alpha\prime}H^3$ group) are observed in all the studied ILs. However, several IL-specific features are also apparent. Namely, the localization of anions becomes progressively more diffuse in the order $BF_4^- \approx PF_6^- < TFO^- < TFSI^-$. Particularly, at the $C–H^2$ site the nature of the distribution of anions above/below and in the imidazolium ring plane is strongly IL dependent. For example, $C_4mimTFSI$ the distribution seems to be rather uniform over quite a broad range of orientations.

In order to study the latter aspect more precisely we decided to follow the distribution of the first nearest neighboring anions with respect to cation's main sites of interest. Indeed, it is primarily the nearest neighbor that defines the local environment of a reference site. Thus, by analyzing different structural properties taking into account only the first nearest neighbors[43-45] one samples over a small yet significantly reasonable volume of space. In this regard we described the position of the first nearest neighboring coordination group of anions with respect to one of the three ring hydrogen atoms $H^{2/4–5}$ of C_4mim^+ cation in terms of the distance $H^i\cdots X$ and the angle φ_i between the imidazolium ring normal vector and the radius-vector $H^i\cdots X$ (see Figure 3.4 for the scheme). Thus, a perfect in-plane arrangement of the observed anion next to the reference H^i site would correspond to the φ_i values around 90 degrees while positions above/below the reference site would contribute to the φ_i values close to 0 and 180 degrees.

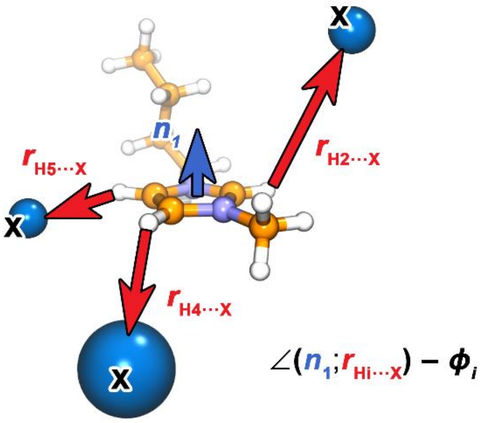

Figure 3.4. Schematic representation of the main parameters used for the description of the relative position of anion with respect to the imidazolium ring $C–H^{2/4–5}$ sites.

The results of the present analysis are shown in Figure 3.5B as combined distribution functions (CDFs) correlating the $H^i\cdots X$ distances and the corresponding φ_i values for the first nearest neighboring anions with respect to $H^{2/4–5}$. By construction, these contour plots are very similar to the slicing plane in Figure 3.3 that contains the $C–H^2$ line. However, due to restriction to the first nearest neighbor with respect to each specific reference site these CDFs bring about more information.

A common point of all the studied ILs here is that both angular and radial distributions are more diffuse in the case of $H^{4–5}$ than in the case of H^2. This means that the general position of anion is more localized around the H^2 site which obviously stems from its higher positive charge.[4,7,41] At the same time, there is still plenty of anion-specific information. For example, the considered here anions show a distinct preference towards above/below H^2 arrangement. This effect is pronounced the most in C_4mimPF_6, then to a similar extent in C_4mimBF_4 and $C_4mimTFO$, while $C_4mimTFSI$ reveals the most diffuse distribution of anion around the H^2 site. As for the distribution of the perfluorinated anions around the $H^{4–5}$ atoms some anion-specific details are also apparent. In C_4mimBF$_4$ and C_4mimTFO anions tend to be localized around the in-plane positions next to the $H^{4–5}$ sites while as in C_4mimTFSI the bulky anion is mainly found above and below these sites. In the letter case, one has to notice as well that the distribution is even more diffuse than in the case of H^2. Finally, PF_6^- occupies mainly in-plane position next to H^5 and slightly prefers above/below H^4 arrangement.

Clearly, the above/below arrangement of the nearest neighboring to the imidazolium ring anions plays a non-negligible if not the dominant (depending on the anion) role in the local microscopic structure around a reference C_4mim^+ cation. In an attempt to characterize such contributions which could have been overlooked in the presented above analysis we studied the distribution of the nearest neighboring to the CoR anions that are at the same time *not* the first nearest neighbors of any of the imidazolium ring C–$H^{2/4–5}$ sites, those that are not taken into account in the previous analysis. Figure 3.5A presents the results of such analysis in the form of contour plots of the density of projections of anion's position on the imidazolium ring plane. The percentages shown in the plots indicate the fraction of the nearest to the CoR anions that satisfy the second condition, *i.e.*, which are not the nearest neighbors of any of $H^{2/4–5}$.

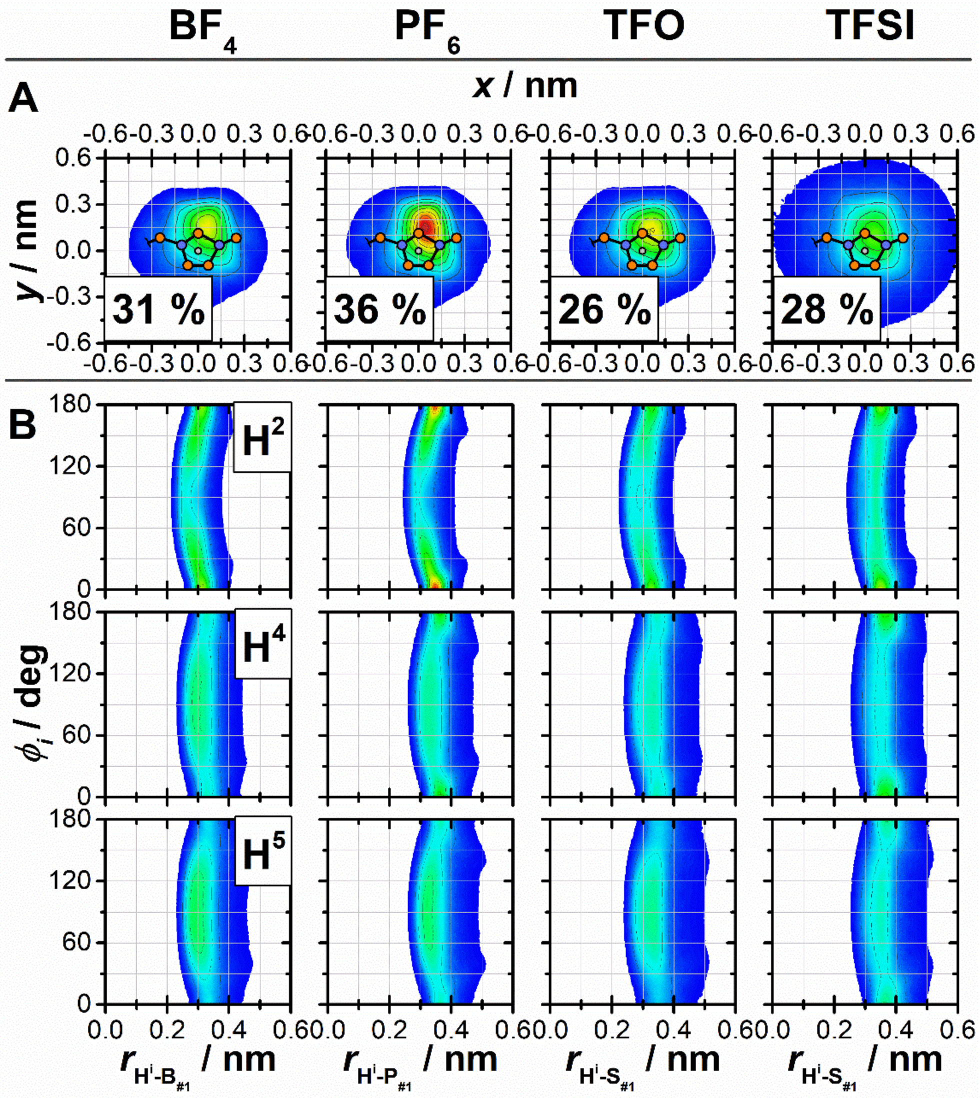

Figure 3.5. A) Contour plots of the density of projections on the imidazolium ring plane of the nearest to the CoR anions that are at the same time *not* the nearest neighbors of any of $H^{2/4–5}$ sites. The projection plane is centered at the CoR (grey circle) and part of the skeleton of a reference C_4mim^+ is shown for clarity. The percentages indicate the fraction of the nearest to the CoR anions that satisfy the second condition, *i.e.*, which are not the nearest neighbors of any of $H^{2/4–5}$. Color scaling range is different in A and B, but the same for all the studied ILs and reference sites. B) Combined distribution functions relating the distance of the vector connecting the imidazolium ring hydrogen sites H^2 (*top row*), H^4 (*middle row*), H^5 (*middle row*) of C_4mim^+ cation and the nearest central atom of coordinating group of anions and the angle between this angle and the normal to the imidazolium ring plane (*φ*).

In concordance with what was mentioned above all the studied ILs show very similar distributions centered between C^2 and N^3 with intensities following the order PF_6^- > BF_4^- ≈ TFO^- > $TFSI^-$.

The obtained trend is in excellent agreement with numerous results on related systems. The examples include MD simulations of Hardacre *et al.* targeted at reproducing neutron diffraction data on C_1mimCl/PF_6/TFSI and C_2mimAc[40,46-50], NMR, classical MD simulations and static *ab initio* calculations on ion pair dimers performed by Matthews and colleagues on C_1mimCl/TFO/NO_3/BF_4/$MeSO_4$ and C_4mimCl/TFO/SCN/TFSI/Me_2PO_4.[5,6] These results were, however, mainly based on conventional SDFs with an arbitrary isovalue. The conclusions can be typically summarized as follows: the bigger and the less coordinating (H-bond accepting) the anion is, the more it prefers to occupy the above/below C–H^2 sites. A more quantitative assessment of this issue was given by Skarmoutsos *et al.*[7] who reported a similar angular distribution for anions that is localized at distance lower than the H-bonding criteria at the C–H^2 site in C_4mimCl. Kirchner's group reported so far the results of the relative anion arrangement of similar level of details to ours for *ab initio* and classical MD simulations of C_2mim^+ coupled with cyano-based anions,[36] mixtures of C_2mimAc with water,[42] neat C_4mimBr/I/Ac/CF_3COO/TFSI ILs,[37] and C_2mimCl-C_2mimSCN IL mixtures.[51] Nonetheless their results mainly dealt with C–H^2 or CoR centered description. In the present study we present a particular level of structural details by considering nearest neighboring anions with respect to each relevant cation interaction site.

As for the nature of the interactions underlying the revealed structural motifs we firstly highlight that the present results are an outcome of a classical force-field meaning that one can speculate not more than about the effects of size and charge distribution. Nonetheless, several static and dynamic *ab initio* studies have already tackled this question. It is assumed that the on-top arrangement of anions results from the so-called anion-π^+ interaction[5-7,52] which is a complex interplay of electrostatics and dispersion interactions.[5-7,36,52]

3.2.2 Cation···anion H-bonding

It is well appreciated in the literature, that apart from the strong electrostatic interactions the local microscopic structure in imidazolium ILs is significantly influenced by cation-anion H-bonding, though the extent and the importance of this contribution to the overall potential energy landscape is still under debate.[7,11,15,35,53,54] The issue of cation-anion H-bonding in ILs has mainly been assessed from simulations within a certain H-bond criterion. Typically, this implies a combination of a radial cut-off between a given hydrogen atom and the corresponding H-bond acceptor and an angular cut-off for the pseudo-valent H-bond angle (D–H···A, where D and A stand for H-bond donor and acceptor, respectively).[55] However, more sophisticated criteria have also been used.[7] Moreover, some authors claim that poorly selected cut-off values can significantly bias the results[7] while the others stipulate that their results are rather robust towards the cut-offs.[35]

To get insight on the relative strength of the interionic H-bonding interactions we started from the general radial distribution between the imidazolium ring hydrogen sites $H^{2/4–5}$ and H-bond accepting atoms of the anions Y, where Y corresponds to F in BF_4^- and PF_6^-, O in TFO^- and $TFSI^-$. Obtained results presented in Figure 3.6 shows the similar RDFs profiles for all the studied ILs with the sharpest first maxima located at 0.20-0.22 nm for H^2 and 0.22-0.24 nm for $H^{4–5}$ and the numerous hollows and humps at larger distances. This indicate that the relatively strong H-bonding interactions between the C_4mim^+ ring and the anions occurs at H^2 site, whereas the weakest interactions observed at $H^{4–5}$. Furthermore, to the distinctive features of these RDFs can be also attributed the difference in the intensities of the first maxima. For all the considered ILs the position of the first maxima located at the same positions with the exception of C_4mimTFSI shifted to the larger distances. This can be interpreted, that the H-bonding interactions between the imidazolium ring hydrogens and $TFSI^-$ are rather weaker than in other ILs.

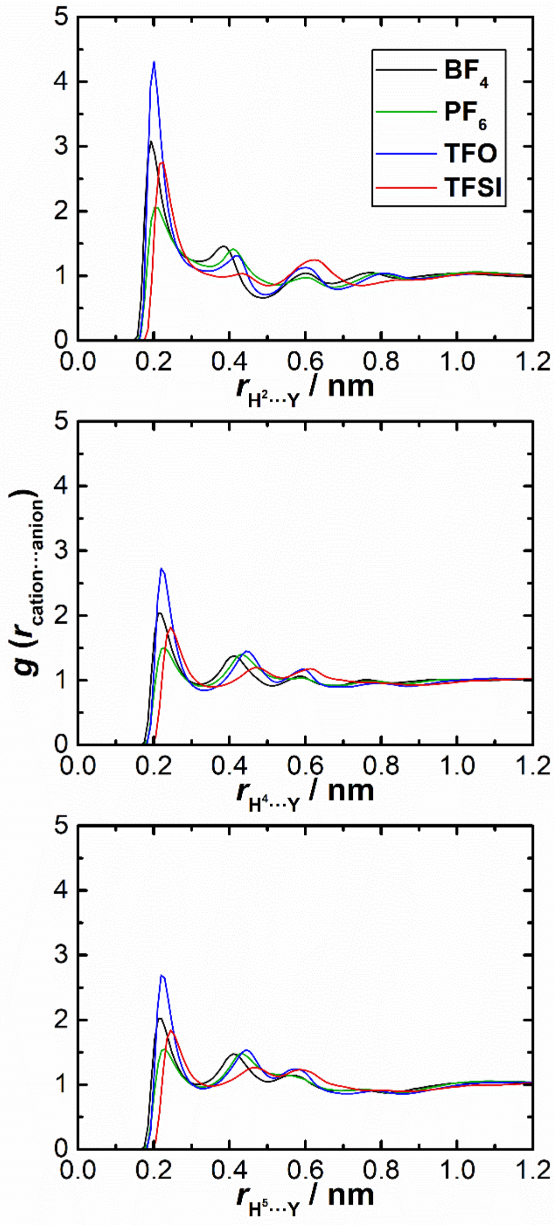

Figure 3.6. Example of the cation···anion radial distribution functions for the pure ILs considered in terms of the H-bonding interactions between the imidazolium ring hydrogen sites $H^{2/4–5}$ and H-bond accepting atoms of the anions Y, H^i···Y (F in BF_4^- and PF_6^-, O in TFO^- and $TFSI^-$).

To get a detailed information on the nature of H-bonding interactions between the different anions in the present study we refrain from any H-bonding criteria and present in Figure 3.7 CDFs correlating the H-bond pseudovalent angle and the corresponding H-bonding distance between the imidazolium ring hydrogen atoms H^i and the nearest neighboring H-bond accepting atom of anion. Similarly to the general distribution of anions around the ring sites discussed before, several apparent features are common for all the studied ILs here. Namely, both angular and radial distributions are more diffuse at H^{4-5} than at H^2. Also the linearity of H-bond is more important at H^5 than at H^4 and sometimes even than at H^2.

As for the IL-specific observations on cation-anion H-bonding at the imidazolium ring sites one should mention that the relative strength of H-bonds estimated from their linearity/length follows the order $TFO^- \geq BF_4^- > TFSI^- \approx PF_6^-$. Despite the fact that the main peaks are located at H-bonding distances, very close to linear arrangements and with intensities comparable to those of C_4mimTFO one sees broad low intensity features reaching rather large distances and low angle values.

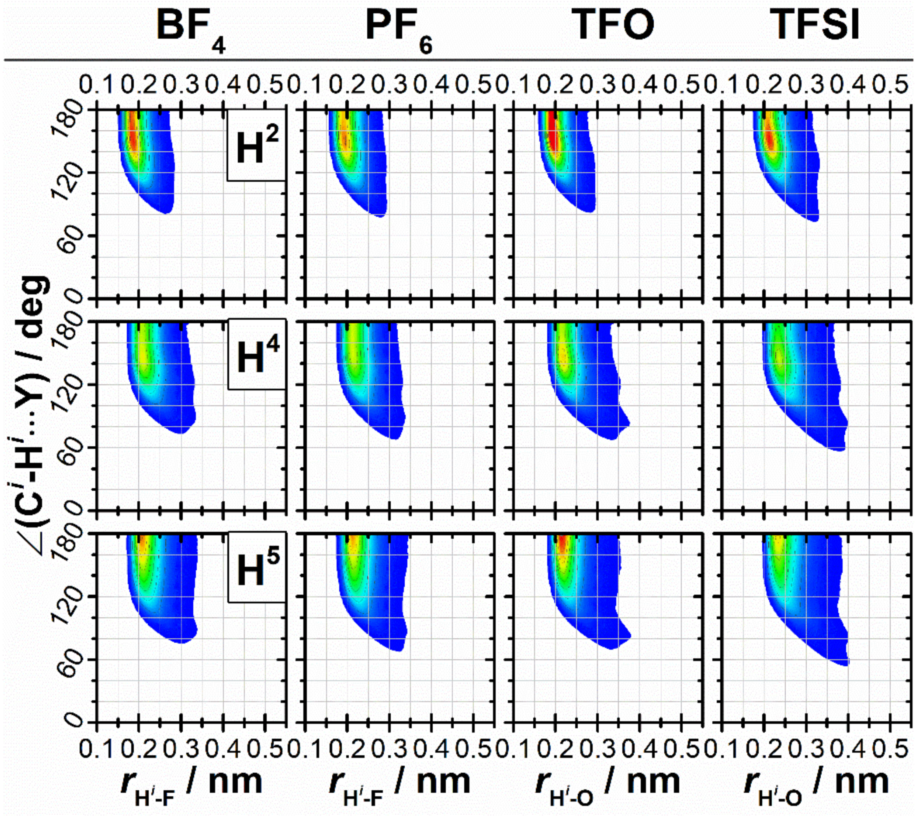

Figure 3.7. Combinated distribution functions relating the distance and the corresponding pseudovalent angle of H-bond like interactions between the imidazolium ring hydrogen atoms H^2 (*top row*), H^4 (*middle row*), H^5 (*bottom row*) of C_4mim^+ cation and the nearest neighboring primary H-bond accepting atom of anion (F for BF_4^- and PF_6^-, O for TFO^-, and $TFSI^-$).

In the recent NMR study on neat C_4mimBF_4, C_4mimPF_6, $C_4mimTFO$, and $C_4mimTFSI$ and in mixtures with acetonitrile over a broad concentration range[13] apart from the relative strength of cation-anion H-bonding in these ILs we also discovered an interesting result concerning the relative strength of H-bonds at H^2 and at $H^{4–5}$ sites. In particular, it was established that H-bonding at H^2 is much stronger than at $H^{4–5}$ in $C_4mimTFO$ and $C_4mimTFSI$, while as this difference is less pronounced in C_4mimBF_4 and C_4mimPF_6. Given that the radial and the angular distribution of the H-bonding interactions are quite similar in these ILs we additionally verify experimental finding by calculating the average distances, $C^i\cdots Y$ and $H^i\cdots Y$, representing the H-bonding geometry between the imidazolium ring sites and the corresponding H-bond accepting atom of anion Y, *i.e.*, F in BF_4^- and PF_6^-, O in TFO^- and $TFSI^-$ (Figure 3.8). It is readily apparent that the difference in the average distances at H^2 and $H^{4–5}$ is larger in the case of $C_4mimTFO$ and $C_4mimTFSI$ compared to C_4mimBF_4 and C_4mimPF_6. Despite that the distances between the imidazolium ring hydrogen sites and the anions are rather larger in $C_4mimTFO$ and $C_4mimTFSI$ it can be clearly seen that the respective H-bonding angle in $C_4mimTFO$ is more linear than in C_4mimPF_6. This may indicate the rather strong H-bonding interactions in $C_4mimTFO$. The MD results are in accordance with the previous experimental findings which were also partly supported in another our work on quantum-chemical calculations of ion pair dimers of these ILs.[14]

One of the main experimental evidence used by us in this regard was the IR bandshape of the stretching vibration of the imidazolium $C–H^i$ bonds, namely, the particularly strong low frequency shoulder corresponding to the $C–H^2$ stretching vibration.[13] The results presented in Figure 3.8 suggest that $C_4mimTFO$ and $C_4mimTFSI$ also reveal significantly enhanced H-bonding strength at H^2.

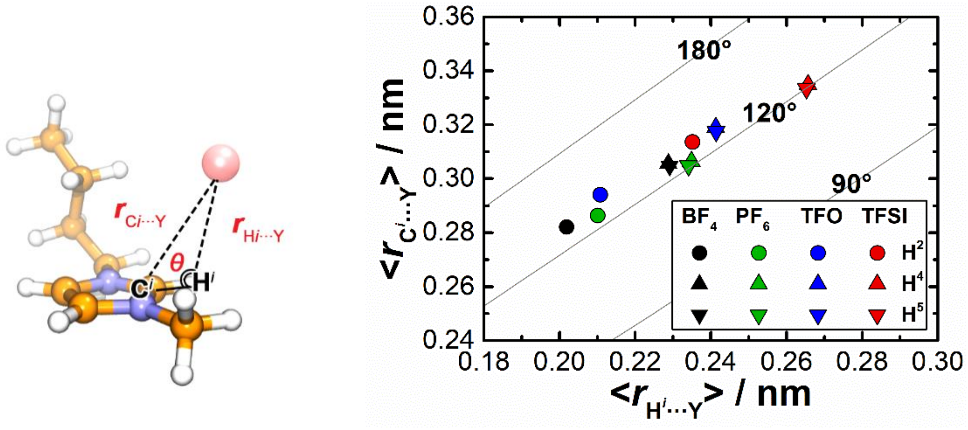

Figure 3.8. Average distances, $C^i\cdots Y$ and $H^i\cdots Y$, representing H-bonding geometry between the imidazolium ring hydrogen atoms $H^{2/4–5}$ of C_4mim^+ cation and the nearest neighboring primary H-bond accepting atom of anion Y (where Y corresponds to F in $BF_4^–$ and $PF_6^–$, O in $TFO^–$, and $TFSI^–$).

All the anions considered in this study can form multiple H-bonds with a given hydrogen atom. This point has been mainly studied in acetate-based systems;[40,42] however, numerous static quantum-chemical calculations on representative ion pair clusters suggest that this issue is important as well in ILs with perfluorinated anions.[11,14,56] As we stick to the idea of the nearest neighbor approach and try avoiding use of any H-bonding criteria here we propose to follow the correlations between the distances from a given ring hydrogen atom to H-bond accepting atoms of the nearest neighboring anion. The nearest neighboring anion here was defined with respect to the distance between the ring hydrogen atoms $H^{2/4–5}$ and the central atom of anion's coordinating group (see above). The obtained CDFs are shown in Figure 3.9.

All the other anions have at least three atoms that could possibly simultaneously coordinate a given hydrogen atom the visualization of such multidimensional data is rather complicated. In order to simplify the representation, we analyzed only those nearest neighboring anions that have one H-bond with a given hydrogen atom. This was realized by applying a condition that the distance from a given hydrogen atom to an H-bond-accepting atom of the nearest neighboring anion is within the standard deviation from the average position of the first nearest neighbor of this type in Figure 3.8. Then, after selecting the configurations that fit these conditions, we analyzed the CDFs of the distances from the selected hydrogen atom to two other H-bond accepting atoms of the nearest neighboring anion that were not used in the condition. In other words, these CDFs, presented in Figure 3.9, correspond to an observation of two different atoms (a three-body analysis) with a condition applied to a third one.

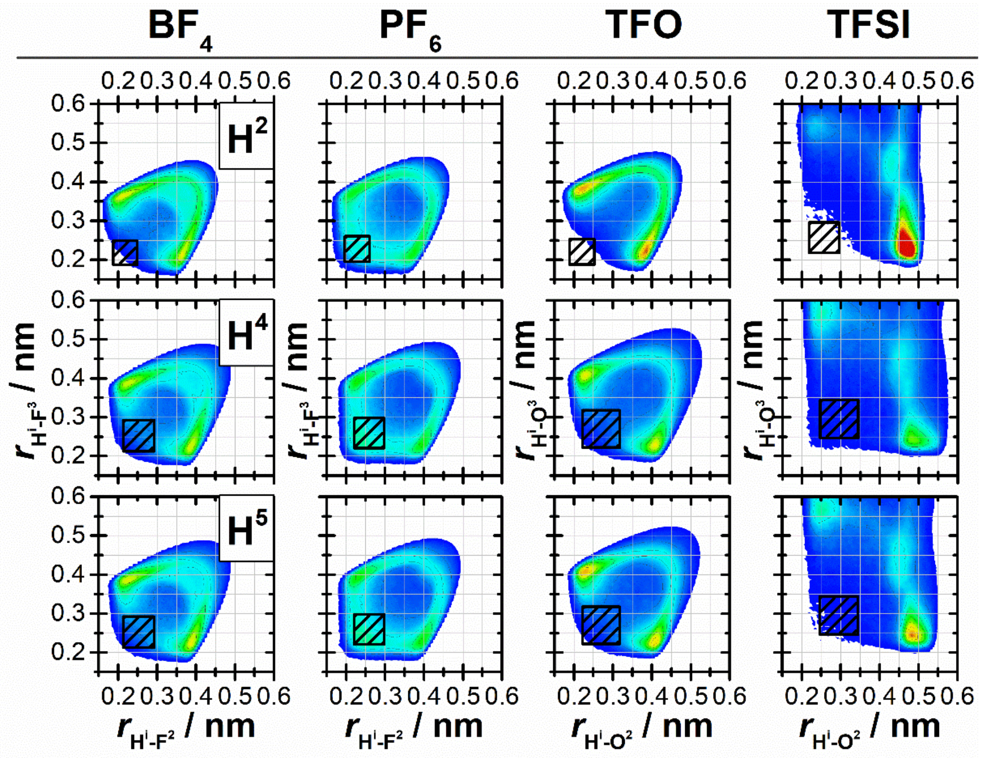

Figure 3.9. Combined distribution functions relating the distances from H^2 (*top row*), H^4 (*middle row*), H^5 (*bottom row*) of C$_4$mim$^+$ cation to the two different H-bond accepting atoms of the nearest anion (F for BF$_4^-$ and PF$_6^-$, O for TFO$^-$, and TFSI$^-$) under condition that a third atom is within a certain distance condition as explained in the text.

Within this framework a monodentate coordination means that only the first H-bond accepting atom of the nearest neighboring anion, *i.e.*, the one that served for the condition, is within the typical H-bonding distance away from a given hydrogen atom. In other words, in the CDFs shown in Figure 3.9 such configurations would contribute to the probability density corresponding to high values of both observed distances. Similarly, a bidentate coordination implies that apart from the first H-bond accepting atom one of the two observed ones should be observed at short H-bonding-like distances while the other one being much farther from a given hydrogen atom. Finally, a tridentate coordination would give rise to a cross-peak on diagonal at short distances. For this set of systems we highlight the range of H-bonding distances used as criteria for the first H-bond accepting atom with hatched squares in Figure 3.9.

In C_4mimBF_4, C_4mimPF_6, and $C_4mimTFO$ the anions can potentially form up to three H-bonds with a given hydrogen atom using three equivalent H-bond accepting atoms. As one can see from Figure 3.8, several observations are universally applicable to all the three ring sites in this set of ILs. Firstly, the most probable H-bonding mode is the bidentate one as indicated by the strongest peaks (at 0.20–0.25 nm / 0.35–0.45 nm) symmetric with respect to diagonal. Secondly, tridentate configurations are more probable at $H^{4–5}$ sites than at H^2 (note the higher intensity close to the hatched regions in the case of $H^{4–5}$ compared to H^2). Finally, transition from the dominating bidentate configuration to either monodentate or tridentate ones passes through a monotonic decrease of probability. The latter finding makes quantitative distinguishing between different H-bonding coordination patterns rather ambiguous. It is also worth noting that the previously reported by us stable ion pair geometries of C_4mimBF_4, C_4mimPF_6, and $C_4mimTFO$[14] with anion on top of the $C–H^2$ fragment are fully compatible with the prevailing bidentate H-bonding mode revealed here.

As for IL specific features of multiple H-bonding of a given ring C–H site with the nearest anion we note a significant population of tridentate configuration, comparable to the monodentate one, in the case of C_4mimPF_6. In C_4mimBF_4 and $C_4mimTFO$ the tridentate H-bonding is less frequent than the monodentate one. Among the two ILs it is C_4mimBF4 that exhibits more tridentate H-bonding. In other words, the average number of close H-bond like contacts with the nearest neighboring anion follows the order $C_4mimPF_6 > C_4mimBF_4 > C_4mimTFO$.

Lastly, we describe the multiple H-bonding with the nearest TFSI anion. Here the two H-bond like distances analyzed in Figure 3.8 refer to the non-equivalent oxygen atoms. Namely, the distance corresponding to the horizontal axis of the graph is that to the O^2 oxygen atom which resides on the same SO_2 moiety as the oxygen atom O^1 used for defining the condition. Accordingly, the distance plotted along the vertical axis is that to the O^3 oxygen atom, corresponding to the second SO_2 group. The main peak at 0.45 nm / 0.25 nm implies a very strong preference, particularly at the C–H^2 site, to the bidentate H-bonding between oxygen atoms of two different SO_2 groups is clearly observed. Nevertheless, weak populations of monodentate and bidentate configurations within the same SO_2 group are also apparent. Similarly to C_4mimBF_4 and C_4mimTFO tridentate configurations are hardly observed at the C–H^2 site while they are encountered at $H^{4–5}$ though with a very low probability.

Our final insight into cation···anion H-bonding concerns such non-conventional H-bond donors as aliphatic C–H sites of the butyl and methyl groups of C_4mim$^+$ cation. It has been often acknowledged in molecular modeling studies[6,7,11,14,52,56] that anions located close to the imidazolium ring C–H sites can also establish slightly weaker H-bonds with the adjacent alkyl hydrogen atoms of the alkyl chains. This claim has been experimentally confirmed in neat ILs via the isotopic shift of ^{19}F NMR signals after selective deuteration of C_4mim$^+$ cation in C_4mimBF_4 and C_4mimPF_6[57] and also in solutions in various molecular solvents from concentration dependent chemical shifts.[13,20,21]

Similarly to Figure 3.7 we present in Figure 3.10 the CDFs relating H-bonding distance and the corresponding pseudovalent angle between different alkyl hydrogen atoms of C_4mim$^+$ cation and the nearest neighboring H-bond accepting atom of anions. Not surprisingly, the H-bonds involving the alkyl hydrogen atoms are less frequent, longer and less directional than those involving the imidazolium ring C–H sites. The fact that the distributions are the least diffuse for the $H^{\alpha'}$ site can be traced back to its better special accessibility. Moreover, it can contribute to the cation-anion H-bonding not only via configurations where anion is simultaneously bound to H^2 or H^4 of the same C_4mim$^+$ cation but also via configurations in which anion is directly in front of the N^3-$C^{\alpha\prime}H^3$ seen as a weak probability zone in cross-sections in Figure 3.3. This findings supports the importance of $H^{\alpha/\alpha'}$ hydrogen atoms not only in the analysis of the cation···anion interactions in ILs but in the potential model development as well.

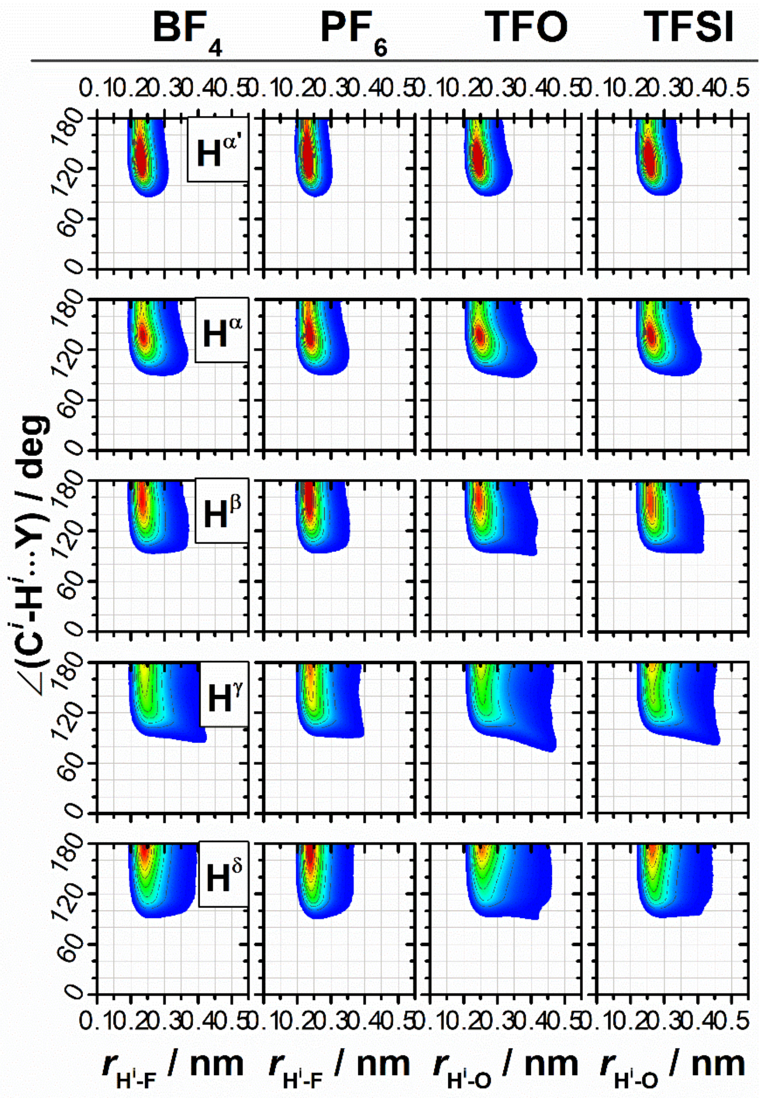

Figure 3.10. Combined distribution functions relating the distance and the corresponding pseudovalent angle of H-bond like interactions between the alkyl hydrogen atoms of C_4mim^+ cation and the nearest neighboring primary H-bond accepting atom of anion (F for BF_4^- and PF_6^-, O for TFO^-, and $TFSI^-$). Intensity scale is two times smaller than that in Figure 3.7.

In general, the H-bonds with hydrogen atoms of the butyl chain become progressively weaker as one gets further away from the imidazolium ring. The only obvious exception here is C_4mimPF_6 as it reveals rather equally strong H-bonds with all types of alkyl hydrogen atoms along the butyl chain of C_4mim^+ cation. This finding can be related to the well defined localization of PF_6^- anion above/below the C–H^2 site and could be one of the reasons of its surprisingly high viscosity of *ca.* 280 mPa s[58].

3.2.3 Cation···cation arrangement

Despite the fact that the local environment of cations in imidazolium-based ILs is mainly determined by the surrounding counterions it is well understood that cation···cation contacts also play significant role. Two typical kinds of contacts have been reported in imidazolium-based ILs: tail-tail and ring-ring (*e.g.* π^+-π^+ stacking).[6,17,37,56] The former one is known to be at the origin of microheterogeneity observed both experimentally [17,59,60] and by molecular simulations.[8,25,26] The latter, in contrast, is much less common and was initially suggested to rationalize some NMR spectroscopic data[61-63] and later was also confirmed by MD simulations including those reproducing neutron and X-ray scattering data.[46,50,64]

It is interesting to note that in the available experimental crystal structures of C_4mim^+-based ILs corresponding to some of the ILs studied here no stacking type close contacts were observed, though the neighboring ring planes are often, but not always, parallel and displaced.[65,66] Several recent quantum-chemical calculations on representative clusters of ion pairs of C_4mim^+-based ILs have also revealed the importance of π^+-π^+ stacking in such systems.[5,6,14,52,56,67-69]

We address these two types of cation-cation contacts with classical RDFs (Figure 3.11) between the centers of imidazolium rings (CoR) and between the terminal carbon atoms of the butyl chain (C^δ). It is readily apparent that the chain-chain aggregation is much less IL specific though it is obviously stronger than the π^+-π^+ stacking. The first peak in the $C^\delta\cdots C^\delta$ RDFs is located at 0.40 nm with a distinct shoulder at *ca.* 0.50 nm. The main peak accommodates approximately one neighbour whereas integration up to the first minimum located at 0.65-0.70 nm gives around 0.30-0.35 neighbours except for C_4mimTFSI where the coordination number is close to 2 due to the bulkiness of the anion. The second shell of chain-chain contacts is hardly discernable.

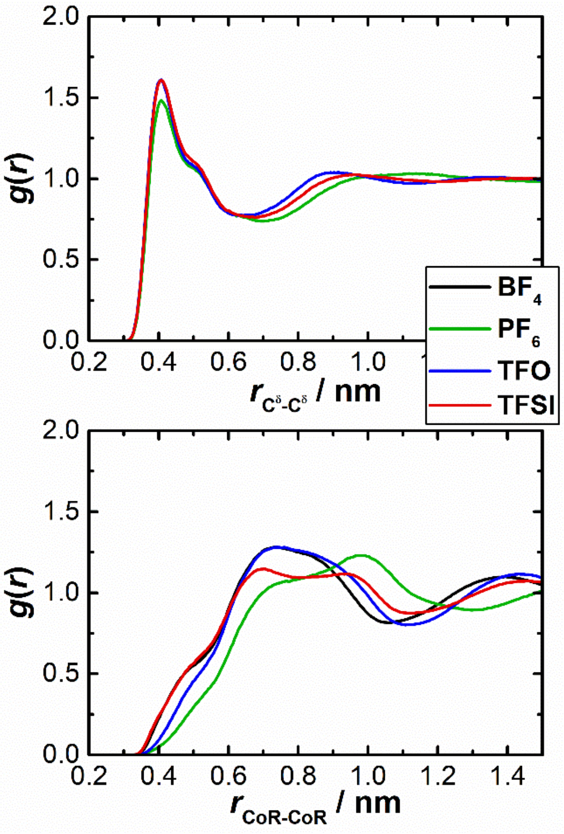

Figure 3.11. Example of the cation···cation radial distribution functions relating two main types of C_4mim^+aggregation: between the butyl chains (*top*) and between the imidazolium rings (*bottom*).

As already mentioned before, the CoR···CoR distributions are much more complex and sensitive to the type of anion. Firstly, none of these distributions exhibits a distinct strong first peak. One rather observes a series of shoulders and humps with a complicated structure. Secondly, the initial slope of the curve corresponding to stacking contributions at 0.30-0.40 nm follows the order $BF_4^- \approx TFO^- > PF_6^- > TFSI^-$. This trend only represents the general tendency for stacking. In order to resolve the orientational aspects of this interaction we study several angular distributions (see Figure 3.12) for the first nearest neighbor with respect to the CoR···CoR distance. The results are presented in Figure 3.13 as CDFs correlating one of the selected angles and the distance between the centers of two closest imidazolium rings.

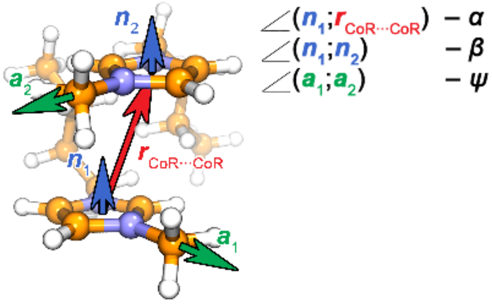

Figure 3.12. Schematic representation of the parameters used to description of the relative orientation of two C_4mim^+ cations.

The first investigated angle, designated here as *α*, is the angle between the normal vector of the imidazolium ring plane of the reference C_4mim^+ cation and the radius vector connecting the centers of ring of the reference cation and the observed nearest neighboring C_4mim^+ cation. This angle is analogous to the *φ* angle that we used to describe the relative position of anion with respect to cation. If the center of the imidazolium ring of the observed cation is located exactly above/below that of the reference one, such situation will produce contributions at *α* values close to 0 and 180 degrees. Similarly, an in-plane arrangement of the observed nearest neighboring cation corresponds to *α* around 90 degrees. One can clearly see from Figure 3.12 that in all the investigated ILs the nearest neighboring cation prefers to occupy the above/below positions at typical stacking distances around 0.35-0.45 nm. Noteworthy, the distributions for C_4mimPF_6 and $C_4mimTFSI$ are much weaker and their radial parts are much broader and shifted to longer distances.

Stacking interactions including those in imidazolium-based ILs [37,70,71] imply not only good relative above/below arrangement of the interacting planes but also their essential parallel configuration. The latter is probed via the angle *β*, *i.e.* the angle between the normal vectors of the imidazolium ring plane of the reference and observed molecules. Again, a perfectly parallel arrangement of the planes corresponds to *β* values of 0 or 180 degrees, whereas the values around 90 degrees are indicative of T-shaped relative arrangement of the two rings. For all the studied here ILs (except $C_4mimTFSI$ which doesn't show any distinct preferences for stacking) we observe a strong bias towards parallel alignment of the imidazolium ring plane of the first nearest neighboring cation. This tendency is even slightly stronger than for the above/below arrangement. In other words the angular distribution of α is broader than that of θ.

So far we have established that the nearest neighboring cation ring prefers parallel stacking with direct above/below arrangement though some displacement is possible. C_4mimPF_6 and C_4mimTFSI exhibit hardly any particular stacking type arrangements due to the preferential above/below the ring plane localization of anions and their big size (the latter particularly applies to C_4mimTFSI). C_4mimBF_4 and C_4mimTFO constitute an intermediate case of π^+-π^+ stacking. We remind, however, that the present results are obtained from classical MD simulations, *i.e.* they stem from merely point-charge electrostatics and molecular packing considerations while quantum-chemical treatment of π^+-π^+ interactions are out of scope here. Static quantum-chemical calculations on a set of ion pair dimers of C_1mim^+-based ILs reported recently by Matthews *et al.* [56] also highlighted the tendency of multidentate big anions to prefer the on-top arrangement thus preventing cations from stacking. In their subsequent combined NMR/MD study on mixtures of C_4mim^+-based ILs with different anions they reinforced their findings that smaller anions showing higher H-bond accepting capacity stabilize π^+-π^+ stacking, whereas bulky anions with diffuse charge distribution favor the anion- π^+ interactions.[5] However, a very recent *ab initio* MD study of C_2mim^+-based ILs with cyano-bearing anions by Weber and Kirchner [36] suggests that cation stacking and on-top anion arrangement are not always in direct competition.

One can also get an idea about the relative orientation of two stacked imidazolium rings by following the angle ψ, which is the angle between the vectors N^3-$C^{\alpha'}$ in the reference and observed C_4mim^+ cations. Orientations where the equivalent alkyl groups point to the same direction correspond to the ψ values of 0 degrees. It is apparent from the bottom row in Figure 3.13 that the four ILs prone to stacking show equal preference towards parallel and anti-parallel arrangements of the alkyl groups.

Brehm *et al.* inferred from small but still representative *ab initio* MD simulations of neat $C_2mimOAc$ and its mixtures with water [42] that the nearest neighboring cations in the corresponding stacking arrangement (*on top* and parallel with respect to the reference one) are oriented in an orthogonal fashion. On the one hand, this result could stem from the better description of the manifold of interactions between the ions in *ab initio* MD compared to the classical MD used in the present study. On the other hand, in the case of C_4mim^+-based ILs one would naturally expect stronger bias towards (anti)parallel arrangement of the alkyl chains due to packing restrictions and aggregation of the nonpolar moieties. Moreover, many published to date structures of quantum-chemically optimized ion pair clusters of C_4mim^+-based ILs[14,67,69] reveal collinear arrangement of the butyl chains.

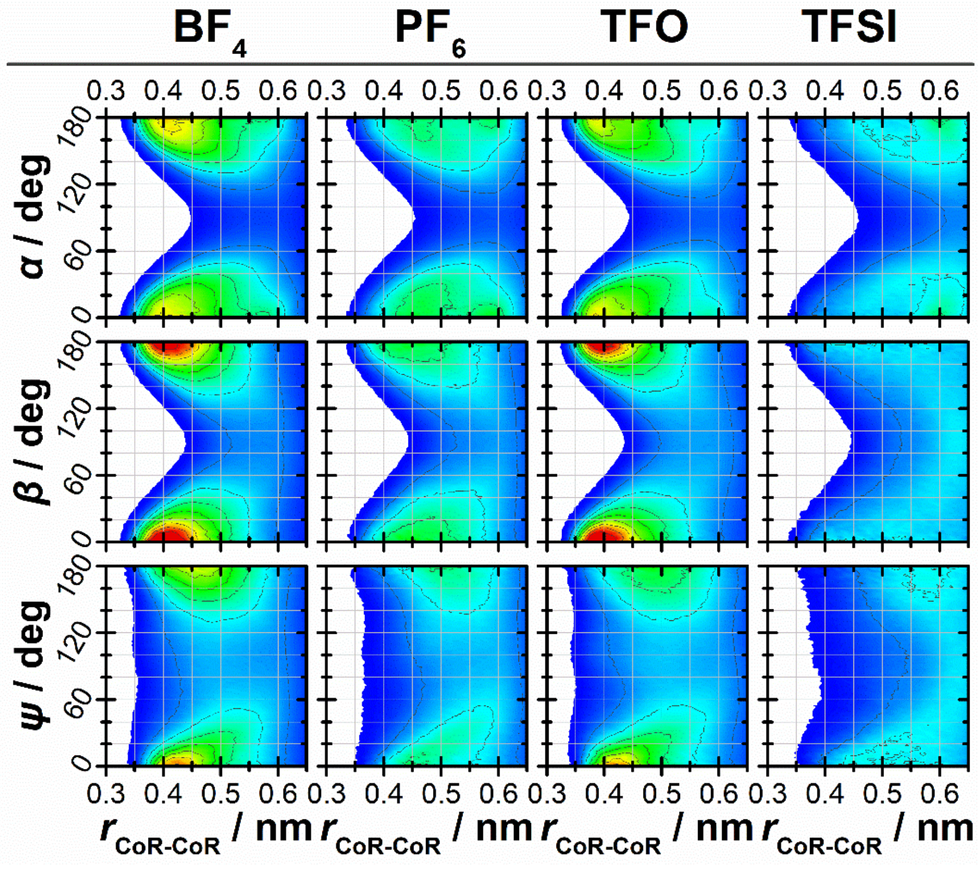

Figure 3.13. Combined distribution functions relating the *first* nearest neighbor CoR···CoR distance between two C_4mim^+ cations and the three representative angles α (*top row*), β (*middle row*), and ψ (*bottom row*) reporting their relative orientation.

The latter observation highlights the fact that the ring stacking of cations can occur simultaneously with the aggregation of butyl chains. In order to study this aspect more precisely we present in Figure 3.14 the CDFs correlating the $C^{\delta}\cdots C^{\delta}$ and CoR···CoR radial distributions under two alternative conditions. The first one implies that the observed cation is the nearest neighbor with respect to the distance between the terminal carbon atoms C^{δ} of the butyl chain whilst the second type of condition applied refers to the nearest neighbor with respect to the CoR···CoR distance. The results suggest that if two neighboring C_4mim^+ cations are aggregated via their butyl chain the most probable distance between their centers of the imidazolium rings is around 0.75-0.80 nm in all the ILs.

In the opposite case, *i.e.*, when one considers a pair of stacked C_4mim^+ cations the distribution of distances between the terminal carbon atoms of the butyl chains is rather broad and featureless within the range of 0.40-0.80 nm peaking at 0.40 nm. In other words, in the studied ILs, the stacking of cations does not impose any particular arrangement between their corresponding butyl chains.

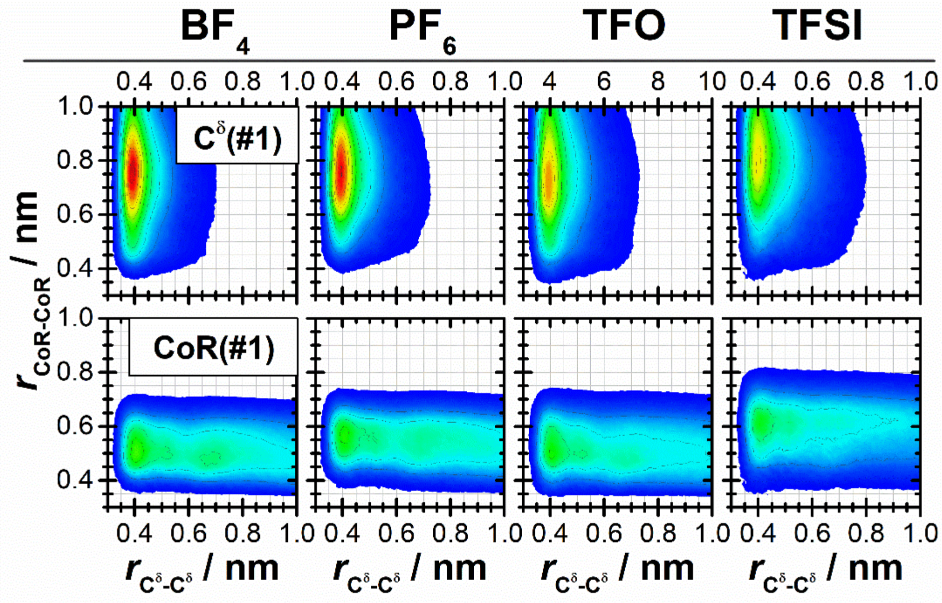

Figure 3.14. Combined distribution functions relating the distance between the terminal carbon atoms C^{δ} and the distance between the centers of rings (CoR) for a pair of closest C_4mim^+ cations with respect to their C^{δ} (*top row*) or their CoR (*bottom row*).

3.3. Conclusions

We have studied site-specific nearest neighboring local environment of cations in six ionic liquids bearing C_4mim^+ cation coupled with BF_4^-, PF_6^-, TFO⁻, and TFSI⁻ anions by means of classical MD simulations. Particular attention was paid to the issues of the influence of the nature of anion on the relative cation···anion and cation···cation localization, as well as on cation···anion H-bonding in terms of radial and orientational distributions of the nearest neighbors.

The results suggest that position of anion with respect to the imidazolium ring plane of cation is strongly anion-dependent, especially at the C–H^2 site. Namely, all the anions strongly prefer to occupy the on-top arrangement. The corresponding distribution at the C–$H^{4–5}$ sites is much more diffuse.

H-bonding at the H^2 site is strongly enhanced compared to the H^{4-5} sites in the case of asymmetric and/or strongly basic anions like TFO⁻ or TFSI⁻ which is in accordance with recent spectroscopic and theoretical claims.[5,13,14] Multiple H-bonding (bi- and even tri-dentate, where possible) with the nearest neighboring anion was observed to be prevailing at the $H^{4–5}$ sites compared to the H^2 one in all the considered ILs. H-bonding like short contacts were also found between the anions and alkyl C–H groups in all the studied anions though remarkably less frequent and directional.

Finally, cation-cation contacts via the aggregation of the butyl chains is much stronger and less anion-dependent than the π^+-π^+ stacking of the imidazolium rings. The latter, however, can occur simultaneously with the alkyl chain aggregation.

3.4. References for Chapter 3

(1) Chaban, V. V.; Prezhdo, O. V. A new force field model of 1-butyl-3-methylimidazolium tetrafluoroborate ionic liquid and acetonitrile mixtures. *Phys. Chem. Chem. Phys.* **2011**, *13*, 19345-19354.

(2) Chaban, V. Polarizability versus mobility: atomistic force field for ionic liquids. *Phys. Chem. Chem. Phys.* **2011**, *13*, 16055-16062.

(3) Mondal, A.; Balasubramanian, S. A Refined All-Atom Potential for Imidazolium-Based Room Temperature Ionic Liquids: Acetate, Dicyanamide, and Thiocyanate Anions. *J. Phys. Chem. B* **2015**, *119*, 11041-11051.

(4) Mondal, A.; Balasubramanian, S. Quantitative Prediction of Physical Properties of Imidazolium Based Room Temperature Ionic Liquids through Determination of Condensed Phase Site Charges: A Refined Force Field. *J. Phys. Chem. B* **2014**, *118*, 3409-3422.

(5) Matthews, R. P.; Villar Garcia, I. J.; Weber, C. C.; Griffith, J. A.; Cameron, F.; Hallett, J.; Hunt, P.; Welton, T. A structural investigation of ionic liquid mixtures. *Phys. Chem. Chem. Phys.* **2016**.

(6) Matthews, R. P.; Welton, T.; Hunt, P. A. Competitive pi interactions and hydrogen bonding within imidazolium ionic liquids. *Phys. Chem. Chem. Phys.* **2014**, *16*, 3238-3253.

(7) Skarmoutsos, I.; Dellis, D.; Matthews, R. P.; Welton, T.; Hunt, P. A. Hydrogen Bonding in 1-Butyl- and 1-Ethyl-3-methylimidazolium Chloride Ionic Liquids. *J. Phys. Chem. B* **2012**, *116*, 4921-4933.

(8) Kirchner, B.; Hollóczki, O.; Canongia Lopes, J. N.; Pádua, A. A. H. Multiresolution calculation of ionic liquids. *Wiley Interdisciplinary Reviews: Computational Molecular Science* **2015**, *5*, 202-214.

(9) Tsuzuki, S.; Tokuda, H.; Mikami, M. Theoretical Analysis of the Hydrogen Bond of Imidazolium C_2–H with Anions. *Phys. Chem. Chem. Phys.* **2007**, *9*, 4780-4784.

(10) Tsuzuki, S.; Tokuda, H.; Hayamizu, K.; Watanabe, M. Magnitude and Directionality of Interaction in Ion Pairs of Ionic Liquids: Relationship with Ionic Conductivity. *J. Phys. Chem. B* **2005**, *109*, 16474-16481.

(11) Hunt, P. A.; Ashworth, C. R.; Matthews, R. P. Hydrogen bonding in ionic liquids. *Chem. Soc. Rev.* **2015**, *44*, 1257-1288.

(12) Hunt, P. A.; Gould, I. R. Structural characterization of the 1-butyl-3-methylimidazolium chloride ion pair using ab initio methods. *J. Phys. Chem. A* **2006**, *110*, 2269-2282.

(13) Marekha, B.; Kalugin, O.; Bria, M.; Idrissi, A. Probing structural patterns of ion association and solvation in mixtures of imidazolium ionic liquids with acetonitrile by means of relative ^{1}H and ^{13}C NMR chemical shifts. *Phys. Chem. Chem. Phys.* **2015**, *17*, 23183 - 23194.

(14) Marekha, B. A.; Kalugin, O. N.; Idrissi, A. Non-covalent interactions in ionic liquid ion pairs and ion pair dimers: a quantum chemical calculation analysis. *PCCP* **2015**, *17*, 16846-16857.

(15) Zahn, S.; Bruns, G.; Thar, J.; Kirchner, B. What keeps ionic liquids in flow? *Phys. Chem. Chem. Phys.* **2008**, *10*, 6921.

(16) Chaban, V. V.; Prezhdo, O. V. Ionic and Molecular Liquids: Working Together for Robust Engineering. *J. Phys. Chem. Lett.* **2013**, *4*, 1423-1431.

(17) Hayes, R.; Warr, G. G.; Atkin, R. Structure and Nanostructure in Ionic Liquids. *Chem. Rev.* **2015**, *115*, 6357-6426.

(18) Plechkova, N. V.; Seddon Kenneth, R.: *Ionic liquids completely uncoiled: critical expert overview*; John Wiley & Sons, Inc.: Hoboken, New Jersey, 2015.

(19) Dommert, F.; Wendler, K.; Berger, R.; Delle Site, L.; Holm, C. Force Fields for Studying the Structure and Dynamics of Ionic Liquids: A Critical Review of Recent Developments. *ChemPhysChem* **2012**, *13*, 1625-1637.

(20) Marekha, B. A.; Bria, M.; Moreau, M.; De Waele, I.; Miannay, F.-A.; Smortsova, Y.; Takamuku, T.; Kalugin, O. N.; Kiselev, M.; Idrissi, A. Intermolecular interactions in mixtures of

1-n-butyl-3-methylimidazolium acetate and water: Insights from IR, Raman, NMR spectroscopy and quantum chemistry calculations. *J. Mol. Liq.* **2015**, *210, Part B*, 227-237.

(21) Takamuku, T.; Hoke, H.; Idrissi, A.; Marekha, B. A.; Moreau, M.; Honda, Y.; Umecky, T.; Shimomura, T. Microscopic interactions of the imidazolium-based ionic liquid with molecular liquids depending on their electron-donicity. *PCCP* **2014**, *16*, 23627-23638.

(22) Shirota, H.; Kakinuma, S.; Itoyama, Y.; Umecky, T.; Takamuku, T. Effects of Tetrafluoroborate and Bis(trifluoromethylsulfonyl)amide Anions on the Microscopic Structures of 1-Methyl-3-octylimidazolium-Based Ionic Liquids and Benzene Mixtures: A Multiple Approach by ATR-IR, NMR, and Femtosecond Raman-Induced Kerr Effect Spectroscopy. *J. Phys. Chem. B* **2016**, *120*, 513-526.

(23) Hallett, J. P.; Welton, T. Room-Temperature Ionic Liquids: Solvents for Synthesis and Catalysis. 2. *Chem. Rev.* **2011**, *111*, 3508-3576.

(24) Wang, H.; Gurau, G.; Rogers, R. D. Ionic liquid processing of cellulose. *Chem. Soc. Rev.* **2012**, *41*, 1519-1537.

(25) Shimizu, K.; Costa Gomes, M. F.; Pádua, A. A. H.; Rebelo, L. P. N.; Canongia Lopes, J. N. Three commentaries on the nano-segregated structure of ionic liquids. *J. Mol. Struct.: THEOCHEM* **2010**, *946*, 70-76.

(26) Shimizu, K.; Bernardes, C. E. S.; Canongia Lopes, J. N. Structure and Aggregation in the 1-Alkyl-3-Methylimidazolium Bis(trifluoromethylsulfonyl)imide Ionic Liquid Homologous Series. *J. Phys. Chem. B* **2014**, *118*, 567-576.

(27) Červinka, C.; Pádua, A. A. H.; Fulem, M. Thermodynamic Properties of Selected Homologous Series of Ionic Liquids Calculated Using Molecular Dynamics. *J. Phys. Chem. B* **2016**.

(28) Köddermann, T.; Reith, D.; Ludwig, R. Comparison of Force Fields on the Basis of Various Model Approaches—How To Design the Best Model for the [CnMIM][NTf2] Family of Ionic Liquids. *ChemPhysChem* **2013**, *14*, 3368-3374.

(29) Marekha, B. A.; Koverga, V. A.; Moreau, M.; Kiselev, M.; Takamuku, T.; Kalugin, O. N.; Idrissi, A. Intermolecular interactions, ion solvation, and association in mixtures of 1-n-butyl-3-methylimidazolium hexafluorophosphate and γ-butyrolactone: insights from Raman spectroscopy. *J. Raman Spectrosc.* **2015**, *46*, 339-352.

(30) Giernoth, R.: NMR Spectroscopy in Ionic Liquds. In *Ionic Liquids*; Kirchner, B., Ed.; Topics in Current Chemistry; Springer Berlin Heidelberg, 2010; Vol. 290; pp 263-283.

(31) Damodaran, K.: Recent NMR Studies of Ionic Liquids. In *Annual Reports on NMR Spectroscopy*; Academic Press.

(32) Kiefer, J.: Vibrational Spectroscopy for Studying Hydrogen Bonding in Imidazolium Ionic Liquids and their Mixtures with Cosolvents. In *Hydrogen Bonding and Transfer in the Excited State*; John Wiley & Sons, Ltd, 2010; pp 341-352.

(33) Ramya, K. R.; Kumar, P.; Venkatnathan, A. Molecular Simulations of Anion and Temperature Dependence on Structure and Dynamics of 1-Hexyl-3-methylimidazolium Ionic Liquids. *J. Phys. Chem. B* **2015**, *119*, 14800-14806.

(34) Zhang, S.; Shi, R.; Ma, X.; Lu, L.; He, Y.; Zhang, X.; Wang, Y.; Deng, Y. Intrinsic Electric Fields in Ionic Liquids Determined by Vibrational Stark Effect Spectroscopy and Molecular Dynamics Simulation. *Chem. – Eur. J.* **2012**, *18*, 11904-11908.

(35) Stark, A.; Brehm, M.; Brüssel, M.; Lehmann, S. C.; Pensado, A.; Schöppke, M.; Kirchner, B.: A Theoretical and Experimental Chemist's Joint View on Hydrogen Bonding in Ionic Liquids and Their Binary Mixtures. In *Electronic Effects in Organic Chemistry*; Kirchner, B., Ed.; Topics in Current Chemistry; Springer Berlin Heidelberg, 2014; Vol. 351; pp 149-187.

(36) Weber, H.; Kirchner, B. Complex Structural and Dynamical Interplay of Cyano-Based Ionic Liquids. *J. Phys. Chem. B* **2016**.

(37) Weber, H.; Hollóczki, O.; Pensado, A. S.; Kirchner, B. Side chain fluorination and anion effect on the structure of 1-butyl-3-methylimidazolium ionic liquids. *J. Chem. Phys.* **2013**, *139*, 084502.

(38) Wilson, G. J.; Hollenkamp, A. F.; Pandolfo, A. G. Resolving Ambiguous Naming for an Ionic Liquid Anion. *Chemistry International - Newsmagazine for IUPAC* **2007**, *29*, 16-18.

(39) MacFarlane, D. R.; Tachikawa, N.; Forsyth, M.; Pringle, J. M.; Howlett, P. C.; Elliott, G. D.; Davis, J. H.; Watanabe, M.; Simon, P.; Angell, C. A. Energy applications of ionic liquids. *Energy Environ. Sci.* **2014**, *7*, 232-250.

(40) Bowron, D. T.; D'Agostino, C.; Gladden, L. F.; Hardacre, C.; Holbrey, J. D.; Lagunas, M. C.; McGregor, J.; Mantle, M. D.; Mullan, C. L.; Youngs, T. G. A. Structure and Dynamics of 1-Ethyl-3-methylimidazolium Acetate via Molecular Dynamics and Neutron Diffraction. *J. Phys. Chem. B* **2010**, *114*, 7760-7768.

(41) Kohagen, M.; Brehm, M.; Thar, J.; Zhao, W.; Müller-Plathe, F.; Kirchner, B. Performance of Quantum Chemically Derived Charges and Persistence of Ion Cages in Ionic Liquids. A Molecular Dynamics Simulations Study of 1-*n*-Butyl-3-methylimidazolium Bromide. *J. Phys. Chem. B* **2011**, *115*, 693-702.

(42) Brehm, M.; Weber, H.; Pensado Alfonso, S.; Stark, A.; Kirchner, B.: Liquid Structure and Cluster Formation in Ionic Liquid/Water Mixtures – An Extensive ab initio Molecular Dynamics Study on 1-Ethyl-3-Methylimidazolium Acetate/Water Mixtures – Part 2. In *Zeitschrift für Physikalische Chemie International journal of research in physical chemistry and chemical physics*, 2013; Vol. 227; pp 177.

(43) Vyalov, I.; Kiselev, M.; Tassaing, T.; Soetens, J. C.; Idrissi, A. Investigation of the Local Structure in Sub and Supercritical Ammonia Using the Nearest Neighbor Approach: A Molecular Dynamics Analysis. *J. Phys. Chem. B* **2010**, *114*, 15003-15010.

(44) Idrissi, A.; Gerard, M.; Damay, P.; Kiselev, M.; Puhovsky, Y.; Cinar, E.; Lagant, P.; Vergoten, G. The Effect of Urea on the Structure of Water: A Molecular Dynamics Simulation. *J. Phys. Chem. B* **2010**, *114*, 4731-4738.

(45) Idrissi, A.; Vyalov, I.; Damay, P.; Frolov, A.; Oparin, R.; Kiselev, M. Assessment of the Spatial Distribution in Sub- and Supercritical CO2 Using the Nearest Neighbor Approach: A Molecular Dynamics Analysis. *J. Phys. Chem. B* **2009**, *113*, 15820-15830.

(46) Hardacre, C.; McMath, S. E. J.; Nieuwenhuyzen, M.; Bowron, D. T.; Soper, A. K. Liquid structure of 1, 3-dimethylimidazolium salts. *J. Phys.: Condens. Matter* **2003**, *15*, S159–S166.

(47) Hardacre, C.; Holbrey, J. D.; Mullan, C. L.; Youngs, T. G. A.; Bowron, D. T. Small angle neutron scattering from 1-alkyl-3-methylimidazolium hexafluorophosphate ionic liquids ([$C_n$mim][PF_6], n=4, 6, and 8). *J. Chem. Phys.* **2010**, *133*, 074510.

(48) Deetlefs, M.; Hardacre, C.; Nieuwenhuyzen, M.; Padua, A. A. H.; Sheppard, O.; Soper, A. K. Liquid Structure of the Ionic Liquid 1,3-Dimethylimidazolium Bis{(trifluoromethyl)sulfonyl}amide. *J. Phys. Chem. B* **2006**, *110*, 12055-12061.

(49) Hardacre, C.; Holbrey, J. D.; McMath, S. E. J.; Bowron, D. T.; Soper, A. K. Structure of molten 1,3-dimethylimidazolium chloride using neutron diffraction. *J. Chem. Phys.* **2003**, *118*, 273-278.

(50) Hardacre, C.; Holbrey, J. D.; Nieuwenhuyzen, M.; Youngs, T. G. A. Structure and Solvation in Ionic Liquids. *Acc. Chem. Res.* **2007**, *40*, 1146-1155.

(51) Brussel, M.; Brehm, M.; Pensado, A. S.; Malberg, F.; Ramzan, M.; Stark, A.; Kirchner, B. On the ideality of binary mixtures of ionic liquids. *Phys. Chem. Chem. Phys.* **2012**, *14*, 13204-13215.

(52) Matthews, R. P.; Welton, T.; Hunt, P. A. Hydrogen bonding and [small pi]-[small pi] interactions in imidazolium-chloride ionic liquid clusters. *PCCP* **2015**, *17*, 14437-14453.

(53) Fumino, K.; Peppel, T.; Geppert-Rybczynska, M.; Zaitsau, D. H.; Lehmann, J. K.; Verevkin, S. P.; Kockerling, M.; Ludwig, R. The influence of hydrogen bonding on the physical properties of ionic liquids. *Phys. Chem. Chem. Phys.* **2011**, *13*, 14064-14075.

(54) Roth, C.; Peppel, T.; Fumino, K.; Köckerling, M.; Ludwig, R. The Importance of Hydrogen Bonds for the Structure of Ionic Liquids: Single-Crystal X-ray Diffraction and Transmission and Attenuated Total Reflection Spectroscopy in the Terahertz Region. *Angew. Chem., Int. Ed.* **2010**, *49*, 10221-10224.

(55) Gilli, G.; Gilli, P.: *The Nature of the Hydrogen Bond: Outline of a Comprehensive Hydrogen Bond Theory*; Oxford University Press, 2009.

(56) Matthews, R. P.; Ashworth, C.; Tom, W.; Patricia, A. H. The impact of anion electronic structure: similarities and differences in imidazolium based ionic liquids. *J. Phys.: Condens. Matter* **2014**, *26*, 284112.

(57) Khrizman, A.; Cheng, H. Y.; Bottini, G.; Moyna, G. Observation of Aliphatic C-H···X Hydrogen Bonds in Imidazolium Ionic Liquids. *Chem. Commun.* **2015**, *51*, 3193-3195.

(58) Marekha, B. A.; Kalugin, O. N.; Bria, M.; Buchner, R.; Idrissi, A. Translational Diffusion in Mixtures of Imidazolium ILs with Polar Aprotic Molecular Solvents. *J. Phys. Chem. B* **2014**, *118*, 5509-5517.

(59) Russina, O.; Triolo, A. New experimental evidence supporting the mesoscopic segregation model in room temperature ionic liquids. *Faraday Discuss.* **2012**, *154*, 97-109.

(60) Russina, O.; Triolo, A.; Gontrani, L.; Caminiti, R. Mesoscopic Structural Heterogeneities in Room-Temperature Ionic Liquids. *J. Phys. Chem. Lett.* **2011**, *3*, 27-33.

(61) Avent, A. G.; Chaloner, P. A.; Day, M. P.; Seddon, K. R.; Welton, T. Evidence for hydrogen bonding in solutions of 1-ethyl-3-methylimidazolium halides, and its implications for room-temperature halogenoaluminate(III) ionic liquids. *J. Chem. Soc., Dalton Trans.* **1994**, 3405-3413.

(62) Bonhôte, P.; Dias, A.-P.; Papageorgiou, N.; Kalyanasundaram, K.; Grätzel, M. Hydrophobic, Highly Conductive Ambient-Temperature Molten Salts. *Inorg. Chem.* **1996**, *35*, 1168-1178.

(63) Mele, A.; Tran, C. D.; De Paoli Lacerda, S. H. The Structure of a Room-Temperature Ionic Liquid with and without Trace Amounts of Water: The Role of C-H···O and C-H···F Interactions in 1-n-Butyl-3-Methylimidazolium Tetrafluoroborate. *Angew. Chem., Int. Ed.* **2003**, *42*, 4364-4366.

(64) Zahn, S.; Brehm, M.; Brüssel, M.; Hollóczki, O.; Kohagen, M.; Lehmann, S.; Malberg, F.; Pensado, A. S.; Schöppke, M.; Weber, H.; Kirchner, B. Understanding ionic liquids from theoretical methods. *J. Mol. Liq.* **2014**, *192*, 71-76.

(65) Choudhury, A. R.; Winterton, N.; Steiner, A.; Cooper, A. I.; Johnson, K. A. In situ Crystallization of Low-Melting Ionic Liquids. *J. Am. Chem. Soc.* **2005**, *127*, 16792-16793.

(66) Hamaguchi, H.-O.; Ozawa, R.: Structure of Ionic Liquids and Ionic Liquid Compounds: Are Ionic Liquids Genuine Liquids in the Conventional Sense? In *Advances in Chemical Physics*; John Wiley & Sons, Inc., 2005; pp 85-104.

(67) Izgorodina, E. I.; Rigby, J.; MacFarlane, D. R. Large-scale ab initio calculations of archetypical ionic liquids. *Chem. Commun.* **2012**, *48*, 1493-1495.

(68) Cabaço, M. I.; Besnard, M.; Danten, Y.; Coutinho, J. A. P. Solubility of CO_2 in 1-Butyl-3-methyl-imidazolium-trifluoro Acetate Ionic Liquid Studied by Raman Spectroscopy and DFT Investigations. *J. Phys. Chem. B* **2011**, *115*, 3538-3550.

(69) Danten, Y.; Cabaço, M. I.; Besnard, M. Interaction of water diluted in 1-butyl-3-methyl imidazolium ionic liquids by vibrational spectroscopy modeling. *J. Mol. Liq.* **2010**, *153*, 57-66.

(70) Pensado, A. S.; Brehm, M.; Thar, J.; Seitsonen, A. P.; Kirchner, B. Effect of Dispersion on the Structure and Dynamics of the Ionic Liquid 1-Ethyl-3-methylimidazolium Thiocyanate. *ChemPhysChem* **2012**, *13*, 1845-1853.

(71) Wendler, K.; Zahn, S.; Dommert, F.; Berger, R.; Holm, C.; Kirchner, B.; Delle Site, L. Locality and Fluctuations: Trends in Imidazolium-Based Ionic Liquids and Beyond. *J. Chem. Theory Comput.* **2011**, *7*, 3040-3044.

Chapter 4. Local structure organization and orientational aspects in molecular solvents

The material presented in this chapter forms the basis of publication

Koverga, V. A.; Korsun, O. M.; Kalugin, O. N.; Marekha, B. A.; Idrissi, A. A new potential model for acetonitrile: insight into the local structure organization. **J. Mol. Liquids**, 2017, 233, 251-261

Koverga, V.A., Kalugin O. N.; Idrissi, A. Local structure organization and orientational aspects in γ-butyrolactone and propylene carbonate: molecular dynamics simulation. Submitted to **J. Phys. Chem. B**

The local structure of neat liquid acetonitrile (AN), γ-butyrolactone (GBL) and propylene carbonate (PC) was analyzed in a framework of the nearest neighbor approach. The closest neighbors have a dominant antiparallel dipoles orientation with respect to a reference one, while for the further nearest neighbors perpendicular and parallel mutual orientation is observed.

The nearest neighbors approach in combination with angular distribution functions was used for the estimation of the Kirkwood factor. Our results shows that in order to reproduce the corresponding experimental values derived in the framework of the Onsager-Kirkwood-Fröhlich theory, it is necessary to take in account the mutual orientation of the 5~6 nearest neighbors.

The analysis of H-bonding interactions in AN, GBL and PC shows the presence of the weak hydrogen bonds between the two closest molecules.

4.1. Introduction

A set of complementary experimental techniques such as spectroscopic (IR, Raman, X-ray, neutron scattering, NMR *etc.*) and/or dielectric relaxation enables to inspect the microscopic structure organization in these dipolar. Indeed, by studying the so-called noncoincidence effect (NCE),[1] it was found that dipolar solvent orientation in aggregates of aprotic dipolar solvents (particularly, in carbonyl[2-8] and sulfoxide[9-12] compounds, where NCE effect is more pronounced[12]) is typically characterized by the favorable antiparallel dipolar orientation that give rises to a positive NCE value. Similar observations on the orientation in these dipolar liquids were reached using X-ray and neutron diffraction measurements as well.[13-19]

The numerous studies focusing on the dielectric properties of dipolar solvents such as, acetonitrile,[20-36] dimethylsulfoxide,[21,37-41] ethylene[42,43] and propylene[5,41,42,44,45] carbonate, provide notable discrepancies in the assessment of the type of dipolar orientation derived through the Kirkwood correlation factor.[46] The most prominent example was considered by Świergiel *et al.*[47-49] in PC. Depending on the selected values of the high-frequency permittivity, ε_∞, two Kirkwood factor values at room temperature were obtained. The first value equals 1.23 (indicating a collinear dipolar association or a "head-to-tail" geometry) and the second one equals 0.57[41] (indicating rather strong association with antiparallel oriented molecular dipoles).

Considering the short-order organization in neat dipolar liquids, the several types of arrangements were proposed. Commonly the antiparallel configuration (stacked to each other in case of cyclic solvents) formed by strong dipole-dipole interactions was shown to occur and it is stabilized by the intermolecular H-bonding formation between the H-bond accepting atom of one molecule and the hydrogen atoms of the $C{-}H^i$ groups of another one. Thus, the numerous quantum-chemical calculations point out that the relative stability of the AN aggregates may be explained on the basis of H-bond intermolecular $C{-}H\cdots N$ interactions.[50-54] Based on these calculations the two types of arrangement was found with antiparallel oriented dipoles and "head-to-tail" configurations with existing H-bonds. The issue of mutual arrangement of AN molecules also has been addressed using MD simulations by following the distribution of the angles between the molecular dipoles as a function of the distance between the molecular centers of mass.[55-59] However, the reliability of the simulations to reproduce a wide set of experimental properties and then to get a microscopic level insight largely depends on the accuracy of the force field model used.

However, there are some discrepancies among the configurations revealed by the quantum-chemical and those inferred from MD simulation studies on cyclic solvents such as GBL and PC. Indeed, using quantum-chemical calculations Aparicio and Alcalde[60] found that the cyclic in-plane structure of GBL is energetically more favorable than the antiparallel one, however the existence of such configuration has been refuted later in the analysis by MD simulation results. Similar conclusions were drawn by Vaz and Ribeiro-Carlo[61] who suggested the occurrence of the rotated stacked and the cyclic in-plane configurations in addition to the antiparallel one. Furthermore, Hesse and Suhm[62] reported a series of stacked rotated configurations of GBL with an asymmetric H-bonded monomers involving both the carbonyl and the ester oxygen atoms. Combining Raman spectroscopy and quantum calculations, similar structures also were reported in our previous study on the mixtures of GBL with $BmimPF_6$.[63] MD simulation study of the pure GBL performed by Masia and Rey[64] suggested that there is no preferential orientation of molecular dipoles. This interpretation was based on the fact that the radial distribution functions between the carbonyl groups atoms have no maxima.

As for PC, owing to its chirality, it is capable to form two main groups of configurations, homochiral and heterochiral.[65] The first group includes the interactions between the identical types of isomers, e.g *RR*- or *SS*-configuration, whereas the latter one implies configuration formed by *R*- and *S*-isomer. Wang and Balbuena[66] showed that the antiparallel oriented PC molecules are associated mainly through the H-bonding interactions between the oxygen atom of carbonyl group and hydrogen of CH group, whereas Silva and Freitas[67] discover another type of homochiral antiparallel stacked configuration with a contact between carbonyl oxygen and the CH_3 group. The latter, however, noted that antiparallel orientation of the dipoles is not predominant in the liquid PC and such arrangement corresponds to the most energetically favorable in the gas phase. Kollipost *et al.*[65] also confirm the antiparallel alignment of the molecular dipoles in PC with a favorable heterochiral configuration that involves both molecules in the equatorial orientation. Soetens *et al.*[13] using MD simulation also found the favorable antiparallel orientation of molecular dipoles. This result later was confirmed by You *et al.*[68] However, recent computational study[69] on PC suggests an appreciable contribution of parallel oriented molecular configurations along with antiparallel ones. Combining neutrons scattering experiment and the Empirical Potential Structure Refinement (EPSR) approach it was concluded that PC exhibits a strong orientational correlation in the liquid state generated by C−O···H−C "head-to-tail" H-bonding forming chains [70]. These orientations are similar to those suggested for GBL molecules based on the experimental measurements.[71]. Finally, it should be mentioned that as a consequence of these dipole-dipole interactions, many experimental[60-63,65,71] and theoretical [60-67,70] studies on GBL/PC point out to their self-association.

These results point out to the fact that the local structure (radial and orientational distribution) in dipolar liquids is the results of a balance between the dipole-dipole interactions, the H-bonding and the interactions between the ring planes, particularly for GBL and PC (designated here as stacking interactions). The accurate description of the dipole orientation requires to take in account collective effects that are lacking in quantum calculations where the probable orientation is associated with the minimum energy of a dimer or at best a small size cluster of dipolar molecules. Therefore, we consider in this work to analyze the effect of dipole-dipole, H-bonding and stacking interactions on the resultant local structure in these dipolar liquids. The description of the molecular local structure is very often based solely on the pair RDFs. However, these RDFs show little detail as they sample all the possible orientations between molecules. We then used the approach of the nearest neighbor radial and orientation distribution that helps to unambiguously describe the local arrangement between molecules.[72-81]

Here we present a systematic MD simulation study on the local microscopic structure of the three molecular solvents as AN, GBL and PC. By studying different radial and various angular orientation describing the above/below, the stacking and the dipole-dipole orientations, we seek to systematize the previous results on these systems and quantify the contribution of dipole-dipole and H-bonding interactions on the resultant local arrangement.

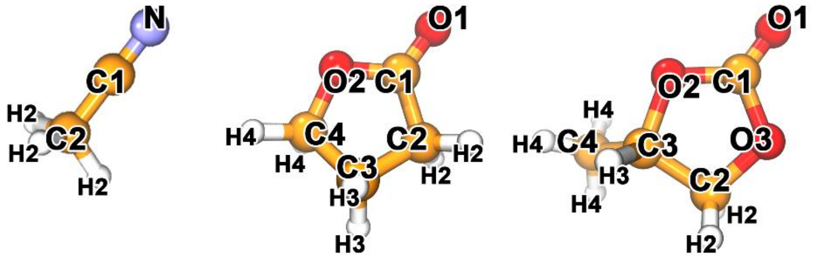

Figure 4.1. Molecular structures of AN, GBL and PC with atomic labeling used for the analysis of the structure properties.

4.2. Results and discussion

4.2.1 Radial distribution function

In a first step on the analysis of the local structure in the studied dipolar liquids, we calculated the RDFs between the H-bond accepting atoms (N for AN, O^1 for GBL and PC) of the reference molecule and the corresponding hydrogens/carbons of the observed one. Furthermore, we also analyzed RDFs between the corresponding geometrical centers of the reference and observed molecules ($C^1 \cdots C^1$ for AN, and CoR – center of the ring – for GBL and PC). As it shown in Figure 4.2, there is a strong similarity in the RDFs between the three studied systems. The $O^1 \cdots H^i$ (i = 2, 3, 4) RDFs have a strong and narrow first peak at almost the same distances at *ca.* 0.23-0.26 nm for both GBL and PC molecules, while for AN in $N \cdots H^2$ RDF this peak located at slightly higher distances around

0.28 nm. The occurrence of these peaks is interpreted as H-bonding formation between these atoms, where for AN the strength of H-bonding interactions is slightly weaker than in GBL and PC. The shape of these RDFs and the positions of the maxima are in excellent agreement with the previous computational studies.[50,56,58,60,62,64-68,70,82-88] We also found some discrepancy in the shape and positions of the $O^1\cdots H^i$ peaks in our study with those reported by Masia and Rey[64] with numerous shoulder and humps. We suppose that such a difference may be connected to significant contribution of the intramolecular interactions between the corresponding pairs, which were erroneously taken into account in the cited work.

The shape of the first peak in $N\cdots C^1$ and $O^1\cdots C^1$ and RDFs has a complex structure with a shoulders and humps compared with other $N\cdots C^2$ and $O^1\cdots C^{3-4}$ RDFs. These features indicate that the nitrogen (AN) or carbonyl oxygens (GBL and PC) in the reference molecule and C^1 in observed one tend to stay away from each other, which is attributed by their specific dipolar orientation. From the other hand, the similarity in the behavior of the $N\cdots C^2$ and $O^1\cdots C^{3-4}$ RDFs at the same distances around 0.32-0.34 nm, may be correlated with the behavior of the $N\cdots H^2$ and $O^1\cdots H^{3-4}$ RDFs. For both liquids, integrating the peaks in the $N\cdots C^i$ and $O^1\cdots C^i$ RDFs up to their first minima yields consistently a number of approximately 6 neighbors in each case.

Finally, we begin to analyze the RDFs between the geometrical centers of AN ($C^1\cdots C^1$), GBL and PC (CoR⋯CoR). The position of the first peak and the first minimum in AN found to be located at shorter distances (0.47-0.50 and 0.64 nm, respectively) compared with GBL and PC. For both cyclic solvents located at the same distances with a well-defined first coordination shell, featuring a maximum at 0.54 nm and a first minimum at 0.74 nm. These values are similar to those previously obtained for tetrahydrofuran molecule.[89,90] However, a shoulder appears clearly in PC while it is not resolved in the first peak. This may be assigned to different stacking structures in the cyclic molecules. The coordination numbers for $C^1\cdots C^1$ and CoR⋯CoR RDFs at the first minimum is essentially identical and give approximately 12 neighbors.

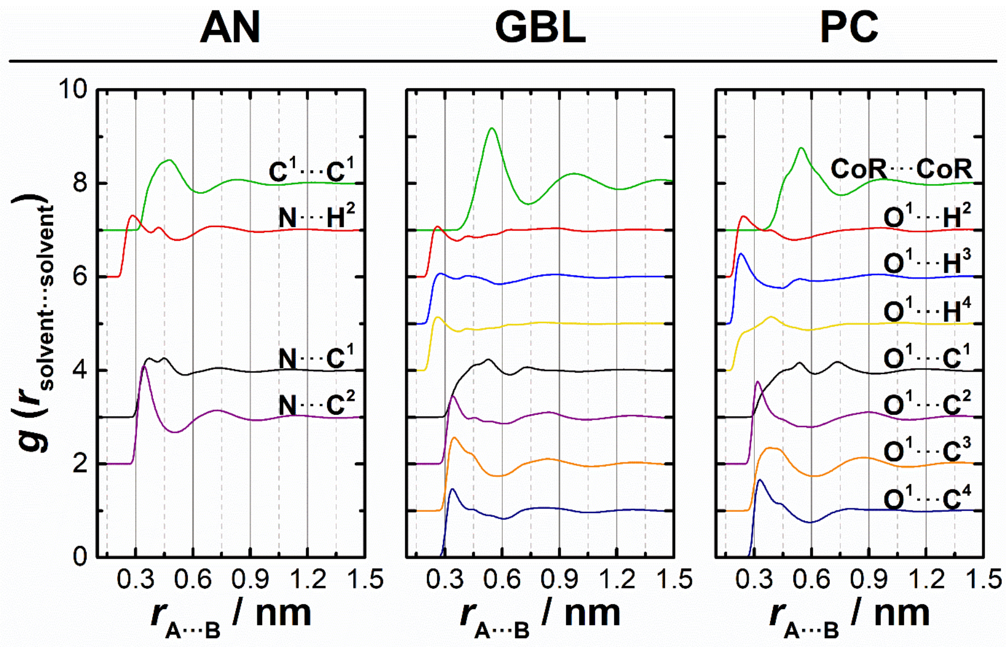

Figure 4.2. Site-site radial distribution functions of pure AN, GBL and PC between the geometrical centers ($C^1 \cdots C^1$ for AN, and CoR for GBL and PC) and between the H-bonds accepting atom of the reference molecule (N for AN, O^1 for GBL and PC) and corresponding C^i or H^i of the observed one calculated at 298.15 K, where $i = 2, 3, 4$.

4.2.2 Spatial distribution function

In order to get a general view on the spatial distribution around a reference molecule, we calculated the spatial distribution functions (SDFs). In Figure 4.3 the SDFs represents a three-dimensional map of the density distribution calculated for the H-bond accepting atoms (N of AN, O^1 in GBL and PC designated as blue and red, respectively) and geometrical centers (C^1 of AN, CoR of GBL and PC designated as gray) around the reference solvent molecules. In case of AN, the wide isosurface of the nitrogen has a belt shape around the CH_3 group with some distribution probability along the C≡N axis. Such space arrangement of the observed nitrogen may indicate the formation of H-bonding interactions by the antiparallel aligned molecules and on the “head-to-tail” manner as well. For cyclic GBL and PC molecules rather different situation observed for the distribution of the carbonyl oxygen. For the GBL the strong localization of O^1 atom observed above and below the reference $C–H^{2–3}$ group, whereas the respective distribution for PC form an approximate hemisphere encompassing the $C–H^{2/4}$. Similar to AN, these results correlating with the fact of H-bonding formation in GBL and PC. Apart the above/below configuration around the reference molecule in PC the “head-to-tail” orientation is also possible.

The arrangement of the carbonyl oxygen’s in GBL and PC is consistent with distribution of the respective geometrical centers, however the in-plane localization is quite weak compared with those arranged above and below the reference PC. The broader CoR distribution around the reference GBL is also diffuse at the in-plane position and more localized above/below, which may point to a similar packing ordering of the GBL and PC molecules in bulk liquid. As for the distribution of AN molecules, the resulting pattern is identical to the abovementioned distribution of the nitrogen. This arrangement confirms our suggestion concerning coexistence of the two possible configurations in bulk AN with antiparallel and “head-to-tail” orientation of the molecules.

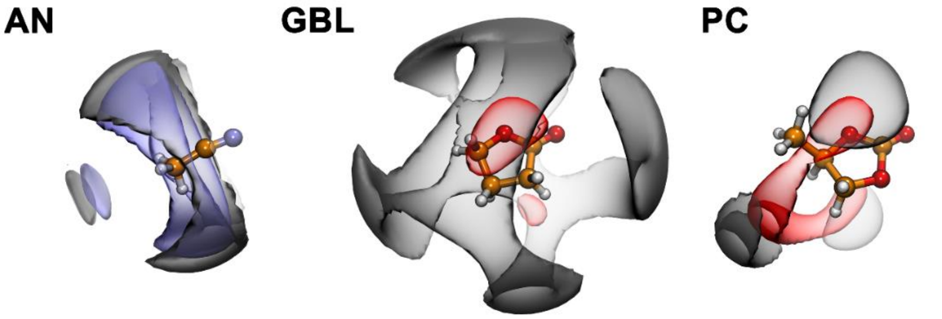

Figure 4.3. Spatial distribution functions with 30% density probability of the H-bond accepting atoms (N of AN, O^1 in GBL and PC designated as blue and red, respectively) and geometrical centers (C^1 of AN, CoR of GBL and PC designated as gray) around the reference AN, GBL and PC.

4.2.3 Spatial arrangement of the solvent molecules

In order to study the orientational aspects in more detail, we have decided to calculate several combined angular and distance distributions where the angles are defined in Figure 4.4, while the distance conditions is that between a reference center of geometry (C^1 of AN, CoR of GBL and PC) and the several neighboring molecules corresponding to the number of coordinated molecules, *n*, by these sites.

The first investigated angle, designated here as ψ is that between the vectors along C=O (GBL and PC) and C≡N (AN) bonds in the reference and observed molecules. The ψ values close to 0 and 180 degrees, indicate a parallel and/or antiparallel orientation, respectively. Similarly, a T-shaped arrangement of the observed nearest neighboring molecules corresponds to a ψ value around 90 degrees.

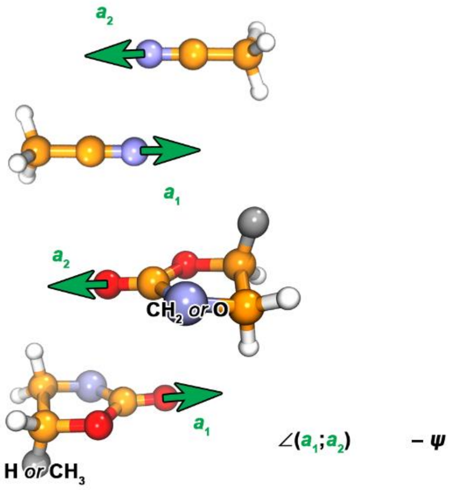

Figure 4.4. Schematic representation of the GBL/PC and AN dimer with geometric characteristics used for description of the dipolar orientation of the molecules in neat liquid. The *blue* atoms on GBL/PC corresponds to methylene group (GBL) or oxygen (PC); *grey* – to hydrogen (GBL) or methyl group (PC), respectively.

As can be seen in Figure 4.5 for the case of AN the corresponding ADFs for the first and second neighbors the angle ψ have the most probable values between 120 and 180 degrees, indicating a strong preferences for the antiparallel orientation of C≡N bonds. The distribution probability of angle ψ here is much more localized compared with GBL and PC that may be caused by the stronger dipolar interactions between the small linear AN molecules. Nevertheless, as a comparison with that of the first neighbors, the intensity of the CDFs of the further ones is very weak and it is associated with undefined angle values. This indicates that several mutual orientations coexist for these neighbors. The mutual orientation between a reference AN molecule and its third and fourth neighbors is clearly parallel. A contribution of a T-shaped orientation coexist with the parallel one for the *n* = 5–6 neighbors. Starting from n = 11, the mutual orientation becomes random with respect to the ψ angle.

For GBL and PC the values of the probability distributions of angle ψ indicate that in both systems, with respect to a reference molecule, the first neighbor is characterized by the preferential antiparallel orientation. The antiparallel dipole orientation is mote pronounced in GBL than in PC while in both liquids, the parallel orientation of C=O also occurs however with less probability than the antiparallel one. In both systems, the staking orientation is random for the second neighbor and a transition to a T-shape orientation is observed for the third neighbor while it becomes gradually random for farther neighbors. Both a distorted antiparallel and parallel orientations occurs for the second neighbor and when considering farther neighbors these orientations become loose. Finally, all these orientations become almost random for farther neighbors.

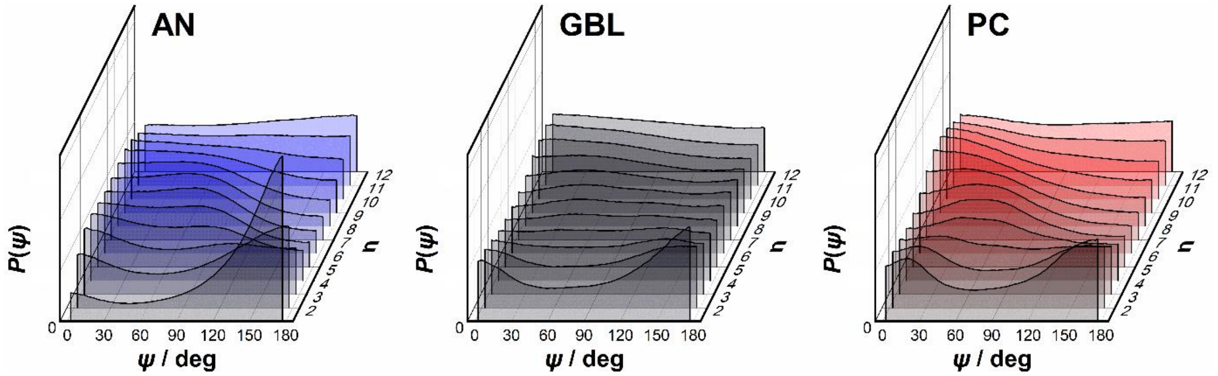

Figure 4.5. Angular distribution functions for n nearest neighbors for the angle between two unit vectors along C≡N and C=O bond ψ calculated for AN, GBL and PC.

For GBL and PC, due to their cyclic structure, it is possible to estimate additionally the relative arrangement of the ring planes with respect to the reference molecule. In this regard we have analyzed the two representative angles using the same distances conditions as in the previous case for angle ψ. The first investigated angle, designated here as α (see Figure 4.6 for the scheme), is the angle between the normal vector of the GBL/PC ring plane of the reference molecule and the distance vector connecting the ring centers of the reference and observed molecules. Thus, positions above/below the reference molecule would correspond to α angle around 0 and 180 degrees, while perfect in-plane arrangement of the observed molecules would contribute to the α values close to 90 degrees. The second investigated angle is β formed by the normal vectors of the ring planes between the reference and observed molecules. As in the previous case a perfectly plane-parallel arrangement corresponds to β values of 0 and 180 degrees, whereas the values around 90 degrees are indicative of a T-shaped relative arrangement of the two rings.

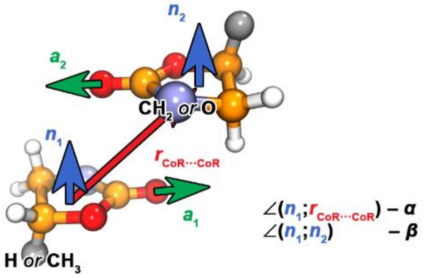

Figure 4.6. Schematic representation of the GBL/PC dimer with geometric characteristics used for description of the mutual orientation of the molecules in neat liquid. The *blue* atoms corresponds to methylene group (GBL) or oxygen (PC); *grey* – to hydrogen (GBL) or methyl group (PC), respectively.

As can be seen from the Figure 4.7, PC molecules tend to occupy the perfect above/below position in the bulk system, while for GBL the corresponding probabilities are notably lower. Moreover, the first peak denoting below position is displaced to the higher angular values that could be interpreted as possible near-plane orientation. From the other side, considering the first neighboring GBL/PC molecule, the tendency to below position preference is much weaker in GBL, and the corresponding peaks are much broader along the angular variable than those in PC. For the distant neighbors the intensities corresponding above/below positions become weaker, and the angular distributions much broader up to the third neighbor. Starting from the fourth nearest neighbor a contribution of approximately in-plane orientation equally coexist with those located above/below. The latter ones, however are more diffuse starting from the sixth neighbors, while the in-plane arrangement becomes a dominant one. It should be noted, that for PC molecules such transition occurred from the slightly below shifted plane orientation, while for GBL contribution from above/below orientation was equivalent.

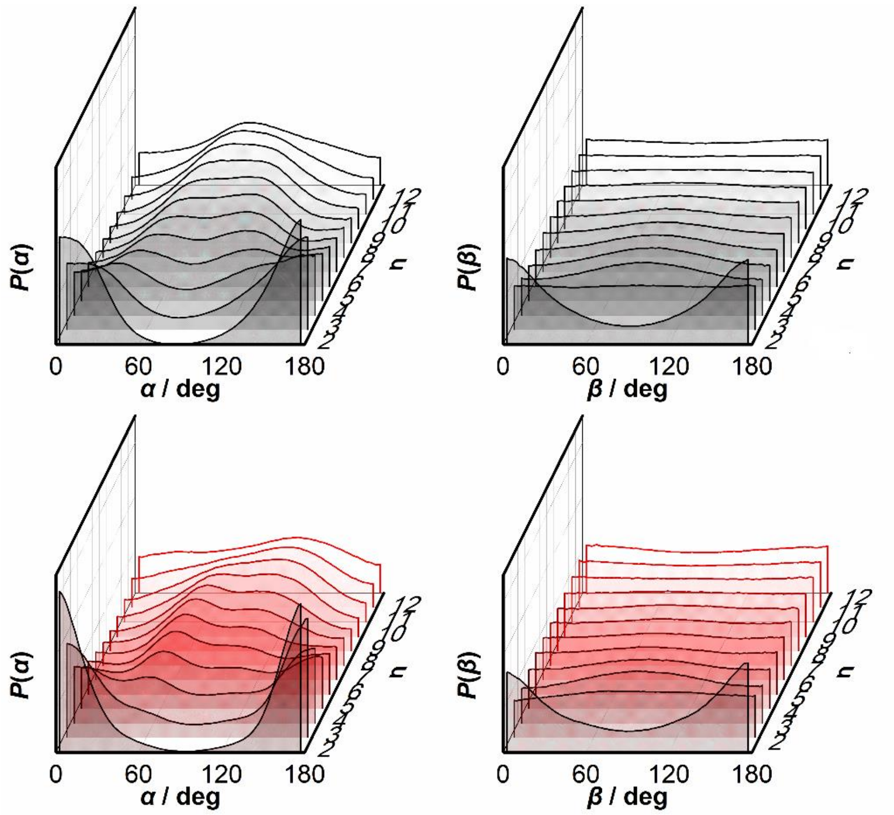

Figure 4.7. Angular distribution functions for *n* nearest neighbors for the two representative angles α (*left*) and β (*right*) calculated for GBL (*top*) and PC (*bottom*).

As it follows from the Figure 4.7 the strong above/below parallel alignment with the same probability of GBL/PC ring planes is preferential for in the bulk systems as well as for the first neighboring molecule. Starting from the second neighbor of GBL the contribution of T-shaped orientation appears along with plane-parallel arrangement up to the twelfth neighbor where the mutual orientation becomes random with respect to the reference molecule. For the third neighbor such orientation become more favorable and then smoothly decay up to the ninth neighbor, and similarly to second neighbor become random oriented with respect to the reference molecule. Thus, considered dimeric configuration in both molecules, the above/below plane-parallel arrangement of the molecules is the dominant one similar to abovementioned quantum-chemical investigations. From the other hand, such configuration undergoes the significant changes for the distant neighbors, where the T-lake in-plane structural interaction motif is a dominant one.

In a framework of nearest neighbors approach it is also possible to estimate the behavior of the average distance and its standard deviation from the individual RDFs with respect to the number of neighboring molecules between the geometrical centers (C^1 of AN, CoR of GBL and PC) of the reference molecule and the observed ones. As it clearly seen from the Figure 4.8 the average distance increasing roughly linearly with the neighbor's order. The average distance for the closest neighbors between GBL and PC is quite close to each other, while they are notably higher compared with those in AN. Until the fourth neighbor the average distance between CoRs for GBL and PC is almost identical, while for distant molecules the average distances for GBL is notably lower compared with those for PC.

Another important parameter is the distance variance fluctuations, which is characterized by a complex behavior associated with particular organization of the local structure. The behavior of standard deviation with respect to the number of neighbors has a wave-like shape with a minimum at n = 4-6 and maximum at n = 11-12, where the distance deviation follow the sequence PC > AN > GBL. From the previous studies[91,92] it is known that existence of such maximum indicates that the molecules occupying this position exhibit important "fluctuations" in their radial distances and defines the spatial border of the first coordination shell coinciding for all the studied liquids, while the nature of the minimum is still ambiguous. We assume that this minimum can be assigned to a specific transition state when the molecules change their original orientation to another one Indeed, tracing the evolution of representative angles reporting the relative orientation between the reference and neighboring molecules, one can see a strong correlation between angle ψ and behavior of distance fluctuations, where ψ after reaching the minimum, of fluctuations increase the contribution of parallel alignment molecules.

Along with this such reorientation of C≡N-group in AN and C=O-groups in GBL and PC entails rearrangement of the molecules (ring planes positions in case of cyclic solvents) from the antiparallel to “head-to-tail” (in-plane) arranged. Moreover, a rather high dipole moment in PC promotes the strongest effect on the neighboring molecules that reflects in the sharpest minimum in distance fluctuations compared with smooth decay in AN and GBL, and the respective configuration arranged in less fixed distances.

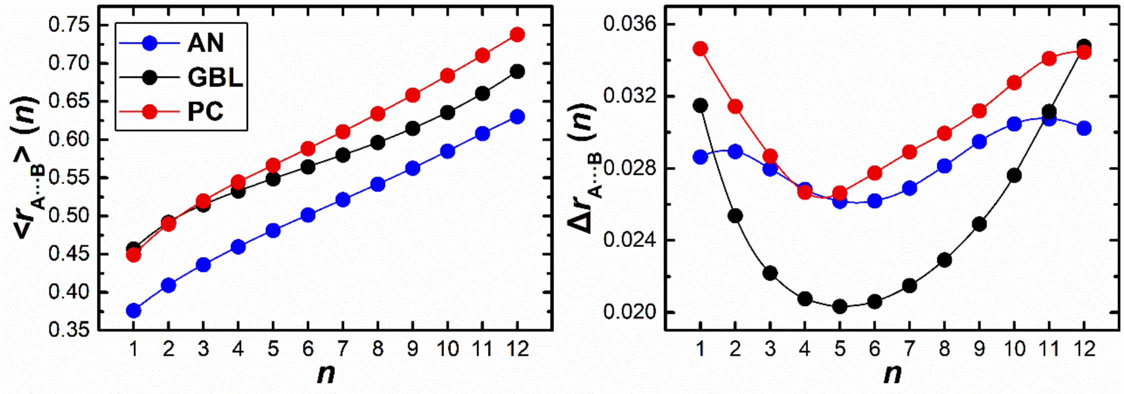

Figure 4.8. Average distance (*left*) and its standard deviation (*right*) with respect to the number of nearest neighbors between the geometrical centers (C^1 of AN, CoR of GBL and PC) of reference and observed AN, GBL and PC.

4.2.4 Manifestation of the molecular orientation in the dielectric properties

In the framework of the Onsager-Kirkwood-Fröhlich (OKF) theory[93] the experimental value of the static dielectric constant, ε, can be used for estimation of the Kirkwood correlation factor, g_K, that reflects the spatial correlations (mutual orientation) of the dipoles of the nearest neighbors around the chosen molecule. This is given by the relation:

$$g_K = 1 + z\langle\cos\psi\rangle, \qquad (3.1)$$

where z is the number of the considered nearest neighbor molecules around a given central molecule and $\langle\cos\psi\rangle$ is the average cosine of the angle between the dipole moment of the central molecule and those of the neighboring molecules. The case of g_K < 1 corresponds to the antiparallel dipolar correlation while the case of g_K > 1 reflects the parallel correlation of the neighboring dipoles. The mutual orientation between molecules has a complex effect on the values of both the apparent molecular dipole moment in the liquid phase and the dielectric constant.

Unfortunately, there is no clear understanding on how one can estimate the value of *z*. In the case of water, *z* was chosen equal to 4 based on the tetrahedral distribution of water. By considering the mutual orientation of the four neighbors with respect to a reference water molecule, it was possible to estimate the dielectric constant of water.[94] In the case of AN, the local environment of AN as well as other polar aprotic solvents is mainly determined by the preferential antiparallel dipole orientation,[16-23] however, it was noted that such orientation is inherent just for the *few* nearest neighbors.[55,56]

Following the nearest neighbor approach, we offer here a rigorous way to calculate the Kirkwood correlation factor g_K . Indeed, we used the ADFs shown in Fgure 4.4 for this purpose since the $\mathbf{a}_1$ and $\mathbf{a}_2$ unit vectors coincide with the direction of the dipole moments of the chosen neighbors. So, the Equation 1 can be expressed in the form

$$g_K(n) = 1 + \sum_{i=1}^{n} \langle \cos\psi \rangle_i \tag{3.2}$$

where the *i* index corresponds to the i^{th} neighbor and $\langle \cos\psi \rangle_i$ can be calculated by averaging all the accessible values of the $\cos\psi_i$ taking in account all the i^{th} first neighbors around the reference one.

The calculated values of the Kirkwood factor as a function of the mean position of each of the nearest neighbor taken into account for its calculation along with correspondent $\langle \cos\psi \rangle_i$ value at 298 K is shown in Figure 4.9. The horizontal lines correspond to the experimental values of g_K that were obtained from the dielectric experiment.[20-23] For AN it is evident that g_K values are below 1 when considering up to the 7th nearest neighbors. It goes through a minimum indicating that the two first neighbors have a strong tendency towards the antiparallel orientation. Figure 4.9 clearly demonstrates that the dipole correlation sphere of a chosen AN molecule in terms of the OKF is restricted by ~0.48-0.5 nm and includes ~5-6 nearest neighbors.

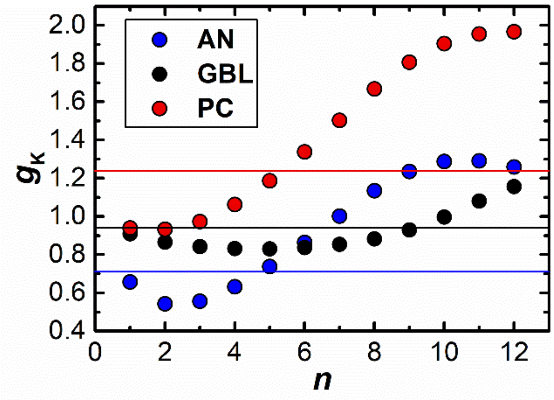

Figure 4.9. Behavior of Kirkwood correlation factor with respect to the neighbors order *n* between centers of geometry (C^1 in AN, COR in GBL and PC) of reference molecules and its nearest neighbors for AN, GBL and PC. Solid lines corresponds to experimental values of Kirkwood correlation factor for AN, GBL and PC, respectively.

As for GBL and PC, when considering only the first neighbor, the Kirkwood factor value is slightly less than one, and is the result of the averaging between the antiparallel configuration occurring with highest probability that gives negative contribution and the parallel one occurring with low probability that gives positive contribution to the final value of g_K ($n = 1$). As a consequence, the increase of g_K(n) values is an indication of the dominance of parallel orientation of the neighbor molecules in the case of PC while the (distorted) antiparallel and parallel ones coexist in GBL (with a dominance of the first one) for the $n < 8$ and for further increase of *n*, the parallel configuration start to dominate. The stronger dominance of the dipole-dipole antiparallel configuration in GBL than in PC indicates that in GBL liquid the packing is more important.

4.2.5 H-bond interactions

Although the dipole-dipole interactions are major contributors to the organization of the local structure, the weak hydrogen bond interactions may a play role in the local structure of the studied solvents. Indeed, the analysis of the RDFs shown in Figure 4.2, indicates that the distance between nitrogen and/or carbonyl oxygen and the respective hydrogen atoms is the shortest among all the possible pair distributions. This indicates a possible formation of weak hydrogen bond between the two atoms. The H-bonding formation can be easily described through the combined distribution function (CDF) that correlating the H-bond pseudo-valence angle C^i–$H^i\cdots Y$ and the corresponding H-bonding distance between the hydrogen H^i of the reference molecule and neighboring atom Y, where Y corresponds to the H-bond accepting atom of the solvent N in AN and O^1 in GBL and PC. From the Figure 4.10 it can be seen that all the studied liquids are able to form weak H-bonding at 0.20-0.27 nm. However, the distributions in PC along angular variable considerably vary with those in GBL and AN, and between each other. For the GBL the corresponding H-bonding angle is slightly bent and is common for all the positions, whereas in PC the H-bonding angle close to the linear arrangement. The exception is interaction at H^3 site which is notably weaker bonded compared with other sites. This indicates that the C–H^3 group is less spatially accessible for the interactions compared with other ones. The obtained results are in line with previous quantum-chemical calculations [50-54] and experimental studies[95] on the considered liquids.

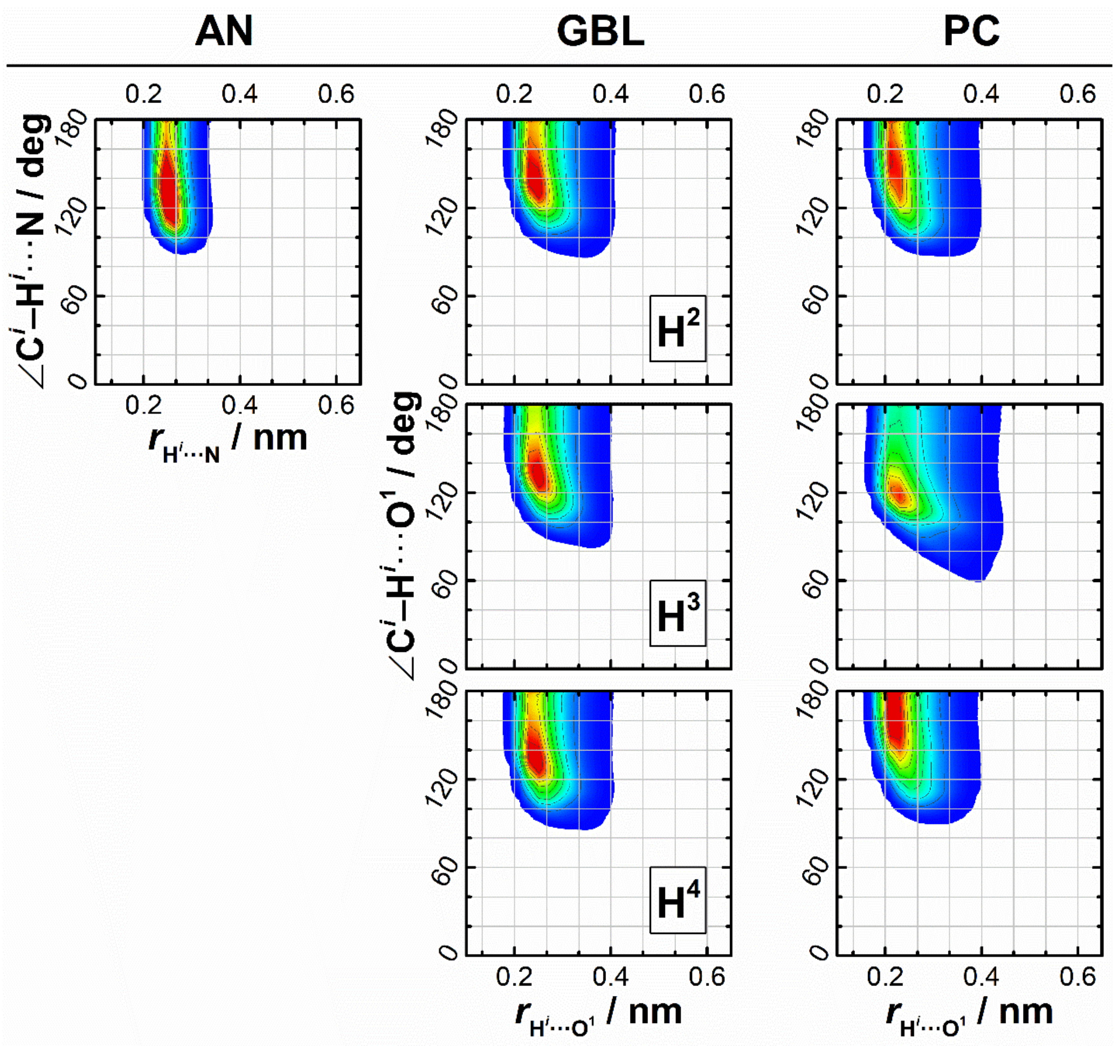

Figure 4.10. Combined distribution functions relating the corresponding pseudo-valence angle of H-bonding interaction and the distance between the hydrogen H^{i} atoms of the reference molecule and the nearest neighboring H-bond accepting atom Y for AN, GBL and PC, where Y corresponds to N in AN, O^{1} in GBL and PC.

In addition to assess the extent of this H-bonding, similar to pure ILs, we analyzed the dependence of two distances characteristic of hydrogen bonding, the first one is that between H$^{i}\cdots$Y, and the distance between C$^{i}\cdots$Y, where *i* indicates the position of the C and H atoms and *i* is equal to 2, 3 and 4. In the case of a linear hydrogen bonding and then a strong one, the C$^{i}\cdots$Y distance will be equal to the sum of C^{i}- H^{i} intramolecular distance and of the intermolecular H$^{i}\cdots$Y distance . This case corresponds to a strong hydrogen bonding interactions. In the case of a bent hydrogen bonding, with a given θ angle, the C$^{i}\cdots$O^{1} distance is shorter and can be estimated using the law of cosines. We calculated these distances using the nearest neighbor approach, and their behavior is illustrated in Figure 4.11. The comparison between the calculated values and those obtained in the case of a linear hydrogen bonding geometry indicates clearly that the hydrogen bond interactions in the three liquids are very weak, and particularly they are the weakest in GBL.

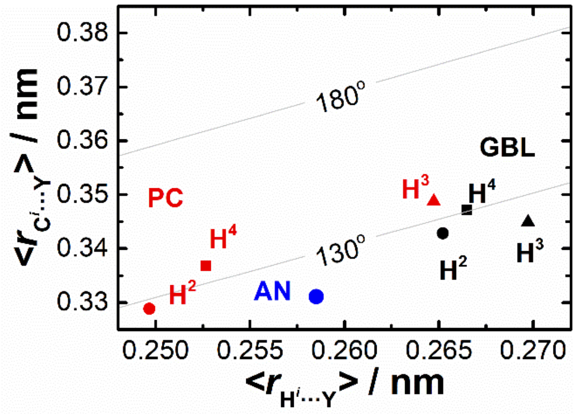

Figure 4.11. Average distances, $C^i \cdots Y$ and $H^i \cdots Y$, representing H-bonding geometry between the AN, GBL and PC hydrogen atoms H^2, H^3, H^4 of the reference molecule and the most electronegative neighboring H-bond accepting atom Y of the observed molecules, where Y corresponds to N in AN, O^1 in GBL and PC.

4.3. Conclusions

The mutual orientation of three solvents, namely AN, GBL and PC, has been characterized, using molecular dynamics simulation, the dipole-dipole orientation as well as the extent of the hydrogen bonding in these molecular liquids. We used the nearest neighbor approach in order to unambiguously characterize the distance and the orientation between a reference molecule and its first, second and n^{th} neighbors. Our results show that although the dominant dipole-dipole orientation between a reference molecule and first neighbor is the antiparallel one, the parallel one has an effect on the outcome of the Kirkwood correlation factor. For the subsequent neighbors the antiparallel orientation is gradually weakened in favor of the parallel one. More distant neighbors tend to be parallel to the reference molecule. Some of the solvents molecules located at intermediate distances are arranged in T-shaped orientation. Furthermore, for the cyclic solvents GBL and PC the above/below and the stacking arrangements between a reference molecules and it first neighbor, are present in both liquids.

Based on the nearest neighbor approach, we calculated the Kirkwood correlation factor for the twelfth neighbor to a reference one. Our results show that it is necessary to take in account the 4~6 nearest neighbor in the calculation of g_{K} in order to reproduce the experimental values.

Finally, the analysis of the distance, H···Y, between the reference H atom and the neighbor H-bond accepting atom and the angle $\angle$C–H^{i}···Y indicates that they are compatible with a weak hydrogen bonding.

4.4. References for Chapter 4

(1) Logan, D. E. The non-coincidence effect in the raman spectra of polar liquids. *Chem. Phys.* **1986**, *103*, 215-225.

(2) Xu, W.; Wu, F.; Zhao, Y.; Zhou, R.; Wang, H.; Zheng, X.; Ni, B. Study on the noncoincidence effect phenomenon using matrix isolated Raman spectra and the proposed structural organization model of acetone in condense phase. **2017**, *7*, 43835.

(3) Giorgini, M. G.; Futamatagawa, K.; Torii, H.; Musso, M.; Cerini, S. Solvation Structure around the Li+ Ion in Mixed Cyclic/Linear Carbonate Solutions Unveiled by the Raman Noncoincidence Effect. *J. Phys. Chem. Lett.* **2015**, *6*, 3296-3302.

(4) Giorgini, M. G.; Torii, H.; Musso, M. The influence of alkaline earth ions on the structural organization of acetone probed by the noncoincidence effect of the [small nu](C[double bond, length as m-dash]O) band: experimental and quantum chemical results. *PCCP* **2010**, *12*, 183-192.

(5) Brodin, A.; Jacobsson, P. Dipolar interaction and molecular ordering in liquid propylene carbonate: Anomalous dielectric susceptibility and Raman non-coincidence effect. *J. Mol. Liq.* **2011**, *164*, 17-21.

(6) Giorgini, M. G.; Musso, M.; Asenbaum, A.; DÖGe, G. The non-coincidence effect in N,N-dimethylformamide-CCl4 highly diluted binary mixtures. Experimental and theoretical results. *Mol. Phys.* **2000**, *98*, 783-791.

(7) Fini, G.; Mirone, P.; Fortunato, B. Evidence for short-range orientation effects in dipolar aprotic liquids from vibrational spectroscopy. Part 1.-Ethylene and propylene carbonates. *Journal of the Chemical Society, Faraday Transactions 2: Molecular and Chemical Physics* **1973**, *69*, 1243-1248.

(8) Shelley, V. M.; Yarwood, J. The noncoincidence effect in N,N-dimethylformamide - a comparison of theoretical predictions and experimental results. *Chem. Phys.* **1989**, *137*, 277-280.

(9) Czeslik, C.; Jonas, J. Effect of Pressure on Local Order in Liquid Dimethyl Sulfoxide. *J. Phys. Chem. A* **1999**, *103*, 3222-3227.

(10) Czeslik, C.; Kim, Y. J.; Jonas, J. Raman frequency noncoincidence effect of confined liquid dimethyl sulfoxide. *J. Chem. Phys.* **1999**, *111*, 9739-9742.

(11) Upadhyay, G.; Devi, T. G.; Singh, R. K.; Singh, A.; Alapati, P. R. Solvent dependent frequency shift and Raman noncoincidence effect of SO stretching mode of Dimethyl sulfoxide in liquid binary mixtures. *Spectrochimica Acta Part A: Molecular and Biomolecular Spectroscopy* **2013**, *109*, 239-246.

(12) Fini, G.; Mirone, P. Short-range orientation effects in dipolar aprotic liquids—III. Intermolecular coupling of vibrations in sulfoxides, sulfones, nitriles and other compounds. *Spectrochim. Acta Mol. Biomol. Spectrosc.* **1976**, *32*, 625-629.

(13) Soetens, J.-C.; Millot, C.; Maigret, B.; Bakó, I. Molecular dynamics simulation and X—ray diffraction studies of ethylene carbonate, propylene carbonate and dimethyl carbonate in liquid phase. *J. Mol. Liq.* **2001**, *92*, 201-216.

(14) Onthong, U.; Megyes, T.; Bako, I.; Radnai, T.; Grosz, T.; Hermansson, K.; Probst, M. X-ray and neutron diffraction studies and molecular dynamics simulations of liquid DMSO. *PCCP* **2004**, *6*, 2136-2144.

(15) Soper, A. K.; Luzar, A. Orientation of Water Molecules around Small Polar and Nonpolar Groups in Solution: A Neutron Diffraction and Computer Simulation Study. *The Journal of Physical Chemistry* **1996**, *100*, 1357-1367.

(16) Bertagnolli, H.; Chieux, P.; Zeidler, M. D. A neutron-diffraction study of liquid acetonitrile. *Mol. Phys.* **1976**, *32*, 1731-1736.

(17) Alston Steiner, P.; Gordy, W. Precision measurement of dipole moments and other spectral constants of normal and deuterated methyl fluoride and methyl cyanide. *J. Mol. Spectrosc.* **1966**, *21*, 291-301.

(18) Takamuku, T.; Tabata, M.; Yamaguchi, A.; Nishimoto, J.; Kumamoto, M.; Wakita, H.; Yamaguchi, T. Liquid Structure of Acetonitrile−Water Mixtures by X-ray Diffraction and Infrared Spectroscopy. *J. Phys. Chem. B* **1998**, *102*, 8880-8888.

(19) Humphreys, E. K.; Allan, P. K.; Welbourn, R. J. L.; Youngs, T. G. A.; Soper, A. K.; Grey, C. P.; Clarke, S. M. A Neutron Diffraction Study of the Electrochemical Double Layer Capacitor Electrolyte Tetrapropylammonium Bromide in Acetonitrile. *J. Phys. Chem. B* **2015**, *119*, 15320-15333.

(20) Srinivasan, K. R.; Kay, R. L. The pressure dependence of the dielectric constant and density of acetonitrile at three temperatures. *J. Solution Chem.* **1977**, *6*, 357-367.

(21) Bakshi, M. S.; Singh, J.; Kaur, H.; Ahmad, S. T.; Kaur, G. Thermodynamic Behavior of Mixtures. 3. Mixtures of Acetonitrile with Dimethylacetamide, Dimethyl Sulfoxide, Nitrobenzene, and Methanol at 25 °C. *J. Chem. Eng. Data* **1996**, *41*, 1459-1461.

(22) Jellema, R.; Bulthuis, J.; van der Zwan, G. Ion-ion, ion-solvent and solvent-solvent interactions in electrolyte solutionsDielectric relaxation of acetonitrile-water mixtures. *J. Mol. Liq.* **1997**, *73*, 179-193.

(23) Stoppa, A.; Nazet, A.; Buchner, R.; Thoman, A.; Walther, M. Dielectric response and collective dynamics of acetonitrile. *J. Mol. Liq.* **2015**, *212*, 963-968.

(24) Torras, J.; Alemán, C. Determination of New Cu+, Cu2+, and Zn2+ Lennard-Jones Ion Parameters in Acetonitrile. *J. Phys. Chem. B* **2013**, *117*, 10513-10522.

(25) Rizzuto, A. M.; Pennington, R. L.; Sienerth, K. D. Study of the BMIM-PF6: Acetonitrile binary mixture as a solvent for electrochemical studies involving CO2. *Electrochim. Acta* **2011**, *56*, 5003-5009.

(26) Fang, S.; Zhang, Z.; Jin, Y.; Yang, L.; Hirano, S.-i.; Tachibana, K.; Katayama, S. New functionalized ionic liquids based on pyrrolidinium and piperidinium cations with two ether groups as electrolytes for lithium battery. *J. Power Sources* **2011**, *196*, 5637-5644.

(27) Schmidt, A. H. Validated HPLC Method for the Determination of Residues of Acetaminophen, Caffeine, and Codeine Phosphate on Swabs Collected from Pharmaceutical Manufacturing Equipment in Support of Cleaning Validation. *J. Liq. Chromatogr. Related Technol.* **2006**, *29*, 1663-1673.

(28) Wen, Z.-Q.; Li, G.; Ren, D. Detection of Trace Melamine in Raw Materials Used for Protein Pharmaceutical Manufacturing Using Surface-Enhanced Raman Spectroscopy (SERS) with Gold Nanoparticles. *Appl. Spectrosc.* **2011**, *65*, 514-521.

(29) Barrosse-Antle, L. E.; Bond, A. M.; Compton, R. G.; O'Mahony, A. M.; Rogers, E. I.; Silvester, D. S. Voltammetry in Room Temperature Ionic Liquids: Comparisons and Contrasts with Conventional Electrochemical Solvents. *Chemistry – An Asian Journal* **2010**, *5*, 202-230.

(30) Zhang, Z.-a.; Lai, Y.-q.; Li, J.; Liu, Y.-x. Electrochemical behavior of wound supercapacitors with propylene carbonate and acetonitrile based nonaqueous electrolytes. *J. Cent. South Univ. Technol.* **2009**, *16*, 247-252.

(31) Arulepp, M.; Permann, L.; Leis, J.; Perkson, A.; Rumma, K.; Jänes, A.; Lust, E. Influence of the solvent properties on the characteristics of a double layer capacitor. *J. Power Sources* **2004**, *133*, 320-328.

(32) Kalugin, O. N.; Voroshylova, I. V.; Riabchunova, A. V.; Lukinova, E. V.; Chaban, V. V. Conductometric study of binary systems based on ionic liquids and acetonitrile in a wide concentration range. *Electrochim. Acta* **2013**, *105*, 188-199.

(33) Bešter-Rogač, M.; Stoppa, A.; Buchner, R. Ion Association of Imidazolium Ionic Liquids in Acetonitrile. *J. Phys. Chem. B* **2014**, *118*, 1426-1435.

(34) Majdan-Cegincara, R.; Zafarani-Moattar, M. T.; Shekaari, H. The study of solute–solvent interactions in 1-butyl-1-methylpyrrolidinium trifluoromethanesulfonate + acetonitrile from solvent activity, density, speed of sound, viscosity, electrical conductivity and refractive index measurements. *J. Mol. Liq.* **2015**, *203*, 198-203.

(35) Liu, W.; Yan, X.; Lang, J.; Xue, Q. Effects of concentration and temperature of EMIMBF4/acetonitrile electrolyte on the supercapacitive behavior of graphene nanosheets. *J. Mater. Chem.* **2012**, *22*, 8853-8861.

(36) Lin, R.; Taberna, P.-L.; Fantini, S.; Presser, V.; Pérez, C. R.; Malbosc, F.; Rupesinghe, N. L.; Teo, K. B. K.; Gogotsi, Y.; Simon, P. Capacitive Energy Storage from −50 to 100 °C Using an Ionic Liquid Electrolyte. *J. Phys. Chem. Lett.* **2011**, *2*, 2396-2401.

(37) Kaatze, U.; Pottel, R.; Schaefer, M. Dielectric spectrum of dimethyl sulfoxide/water mixtures as a function of composition. *The Journal of Physical Chemistry* **1989**, *93*, 5623-5627.

(38) Vechi, S. M.; Skaf, M. S. Collision-Induced Effects on the Dielectric Properties of Liquid Dimethylsulfoxide. *Journal of the Brazilian Chemical Society* **2002**, *13*, 583-591.

(39) Amey, R. L. Extent of association in liquid dimethyl sulfoxide. *The Journal of Physical Chemistry* **1968**, *72*, 3358-3359.

(40) Hunger, J.; Buchner, R.; Kandil, M. E.; May, E. F.; Marsh, K. N.; Hefter, G. Relative Permittivity of Dimethylsulfoxide and N,N-Dimethylformamide at Temperatures from (278 to 328) K and Pressures from (0.1 to 5) MPa. *J. Chem. Eng. Data* **2010**, *55*, 2055-2065.

(41) Barthel, J.; Bachhuber, K.; Buchner, R.; Gill, J. B.; Kleebauer, M. Dielectric spectra of some common solvents in the microwave region. Dipolar aprotic solvents and amides. *Chem. Phys. Lett.* **1990**, *167*, 62-66.

(42) Payne, R.; Theodorou, I. E. Dielectric properties and relaxation in ethylene carbonate and propylene carbonate. *The Journal of Physical Chemistry* **1972**, *76*, 2892-2900.

(43) Sagawa, N.; Takabatake, S.; Shikata, T. A Dielectric Spectroscopic Study of Ethylene Carbonate in Solution. *Bull. Chem. Soc. Jpn.* **2016**, *89*, 1018-1025.

(44) Simeral, L.; Amey, R. L. Dielectric properties of liquid propylene carbonate. *The Journal of Physical Chemistry* **1970**, *74*, 1443-1446.

(45) Świergiel, J.; Płowaś, I.; Jadżyn, J. Charge Relaxation and Stokes–Einstein Relation in Diluted Electrolyte Solution of Propylene Carbonate and Lithium Perchlorate. *Industrial & Engineering Chemistry Research* **2015**, *54*, 2108-2113.

(46) Kirkwood, J. G. The Dielectric Polarization of Polar Liquids. *J. Chem. Phys.* **1939**, *7*, 911-919.

(47) Płowaś, I.; Świergiel, J.; Jadżyn, J. Dipolar Self-Assembling in Mixtures of Propylene Carbonate and Dimethyl Sulfoxide as Revealed by the Orientational Entropy. *J. Phys. Chem. B* **2016**, *120*, 7920-7925.

(48) Świergiel, J.; Płowaś, I.; Jadżyn, J. On investigation of aggregation of molecular dipoles in liquids. *J. Mol. Liq.* **2016**, *220*, 879-882.

(49) Świergiel, J.; Płowaś, I.; Jadżyn, J. Orientational entropy and dipolar aggregation in mixtures of propylene carbonate + N,N-dimethylacetamide. *J. Mol. Liq.* **2016**, *223*, 628-634.

(50) Albertí, M.; Amat, A.; De Angelis, F.; Pirani, F. A Model Potential for Acetonitrile: from Small Clusters to Liquid. *J. Phys. Chem. B* **2013**, *117*, 7065-7076.

(51) Ford, T. A.; Glasser, L. Ab initio calculations of the structural, energetic, and vibrational properties of some hydrogen bonded and van der Waals dimers. Part 4. The acetonitrile dimer. *Int. J. Quantum Chem* **2001**, *84*, 226-240.

(52) Mata, R. A.; Costa Cabral, B. J. Structural, energetic, and electronic properties of (CH3CN)2–8 clusters by density functional theory. *Journal of Molecular Structure: THEOCHEM* **2004**, *673*, 155-164.

(53) Remya, K.; Suresh, C. H. Cooperativity and cluster growth patterns in acetonitrile: A DFT study. *J. Comput. Chem.* **2014**, *35*, 910-922.

(54) Chen, J.; Sit, P. H. L. Ab initio study of the structural properties of acetonitrile–water mixtures. *Chem. Phys.* **2015**, *457*, 87-97.

(55) Radnai, T.; Bakó, I.; Jedlovszky, P.; Pálinkás, G. Local Order in Some Aprotic Dipolar Liquids. *Mol. Simul.* **1996**, *16*, 345-358.

(56) Cabaleiro-Lago, E. M.; RÍOs, M. A. Intermolecular potential for acetonitrile based on ab initio calculations. *Mol. Phys.* **1999**, *96*, 309-321.

(57) Edwards, D. M. F.; Madden, P. A. A computer simulation study of the dielectric properties of a model of methyl cyanide. *Mol. Phys.* **1984**, *51*, 1163-1179.

(58) Orhan, M. Dielectric and Transport Properties of Acetonitrile at Varying Temperatures: a Molecular Dynamics Study. *Bull. Korean Chem. Soc.* **2014**, *35*, 1469-1478.

(59) Guàrdia, E.; Pinzón, R.; Casulleras, J.; Orozco, M.; Luque, F. J. Comparison of Different Three-site Interaction Potentials for Liquid Acetonitrile. *Mol. Simul.* **2001**, *26*, 287-306.

(60) Aparicio, S.; Alcalde, R. Characterization of two lactones in liquid phase: an experimental and computational approach. *PCCP* **2009**, *11*, 6455-6467.

(61) Vaz, P. D.; Ribeiro-Claro, P. J. A. C≡H ·s O Hydrogen Bonds in Small Ring Carbonyl Compounds: Vibrational Spectroscopy and Ab initio Calculations. *Struct. Chem.* **2005**, *16*, 287-293.

(62) Hesse, S.; Suhm, M. A. On the low volatility of cyclic esters: an infrared spectroscopy comparison between dimers of [gamma]-butyrolactone and methyl propionate. *PCCP* **2009**, *11*, 11157-11170.

(63) Marekha, B. A.; Koverga, V. A.; Moreau, M.; Kiselev, M.; Takamuku, T.; Kalugin, O. N.; Idrissi, A. Intermolecular interactions, ion solvation, and association in mixtures of 1-n-butyl-3-methylimidazolium hexafluorophosphate and γ-butyrolactone: insights from Raman spectroscopy. *J. Raman Spectrosc.* **2015**, *46*, 339-352.

(64) Masia, M.; Rey, R. Computational Study of γ-Butyrolactone and Li+/γ-butyrolactone in Gas and Liquid Phases. *J. Phys. Chem. B* **2004**, *108*, 17992-18002.

(65) Kollipost, F.; Hesse, S.; Lee, J. J.; Suhm, M. A. Dimers of cyclic carbonates: chirality recognition in battery solvents and energy storage. *PCCP* **2011**, *13*, 14176-14182.

(66) Wang, Y.; Balbuena, P. B. Associations of Alkyl Carbonates: Intermolecular C−H···O Interactions. *J. Phys. Chem. A* **2001**, *105*, 9972-9982.

(67) Silva, L. B.; Freitas, L. C. G. Structural and thermodynamic properties of liquid ethylene carbonate and propylene carbonate by Monte Carlo Simulations. *Journal of Molecular Structure: THEOCHEM* **2007**, *806*, 23-34.

(68) You, X.; Chaudhari, M. I.; Pratt, L. R.; Pesika, N.; Aritakula, K. M.; Rick, S. W. Interfaces of propylene carbonate. *J. Chem. Phys.* **2013**, *138*, 114708.

(69) Wang, L.; Peng, Q.; Ye, S.; Morita, A. Surface Structure of Organic Carbonate Liquids Investigated by Molecular Dynamics Simulation and Sum Frequency Generation Spectroscopy. *The Journal of Physical Chemistry C* **2016**, *120*, 15185-15197.

(70) Delavoux, Y. M.; Gilmore, M.; Atkins, M. P.; Swadzba-Kwasny, M.; Holbrey, J. D. Intermolecular structure and hydrogen-bonding in liquid 1,2-propylene carbonate and 1,2-glycerol carbonate determined by neutron scattering. *PCCP* **2017**, *19*, 2867-2876.

(71) Perelygin, I. S.; Itkulov, I. G. Spontaneous raman spectroscopic study of the association of liquid γ-butyrolactone molecules. *J. Struct. Chem.* **1996**, *37*, 928-932.

(72) Idrissi, A.; Damay, P.; Kiselev, M. Nearest neighbor assessments of spatial distribution in CO2: A molecular dynamics analysis. *Chem. Phys.* **2007**, *332*, 139-143.

(73) Idrissi, A.; Gerard, M.; Damay, P.; Kiselev, M.; Puhovsky, Y.; Cinar, E.; Lagant, P.; Vergoten, G. The Effect of Urea on the Structure of Water: A Molecular Dynamics Simulation. *J. Phys. Chem. B* **2010**, *114*, 4731-4738.

(74) Idrissi, A.; Marekha, B.; Kiselev, M.; Jedlovszky, P. The local environment of the molecules in water-DMSO mixtures, as seen from computer simulations and Voronoi polyhedra analysis. *PCCP* **2015**, *17*, 3470-3481.

(75) Idrissi, A.; Marekha, B. A.; Barj, M.; Miannay, F. A.; Takamuku, T.; Raptis, V.; Samios, J.; Jedlovszky, P. Local structure of dilute aqueous DMSO solutions, as seen from molecular dynamics simulations. *J. Chem. Phys.* **2017**, *146*, 234507.

(76) Idrissi, A.; Oparin, R. D.; Krishtal, S. P.; Krupin, S. V.; Vorobiev, E. A.; Frolov, A. I.; Dubois, L.; Kiselev, M. G. The study of correlations between hydrogen bonding characteristics in liquid, sub- and supercritical methanol. Molecular dynamics simulations and Raman spectroscopy analysis. *Faraday Discussions* **2013**, *167*, 551-566.

(77) Idrissi, A.; Vyalov, I.; Damay, P.; Frolov, A.; Oparin, R.; Kiselev, M. Assessment of the Spatial Distribution in Sub- and Supercritical CO2 Using the Nearest Neighbor Approach: A Molecular Dynamics Analysis. *J. Phys. Chem. B* **2009**, *113*, 15820-15830.

(78) Idrissi, A.; Vyalov, I.; Damay, P.; Kiselev, M. In *Tilte*, 2009.

(79) Idrissi, A.; Vyalov, I.; Georgi, N.; Kiselev, M. On the Characterization of Inhomogeneity of the Density Distribution in Supercritical Fluids via Molecular Dynamics Simulation and Data Mining Analysis. *The Journal of Physical Chemistry B* **2013**, *117*, 12184-12188.

(80) Marekha, B. A.; Koverga, V. A.; Chesneau, E.; Kalugin, O. N.; Takamuku, T.; Jedlovszky, P.; Idrissi, A. Local Structure in Terms of Nearest-Neighbor Approach in 1-Butyl-3-methylimidazolium-Based Ionic Liquids: MD Simulations. *J. Phys. Chem. B* **2016**, *120*, 5029-5041.

(81) Vyalov, I.; Kiselev, M.; Tassaing, T.; Soetens, J. C.; Idrissi, A. Investigation of the Local Structure in Sub and Supercritical Ammonia Using the Nearest Neighbor Approach: A Molecular Dynamics Analysis. *J. Phys. Chem. B* **2010**, *114*, 15003-15010.

(82) Nikitin, A. M.; Lyubartsev, A. P. New six-site acetonitrile model for simulations of liquid acetonitrile and its aqueous mixtures. *J. Comput. Chem.* **2007**, *28*, 2020-2026.

(83) Böhm, H. J.; McDonald, I. R.; Madden, P. A. An effective pair potential for liquid acetonitrile. *Mol. Phys.* **1983**, *49*, 347-360.

(84) Böhm, H. J.; Lynden-Bell, R. M.; Madden, P. A.; McDonald, I. R. Molecular motion in a model of liquid acetonitrile. *Mol. Phys.* **1984**, *51*, 761-777.

(85) Siebers, J. G.; Buck, U.; Beu, T. A. Calculation of structures and vibrational spectra of acetonitrile clusters. *Chem. Phys.* **1998**, *239*, 549-560.

(86) Grabuleda, X.; Jaime, C.; Kollman, P. A. Molecular dynamics simulation studies of liquid acetonitrile: New six-site model. *J. Comput. Chem.* **2000**, *21*, 901-908.

(87) Price, M. L. P.; Ostrovsky, D.; Jorgensen, W. L. Gas-phase and liquid-state properties of esters, nitriles, and nitro compounds with the OPLS-AA force field. *J. Comput. Chem.* **2001**, *22*, 1340-1352.

(88) Oldiges, C.; Wittler, K.; Tönsing, T.; Alijah, A. MD Calculated Structural Properties of Clusters in Liquid Acetonitrile/Water Mixtures with Various Contents of Acetonitrile. *J. Phys. Chem. A* **2002**, *106*, 7147-7154.

(89) Bowron, D. T.; Finney, J. L.; Soper, A. K. The Structure of Liquid Tetrahydrofuran. *J. Am. Chem. Soc.* **2006**, *128*, 5119-5126.

(90) Bowron, D. T.; Finney, J. L.; Soper, A. K. Structural Characteristics of a 0.23 Mole Fraction Aqueous Solution of Tetrahydrofuran at 20 °C. *J. Phys. Chem. B* **2006**, *110*, 20235-20245.

(91) Idrissi, A.; Damay, P.; Kiselev, M. Nearest neighbor assessments of spatial distribution in CO2: A molecular dynamics analysis. *Chem. Phys.* **2007**, *332*, 139-143.

(92) Idrissi, A.; Vyalov, I.; Damay, P.; Frolov, A.; Oparin, R.; Kiselev, M. Assessment of the Spatial Distribution in Sub- and Supercritical CO2 Using the Nearest Neighbor Approach: A Molecular Dynamics Analysis. *J. Phys. Chem. B* **2009**, *113*, 15820-15830.

(93) Fröhlich, H. H.: *Theory of dielectrics : dielectrics constant and dielectric loss*; 2nd ed ed.; Clarendon Press, 1986.

(94) Oster, G.; Kirkwood, J. G. The Influence of Hindered Molecular Rotation on the Dielectric Constants of Water, Alcohols, and Other Polar Liquids. *J. Chem. Phys.* **1943**, *11*, 175-178.

(95) Stolov, A. A.; Kamalova, D. I.; Borisover, M. D.; Solomonov, B. N.; Remizov, A. B. Hydrogen bonds formed by methyl groups of acetonitrile: Infrared and calorimetric study. *Spectrochim. Acta Mol. Biomol. Spectrosc.* **1994**, *50*, 145-150.

Chapter 5. Local structure in the mixture imidazolium-based ILs with molecular solvents

Local microscopic structure of the nearest neighboring ions in ionic liquids (ILs) is the key prerequisite in obtaining a comprehensive understanding of the influence of the nature of ions and solvents on the properties of mixtures of imidazolium-based ILs. We employed classical molecular dynamics (MD) simulations to study in detail the spatial, radial, and orientational relative distribution of a set of imidazolium ILs based on 1-butyl-3-methylimidazolium (C_4mim^+) cation coupled with acetate tetrafluoroborate (BF_4^-), hexafluorophosphate (PF_6^-), trifluoromethanesulfonate (TFO^-), and bis(trifluoromethanesulfonyl)amide ($TFSI^-$) in the mixture with dipolar aprotic solvents as acetonitrile (AN), γ-butyrolactone (GBL) and propylene carbonate (PC). The main interaction patterns such as cation···anion, cation···solvent, anion···solvent and solvent···solvent H-bonding, cation···cation ring stacking and solvent···solvent dipolar orientation were considered within the framework of the nearest neighbor approach with respect to each particular interaction site.

5.1. Introduction

In this Chapter we use classical MD simulation for the microscopic description and interpretation of structure in mixtures of imidazolium ionic liquids (ILs) with per fluorinated anions on one side and polar aprotic solvents on the other side. These mixtures possess a number of properties which are advantageous for electrochemical application (e.g., high ionic conductivity, thermal and electrochemical stability, low environmental hazardness) and they can be fine tuned due to the full miscibility of the components. Understanding the influence of the nature of the constituents and of the composition of these mixtures on the microscopic structure is of crucial importance for their successful application. Indeed, in this Chapter, the mixtures of four imidazolium ILs with three polar aprotic molecular solvents have been investigated. The ILs contain a common cation 1-n-butyl-3-methlylimidazolium (C_4mim^+). It is combined with perfluorinated anions of different size, shape, symmetry, and electronic structure, namely, tetrafluoroborate (BF4−), hexafluorophosphate (PF6−), trifluoromethylsulfonate (TfO−), and bis(trifluoromethanesulfonyl)imide (TFSI−). Polar aprotic molecular solvents employed in this thesis are those common in electrochemistry of electrolyte solutions: acetonitrile (AN), γ-butyrolactone (GBL), and propylene carbonate (PC), which differ in terms of their polarity, donicity, viscosity, molecular shape and volume.

Originally, dilution of ILs in molecular solvents was considered as a simple mean to optimize the transport properties in the mixture (reduce their high viscosity for the sake of practical handling, increase of diffusion). However, not only does it increase the fluidity, but modifies the overall pattern of intermolecular and interionic interactions and the related properties, e.g., electrical conductivity. It is important to mention that in many ionic liquids/solvent mixtures the electrical conductivity goes through a maximum in the molar fraction range of ionic liquid around 0.2. This stresses the fact that the local microscopic structure of the nearest neighboring around the cation and anion in the ionic liquids/molecular solvent is the key prerequisite in obtaining a comprehensive understanding of the influence of the nature of solvent on the properties of ILs.

The question of how the local structure is affected in this range of molar fraction is a fundamental importance in order to understand the behavior of the spectroscopic results as well as the physical chemical properties of these mixtures such as diffusion, conductivity and viscosity. The local structure may result from a concerted action of the C–H···Y hydrogen bond (hydrogen atoms of the cation ring and Y atoms of the anion or the solvent), that describing the hydrogen bond between the cation···solvent, and the anion···solvent as well as the stacking of the imidazolium rings. Certainly the C–H···Y are much weaker than the O–H···Y hydrogen bond however, in many studies, these hydrogen bond interactions and stacking interactions have been recognized important in determining the local structure (packing, orientation) in IL/molecular solvents mixtures.

Several studies on quantum-chemical calculations[1-4] *ab initio* MD simulations[5] of the complexes of imidazolium-based ILs with molecular solvents report the similar mutual arrangement of the anions and solvent molecules around the imidazolium ring. A common point for the complexes of ion pair with molecular solvent is that the solvent molecule is found closest to H^2 site where it established rather strong H-bonds compared with ones at $H^{4\text{-}5}$ site. Moreover, for the studied configurations the anion and solvent mainly located above the $C–H^2$ group, where the interionic H-bonding interactions found to be stronger compared with those between the cation and solvent. Weaker interaction of the solvent molecule with anion, which is located on top of the $C^2–H^2$ fragment, was also noted.[3,6] Numerous works point out to the strongest interactions between anion and solvent due to the formation of H-bonding interactions.[7-19] Moreover, Ghoshdastidar and Senapati[8] show that at highest x_{IL} water molecules occupy locations between adjacent anions and form water-mediated H-bonded anion bridges, whereas the further increasing of water content in mixtures disrupts these bridges and increasingly forms bifurcated anion···water H-bonds. This behavior leading to the weakening of H-bonding interactions between the cation and anion even at small amount of solvent.[11,16,20]

The most of the research dealing with vibrational spectroscopy of mixtures of the imidazolium ILs with molecular solvents is focused on the ring C–H stretching region, which is significantly more intense and show higher sensitivity to the variations in the microenvironment induced by the changes of the mixture composition. By studying of imidazolium ILs with different counterions in the various binary mixtures with molecular solvents it was found the significant dependence of the spectral profile on the choice of the medium which accompanied by the redshift (C_4mimPF_6-GBL,[21] C_4mimBF_4-MeOH,[22] C_4mimBF_4-DMSO,[1,23,24] C_2mimTFSI-PEO,[25] C_4mimPF_6/BF_4-PEO[26]), blueshift ($C_2mimEtSO_4$-AC,[27] $C_4mimCl/MeSO_4$-EG,[28] C_2mimTFA-H_2O/MeOH[29]) or whitout any apparent shift (C_2mimTFSI-MeOH,[30] C_nmimBF_4-EG,[31] C_2mimTFSI-DiOx,[25] C_4mimBF_4/PF_6-AN[32]). Such behavior may be associated to the fact that with the addition of donating solvents to weakly associated ILs where the solvent molecules can effectively compete with the anions for the ring C–H sites in order to establish stronger H-bonds, which lead to the redshift of the ring C–H vibrations. In case of the absence of any apparent shift of the spectral profiles corresponds to the rather low anion basicity and solvent donicity resulting it the absence of persistent H-bond network in neat ILs and solvent is not capable to perturb the interionic interactions significantly. In all other cases, where the rupture of rather strong interionic H-bonds that is not counterbalanced by the solvation of the cation leads to apparent blueshifts. From another side, by studying $C_3C_3C_3$NHTFO dissolved in different molecular solvents over a wide range of concentration Fumino *et al.*[33] pointed that in case solvents of a low dielectric constant ($CHCl_3$ and THF), there is larger concentration of contact ionic pairs over solvent-separated ionic pairs, whereas for high dielectric constant (DMSO), solvent-separated ion pairs dominate.

On the example of C_4mimBF_4/PF_6/TFO/TFSI in AN[34] it was shown that the most significant effects of the chemical shift variation are observed for the ring H^2 site, where the relative order of thus referenced chemical shifts for the imidazolium ring signals is C_4mimTFO ⩾ C_4mimBF$_4$ > C_4mimTFSI > C_4mimPF$_6$. Particular sensitivity of the H^2 was associated with the higher positive charge acidity of the C^2–H^2 group (that is especially well pronounced for C_4mimTFO and C_4mimTFSI) compared to the C^4–H^4 and C^5–H^5 and, hence, to the higher strength of the corresponding H-bonds. However, for the C_4mimBF$_4$ and C_4mimPF$_6$ it was noted the less pronounced difference between H^2 and $H^{4\text{-}5}$ sites, which was related to the higher symmetry of the counterions.

In the recent NMR study on the same ILs in GBL and PC[35] the influence of the solvents follows the same trend, while the relative chemical shift variations found to be more negative compared with those in AN that was associated by solvating properties of the solvents towards cations but not their polarity. The same trend of chemical shift variation for the imidazolium ring hydrogen atoms was observed for ILs with rather basic anions, which tend to form strong directional H-bonds such as halides Hal$^-$,[36-38] substituted sulfonates RSO$_3^-$[36,39] and sulfates RSO$_4^-$[40] in various molecular solvents and for BF$_4^-$/PF$_6^-$[3,41,42] based ILs. Moreover, the most significant changes on chemical shift variation in IL-solvent mixtures occurred at low ILs content (x_{IL} ~ 0.1–0.2) and even at high dilutions of ILs ($x_{\mathrm{IL}} < 0.1$) that was associated with the disruption of interionic H-bonds and ion dissociation.[43,44]

Furthermore, important information on the local structure can be obtained by analyzing the stacking between the cation that expresses the cation-cation interactions. Indeed, in several theoretical studies, the most stable structures were found to be with imidazolium cations in a stacked antiparallel arrangement. Cations can be offset from the perfect stacked antiparallel arrangement rather easily depending on anion. Two typical kinds of contacts have been reported in imidazolium-based ILs: tail-tail and ring-ring (*e.g.* π^+-π^+ stacking).[45-48] The former one is known to be at the origin of microheterogeneity observed both experimentally [45,49,50] and by molecular simulations.[51-53] The latter, in contrast, is much less common and was initially suggested to rationalize some NMR spectroscopic data[54-56] and later was also confirmed by MD simulations including those reproducing neutron and X-ray scattering data.[57-59] It is interesting to note that in the available experimental crystal structures of C_4mim^+-based ILs corresponding to some of the ILs studied here no stacking type close contacts were observed, though the neighboring ring planes are often, but not always, parallel and displaced.[60,61] Several recent quantum-chemical calculations on representative clusters of ion pairs of C_4mim^+-based ILs have also revealed the importance of π^+-π^+ stacking in such systems.[2,47,48,62-66]

The $H^{2/4–5}\cdots Y$ distance between the acidic hydrogen atoms and any atom of the anion or the solvent molecule as well as the orientation between the $C^{2/45}\cdots H^{2/4-5}$ axes and specific other axes defining the orientation with respect to the anion or solvent molecule are then an important information that can help to characterize the local structure around these acidic hydrogen atoms. Unfortunately, these distances obtained from bulk density or radial distribution functions [9,67-69] determined from X-ray or neutron scattering experiment, doesn’t define them in an unambiguous way. The $H^{2,4–5}\cdots Y$ distance has mainly been assessed from simulations within a certain H-bond criterion. Typically, this implies a combination of a radial cut-off between a given hydrogen atom and the corresponding H-bond acceptor and an angular cut-off for the pseudo-valent H-bond angle (D–H···A, where D and A stand for H-bond donor and acceptor, respectively).[70] However, more sophisticated criteria have also been used.[71] Moreover, some authors claim that poorly selected cut-off values can significantly bias the results[71] while the others stipulate that their results are rather robust towards the cut-offs.[72]

The main difficulty then is to define statistical functions which characterize the local structure in terms of close distance between these hydrogen atoms and other specific atoms of the mixture components.[36] The arrangement of neighbors relative to a given component of the mixture can be described by the nearest neighbor radial distribution.

In order to assess the extent of the hydrogen bonding between the cation and the anion or the solvent molecules, we analyzed the dependence of two distances shown in figure , the first one is between $H^{2/4–5}\cdots Y$, and the distance between , $C^{2/4–}$

$^{5}\cdots$Y, where the H-bond-accepting atom of anions (F in BF_4^- and PF_6^-, O in TFO^- and $TFSI^-$) or of the solvent (N in AN, O^1 in GBL and PC). Furthermore, the H-bonding between the solvent-anion is described by the two distances $H^2\cdots Y$ and $C^2\cdots Y$, where Y corresponds to F in BF_4^- and PF_6^-, O in TFO^- and $TFSI^-$, while H^2 is the hydrogen atom in position 2 as indicated in Figure 3.1 of Chapter 3. In the case of a linear H-bonding that is qualified as strong one, the $C^{2/4\text{–}5}\cdots Y$ distance will be equal to the sum of the intramolecular distance $C^{2/4\text{–}5}$–$H^{2/4\text{–}5}$ and the intermolecular distance $H^{2/4\text{–}5}\cdots Y$, while in the case of a bent H-bonding, with a given θ angle, the $C^{2/4\text{-}5}\cdots X$ distance is shorter than the sum of $C^{2/4\text{–}5}$–$H^{2/4\text{–}5}$ and $C^{2/4\text{–}5}\cdots Y$ and it can be estimated using the law of cosines. We calculated these distances, $C^{2/4\text{–}5}\cdots Y$, $H^{2/4\text{–}5}\cdots Y$, $H^2\cdots Y$ and $C^2\cdots Y$ using the nearest neighbor approach.

To characterize the stacking interactions between the imidazolium rings, the several angles defined in Chapter 3, are used. Namely, the angle defining the above/below, the parallel stacking between the plans of the cation ring and the dipole-dipole orientations. Similar angles also were used to characterize the orientation between the solvent molecules.

As a consequence in this Chapter, we will analyze the structure in the imidazolium-based ILs anions in terms of the $C^{2/4\text{–}5}$–$H^{2/4\text{–}5}\cdots Y$ H-bond, where Y stands for F in BF_4^- and PF_6^-, O in TFO^- and $TFSI^-$, in terms of the cation$\cdots$solvent $H^{2/4\text{–}5}\cdots Y$ H-bond interaction, where Y corresponds to the most electronegative H-bond accepting atom of solvent, *i.e.*, N in AN, O^1 in GBL and PC and in terms of the anion$\cdots$solvent hydrogen bond $Y\cdots H^2$ where Y corresponds to F in BF_4^- and PF_6^-, O in TFO^- and $TFSI^-$ and H^2 stands for the hydrogen atom in position 2 of AN, PC and GBL. Furthermore the stacking between the cations ring will be analyzed as well as the solvent$\cdots$solvent interactions.

5.2. Results and discussion

5.2.1 Hydrogen bonding interactions

5.2.2.1 Spatial Distribution functions

In order to get the general pattern on the mixture composition on the local structure and then on the spatial distribution of the components in the mixture, we first analyze the behavior of the spatial distributions distribution (SDFs) of the anion and solvent around the imidazolium ring in the whole range of the mixture composition. It should be mentioned that only the nearest neighbor anion or solvent molecule to a reference cation was considered in the calculated SDFs. As a representative points we select the H-bond-accepting atom of anions (F in BF_4^- and PF_6^-, O in TFO^- and $TFSI^-$) and solvent molecules (N in AN, O^1 in GBL and PC), around the imidazolium ring.

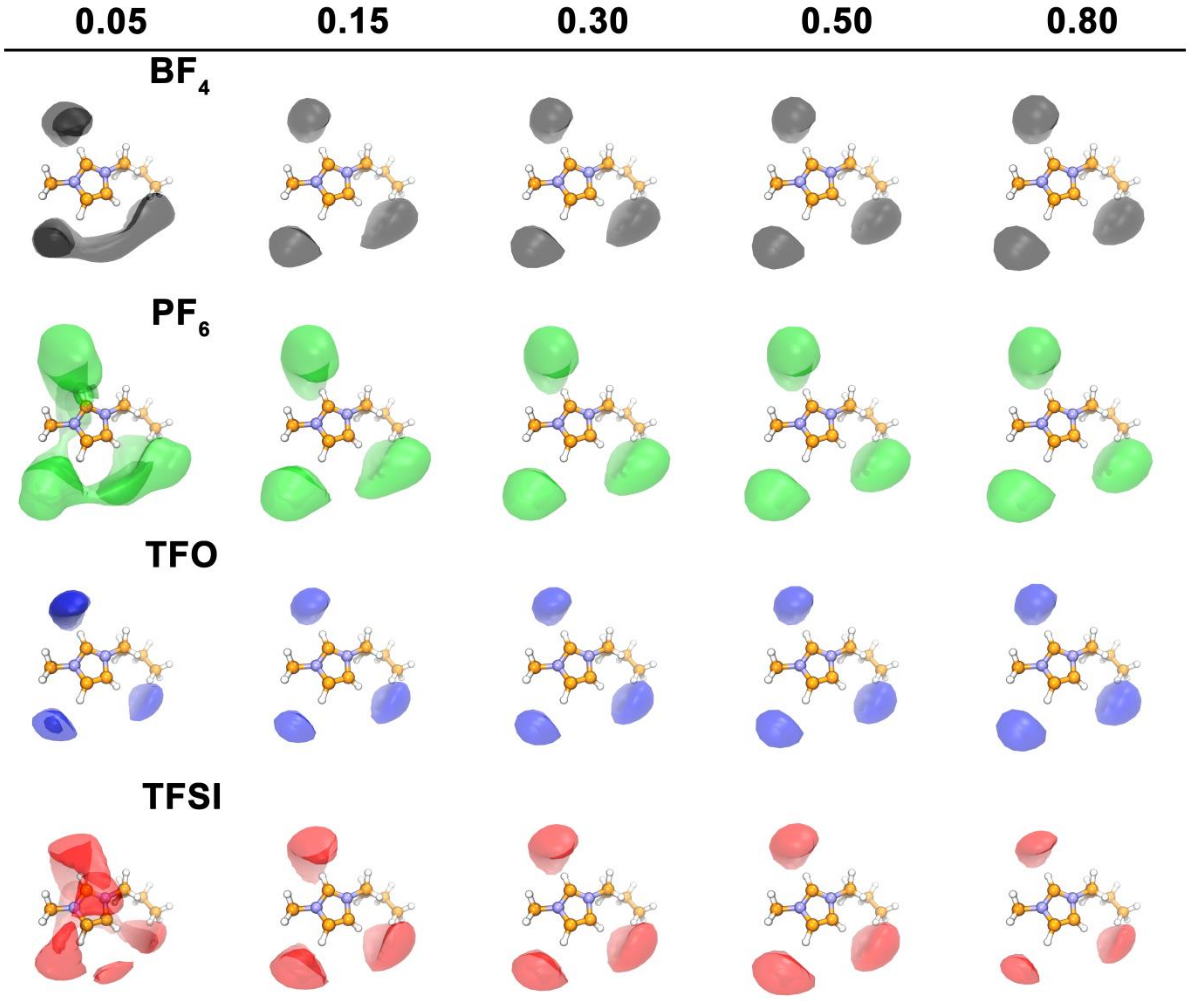

Figure 5.1. Spatial distribution functions of anions around the imidazolium ring for the different mixtures compositions of C_4mimBF_4, C_4mimPF_6, C_4mimTFO and C_4mimTFSI in AN for the different mixtures compositions with density probability of 30%.

The SDFs of the anion around the $H^{2/4-5}$ sites of the set of selected IL are illustrated in Figure 5.1. As it can be seen from the obtained spatial distributions, the anions are prone to occupy the positions around a reference C_4mim^+ cation at $H^{2/4-5}$ sites. In the range of x_{IL} between 0.3 and 1.0, the isosurfaces area do not change drastically indicated that the spatial distribution of the observed anion or solvent molecules is not affected by changing the mixture composition. In particular, the H-bonding interactions between the imidazolium ring hydrogen sites and anions are not affect drastically. A general trend characterizes the SFDs of anion around the $H^{2/4-5}$ sites, at high x_{IL} these SDF are localized and at low x_{IL} than

0.15, they become diffuse to a large extent around H^{4-5} for PF_6^-, $TFSI^-$ and BF_4^- and to less extent around H^2 for TFO^- and BF_4^-.

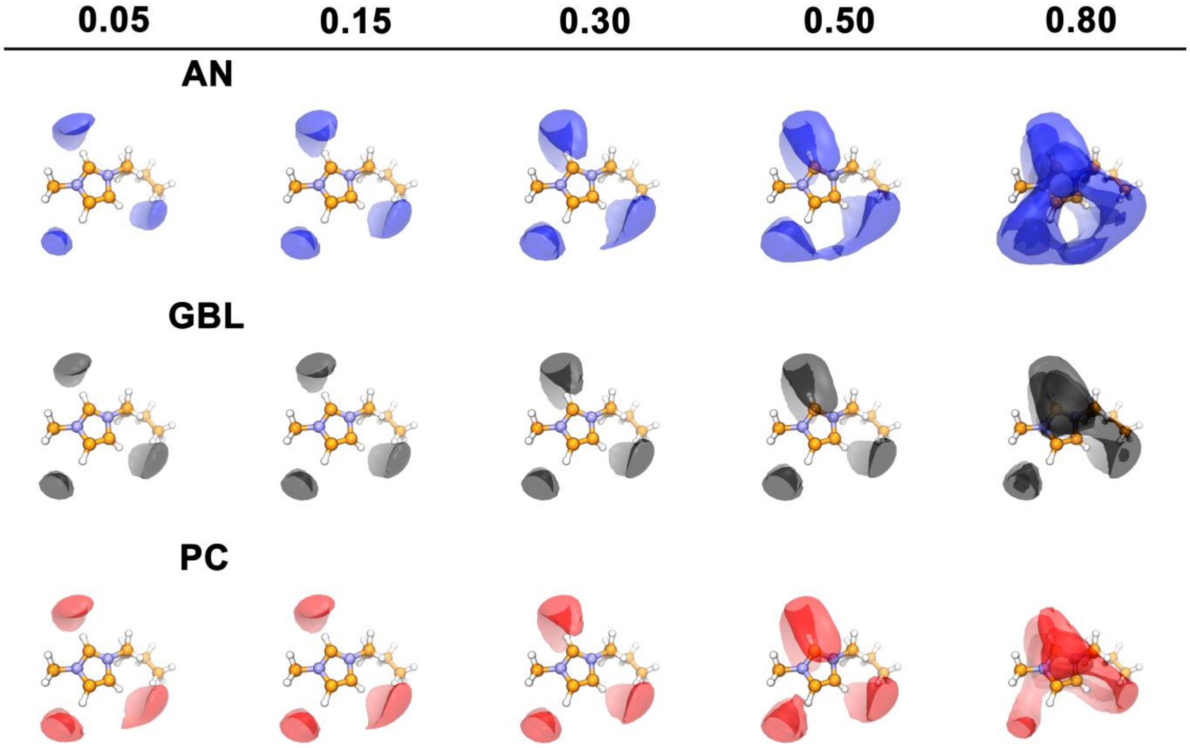

Figure 5.2. Spatial distribution functions of the solvent molecules around the hydrogen atoms $H^{2/4-5}$ of imidazolium ring for the different mixtures compositions of C_4mimBF_4 in AN (*blue*), GBL (*black*) and PC (*red*) for the different mixtures compositions with density probability of 30%.

Similar efforts have been made to analyze the distribution of the solvent around the cation and implicitly to get information of the effect of adding the solvent molecules on the cation anion interactions.

As an illustration, the SDFs of the AN around the $H^{2/4-5}$ sites in C_4mimBF_4 are given in Figure 5.2. Also, in this case a general trend is observed. Indeed, the SDFs of the solvent molecules are diffuse at high x_{IL} and become more localized at low x_{IL}. In particular, at high x_{IL} (between 0.8 and 0.40) we notice that the solvent is not present in the plan of the imidazolium ring at H^2 site.

The comparison between the anion and solvent SDFs around $H^{2/4-5}$ sites points out to the general idea that there is a competition between the anion and the solvent to occupy the position close to the $H^{2/4-5}$ sites.

5.2.2.2 Radial Distribution functions

5.2.2.2.1 Cation···anion interactions

An additional window on the local environment around the imidazolium cation can be provided by the analysis of the radial distribution function of the anion around the $H^{2/4-5}$ atoms. We consider the influence of the three studied solvents on the H-bonding interactions between the cation and anion involving the hydrogen atom at H^2 position and F in BF_4^- and PF_6^-, O in TFO^- and $TFSI^-$, The corresponding RDFs are given in Figure 5.3.

These Figures show that at x_{IL} between 1.0 and 0.4 the shape of the RDFs are not affected neither by the nature of the solvent nor by the change of the x_{IL}. For further decrease of x_{IL} the two peaks at 0.2 nm and 0.4 nm become well resolved and their intensities increase particularly in TFO^- and BF_4^- when they are mixed with GBL.

The coordination number of the anion around the cation is given in the same figure. It shows the same general trend that at low x_{IL}, a noticeable change in the value of the coordination number is observed and it is dependent on the anion type. Their behavior shows that the coordination number of the anion around the cations decreases with the decrease of x_{IL} (although the intensity of the corresponding RDF increase at low x_{IL}).

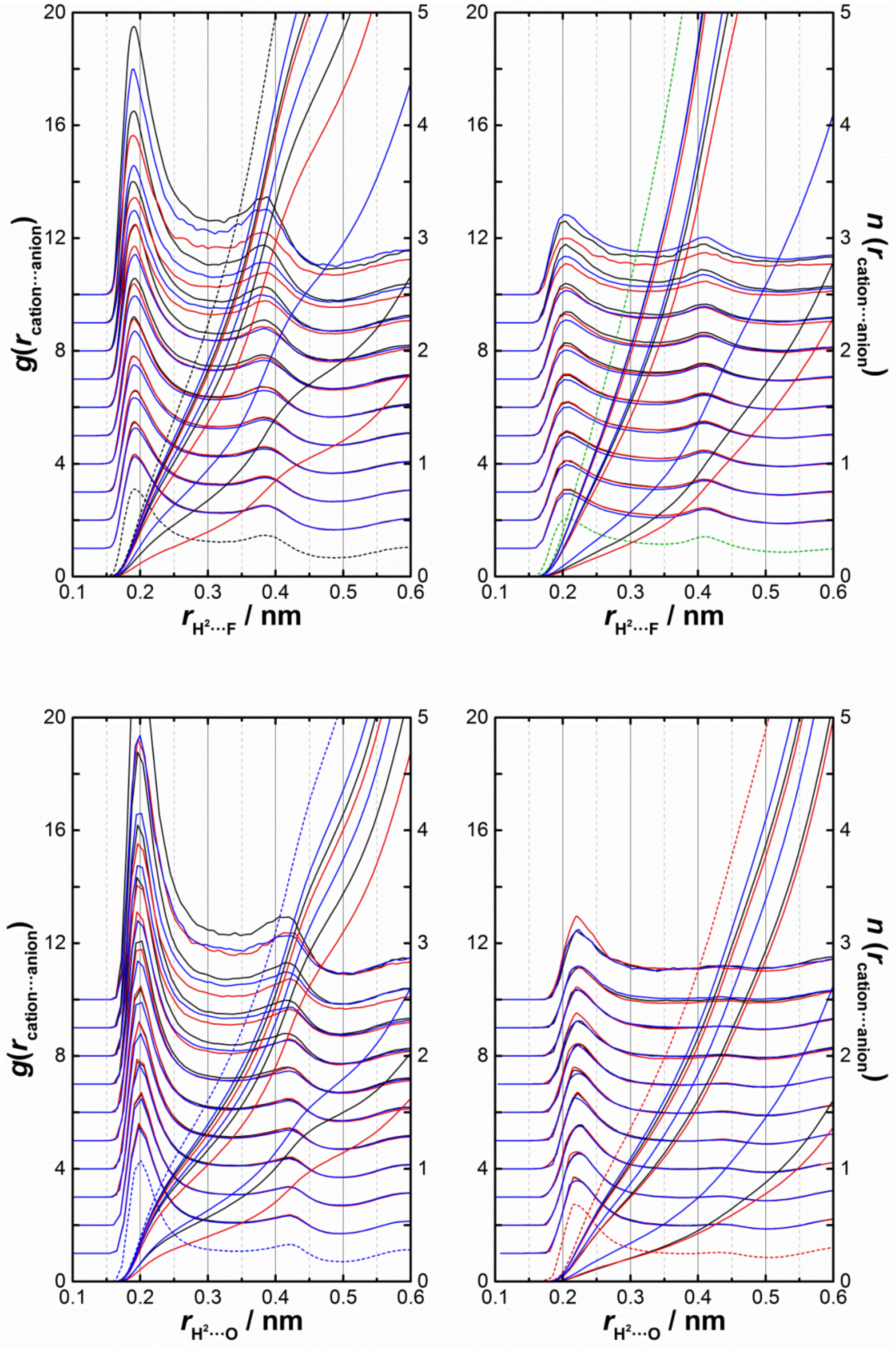

Figure 5.3. Evolution of the cation···anion radial distributions functions, $g(r_{cation\cdots anion})$, in the framework of H-bonding interactions between H^2 and F site in pure C_4mimBF_4 (*dashed black line*), C_4mimPF_6(*dashed green line*), H^2 and O in pure $C_4mimTFO$ (*dashed blue line*) and $C_4mimTFSI$ (*dashed red line*) and in the binary mixtures with AN(*solid blue line*), GBL (*solid black line*) and PC (*solid red line*) for the different mixtures compositions along with the corresponding coordination numbers, $n(r_{cation\cdots anion})$, for 0.05, 0.30, 0.50 and 1.00 x_{IL} (*right panel*). For the subsequent RDFs representations, the same color scheme will be used.

Similar observations are made for the cation···anion interactions involving the two other ring hydrogen atoms H^4 and H^5. The corresponding RDFs are less intense and located at larger distances compared with those involving H^2 site, which indicates rather weaker H-bonding interactions with counterions. This reflected in the lower coordination numbers of anions at $H^{4–5}$, which are also decreasing in the same way as described for H^2 site.

Similar observations concerning the evolution of cation···anion H-bonding interactions were made based on theoretical investigations of the related systems. Particularly, for the imidazolium-based binary mixtures with water (C_2mimAc-H_2O,[5] C_2mimGly-H_2O,[7] C_2mimAc/C_4mimCl/DmimDmp-H_2O,[9] C_4mimBF_4-H_2O,[15] $C_n$mimAc-H_2O,[8,17] C_4mimAc-H_2O,[10] C_4mimI-H_2O,[14] C_4mimPF_6-H_2O,[16] C_4mimBr-H_2O[18]), acetonitrile (C_4mimBF_4-AN,[73,74] C_2mimBF_4/C_4mimBF_4-AN[75]), alcohols (C_2mimMeSO_4-MeOH,[76] C_4mimTFSI-EtOH[13]) and ethers (C_4mimBF_4-diglyme,[11] C_6mimTFSI-tetraglyme[12]) it was found that interionic interactions are weakening with decreasing of x_{IL}.

5.2.2.2.2 Cation···solvent interactions

To get more insight regarding the influence of solvent on the structure of ILs we address the question whether or not solvent molecules interact strongly with anion or cation, *i.e.*, whether there is a competition between them.

As the first step, we considered the cation···solvent interactions in terms of evolution of the respective RDFs in the different mixture compositions. As a representative interaction sites we select the $H^{2/4–5}\cdots Y$ where Y corresponds to the most electronegative H-bond accepting atom of solvent, *i.e.*, N in AN, O^1 in GBL and PC. The first peak positions on the resulting RDFs (Figure 5.4) are located at slightly larger distances around 0.21-0.22 nm compared with those observed for the cation···anion RDFs. This can be interpreted as rather weak H-bonding interactions between the cation and the solvent molecules. Another distinguishing feature of these RDFs is the intensity of the first peak. It is higher in the case of $PF_6^–$ and $TFSI^–$ than that in TFO^- and BF_4^-. This behavior is opposite to that observed in the case of RDFs describing the cation-anions interactions. With decreasing of x_{IL} the respective RDFs intensities is decreasing, whereas the positions of the maxima remain the same in whole mixture composition. The behavior of the observed intensities is dependent on the nature of the solvent.

Taking into account all the observations gathered by analyzing the corresponding SDFs and RDFs, the following conclusions regarding the cation···anion and cation···solvent interactions can be drawn. Upon the dilution the H-bonding interactions between the cation and anion remain relatively unaffected in the range x_{IL} between 1.0 and 0.30. With further decreasing of x_{IL} we observe a large effect on RDFS and SDFs describing the distribution of the anion around the cation. These changes are compatible with the physical picture the solvent molecules compete with anions to be placed closer to the C_4mim^+ ring $H^{2/4\text{–}5}$ hydrogen sites.

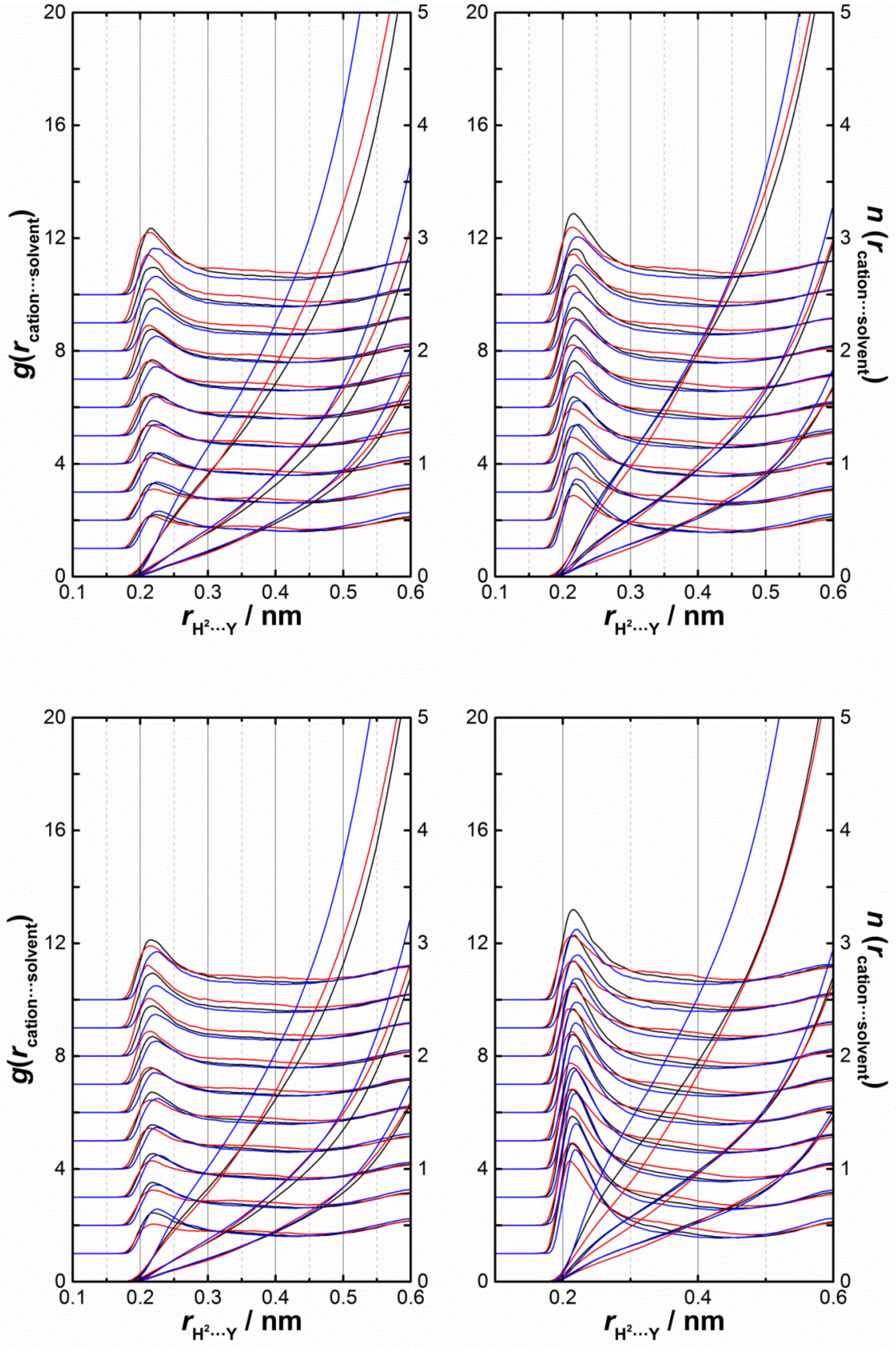

Figure 5.4. Evolution of the cation···solvent radial distributions functions, $g(r_{\text{cation}\cdots\text{solvent}})$, in the framework of H-bonding interactions between H^2 and Y site in the binary mixtures of C_4mimBF_4 (*top left*), C_4mimPF_6 (*top right*), C_4mimTFO (*bottom left*) and C_4mimTFSI (*bottom right*) with AN (*solid blue line*), GBL (*solid black line*) and PC (*solid red line*) for the different mixtures compositions along with the corresponding coordination numbers, $n(r_{\text{cation}\cdots\text{solvent}})$, for 0.05, 0.30 and 0.50 x_{IL} (*right panel*), where Y corresponds to the most electronegative H-bond accepting atom of the solvent N in AN, O in GBL and PC.

5.2.2.2.3 Anion···solvent interactions

Similarly to cation···solvent interactions, the anions are also able to form H-bonding with solvent molecules. In this part, we then considered the anion···solvent interactions in terms of evolution of the respective RDFs in the different mixture compositions. As a representative interaction sites we select the Y···H^2 (Y corresponds F in BF_4^- and PF_6^-, O in TFO^- and $TFSI^-$ and H^2 stands for the hydrogen atom in position 2 of AN, PC and GBL. We showed previously that this H^2 has the ability to from the rather strong intermolecular H-bonding interactions compared with other hydrogen atoms of the solvent molecules.

As it can be seen from the Figure 5.5, the shape of the corresponding RDFs is strongly solvent and mixture composition dependent. In addition, in contrast, to fact that the cation···solvent RDFs were affected only at low x_{IL}, the present RDFS are affected in the whole range of x_{IL}. In all the ionic liquids, the RDFs involving the PC and anion are located at short distances (the intense first maximum at *ca*. 0.21-0.22 nm that is comparable with cation···solvent interactions at C_4mim^+ ring H^2 site) while those involving AN solvent are located at large distance (the first peak position at *ca*. 0.25-0.27 nm) and those involving GBL are located at intermediate distances (0.23-0.26 nm).

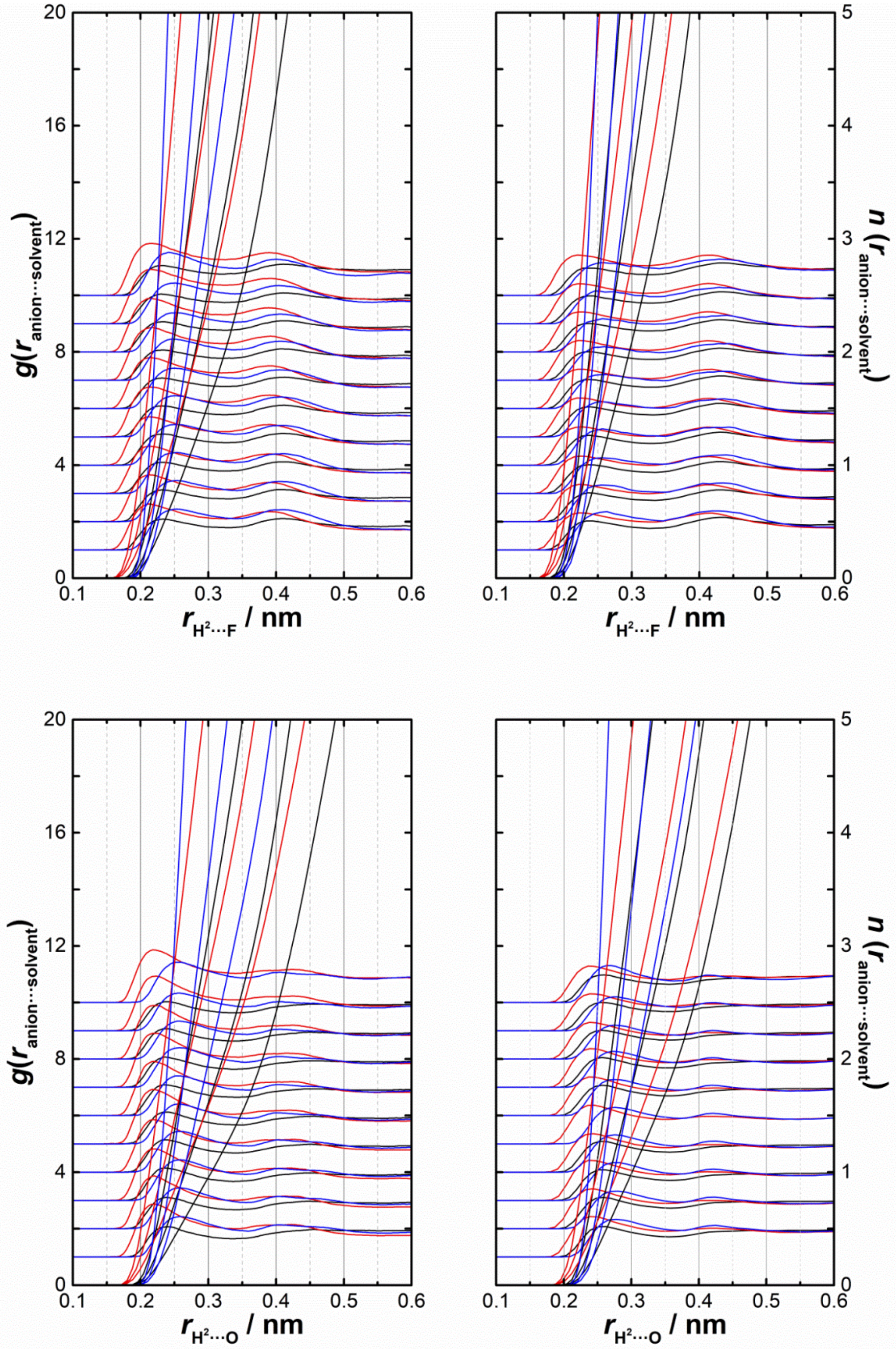

Figure 5.5. Evolution of the anion···solvent radial distributions functions, $g(r_{\mathrm{anion\cdots solvent}})$, in the framework of H-bonding interactions between H^2 site of the solvent and the most electronegative atom of anion (F in BF_4^- and PF_6^-, O in TFO^- and $TFSI^-$) in the binary mixtures of C_4mimBF_4 (*top left*), C_4mimPF_6 (*top right*), $C_4mimTFO$ (*bottom left*) and $C_4mimTFSI$ (*bottom right*) with AN (*solid blue line*), GBL (*solid black line*) and PC (*solid red line*) for the different mixtures compositions along with the corresponding coordination numbers, $n(r_{\mathrm{anion\cdots solvent}})$, for 0.05, 0.30 and 0.50 x_{IL} (*right panel*).

5.2.2.3 Nearest neighbor radial distribution functions

Taking into account these observations for further analysis of the H-bonding interactions we decided to follow the evolution of the nearest neighbor distributions for the two representative complexes: cation···anion and cation···solvent. Here we present a comparative analysis of the strength of the anion···cation and solvent···cation H-bonding interactions. This analysis is based on two distances describing H-bonding geometry between the imidazolium ring carbon/hydrogen atoms and the nearest neighboring H-bond-accepting atom of the anion and solvent, $C^{2/4–5}\cdots Y$ and $H^{2/4–5}\cdots Y$, where Y corresponds F in BF_4^- and PF_6^-, O in TFO^- and $TFSI^-$, N in AN, O^1 in GBL and PC. Thus, we expect to explore in more detail the effects of the different aprotic solvents, as well as the changes in the relative strength between the neighboring ions or solvents molecules upon the change of mixture composition. The behavior of the two distance characteristics of H-bonding for cation···anion, cation···solvent and anion···solvent are drawn in Figure 5.6 and 5.7.

The strategy of our approach is to analyze in the first step the effect of the three solvents on hydrogen bond interactions between the cation and anion of one IL and in the second step to compare the effect of one solvent on the cation and anion of the four type of ILs. In the two cases we calculated the two distance hydrogen bond characteristics for the cation-anion, cation···solvent and anion-solvent interactions in the whole mixture composition range. The effect of the solvent is quantified by comparing these distances as a function of the x_{IL}. The small values of the distances characteristics describing the cation anion interactions at low x_{IL} values, are interpreted as a weak effect of the solvent on the cation···anion interactions while the small values of the distances characteristics describing the cation···solvent and anion···solvent are interpreted as a strong interaction between the solvent and the two ions.

In the case of BF_4^-, the analysis shows that PC solvent is strongly affecting the cation···anion interactions. Indeed, the two characteristic distances, $<r(C^2\cdots Y)>$ and $<r(H^2\cdots Y)>$ in this case is the largest ones, while in the case of

AN solvent the values of these distances are the lowest. However, the analysis of the distances characterizing the cation-solvent hydrogen bonding interactions shows that the strongest interaction is occurring between the cation and AN solvent while in the case of PC and GBL solvents similar cation···solvent interactions are observed.

The same general trend observed for TFO^-, PF_6^- and $TFSI^-$. The extent of the change of the distance characteristics of hydrogen bonding interactions (cation···anion, cation···solvent and anion···solvent) is different for each type of solvent. However, in the case of PF_6^-, the interactions between the cation and the solvent are the strongest in the case of GBL.

In order to quantify the cation···anion, cation···solvent and anion···solvent interaction of the four ionic liquid mixed with one type of the solvent, we gather in figure, the corresponding distance characteristics of hydrogen bonding. In the case of AN, the cation-anion interactions in $TFSI^-$ are the most weakened and this accompanied by a strong interaction between AN and the cation while that between AN and $TFSI^-$ is the weakest one. The cation-anion interactions in BF_4^- are the least affected while the anion-solvent interactions are the strongest ones.

In the case of PC, it induces the large increase of the distances characteristics of hydrogen bond between the cation and anion in both $TFSI^-$ and PF_6^- while those associated with cation···solvent interactions are the strongest in PF_6^- and those associated with the anion···solvent are the weakest.

Similarly to PC, GBL induces a large effect on cation-anion distances characteristics (weakening of hydrogen bond between the cation and anion). The comparison between the distances characteristics describing the cation-solvent interaction, shows that they are the most affected in GBL, while the comparison between those describing the cation-solvent and anion-solvent shows that they are similar to those measured in AN solvent.

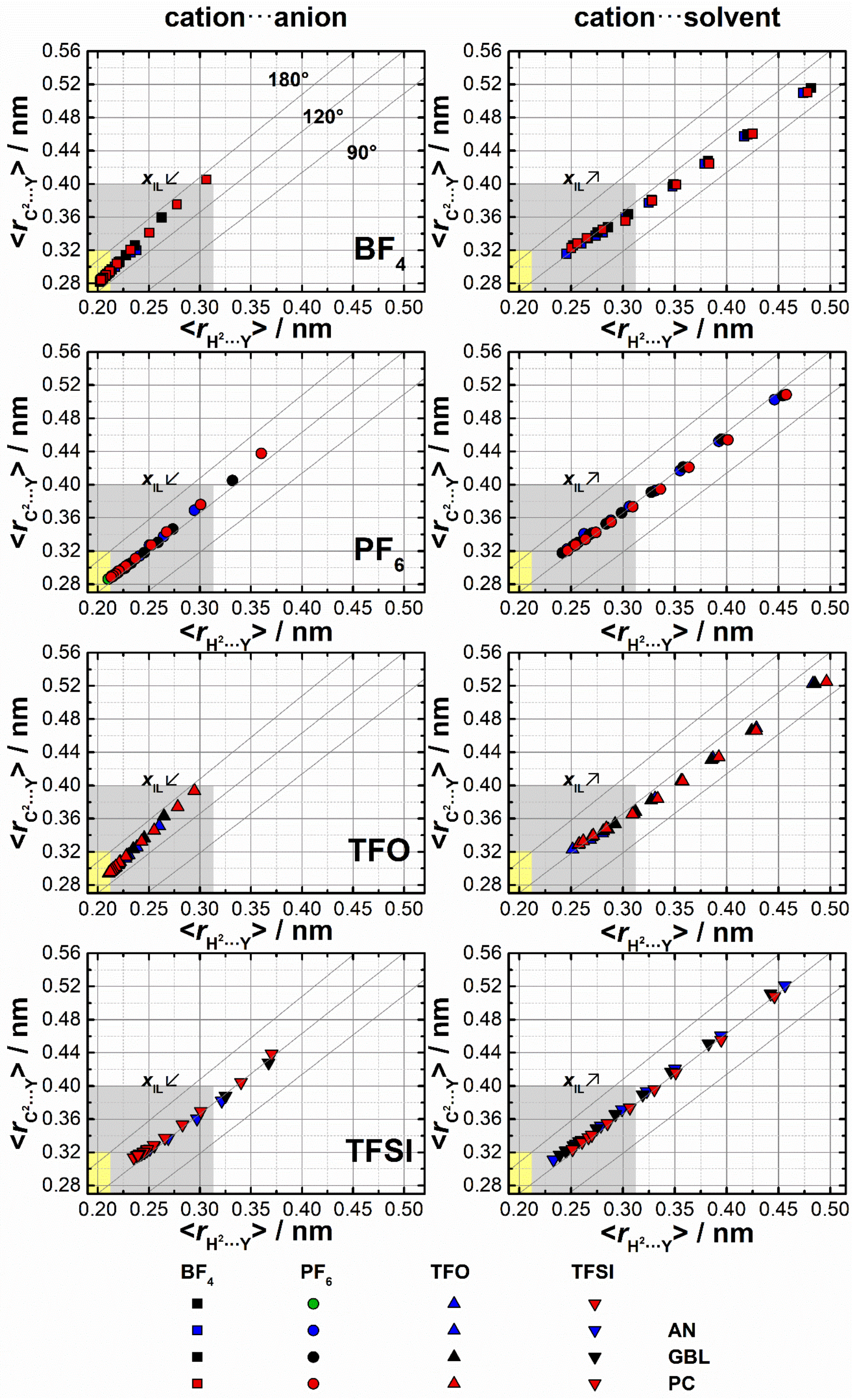
cation···anion
cation···solvent
180°
120°
90°
x_{IL}
BF$_4$
PF$_6$
TFO
TFSI
$<r_{C^2 \cdots Y}>$ / nm
$<r_{H^2 \cdots Y}>$ / nm
0.56
0.52
0.48
0.44
0.40
0.36
0.32
0.28
0.20
0.25
0.30
0.35
0.40
0.45
0.50
AN
GBL
PC

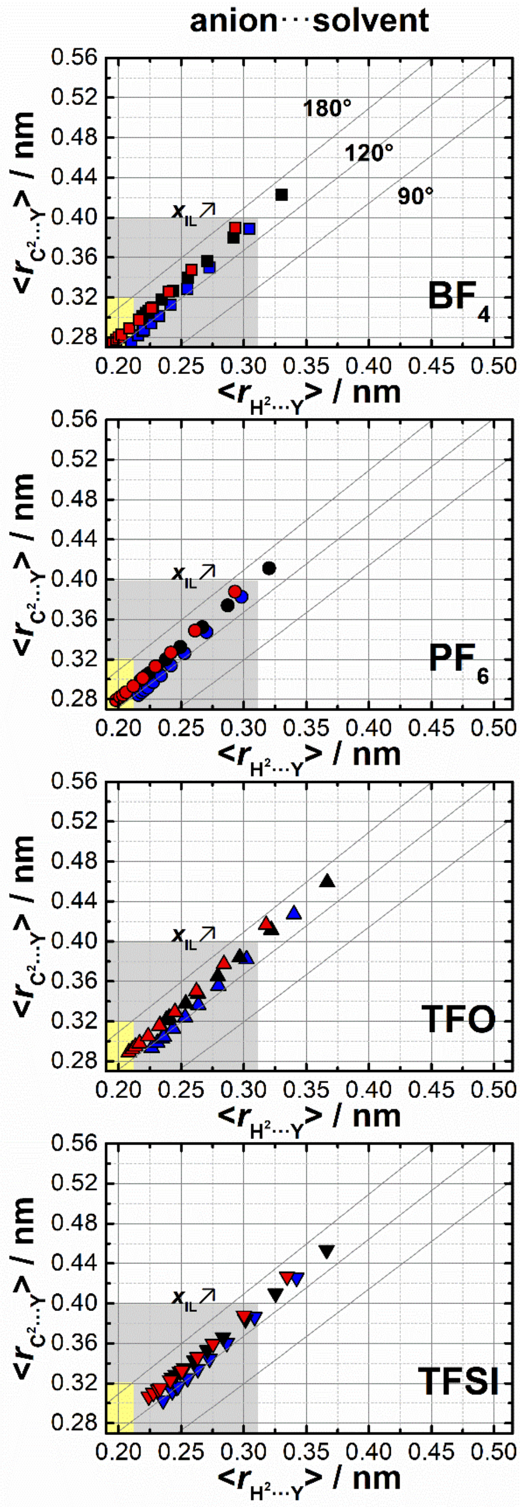

Figure 5.6. The cation···anion, cation···solvent and anion···solvent average distances representing H-bonding geometry between the reference molecule and the nearest neighboring one, $C^i\cdots Y$ and $H^i\cdots Y$, (where Y corresponds F in BF_4^- and PF_6^-, O in TFO^- and $TFSI^-$, N in AN, O^1 in GBL and PC) for pure C_4mimBF_4, C_4mimPF_6, $C_4mimTFO$ and $C_4mimTFSI$ and for the different mixtures compositions in the binary mixtures with AN, GBL and PC. The grey region denote the weak H-bonding interactions and the yellow region denote the H-bonding interactions of the medium strength.

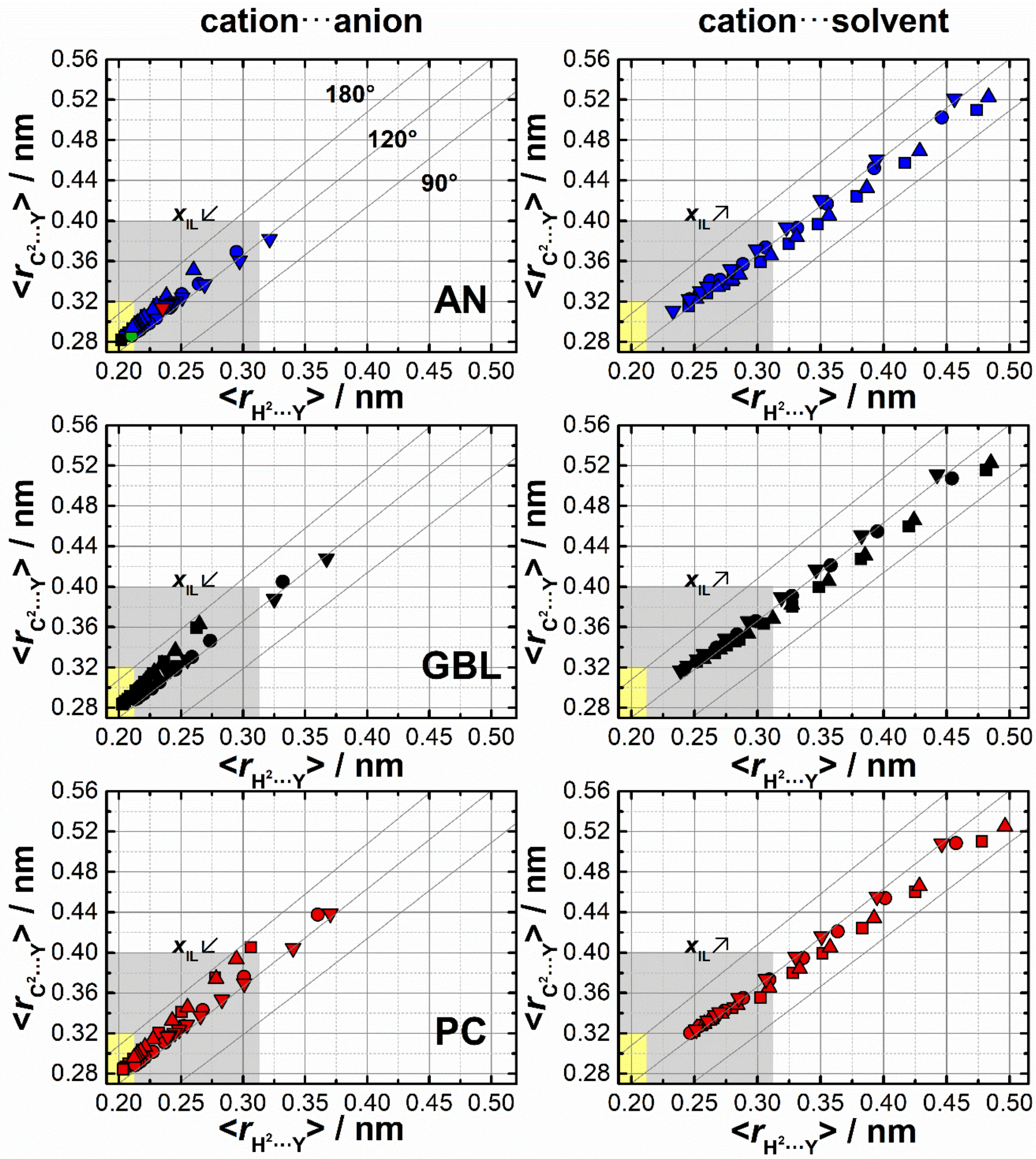
cation···anion
cation···solvent
180°
120°
90°
x_{IL} ↙
x_{IL} ↗
AN
GBL
PC
0.56
0.52
0.48
0.44
0.40
0.36
0.32
0.28
0.20 0.25 0.30 0.35 0.40 0.45 0.50
$<r_{C^2\cdots Y}>$ / nm
$<r_{H^2\cdots Y}>$ / nm

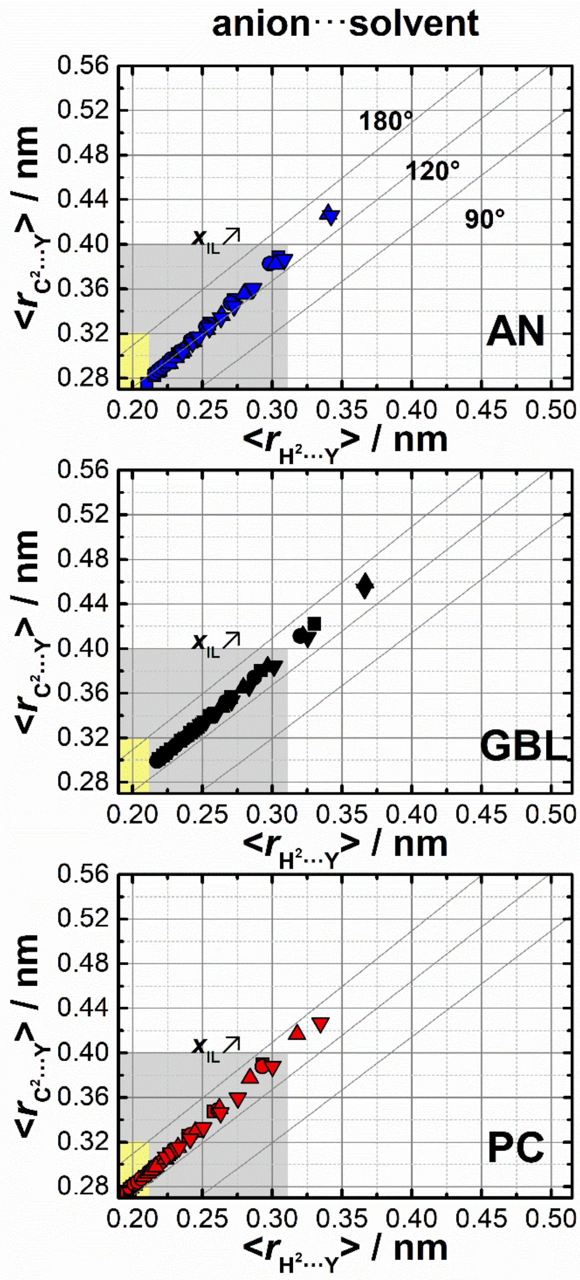

Figure 5.7. The cation···anion, cation···solvent and anion···solvent average distances between the reference molecule and the nearest neighboring one in the framework of H-bonging interactions for the different mixtures compositions in the binary mixtures with AN, GBL and PC, where Y corresponds to the most electronegative H-bond accepting atom of the anion (F in BF_4^- and PF_6^-, O in TFO^- and $TFSI^-$) or solvent (N in AN, O^1 in GBL and PC).

5.2.2 Orientation between the cation···anion and cation···solvent

Another insight into the cation···anion and the cation···solvent competition concerns the relative spatial arrangement of anion and solvent around the imidazolium ring $C–H^{2/4–5}$ sites. For this task, we calculated the distribution of the nearest anions as a function of the distribution of solvent with respect to one of the three ring hydrogen atoms $H^{2/4–5}$ of C_4mim^+ cation. Similar to the angle φ, describing the orientation of the studied anions in pure ILs (see Figure 3.3 Chapter 3), we have added the angle δ which is formed by normal vector and the radius vector between ring hydrogen atoms H^i and the first nearest donor accepting atom of solvent molecule, *i.e.*, N in AN, O^1 in GBL and PC. Thus, the perfect above/below arrangement of anion and solvent around the reference H^i site will shift the angle δ to the values close to 0 and 180 degrees, while an in-plane arrangement will correspond to a δ value around 90 degrees. The results of this analysis are presented in Figure 5.8 as a probability distributions of these angles for each IL in a mixture with the three molecular solvents.

This Figure shows that at high $x_{\mathrm{IL}} = 0.80$, the anion occupies mainly the above/below orientation while the solvent molecules are randomly distributed around the cation. When, the x_{IL} is decreasing, the general trend is that the solvent molecules compete with the anion to have the above/below orientation. However, the extent of this tendency is solvent and IL types dependent. Indeed, in the case of BF_4^- and TFO^-, the probability to occupy the above/below position is higher for the solvent than for the anion while it still remain lower for the $TFSI^-$ and PF_6^-. At very low $x_{\mathrm{IL}} = 0.05$ this probability is almost equal for the anion and the solvent in the case of PF_6^- and $TFSI^-$.

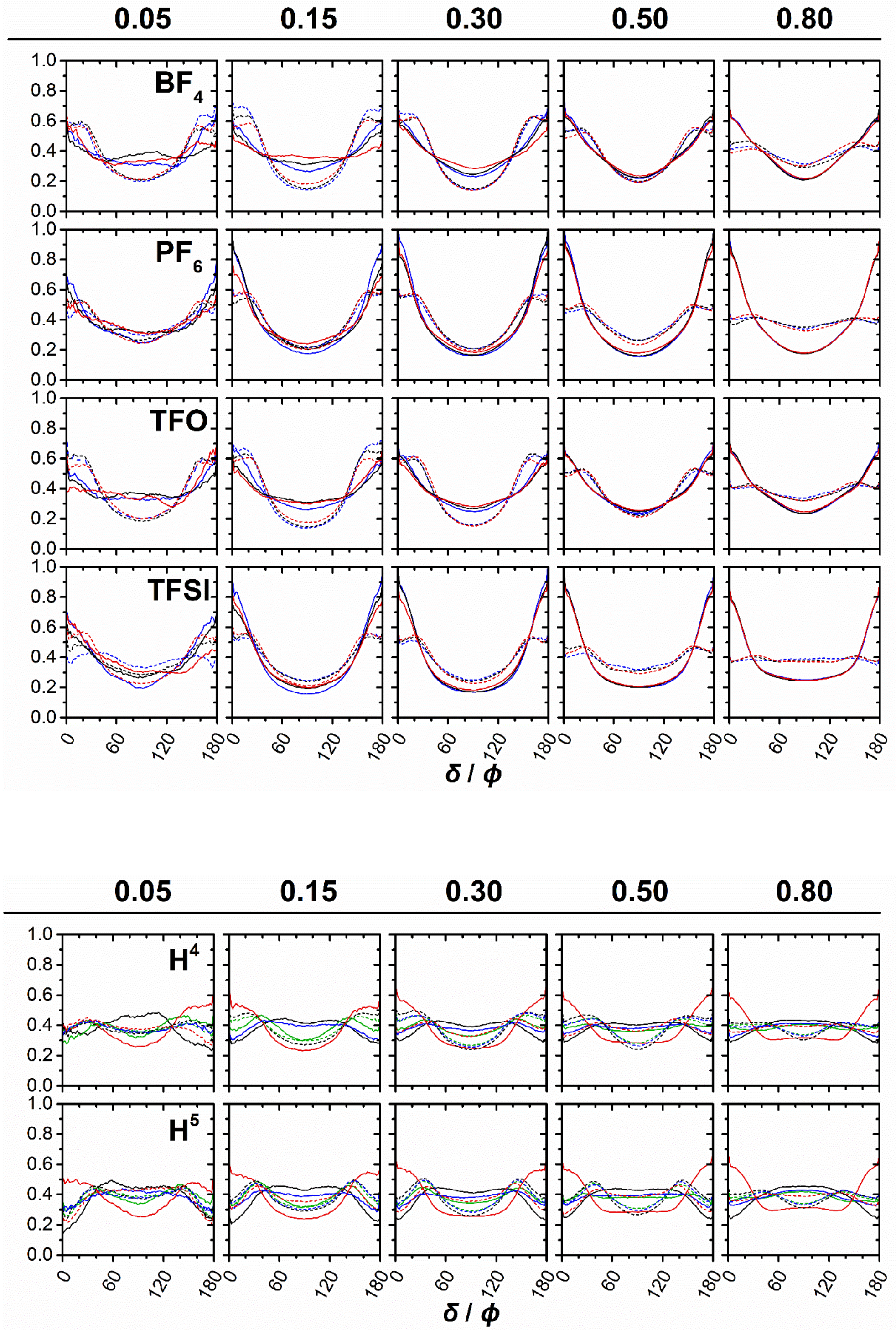

Figure 5. 8. The angular probability distributions $p(\phi)$ and $p(\delta)$ describing the orientation of the anion (*solid line*) and solvent (*dashed line*) orientation between a reference cation and its first neighbor for a chosen x_{IL}. In the top panel, the dependence of the above/below orientation between the cations in the AN (*blue*), GBL (*black*) and PC (*red*) is present at H^2 site, while in the lower panel the dependence of this probability for C$_4$mimBF$_4$ (*black*), C$_4$mimPF$_6$ (*green*), C$_4$mimTFO (*blue*) and C$_4$mimTFSI (*red*) at H$^{4–5}$ in AN solvent is given as an example.

As for the distribution of the anions and solvent molecules around the H^{4-5} atoms, some ILs-specific details are also apparent. In C_4mimBF_4, $C_4mimTFO$ and C_4mimPF_6, the anions tend to be localized around the in-plane positions next to the H^{4-5} sites, while the solvent molecules is mainly located above and below these sites. Upon the dilution of ILs the positions of solvent molecules do not change significantly, while the probability of the above/below anion arrangement slightly increases in $C_4mimTFO$ and C_4mimPF_6. Moreover, the probability of the respective angular distributions also increases for solvent molecules and decreases for anions making it impossible for the simultaneous presence of the solvent molecules and anions in the same position, *e.g.*, in case of C_4mimPF_6 where the angular values coincide. Similar observations are also justified for $C_4mimTFSI$ where the positions of anions are arranged above/below next to the H^{4-5} sites.

5.2.3 Cation···cation stacking interactions

To gain a deeper insight about the impact of concentration effects as well as the effect of different medium on the stacking interactions in the studied ILs we decided to apply consistently the combinations of several angular distributions with respect to the distance between center of the imidazolium rings of the reference and neighboring cations similar to the results for pure ILs reported in Chapter 3. The obtained results presented as the corresponding angular probability distributions and shown in Figure 5.9 for $p(\alpha)$, and in Figure 5.10 for $p(\beta)$ and in Figure 5.11 for $p(\psi)$ and in for each studied IL in combination with AN, GBL and PC.

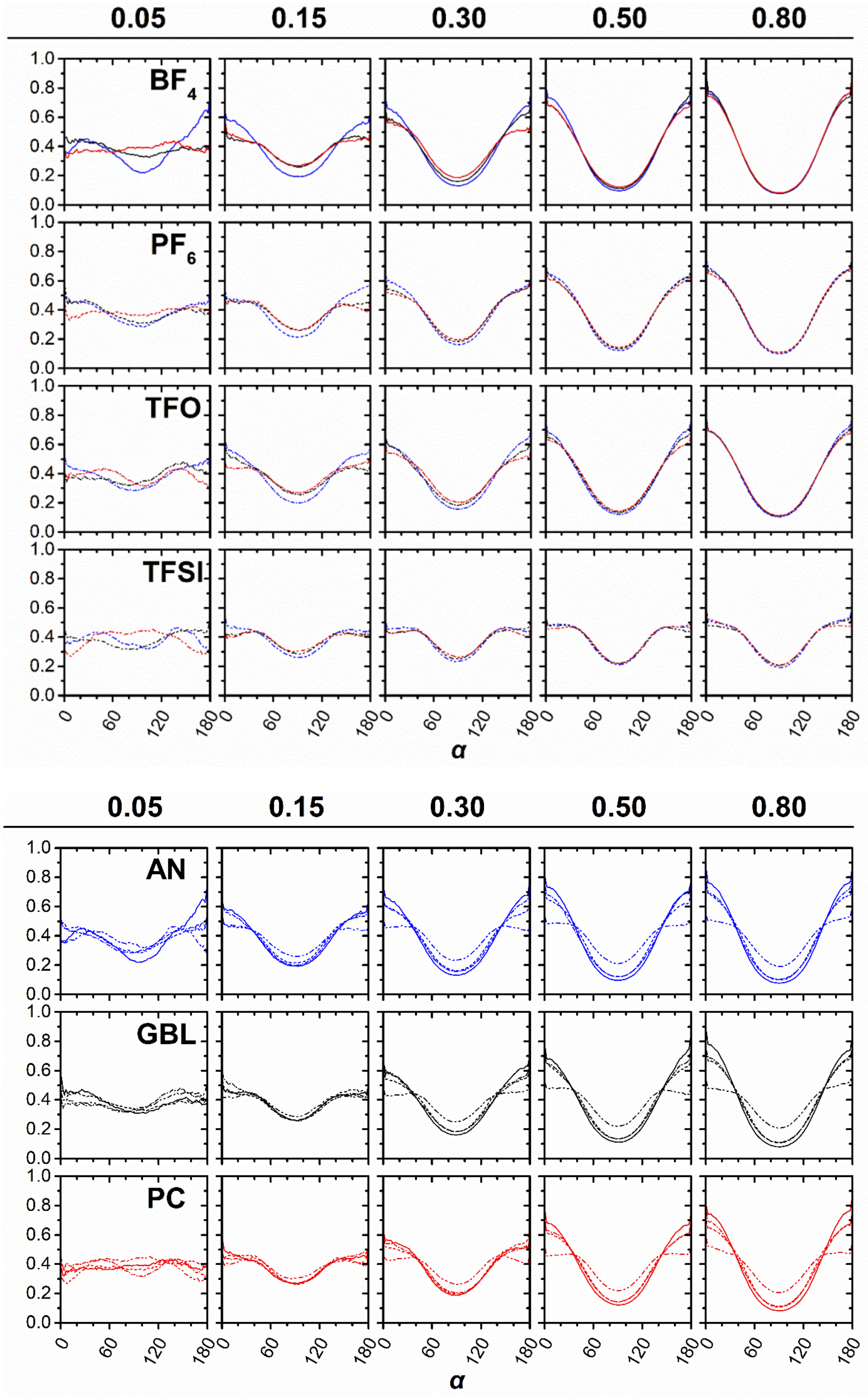

Figure 5.9. The angular probability distributions $p(\alpha)$ describing the above/below orientation between a reference cation and its first neighbor for a chosen x_{IL}. In the top panel, the dependence of the above/below orientation between the cations in the various solvents is present while in the lower panel the dependence of this probability on the solvent for each studied IL is given.

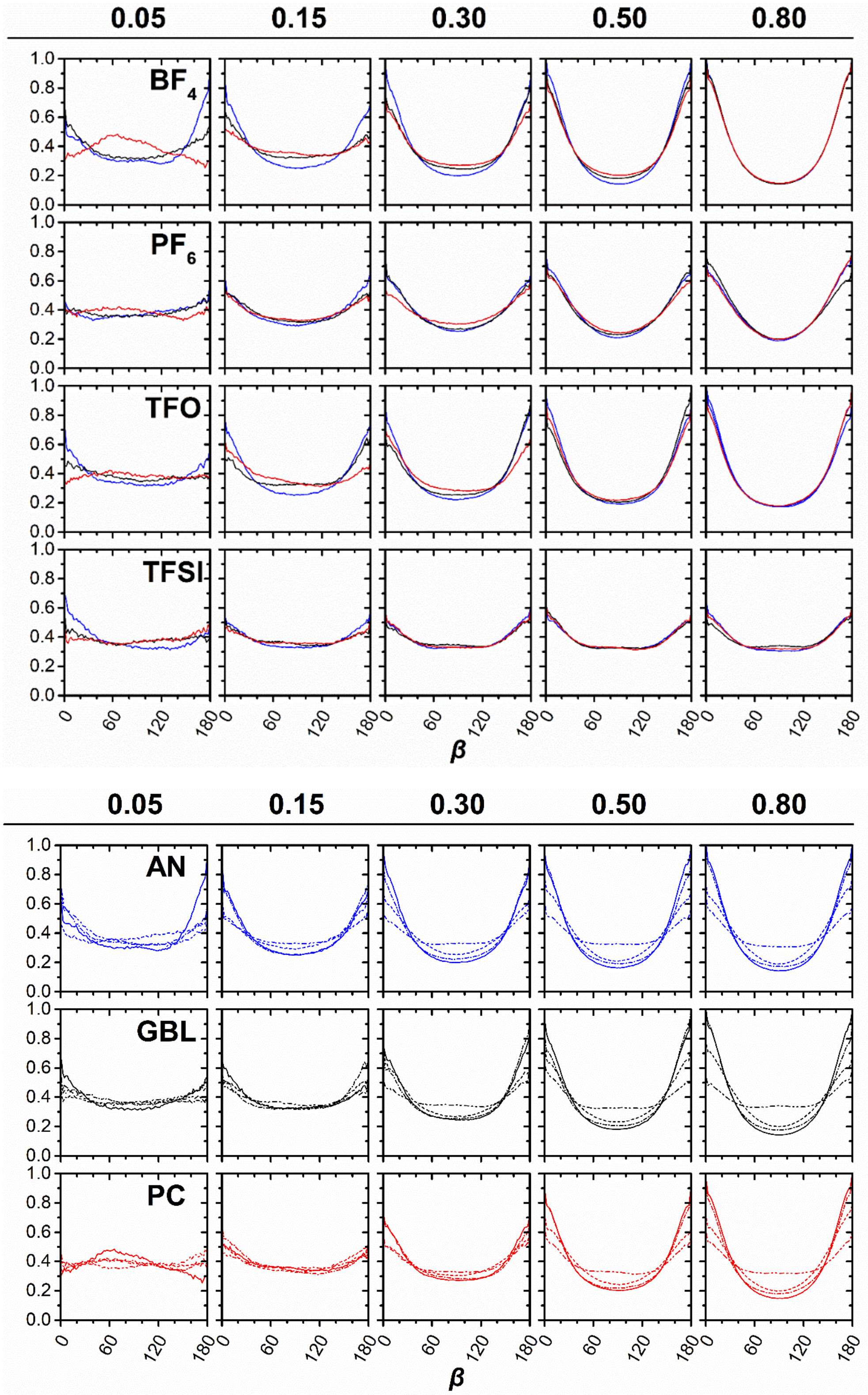

Figure 5.10. The angular probability distributions $p(\beta)$ describing the planar orientation between a reference cation and its first neighbor for a chosen x_{IL}. In the top panel, the dependence of the above/below orientation between the cations in the various solvents is present while in the lower panel the dependence of this probability on the solvent for each studied IL is given.

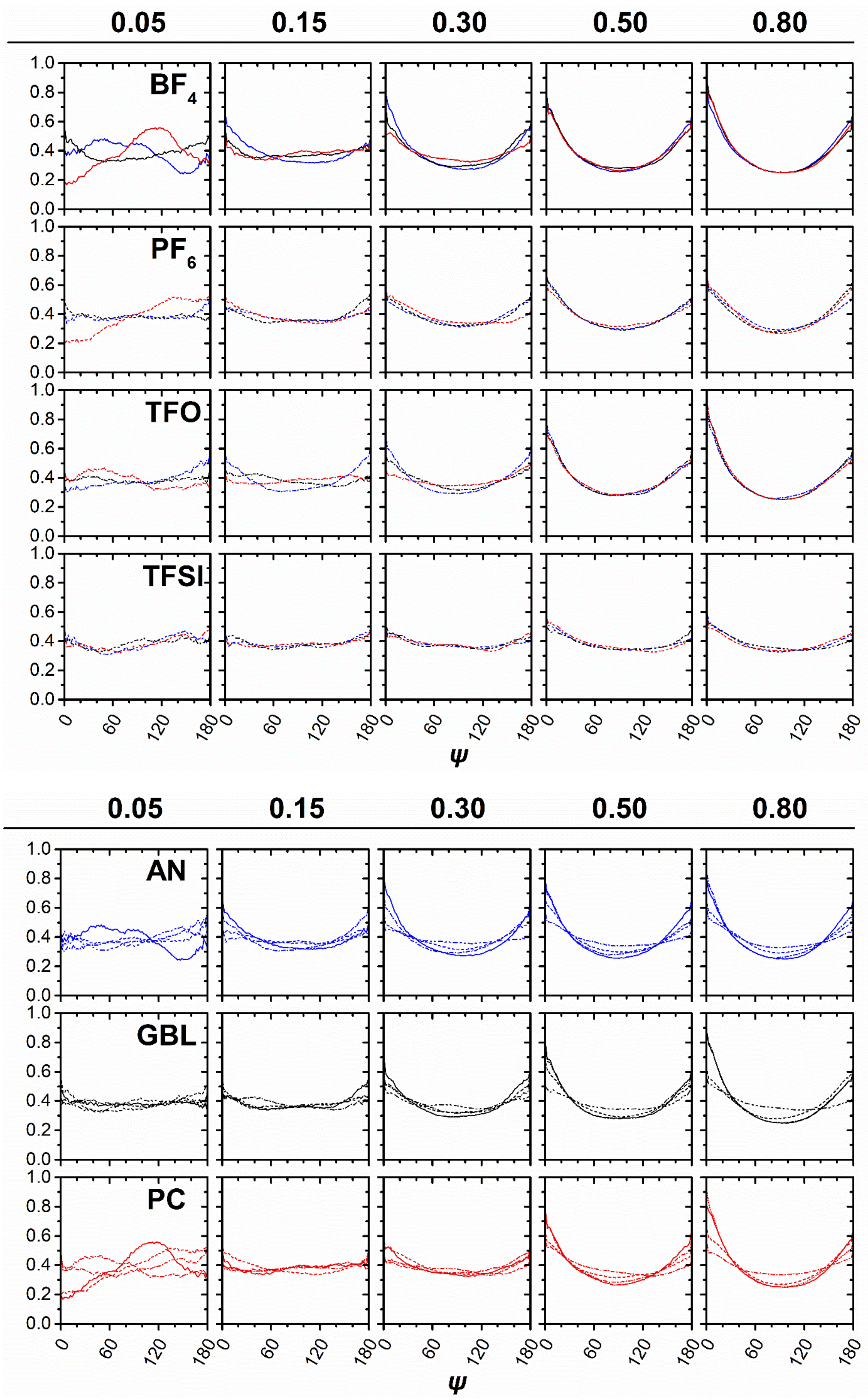

Figure 5. 11. The angular probability distributions $p(\psi)$ describing the parallel and antiparallel orientation between a reference cation and its first neighbor for a chosen x_{IL}. In the top panel, the dependence of the above/below orientation between the cations in the various solvents is present while in the lower panel the dependence of this probability on the solvent for each studied IL is given.

The first investigated angle, designated as α according to the scheme in Figure, indicate a tendency for the above/below arrangement of the neighboring cation around the reference one. When x_{IL} is decreasing this above/below orientation is loosened and becomes almost random at low $x_{\mathrm{IL}} = 0.05$. The extent of these changes is lower for BF_4^- and TFO^-.

The parallel orientation between the rings of two cations neighbors, as described by the β angle undergoes the same general trend. It is almost not affected in the range of x_{IL} between 0.8 and 0.30 and becomes loosed and even random at low x_{IL}. However, the extent of these changes is IL dependent.

In AN, the parallel orientation is less affected for TFO^-, while in GBL and PC solvents this orientation is strongly affected for all the studied IL.

5.2.4 Solvent···solvent interactions

5.2.4.1 Radial distribution function

In order to describe these interactions, we calculated the radial distribution of the H^2 atom of the solvent around a reference atom of the solvent, N in the case of AN and O^1 in the case of PC and GBL. In the following, we will discuss the effect of adding IL on the radial distribution between the solvent molecules. The corresponding RDFs are given in Figure 5.12. Upon the admixing of the studied solvents with ILs the position of the maxima in RDFs is not altered with the variation of x_{IL}, while the intensities are quite sensitive to the type of counterion and decreasing with increasing of x_{IL}. At low $x_{\mathrm{IL}} < 0.30$, the shape and intensities of RDFs are not affected by the addition of ILs, particularly in the case of GBL, while for AN and PC there is a minor difference in the shape of the RDFs. It should be noticed that in this range of $x_{\mathrm{IL}} < 0.30$, the cation···anion and ions···solvent RDFs undergo a large changes. This means these solvent-solvent interactions as described by these RDFs are not affected and remain almost similar to as in pure solvents. With increasing x_{IL}, the shape of these RDFs becomes more affected and the extent of this effect is more pronounced in PC. As it is expected, the coordination number between the solvent molecules is decreasing with the increase of x_{IL}.

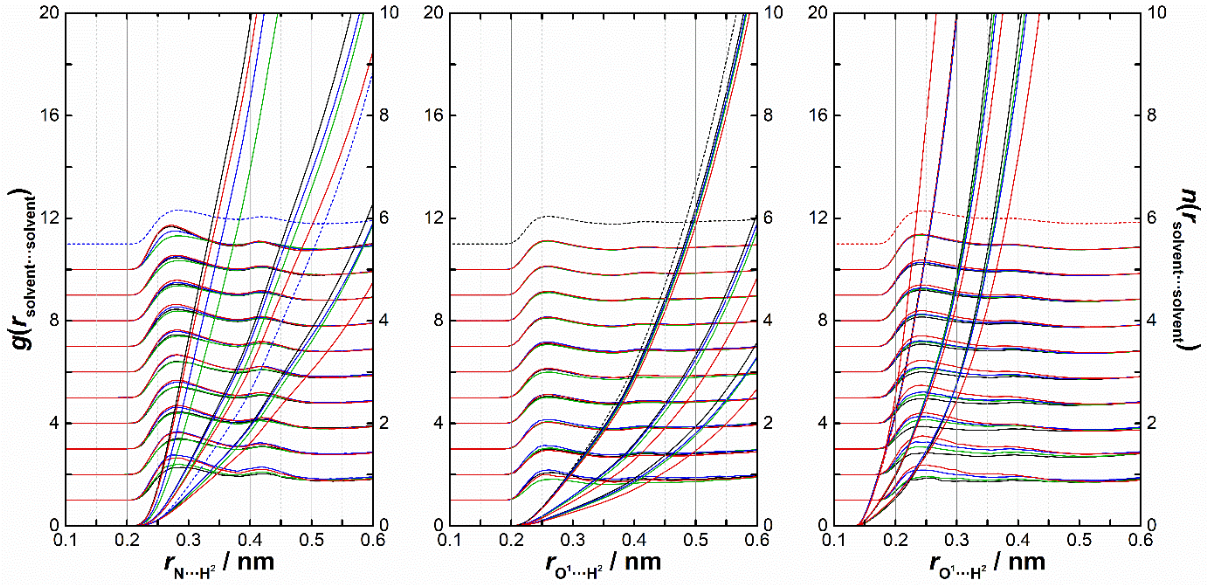

Figure 5.12. Radial distribution functions describing the distribution of the observed solvent molecules around a reference one. The atom of the reference molecule is N for AN and O^1 for PC and GBL while the observed atom is H^2 atom in position 2. Black, green, blue and red lines are for C_4mimBF_4, C_4mimPF_6, C_4mimTFO and C_4mimTFSI, respectively.

5.2.4.2 Nearest neighbor radial distribution

Similarly to the discussion of the hydrogen bonding between the cation-anion, and ions-solvent, we will analyze the H-bonding between the solvent molecules through the two distance characteristics describing the distance $C^2\cdots Y$ and the $H^2\cdots Y$, where Y stands for O^1 in GBL and PC and N in AN, while C^2 and H^2 are the atom occupying the position 2 in the solvent molecules (see Figure 4.9, Chapter 4). The behavior of these distances given in Figure 5.13.

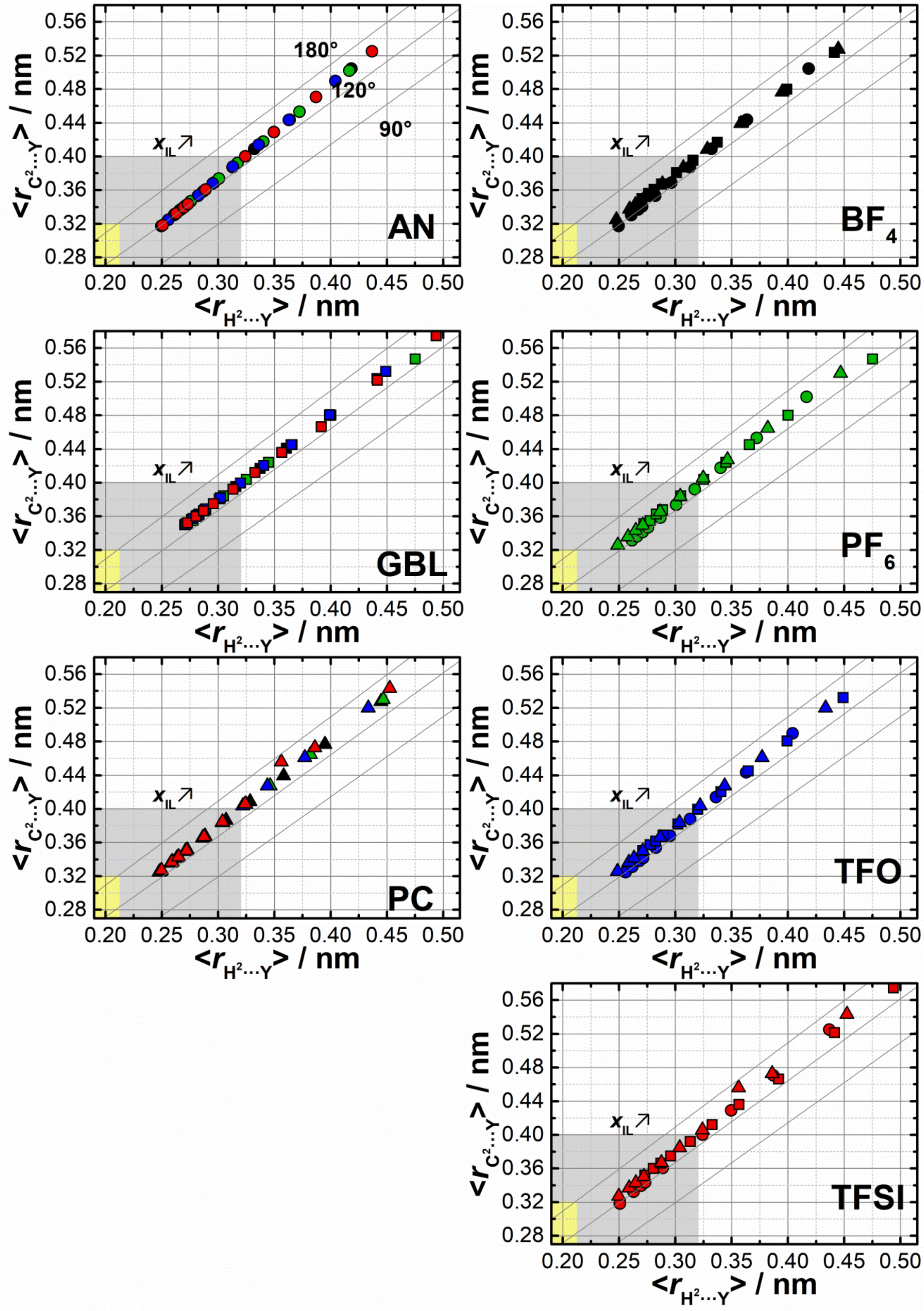

Figure 5.13. Evolution of the solvent···solvent average distances between the reference molecule and the nearest neighboring one in the framework of nonspecific and specific interactions for pure AN, GBL and PC, and for the different mixtures compositions in the binary mixtures with ILs.

This Figure shows that the solvent···solvent hydrogen bonds are weakened with respect to their strength in pure state. In C_4mimTFSI ionic liquid, induces the most important weakening of the solvent-solvent hydrogen bonding in the three solvents, while the least effect observed in C_4mimBF_4 and C_4mimTFO, while it is intermediate in C_4mim PF_6.

5.2.4.3 Orientation between the solvent molecules

In order to study the orientational aspects in more detail, we have decided to calculate several angular probabilities where the angles are defined in Figure 4.5 in Chapter 4. In PC and GBL molecular solvents, the first investigated angle, α describes the above/below the reference molecule would correspond to α angle around 0° and 180°, while perfect in-plane arrangement of the observed molecules would contribute to the α values close to 90°. The second investigated angle is β formed by the normal vectors of the ring planes between the reference and observed molecules. As in the previous case a perfectly parallel arrangement of the planes corresponds to β values of 0° and 180°, whereas the values around 90° are indicative of a T-shaped relative arrangement of the two ring planes. This angle gives information on the stacking between the rings of the solvent molecules. In the three molecular solvents, PC , GBL and AN, the third angle designated as ψ is that between the vectors along C=O bond in PC and in GBL or C≡N bond in AN of the reference solvent molecule and observed like molecules. The ψ values close to 0° and 180°, indicate a parallel and antiparallel orientation, respectively. Thus, this angle gives information about the relative orientation of molecular dipoles. The probability distributions of these angles are illustrated in Figure 5.14, for $p(\alpha)$ and $p(\beta)$ and in Figure 5.15 for $p(\psi)$ as a function of x_{IL}.

The behavior of the probability distribution describing the above/below orientation between PC molecules and between GBL ones, the above/below dominant orientation observed in pure solvents maintained in the range of x_{IL} between 0.05 and 0.50 (in a high mole fraction range of the solvent) and for further increase of x_{IL}, this orientation becomes almost random. As it shown in Figure 5.14

the parallel orientation between the rings of the solvent molecules is similar in the PC and GBL solvents as it is not affected, with respect to that in pure solvents , with adding IL to the molecular solvent.

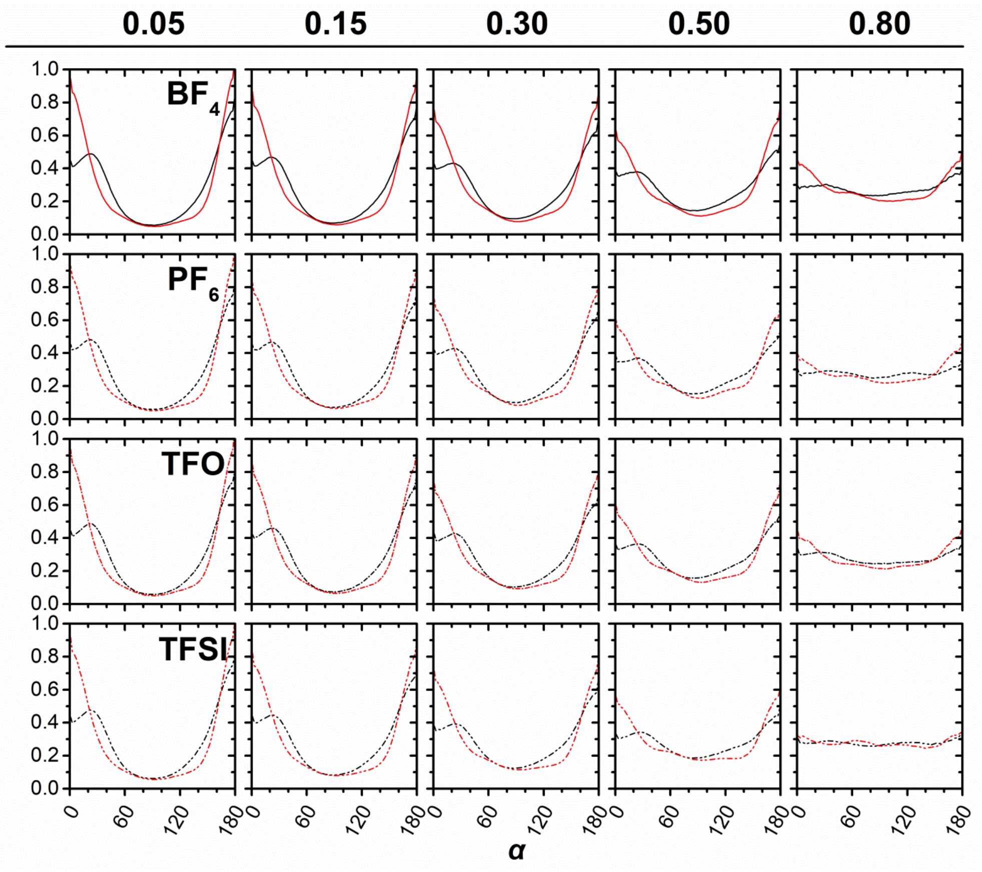

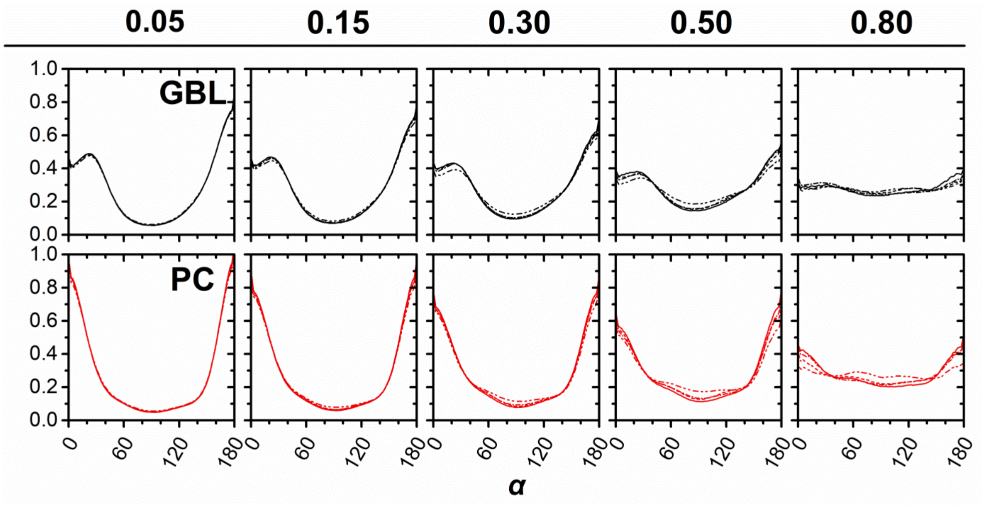

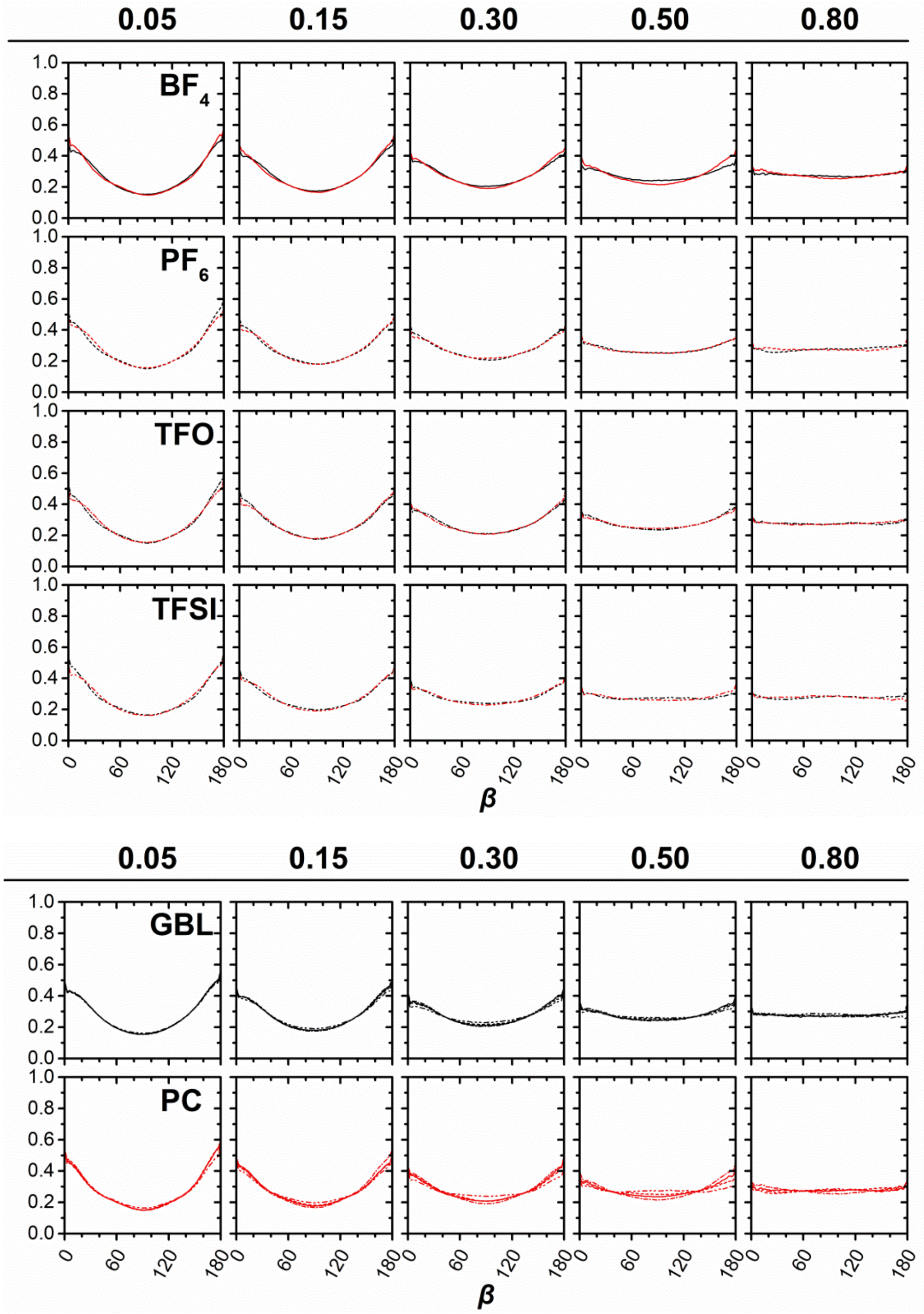

Fig 5.14. The angular probability distributions of the angles α and β describing the above/below and planar parallel orientations between PC and GBL molecular solvents. In each fig, the top one illustrates the comparison between the change of these orientations for the PC and GBL in each type of IL in the down one represents the change of these orientations of each solvent in the four ILs.

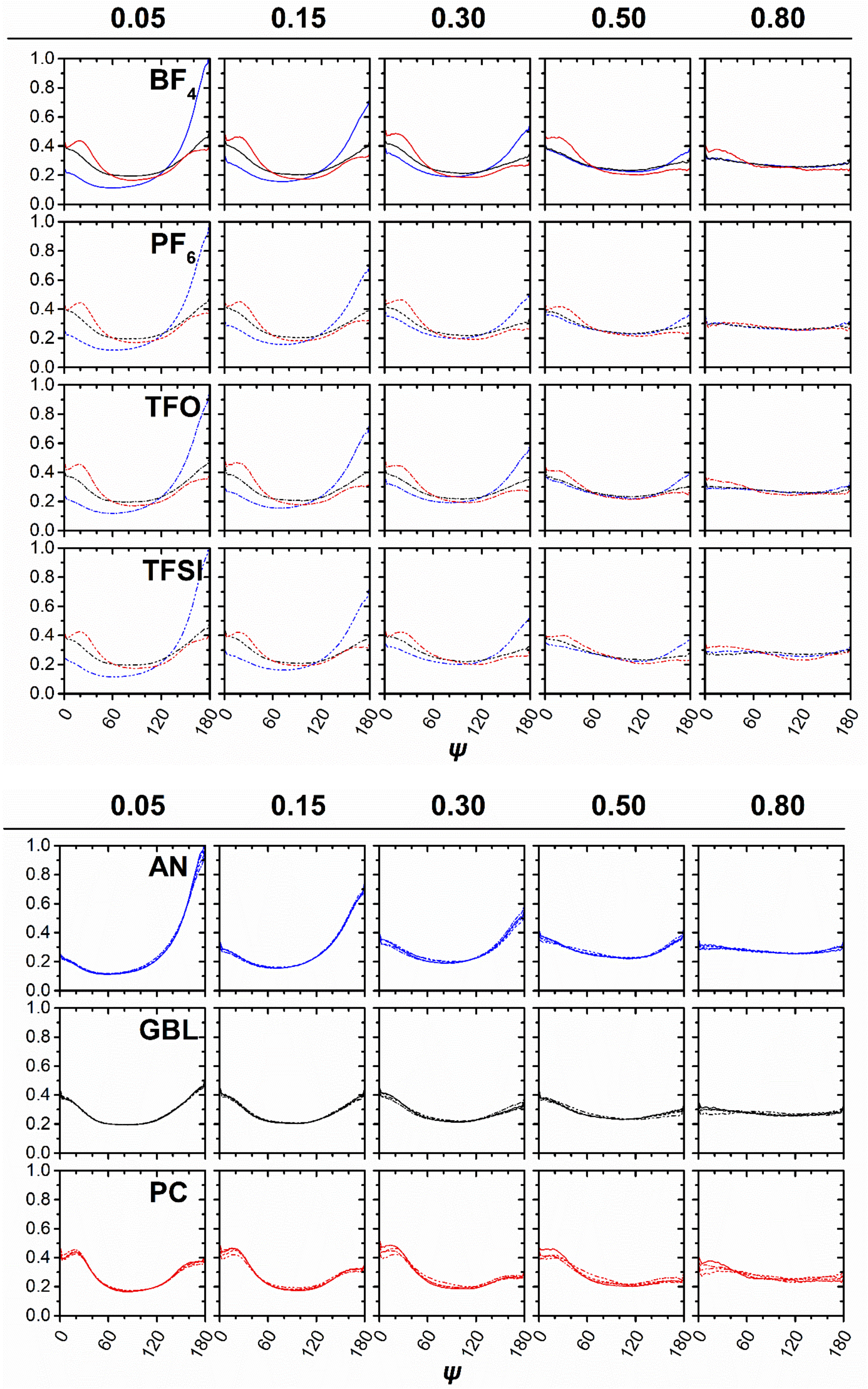

Fig 5.15. The angular probability distributions of the angle ψ describing the dipole-dipole orientation (C≡N axis in AN and C=O axis in PC and GBL) orientations between the molecular solvents. In each fig, the top one illustrates the comparison between the change of these orientations for the three molecular solvents in each type of IL in the down one represents the change of these orientations of each solvent in the four ILs.

The same general trend as a function of x_{IL} is observed for the orientation between the solvent molecules is associated with the orientation between the C≡N axes of AN and between the C=O axes of PC and GBL. These orientations are similar in the four ILs, and the effect of adding IL to the solvent affect slight these orientations in x_{IL} in the range between 0.05 and 0.3 while at further increase of IL in these molecular solvent, these orientations becomes random.

5.3. Conclusions

Classical MD simulation have been used to trace the evolution of the representative interionic, ion-molecular and intermolecular interactions in the binary mixtures of C_4mim^+ cation coupled with BF_4^-, PF_6^-, TFO^-, and $TFSI^-$ with dipolar aprotic solvents.

The results show that in all the studied IL/molecular solvent mixtures, the distribution of the anion around the cation is not drastically affected in the range of x_{IL} between 1 and 0.3 and noticeable changes, traced to the behavior of the SDFs, RDFS and the distance characteristics describing the cation and anion hydrogen bonding interactions, occur. These changes are associated with the expected weakening of the cation and anion interactions. This weakening is more important in PC and GBL in comparison to that in AN and the most affected cation···anion interaction are those in $C_4mimTFSI$ and in C_4mimPF_6 and the least affected are those in C_4mimBF_4 and in $C_4mimTFO$. This trend is in full agreement with the behavior of the C–H vibration mode and the ^1H chemical shift. Our molecular dynamics simulations bring a new insight on the behavior of the cation-solvent and anion-solvent interactions. Indeed, our results the following general trend about the cation···solvent interactions: for the three solvents, the weakest interactions are observed in the case of $C_4mimTFO$ (the values of the distances characteristics describing the cation···solvent are small), while the strongest ones are observed in AN and GBL for $C_4mimTFSI$ and for C_4mimPF_6 in PC.

Concerning the anion···solvent interactions, the three solvent have the weakest interactions with $TFSI^-$, AN and PC solvent have the strongest interaction with BF_4^-, while GBL interacts strongly with PF_6^-.

5.4. References for Chapter 5

(1) Zhang, L.; Wang, Y.; Xu, Z.; Li, H. Comparison of the Blue-Shifted C−D Stretching Vibrations for DMSO-d6 in Imidazolium-Based Room Temperature Ionic Liquids and in Water. *J. Phys. Chem. B* **2009**, *113*, 5978-5984.

(2) Danten, Y.; Cabaço, M. I.; Besnard, M. Interaction of water diluted in 1-butyl-3-methyl imidazolium ionic liquids by vibrational spectroscopy modeling. *J. Mol. Liq.* **2010**, *153*, 57-66.

(3) Zheng, Y.-Z.; Wang, N.-N.; Luo, J.-J.; Zhou, Y.; Yu, Z.-W. Hydrogen-bonding interactions between [BMIM][BF4] and acetonitrile. *PCCP* **2013**, *15*, 18055-18064.

(4) Hu, X.; Lin, Q.; Gao, J.; Wu, Y.; Zhang, Z. Anion–cation and ion–solvent interaction of some typical ionic liquids in solvents with different dielectric constant. *Chem. Phys. Lett.* **2011**, *516*, 35-39.

(5) Brehm, M.; Weber, H.; Pensado, A. S.; Stark, A.; Kirchner, B. Proton transfer and polarity changes in ionic liquid-water mixtures: a perspective on hydrogen bonds from ab initio molecular dynamics at the example of 1-ethyl-3-methylimidazolium acetate-water mixtures-Part 1. *PCCP* **2012**, *14*, 5030-5044.

(6) Chaban, V. V.; Voroshylova, I. V.; Kalugin, O. N. A new force field model for the simulation of transport properties of imidazolium-based ionic liquids. *PCCP* **2011**, *13*, 7910-7920.

(7) Herrera, C.; Costa, L. T.; Atilhan, M.; Aparicio, S. Microscopic characterization of amino acid ionic liquids - water mixtures. *J. Mol. Liq.* **2017**, *236*, 81-92.

(8) Ghoshdastidar, D.; Senapati, S. Nanostructural Reorganization Manifests in Sui-Generis Density Trend of Imidazolium Acetate/Water Binary Mixtures. *J. Phys. Chem. B* **2015**, *119*, 10911-10920.

(9) Niazi, A. A.; Rabideau, B. D.; Ismail, A. E. Effects of Water Concentration on the Structural and Diffusion Properties of Imidazolium-Based Ionic Liquid–Water Mixtures. *J. Phys. Chem. B* **2013**, *117*, 1378-1388.

(10) Zhou, J.; Liu, X.; Zhang, S.; Zhang, X.; Yu, G. Effect of small amount of water on the dynamics properties and microstructures of ionic liquids. *AlChE J.* **2017**, *63*, 2248-2256.

(11) Shimomura, T.; Kodama, D.; Kanakubo, M.; Tsuzuki, S. Solvation Structure of Imidazolium Cation in Mixtures of [C4mim][TFSA] Ionic Liquid and Diglyme by NMR Measurements and MD Simulations. *J. Phys. Chem. B* **2017**, *121*, 2873-2881.

(12) Sharma, A.; Zhang, Y.; Gohndrone, T.; Oh, S.; Brennecke, J. F.; McCready, M. J.; Maginn, E. J. How mixing tetraglyme with the ionic liquid 1-n-hexyl-3-methylimidazolium bis(trifluoromethylsulfonyl)imide changes volumetric and transport properties: An experimental and computational study. *Chem. Eng. Sci.* **2017**, *159*, 43-57.

(13) Alcalde, R.; Atilhan, M.; Aparicio, S. Insights on 1-Butyl-3-methylimidazolium Bis(trifluoromethylsulfonyl)imide + Ethanol Liquid Mixtures: A Molecular Dynamics Approach. *J. Chem. Eng. Data* **2016**, *61*, 2729-2737.

(14) Nickerson, S. D.; Nofen, E. M.; Chen, H.; Ngan, M.; Shindel, B.; Yu, H.; Dai, L. L. A Combined Experimental and Molecular Dynamics Study of Iodide-Based Ionic Liquid and Water Mixtures. *J. Phys. Chem. B* **2015**, *119*, 8764-8772.

(15) Zhong, X.; Fan, Z.; Liu, Z.; Cao, D. Local Structure Evolution and its Connection to Thermodynamic and Transport Properties of 1-Butyl-3-methylimidazolium Tetrafluoroborate and Water Mixtures by Molecular Dynamics Simulations. *J. Phys. Chem. B* **2012**, *116*, 3249-3263.

(16) Sharma, A. Effect of water on structure and dynamics of [BMIM][PF6] ionic liquid: An all-atom molecular dynamics simulation investigation. *J. Chem. Phys.* **2016**, *144*, 114505.

(17) Hegde, G. A.; Bharadwaj, V. S.; Kinsinger, C. L.; Schutt, T. C.; Pisierra, N. R.; Maupin, C. M. Impact of water dilution and cation tail length on ionic liquid characteristics: Interplay between polar and non-polar interactions. *J. Chem. Phys.* **2016**, *145*, 064504.

(18) Migliorati, V.; Zitolo, A.; D'Angelo, P. Using a Combined Theoretical and Experimental Approach to Understand the Structure and Dynamics of Imidazolium-Based Ionic Liquids/Water Mixtures. 1. MD Simulations. *J. Phys. Chem. B* **2013**, *117*, 12505-12515.

(19) Méndez-Morales, T.; Carrete, J.; Cabeza, O.; Gallego, L. J.; Varela, L. M. Molecular Dynamics Simulations of the Structural and Thermodynamic Properties of Imidazolium-Based Ionic Liquid Mixtures. *J. Phys. Chem. B* **2011**, *115*, 11170-11182.

(20) Xu, W.; Wu, F.; Zhao, Y.; Zhou, R.; Wang, H.; Zheng, X.; Ni, B. Study on the noncoincidence effect phenomenon using matrix isolated Raman spectra and the proposed structural organization model of acetone in condense phase. **2017**, *7*, 43835.

(21) Marekha, B. A.; Koverga, V. A.; Moreau, M.; Kiselev, M.; Takamuku, T.; Kalugin, O. N.; Idrissi, A. Intermolecular interactions, ion solvation, and association in mixtures of 1-n-butyl-3-methylimidazolium hexafluorophosphate and γ-butyrolactone: insights from Raman spectroscopy. *J. Raman Spectrosc.* **2015**, *46*, 339-352.

(22) Chang, H.-C.; Jiang, J.-C.; Liou, Y.-C.; Hung, C.-H.; Lai, T.-Y.; Lin, S. H. Effects of water and methanol on the molecular organization of 1-butyl-3-methylimidazolium tetrafluoroborate as functions of pressure and concentration. *J. Chem. Phys.* **2008**, *129*, 044506.

(23) Jiang, J.-C.; Lin, K.-H.; Li, S.-C.; Shih, P.-M.; Hung, K.-C.; Lin, S. H.; Chang, H.-C. Association structures of ionic liquid/DMSO mixtures studied by high-pressure infrared spectroscopy. *J. Chem. Phys.* **2011**, *134*, 044506.

(24) Zheng, Y.-Z.; He, H.-Y.; Zhou, Y.; Yu, Z.-W. Hydrogen-bonding interactions between [BMIM][BF4] and dimethyl sulfoxide. *J. Mol. Struct.* **2014**, *1069*, 140-146.

(25) Jiang, J.-C.; Li, S.-C.; Shih, P.-M.; Hung, T.-C.; Chang, S.-C.; Lin, S. H.; Chang, H.-C. A High-Pressure Infrared Spectroscopic Study on the Interaction of Ionic Liquids with PEO-PPO-PEO Block Copolymers and 1,4-Dioxane. *J. Phys. Chem. B* **2011**, *115*, 883-888.

(26) Chang, H.-C.; Tsai, T.-T.; Kuo, M.-H. Using High-Pressure Infrared Spectroscopy to Study the Interactions between Triblock Copolymers and Ionic Liquids. *Macromolecules* **2014**, *47*, 3052-3058.

(27) Kiefer, J.; Molina, M. M.; Noack, K. The Peculiar Nature of Molecular Interactions between an Imidazolium Ionic Liquid and Acetone. *ChemPhysChem* **2012**, *13*, 1213-1220.

(28) Kumar, B.; Singh, T.; Rao, K. S.; Pal, A.; Kumar, A. Thermodynamic and spectroscopic studies on binary mixtures of imidazolium ionic liquids in ethylene glycol. *The Journal of Chemical Thermodynamics* **2012**, *44*, 121-127.

(29) Zhang, Q.-G.; Wang, N.-N.; Wang, S.-L.; Yu, Z.-W. Hydrogen Bonding Behaviors of Binary Systems Containing the Ionic Liquid 1-Butyl-3-methylimidazolium Trifluoroacetate and Water/Methanol. *J. Phys. Chem. B* **2011**, *115*, 11127-11136.

(30) Roth, C.; Appelhagen, A.; Jobst, N.; Ludwig, R. Microheterogeneities in Ionic-Liquid–Methanol Solutions Studied by FTIR Spectroscopy, DFT Calculations and Molecular Dynamics Simulations. *ChemPhysChem* **2012**, *13*, 1708-1717.

(31) Lin, R.; Taberna, P.-L.; Fantini, S.; Presser, V.; Pérez, C. R.; Malbosc, F.; Rupesinghe, N. L.; Teo, K. B. K.; Gogotsi, Y.; Simon, P. Capacitive Energy Storage from −50 to 100 °C Using an Ionic Liquid Electrolyte. *J. Phys. Chem. Lett.* **2011**, *2*, 2396-2401.

(32) Bhat, M. A.; Dutta, C. K.; Rather, G. M. Exploring physicochemical aspects of N-alkylimidazolium based ionic liquids. *J. Mol. Liq.* **2013**, *181*, 142-151.

(33) Fumino, K.; Stange, P.; Fossog, V.; Hempelmann, R.; Ludwig, R. Equilibrium of Contact and Solvent-Separated Ion Pairs in Mixtures of Protic Ionic Liquids and Molecular Solvents Controlled by Polarity. *Angew. Chem. Int. Ed.* **2013**, *52*, 12439-12442.

(34) Marekha, B. A.; Kalugin, O. N.; Bria, M.; Idrissi, A. Probing structural patterns of ion association and solvation in mixtures of imidazolium ionic liquids with acetonitrile by means of relative 1H and 13C NMR chemical shifts. *PCCP* **2015**, *17*, 23183-23194.

(35) Marekha, B. A.; Kalugin, O. N.; Bria, M.; Takamuku, T.; Gadžurić, S.; Idrissi, A. Competition between Cation–Solvent and Cation–Anion Interactions in Imidazolium Ionic Liquids with Polar Aprotic Solvents. *ChemPhysChem* **2017**, *18*, 718-721.

(36) Russo, J. W.; Hoffmann, M. M. Measurements of Surface Tension and Chemical Shift on Several Binary Mixtures of Water and Ionic Liquids and Their Comparison for Assessing Aggregation. *J. Chem. Eng. Data* **2011**, *56*, 3703-3710.

(37) Remsing, R. C.; Liu, Z.; Sergeyev, I.; Moyna, G. Solvation and Aggregation of N,N′-Dialkylimidazolium Ionic Liquids: A Multinuclear NMR Spectroscopy and Molecular Dynamics Simulation Study. *J. Phys. Chem. B* **2008**, *112*, 7363-7369.

(38) Cesare Marincola, F.; Piras, C.; Russina, O.; Gontrani, L.; Saba, G.; Lai, A. NMR Investigation of Imidazolium-Based Ionic Liquids and Their Aqueous Mixtures. *ChemPhysChem* **2012**, *13*, 1339-1346.

(39) Stark, A.; Zidell, A. W.; Hoffmann, M. M. Is the ionic liquid 1-ethyl-3-methylimidazolium methanesulfonate [emim][MeSO3] capable of rigidly binding water? *J. Mol. Liq.* **2011**, *160*, 166-179.

(40) Zhang, Q.-G.; Wang, N.-N.; Yu, Z.-W. The Hydrogen Bonding Interactions between the Ionic Liquid 1-Ethyl-3-Methylimidazolium Ethyl Sulfate and Water. *J. Phys. Chem. B* **2010**, *114*, 4747-4754.

(41) Moreno, M.; Castiglione, F.; Mele, A.; Pasqui, C.; Raos, G. Interaction of Water with the Model Ionic Liquid [bmim][BF4]: Molecular Dynamics Simulations and Comparison with NMR Data. *J. Phys. Chem. B* **2008**, *112*, 7826-7836.

(42) Su, B.-M.; Zhang, S.; Zhang, Z. C. Structural Elucidation of Thiophene Interaction with Ionic Liquids by Multinuclear NMR Spectroscopy. *J. Phys. Chem. B* **2004**, *108*, 19510-19517.

(43) Dupont, J. On the solid, liquid and solution structural organization of imidazolium ionic liquids. *Journal of the Brazilian Chemical Society* **2004**, *15*, 341-350.

(44) Stassen, H. K.; Ludwig, R.; Wulf, A.; Dupont, J. Imidazolium Salt Ion Pairs in Solution. *Chemistry – A European Journal* **2015**, *21*, 8324-8335.

(45) Hayes, R.; Warr, G. G.; Atkin, R. Structure and Nanostructure in Ionic Liquids. *Chem. Rev.* **2015**, *115*, 6357-6426.

(46) Weber, H.; Hollóczki, O.; Pensado, A. S.; Kirchner, B. Side chain fluorination and anion effect on the structure of 1-butyl-3-methylimidazolium ionic liquids. *J. Chem. Phys.* **2013**, *139*, 084502.

(47) Matthews, R. P.; Ashworth, C.; Tom, W.; Patricia, A. H. The impact of anion electronic structure: similarities and differences in imidazolium based ionic liquids. *J. Phys.: Condens. Matter* **2014**, *26*, 284112.

(48) Matthews, R. P.; Welton, T.; Hunt, P. A. Competitive pi interactions and hydrogen bonding within imidazolium ionic liquids. *Phys. Chem. Chem. Phys.* **2014**, *16*, 3238-3253.

(49) Russina, O.; Triolo, A. New experimental evidence supporting the mesoscopic segregation model in room temperature ionic liquids. *Faraday Discuss.* **2012**, *154*, 97-109.

(50) Russina, O.; Triolo, A.; Gontrani, L.; Caminiti, R. Mesoscopic Structural Heterogeneities in Room-Temperature Ionic Liquids. *J. Phys. Chem. Lett.* **2011**, *3*, 27-33.

(51) Kirchner, B.; Hollóczki, O.; Canongia Lopes, J. N.; Pádua, A. A. H. Multiresolution calculation of ionic liquids. *Wiley Interdisciplinary Reviews: Computational Molecular Science* **2015**, *5*, 202-214.

(52) Shimizu, K.; Bernardes, C. E. S.; Canongia Lopes, J. N. Structure and Aggregation in the 1-Alkyl-3-Methylimidazolium Bis(trifluoromethylsulfonyl)imide Ionic Liquid Homologous Series. *J. Phys. Chem. B* **2014**, *118*, 567-576.

(53) Shimizu, K.; Costa Gomes, M. F.; Pádua, A. A. H.; Rebelo, L. P. N.; Canongia Lopes, J. N. Three commentaries on the nano-segregated structure of ionic liquids. *J. Mol. Struct.: THEOCHEM* **2010**, *946*, 70-76.

(54) Avent, A. G.; Chaloner, P. A.; Day, M. P.; Seddon, K. R.; Welton, T. Evidence for hydrogen bonding in solutions of 1-ethyl-3-methylimidazolium halides, and its implications for room-temperature halogenoaluminate(III) ionic liquids. *J. Chem. Soc., Dalton Trans.* **1994**, 3405-3413.

(55) Bonhôte, P.; Dias, A.-P.; Papageorgiou, N.; Kalyanasundaram, K.; Grätzel, M. Hydrophobic, Highly Conductive Ambient-Temperature Molten Salts. *Inorg. Chem.* **1996**, *35*, 1168-1178.

(56) Mele, A.; Tran, C. D.; De Paoli Lacerda, S. H. The Structure of a Room-Temperature Ionic Liquid with and without Trace Amounts of Water: The Role of C-H···O and C-H···F Interactions in 1-n-Butyl-3-Methylimidazolium Tetrafluoroborate. *Angew. Chem., Int. Ed.* **2003**, *42*, 4364-4366.

(57) Hardacre, C.; McMath, S. E. J.; Nieuwenhuyzen, M.; Bowron, D. T.; Soper, A. K. Liquid structure of 1, 3-dimethylimidazolium salts. *J. Phys.: Condens. Matter* **2003**, *15*, S159–S166.

(58) Hardacre, C.; Holbrey, J. D.; Nieuwenhuyzen, M.; Youngs, T. G. A. Structure and Solvation in Ionic Liquids. *Acc. Chem. Res.* **2007**, *40*, 1146-1155.

(59) Zahn, S.; Brehm, M.; Brüssel, M.; Hollóczki, O.; Kohagen, M.; Lehmann, S.; Malberg, F.; Pensado, A. S.; Schöppke, M.; Weber, H.; Kirchner, B. Understanding ionic liquids from theoretical methods. *J. Mol. Liq.* **2014**, *192*, 71-76.

(60) Choudhury, A. R.; Winterton, N.; Steiner, A.; Cooper, A. I.; Johnson, K. A. In situ Crystallization of Low-Melting Ionic Liquids. *J. Am. Chem. Soc.* **2005**, *127*, 16792-16793.

(61) Hamaguchi, H.-O.; Ozawa, R.: Structure of Ionic Liquids and Ionic Liquid Compounds: Are Ionic Liquids Genuine Liquids in the Conventional Sense? In *Advances in Chemical Physics*; John Wiley & Sons, Inc., 2005; pp 85-104.

(62) Marekha, B. A.; Kalugin, O. N.; Idrissi, A. Non-covalent interactions in ionic liquid ion pairs and ion pair dimers: a quantum chemical calculation analysis. *PCCP* **2015**, *17*, 16846-16857.

(63) Matthews, R. P.; Welton, T.; Hunt, P. A. Hydrogen bonding and [small pi]-[small pi] interactions in imidazolium-chloride ionic liquid clusters. *PCCP* **2015**, *17*, 14437-14453.

(64) Izgorodina, E. I.; Rigby, J.; MacFarlane, D. R. Large-scale ab initio calculations of archetypical ionic liquids. *Chem. Commun.* **2012**, *48*, 1493-1495.

(65) Cabaço, M. I.; Besnard, M.; Danten, Y.; Coutinho, J. A. P. Solubility of CO_2 in 1-Butyl-3-methyl-imidazolium-trifluoro Acetate Ionic Liquid Studied by Raman Spectroscopy and DFT Investigations. *J. Phys. Chem. B* **2011**, *115*, 3538-3550.

(66) Matthews, R. P.; Villar Garcia, I. J.; Weber, C. C.; Griffith, J. A.; Cameron, F.; Hallett, J.; Hunt, P.; Welton, T. A structural investigation of ionic liquid mixtures. *Phys. Chem. Chem. Phys.* **2016**.

(67) Chaban, V. Polarizability versus mobility: atomistic force field for ionic liquids. *PCCP* **2011**, *13*, 16055-16062.

(68) Mondal, A.; Balasubramanian, S. Quantitative Prediction of Physical Properties of Imidazolium Based Room Temperature Ionic Liquids through Determination of Condensed Phase Site Charges: A Refined Force Field. *J. Phys. Chem. B* **2014**, *118*, 3409-3422.

(69) Matthews, R. P.; Villar-Garcia, I. J.; Weber, C. C.; Griffith, J.; Cameron, F.; Hallett, J. P.; Hunt, P. A.; Welton, T. A structural investigation of ionic liquid mixtures. *PCCP* **2016**, *18*, 8608-8624.

(70) Gilli, G.; Gilli, P.: *The Nature of the Hydrogen Bond: Outline of a Comprehensive Hydrogen Bond Theory*; Oxford University Press, 2009.

(71) Skarmoutsos, I.; Dellis, D.; Matthews, R. P.; Welton, T.; Hunt, P. A. Hydrogen Bonding in 1-Butyl- and 1-Ethyl-3-methylimidazolium Chloride Ionic Liquids. *J. Phys. Chem. B* **2012**, *116*, 4921-4933.

(72) Stark, A.; Brehm, M.; Brüssel, M.; Lehmann, S. C.; Pensado, A.; Schöppke, M.; Kirchner, B.: A Theoretical and Experimental Chemist’s Joint View on Hydrogen Bonding in Ionic Liquids and Their Binary Mixtures. In *Electronic Effects in Organic Chemistry*; Kirchner, B., Ed.; Topics in Current Chemistry; Springer Berlin Heidelberg, 2014; Vol. 351; pp 149-187.

(73) Chaban, V. V.; Prezhdo, O. V. A new force field model of 1-butyl-3-methylimidazolium tetrafluoroborate ionic liquid and acetonitrile mixtures. *PCCP* **2011**, *13*, 19345-19354.

(74) Wu, X.; Liu, Z.; Huang, S.; Wang, W. Molecular dynamics simulation of room-temperature ionic liquid mixture of [bmim][BF4] and acetonitrile by a refined force field. *PCCP* **2005**, *7*, 2771-2779.
(75) Chaban, V. V.; Voroshylova, I. V.; Kalugin, O. N.; Prezhdo, O. V. Acetonitrile Boosts Conductivity of Imidazolium Ionic Liquids. *J. Phys. Chem. B* **2012**, *116*, 7719-7727.
(76) Bandlamudi, S. R. P.; Cooney, M. J.; Martin, G. L.; Benjamin, K. M. Molecular Simulation and Experimental Characterization of Ionic-Liquid-Based Cosolvent Extraction Solvents. *Industrial & Engineering Chemistry Research* **2017**, *56*, 3040-3048.

Chapter 6. The Charge distribution effect

Ionic liquids (ILs) constitute a large class of substances which present a considerable scientific interest due to their number of advantageous properties. In many applications ILs are used in mixtures with molecular solvents of different nature. It still remains to be an unresolved task of creating a comprehensive microscopic picture on the structure and dynamics in such systems as a function of mixture composition and nature of the constituents.

6.1. Introduction

In this Chapter, we studied the microscopic organization of the mixture by means of molecular simulations based on atomistic models. The aim is to analyze the effect of the charge distribution on the cation and anion of the C_4mimPF_6 on the microscopic local structure in this mixture. Indeed, the problem we addressed is a global one and is dealing with the validity of the potential model of each component of the mixture, namely the C_4mimPF_6 and AN, (that was optimized to reproduce their neat liquids physical chemical properties) to describe adequately their physical chemical properties in the mixture. In particular, we address in this Chapter the differentiating effect between the x_{IL} dependent scaling charges of the cation and the anion and the one where the scaling of the charges is the same as for the pure IL, on the local structure and in particular the H-bonding interactions between the cation and the anion as well as on the stacking orientation between the two neighboring cations.

In the study of the IL/molecular solvent mixtures the design of the potential model that is able to capture the experimental structural and dynamical properties is important step in the understanding at the microscopic level the above mentioned interactions pertaining to the macroscopic properties. These parameters include the bond, and torsion parameters describing the intramolecular part, the Lennard-Jones describing the intermolecular part and the electrostatic component describing the Coulombic interactions between atom centered point charges. The design process usually takes the following path. First, the parameters of the force field of the components (IL and solvent) are optimized in order to reproduce well the corresponding phisico-chemical properties. It is then often assumed that the same set of parameters should also reproduce the properties of the mixtures. It is obvious that the charge distribution on the cation and anion is expected to play an important role, particularly in describing the various intermolecular interactions in the mixtures with solvent, including the hydrogen bonding between the cation and the anion or between an ion and a solvent molecule, as well as the stacking between the cations. In order to reproduce the transport properties in pure ionic liquids, the net charges on the cation and the anions were scaled down by a factor f_{IL}, in contrast to ±1e netcharge of the isolated counterions[1]. The fundamental argument of the applying such scaling factor is to take in account the mutual polarization of the ions in the given IL. Typical f_{IL} range between 0.7 and 0.8, the individual atomic charges that result in a closer value of the diffusion coefficient to the experimental one with a concomitant correct description of the corresponding experimental local structure of the IL.[2-7] The problem is that the partial charges values can vary substantially for the same ionic liquid.[8] For instance, the partial charges on N atom of the imidazolium cation, vary from negative, through neutral to positive, while the positive partial charges on the C atom of the ring vary substantially, moderately for the carbon in position 2 and 4, 5, respectively depending on the method used to derive these values.[9] Consequently, the interaction potential model (particularly the charge distribution) designed for a specific IL are not portable to other ILs. Indeed, Balasubramanian proposed different set of charge distributions for the C_4mim^+ cation depending on the type of anion.[10]

In the following Chapter we will show the results obtained on the analysis of the effect of the charge distribution for the C_4mim^+ and PF_6^- ions on the local structure and, in particular, on the H-bonding between the cation and the anion or solvent as well as on the stacking orientation between the two neighboring cations. In particular, we discuss the effect of the mole fraction dependent charge distribution model (hereafter referred to as “variable charge model”) of these ions, and that of the model where the fractional charges on the two ions are the same as that in the neat IL (hereafter referred to as “constant charge model”) [see for details subsection 2.3].

6.2. Results and discussion

6.2.1 Hydrogen bonding interactions

6.2.1.1 Spatial distribution function

A physical picture on the relative distribution of the constituents of the mixture around the ring hydrogen atoms may be obtained from the isosurfaces of the SDFs as a function of x_{IL}.[12-17] As we pointed out before this type of representation, however, suffers from somewhat ambiguous choice of the isovalue and also from the lack of information on the distribution of the observed particle density inside the region enclosed by the isosurface. As a consequence, in the calculation of these SDFs, only the first nearest neighbor to a reference constituent was considered. Here we calculated the SDFs of the neighbor anion F atom and the first neighbor N atom of the solvent around the reference ring hydrogen atoms $H^{2,4–5}$ considering both the variable and constant charge distributions. The obtained distributions are shown in Figure 6.2 A and B.

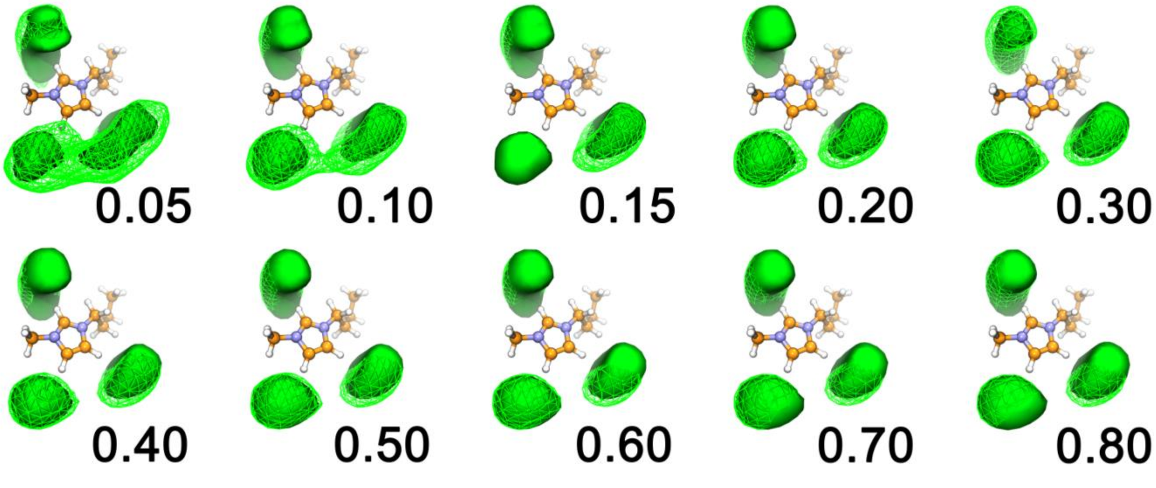

Figure 6.2 A) plots of isosurfaces of spatial distribution functions describing the distribution of the first nearest neighbor F atom of the anion around a reference acidic ring hydrogen atoms $H^{2,4–5}$. The value of the isosurface was equal to 30% of the probability density within the corresponding first nearest neighbor distributions. These surfaces were obtained in the case of the viriable (*solid surface*) and constant (*wireframe surface*) charge models.

In both cases of the variable and constant charge distribution models, the corresponding SDFs have similar shape. The SDF of the anion around the ring hydrogen atoms $H^{2,4–5}$ is more localized than that of the solvent molecules at high x_{IL} values, whereas an opposite behavior occurs at low x_{IL} values. This means that the solvent molecules set apart the cation and the anion and it is particularly clearly seen at x_{IL} lower than 0.20. This means that in the case of the studied mixture, the AN solvent weakens the interaction between the cation and the anion ions and the extent of this effect is more important in the case of the constant charge model.

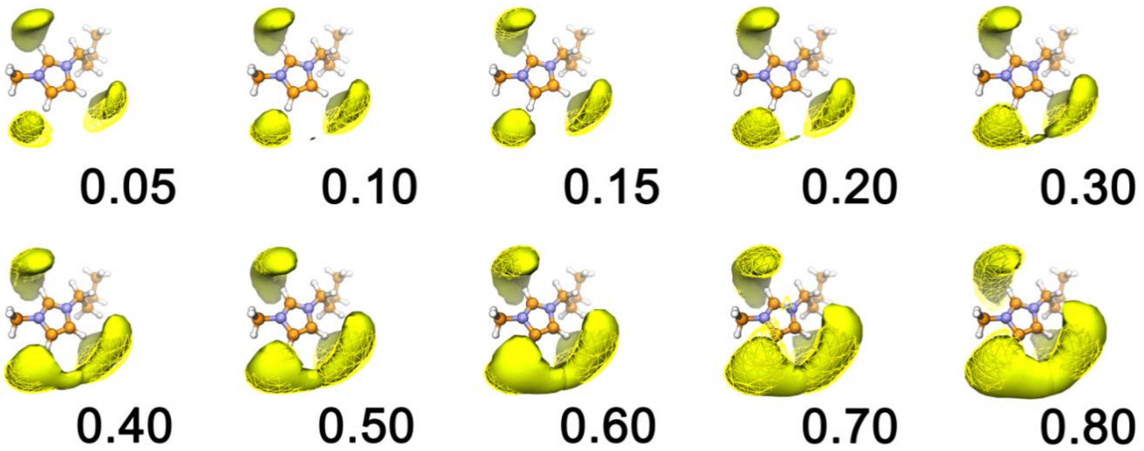

Figure 6.2 B) plots of isosurfaces of spatial distribution functions describing the distribution of the first nearest neighbor N atom of the AN around a reference acidic ring hydrogen atoms $H^{2,4–5}$ of the C_4mim^+ ring. The value of the isosurface was equal to 30% of the probability density within the corresponding first nearest neighbor distributions. These surfaces were obtained in the case of the variable (*solid surface*) and constant (*wireframe surface*) charge distribution models.

6.2.1.2 Radial distributions functions

Insight on effect of the hydrogen bond between the ring hydrogen atoms, $H^{2,4-5}$ and the anion, and the solvent molecules on the change of the local structure of the mixture may be obtained by analyzing the behavior of the corresponding $g_{\mathrm{H^{2,4–5}\cdots F}}(r)$, $g_{\mathrm{H^{2,4-5}\cdots N^s}}(r)$ and $g_{\mathrm{H^s\cdots F}}(r)$. In the two charges distribution models, the $g_{\mathrm{H^{2,4–5}\cdots F}}(r)$ are generally similar to each other at high x_{IL} while they have a quite different shape at $x_{\mathrm{IL}} < 0.20$. The four peaks intensities of $g_{\mathrm{H}^{2,4\text{–}5}\cdots\mathrm{F}}(r)$ increase drastically with decreasing x_{IL}. The extent of this increase is stronger in the case of the variable charge distribution model. However, the objective evaluation of these changes is obtained by analyzing the corresponding coordination number. In the case of $g_{\mathrm{H}^{2,4\text{–}5}\cdots\mathrm{F}}(r)$, the coordination number is decreasing with the decrease of x_{IL} and the extent of this decrease is more important in the case of the constant charge distribution model. The $g_{\mathrm{H}^{2,4\text{–}5}\cdots\mathrm{N}^{s}}(r)$ undergoes noticeable changes in the case of variable charge, while, in both charge distribution models, the coordination number of the solvent molecules around the acidic hydrogen atoms shows a noticeable change and it is increasing with decreasing x_{IL}. The extent of this increase is higher at high x_{IL}.

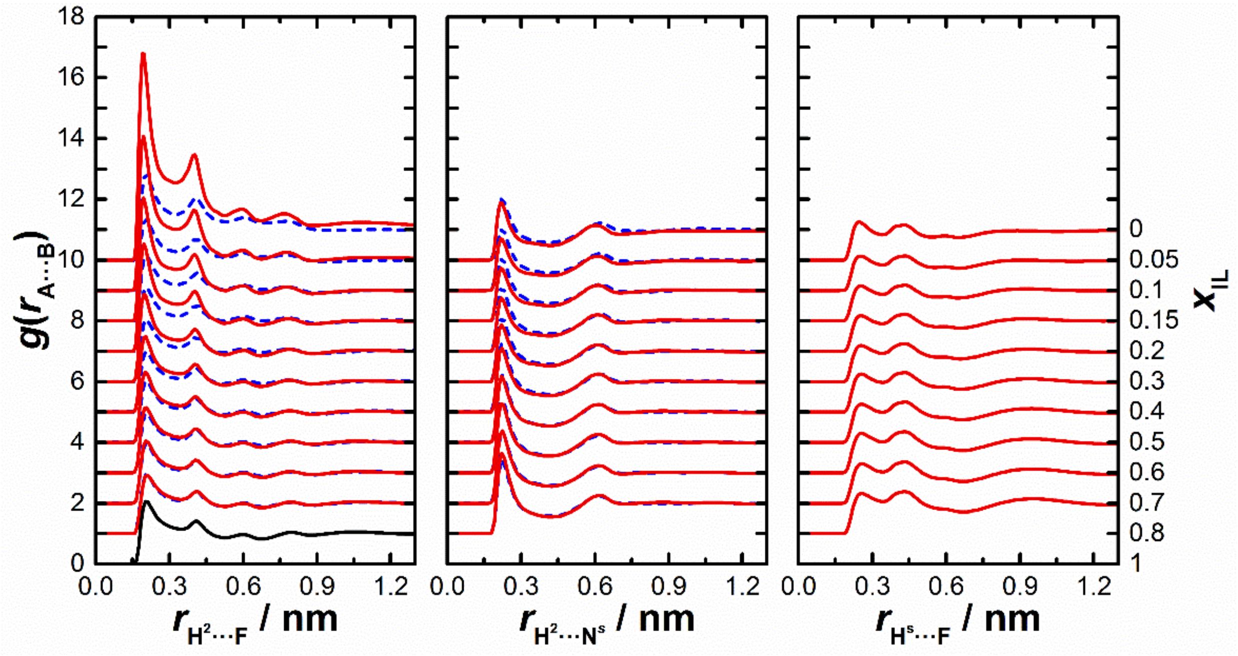

Figure 6.3. The radial distribution functions, $g(r_{\mathrm{A}\cdots\mathrm{B}})$, describing the distribution of anion (F atom) and solvent (N^{s} atom) around the H^{2} of the imidazolium ring as well as the distribution of the F atom around the H^{s} (in position 2) of the solvent. *Red solid lines, blue dashed lines* correspond to the results with variable and constant charge distribution models respectively, *black solid line* correspond to the results for the pure $\mathrm{C_4mimPF_6}$.

The analysis of $g_{\mathrm{H}^s\cdots\mathrm{F}}(r)$ indicates a weak dependence on both x_{IL} and the charge distribution model. However, the corresponding coordination number shows a noticeable dependence on the two parameters. The coordination number of F around H^2 decreases moderately at high x_{IL} values and noticeably at lowest ones.

6.2.1.3 Nearest neighbor radial distributions

The local structure is further analyzed using the nearest neighbor approach, we calculated the nearest neighbor distributions between the acidic hydrogen atoms $H^{2,4\text{–}5}$ and the close F atom of the PF_6^- anion and the N^s atom of the AN as well as that between the H^s of the methyl group of AN and F atom of the anion as a function x_{IL}. Based on these distributions, we calculated the corresponding average distances $<r(\mathrm{H}^2\cdots\mathrm{F})>$ and $<r(\mathrm{H}^2\cdots\mathrm{N}^s)>$. Their behavior as a function of the x_{IL} is illustrated in Figure 6.4.

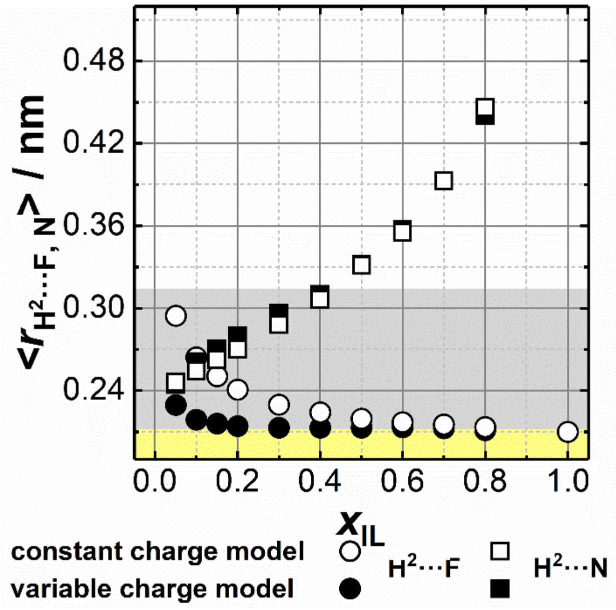

Figure 6.4. The x_{IL} dependence of the average value of the distance between the anion (F atom) and solvent (N^s atom) around the H^2 of the imidazolium ring for both variable (*empty circles*) and constant charge (*filled circles*) distribution models.

In the range of x_{IL} between 1.00 and 0.50, the $\langle \mathrm{r}(\mathrm{H}^2 \ldots \mathrm{F}) \rangle$ is almost independent on both the IL mole fraction and on the charge distribution models while for lower x_{IL}, the extent of the increase of this distance is more important in the case of constant charge model. The behavior of $<r(\mathrm{H}^2\cdots\mathrm{F})>$ is almost independent on the charge distribution models. In both cases, it decreases almost linearly with decreasing x_{IL}. A cross over between $<r(\mathrm{H}^2\cdots\mathrm{F})>$ and $<r(\mathrm{H}^2\cdots\mathrm{N}^s)>$ occurs only in the case of the constant charge model, at around $x_{\mathrm{IL}} = 0.15$. This indicates that in this range the solvent molecules are in average closer to the H^2 than the anion.

It is of great importance to characterize the orientational properties of the hydrogen bonding interactions between donor (ring hydrogen atoms) and acceptor moieties (anion or the solvent). This information is obtained by describing the hydrogen bond geometry, $\mathrm{C}^{2/4\text{–}5}\text{–}\mathrm{H}^{2/4\text{–}5}\cdots\mathrm{F}, \mathrm{N}^s$, involving the cation ring acidic hydrogen atoms and the fluorine or nitrogen atoms of the anion and the solvent molecules, respectively, in terms of two hydrogen bond distances (see chapter 5 for more details): the distance $<r(\mathrm{H}^{2,4\text{–}5}\cdots\mathrm{F}, \mathrm{N}^s)>$ and the distance $<r(\mathrm{C}^{2,4\text{–}5}\cdots\mathrm{F}, \mathrm{N}^s)>$, between the ring carbon atoms in position 2, 4 and 5 and atom F or N^s. The orientation between the donor and acceptor moieties is given by the angle θ.

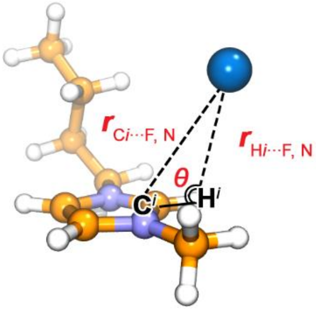

Figure 6.5. Schematic presentation of H-bonding criteria defined by the average distances $\mathrm{H}^i\cdots\mathrm{F}, \mathrm{N}^s$ and $\mathrm{C}^i\cdots\mathrm{F}, \mathrm{N}^s$ between the $\mathrm{C_4mim^+}$ ring hydrogen $\mathrm{H}^{2/4\text{–}5}$ sites and the corresponding electronegative atoms of anion and solvent.

These results confirm the outlined physical picture that the scaled charge distribution model maintains the strong interaction between the cation and the anion while the opposite situation occurs in the unscaled charge distribution model.

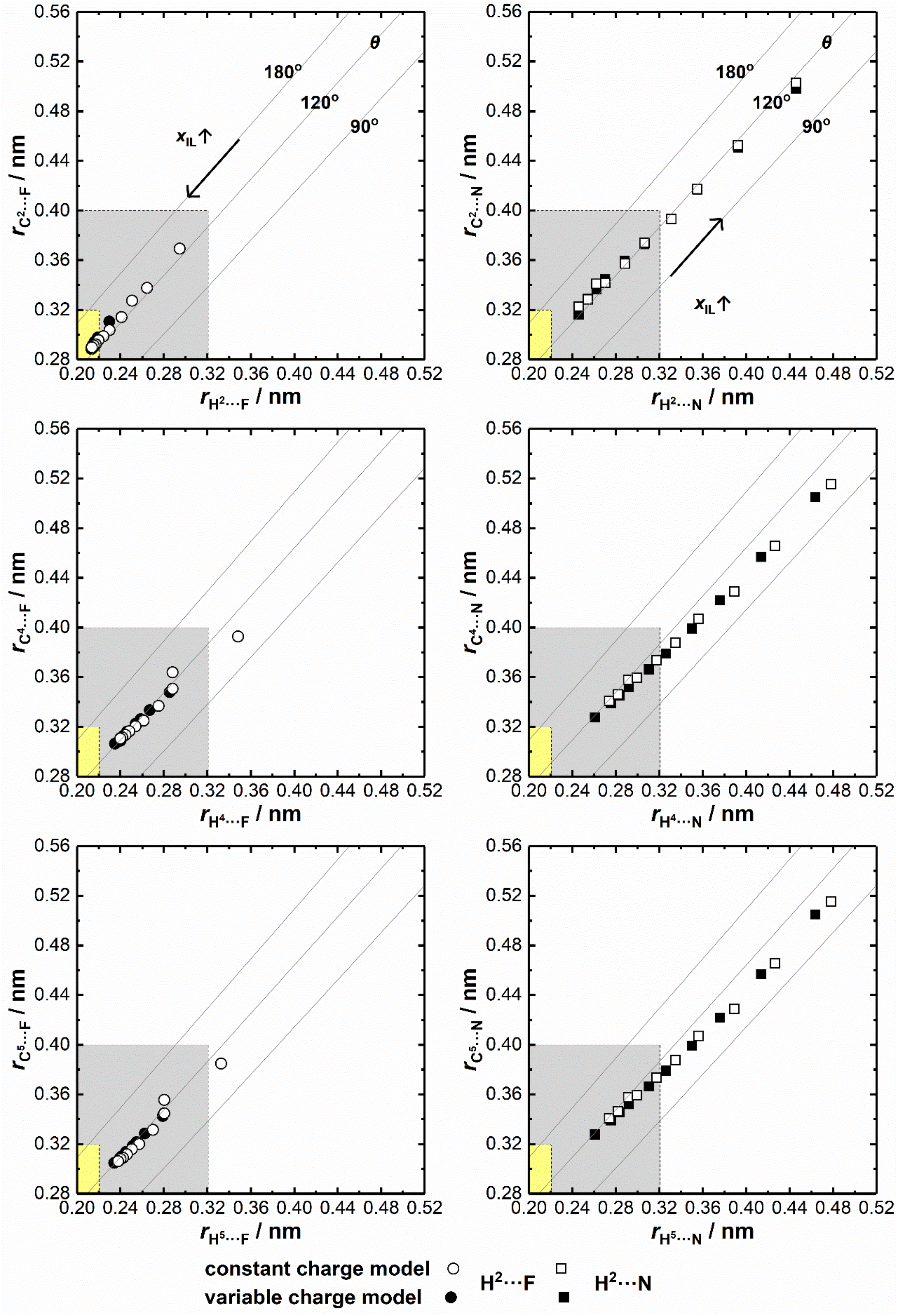

Figure 6.6. The behavior of the two distances characteristics describing the H-bonding interactions between the cation and the anion (*left column*) and solvent (*right column*), $\langle r(\mathrm{H}^{2,4\text{–}5}\cdots \mathrm{F}, \mathrm{N}^{s})\rangle$ and $\langle r(\mathrm{C}^{2,4\text{–}5}\cdots \mathrm{F}, \mathrm{N}^{s})\rangle$. The arrow indicates the direction of the x_{IL} change. The value of θ quantifies the angle between the hydrogen bond donor and acceptor.

In the case of the constant charge model, the distances characteristics are strongly affected by the change in the mixture composition and particularly at x_{IL} lower than 0.15 while they are almost not affected in the whole x_{IL}. In both cases the angle orientation of the hydrogen bond donor-acceptor geometry is not affect by both the charge distribution model. The physical pictures that it merges is that the anion is expelled from its position that it occupies in pure IL without altering drastically the orientation with respect to the cation (in particular with respect to the C^2–H^2 axis) The angular correlation between the two distances $<r(H^2\cdots N^s)>$ and $<r(C^2\cdots N^s)>$ is not dependent on the charge distribution model while these distances decrease with decreasing x_{IL}.

6.2.2 Stacking interactions

In this part of the Chapter we will discuss the effect of changing the mixture composition on the stacking interactions between the two neighboring cations. In addition to the effect of the solvent on the stacking between the cations, we were interested in the effect of the variable and constant charge distribution on this stacking.

6.2.2.1 Radial distribution function

We calculated then the following RDFs: $g_{\mathrm{CoR\cdots CoR}}(r)$, $g_{\mathrm{CoR\cdots P}}(r)$ and $g_{\mathrm{CoR\cdots C^{1s}}}(r)$ describing the interionic and ion-molecular radial distributions, respectively.

The general trend of the effect of both the charge and x_{IL} dependence can be summarized as follow: The shape of the RDFs involving the distribution cation or anion around the cation is slightly affected in all the concentration range, while this shape is strongly affected by both the charge distribution model and by further dilution of the mixture. Indeed, the corresponding intensities are higher in the case the variable charge distribution model and they are well resolved in the case of the CoR···CoR radial distribution. Finally, the RDFs describing the solvent molecules distribution around the cation are slightly affected by both the charge distribution model and the x_{IL}.

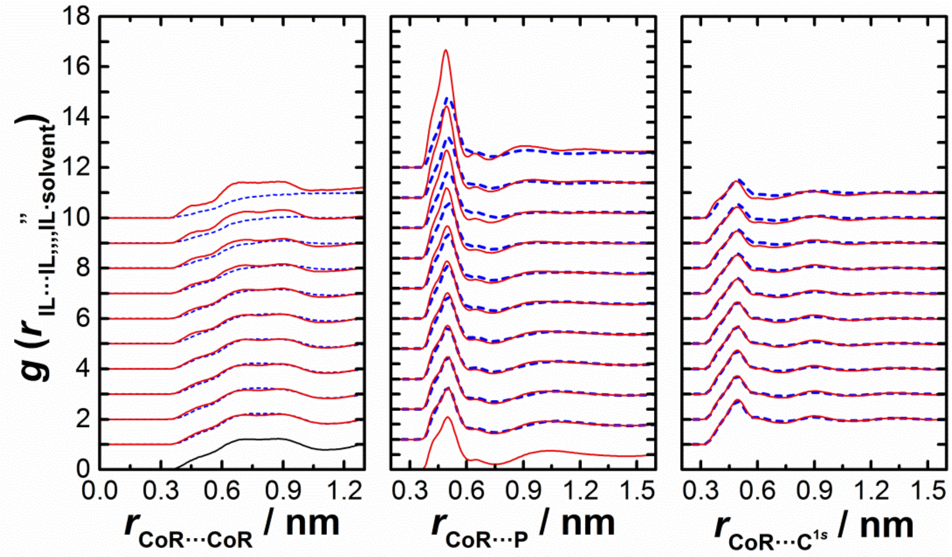

Figure 6.7. Charge distribution model and x_{IL} dependence of the radial distribution functions, $g(r_{\mathrm{IL}\cdots\mathrm{IL},\ \mathrm{solvent}\cdots\mathrm{solvent}})$ describing the distribution of imidazolium cation (CoR) , the anion (P atom of $\mathrm{PF_6^-}$) and solvent (C^{1s} atom of AN) around a reference cation (CoR). *Red solid lines, blue dashed lines* correspond to the results with variable and constant charge distribution models respectively, *black solid line* correspond to the results for the pure $\mathrm{C_4mimPF_6}$.

6.2.2.2 Nearest neighbor radial distributions

In order to get insight the local changes at a level of the neighbor anion or solvent to a reference cation, we calculated the corresponding nearest neighbor radial distributions the behavior of which is illustrated in Figure 6.8. This Figure shows mainly that the radial distribution of the first neighbor cation CoR and first neighbor solvent molecules around a reference cation is not strongly affected by the charge distribution model and the x_{IL} while that between the first neighbor anion is noteavcibly affected at low $x_{\mathrm{IL}} < 0.20$. This Figure also shows that a cross over between the average distances describing the distance of the anion and the solvent molecule to the reference cation. This cross over occurs at $x_{\mathrm{IL}} \sim 0.3$. These results point out to the importance to the optimal choice of the charge distribution to describe as correctly as possible the radial distribution of the constituents of these mixtures and particularly in the low x_{IL} range.

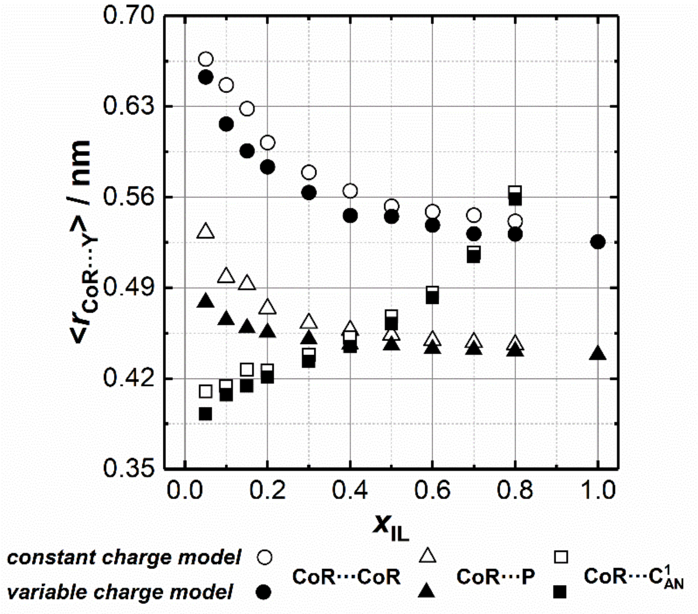

Figure 6.8. Behavior of the average distances, $<r_{CoR\cdots Y}>$, between the CoR of the reference C_4mim^+ ring and the first neighboring site Y of the cation, anion and solvent (CoR of C_4mim^+, P of PF_6^- and C^1_{AN} of AN) as a function of x_{IL} calculated for both charge distribution models

6.2.2.3 Orientation between the cations

In order to study the orientational aspects in more detail, we have decided to calculate several combined angular and distance distributions where the angles are defined in figure while the distance is that between a reference CoR and that of the first neighbor. The first investigated angle, designated here as α, is the angle between the normal vector of the cation ring plane of the reference cation and the distance vector connecting the ring centers of the reference and observed cations. Thus, positions above/below the reference cation would correspond to α angle around 0° and 180°, while perfect in-plane arrangement of the observed cations would contribute to the α values close to 90°. The second investigated angle is β formed by the normal vectors of the ring planes between the reference and observed cations. As in the previous case a perfectly parallel arrangement of the planes corresponds to β values of 0° and 180°, whereas the values around 90° are indicative of a T-shaped relative arrangement of the two ring planes. This angle gives information on the stacking between the rings of the cations. The third angle designated as ψ is that between the vectors along C–H bonds in the reference and observed cations. The ψ values close to 0° and 180°, indicate a parallel and antiparallel orientation, respectively. Thus, this angle gives information about the relative orientation of cation C–H bonds. The probability distributions of these angles are illustrated in Figures 6.9 A, B, and C as a function of x_{IL} and the charge distribution models.

The values of the probability distributions of these angles indicate that at high x_{IL} values, with respect to a reference solvent molecule, the first cation neighbor is characterized by an above/below position, parallel stacking of the rings and antiparallel dipole orientation, while at low x_{IL} (<0.30) these orientations become loose although these orientations remain more localized in the case of the variable charge model and particularly at low x_{IL}.

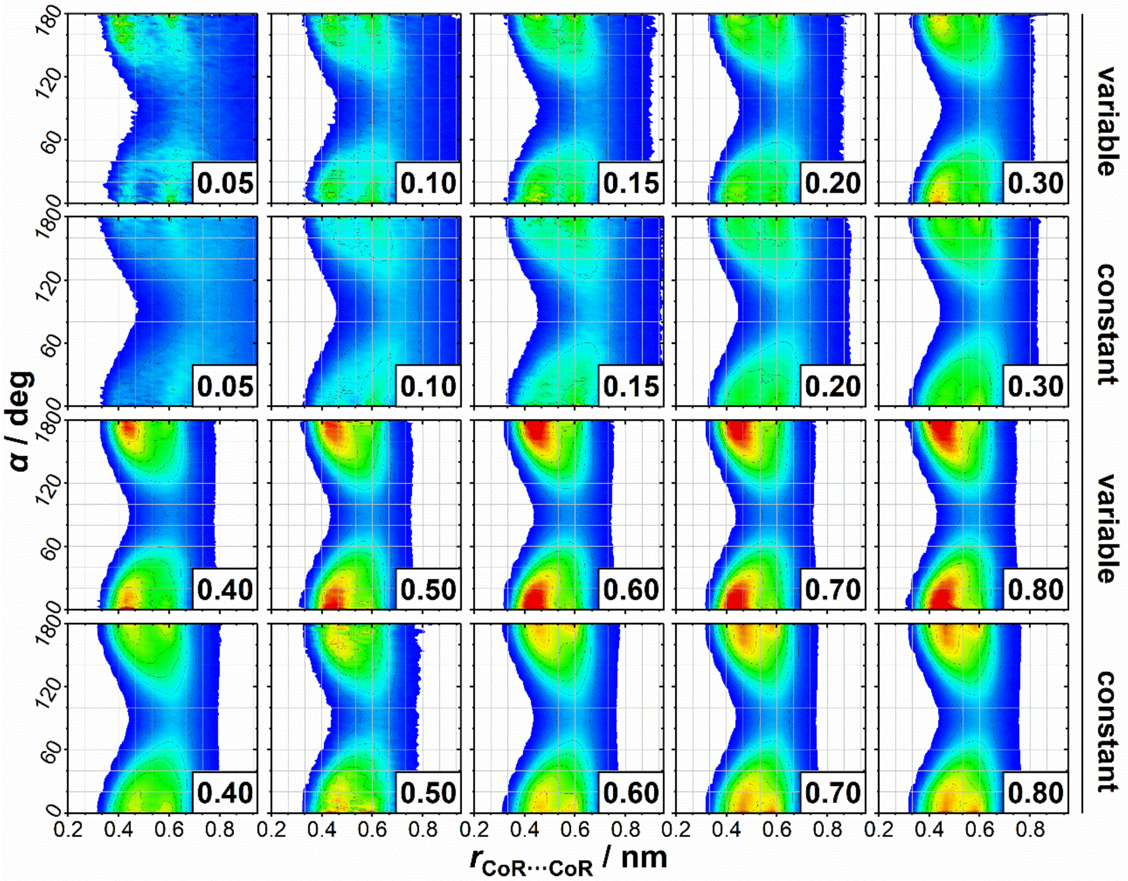

Figure 6.9 A) effect of the charge distribution model and the probability distributions of the angle describing the above/below orientation between the cations.

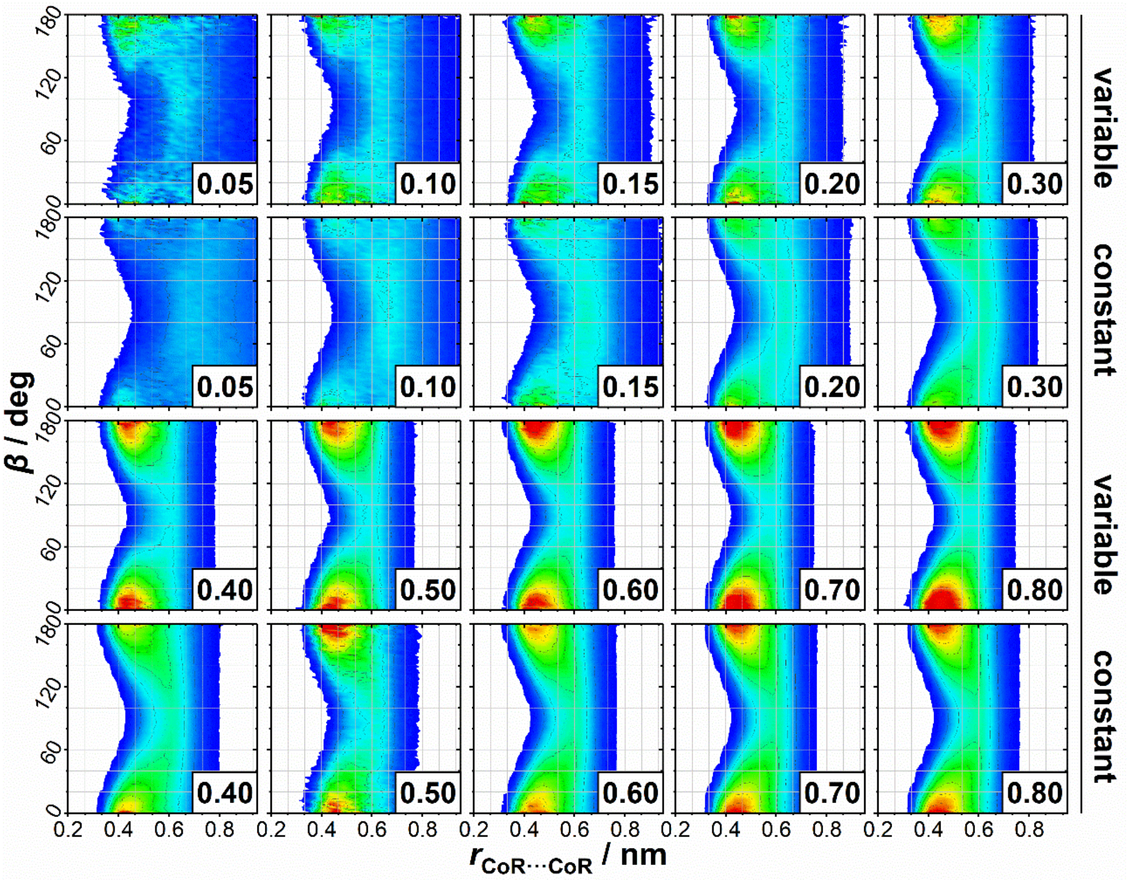

Figure 6.9 B) effect of the charge distribution model and the probability distributions of the angle describing the planar orientation between the cations.

The parallel/antiparallel C–H orientation occur at x_{IL} = 0.80, however the associated probability is higher in the case of scaled than for the unscaled charge. When the x_{IL} decreases, These orientations become less localized (the intensity probability decreases) in both charge distribution models, however the extent of this change is more important in the case of the constant charge distribution model. Finally, all these orientations become almost random in the lowest x_{IL} value.

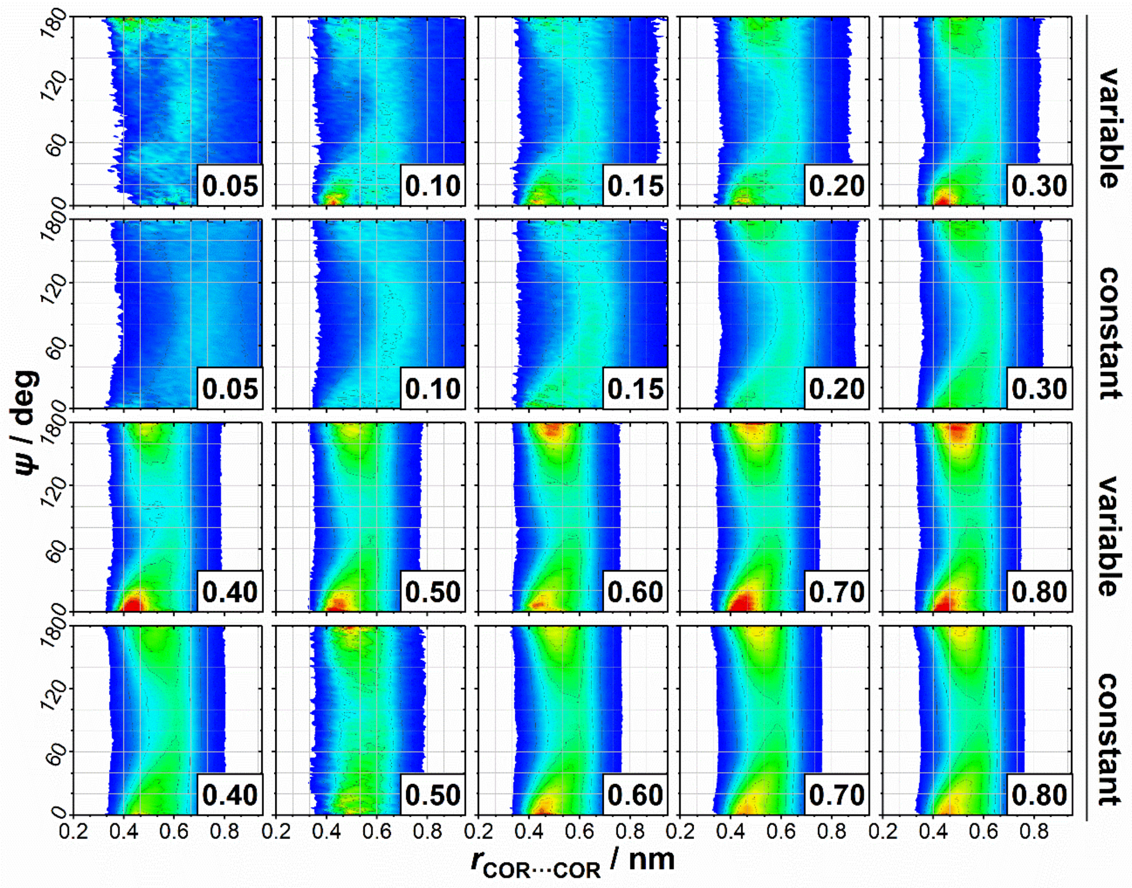

Figure 6.9 C) effect of the charge distribution model and the probability distributions of the angle describing the parallel/antiparallel orientations of the cations.

6.3. Conclusions

In this chapter, we investigate the change in the local structure in a binary mixture of C$_4$mimPF$_6$/AN as a function of the x_{IL}. We considered two charge distribution models, in the first one the charge distribution on the IL was independent of the ionic mole fraction and in the second one the charge distribution was scaled using a dependent mole fraction scaling factor. In the two cases the van der Waals interactions and the intramolecular ones (bond, angles, dihedrals *etc*) are similar. The effect of the charge model distribution on the H-bonding, on the stacking interactions between the cations (below/above, parallel and antiparallel orientations) is analyzed. To this end two distances characteristic of the hydrogen bond between the donor moiety and it close neighbor acceptor one are introduced. Furthermore, a coordinate system that defines unambiguously and stacking orientation between a reference cation and its close neighbor is introduced. It is shown that the variable charge distribution model introduce an artificial large extent of the aggregation of the studied ionic liquid, than in the case of the unscaled charge model.

6.4. References for Chapter 6

(1) Chaban, V. Polarizability Versus Mobility: Atomistic Force Field for Ionic Liquids. *Physical Chemistry Chemical Physics* **2011**, *13*, 16055-16062.

(2) Matsumiya, M.; Hata, K.; Tsunashima, K. Self-diffusion behaviors of ionic liquids by MD simulation based on united-atom force field introduced charge scaling by ab initio MO simulation. *Journal of Molecular Liquids* **2015**, *203*, 125-130.

(3) Borodin, O. Polarizable Force Field Development and Molecular Dynamics Simulations of Ionic Liquids. *Journal of Physical Chemistry B* **2009**, *113*, 11463-11478.

(4) Bedrov, D.; Borodin, O.; Li, Z.; Smith, G. D. Influence of Polarization on Structural, Thermodynamic, and Dynamic Properties of Ionic Liquids Obtained from Molecular Dynamics Simulations. *The Journal of Physical Chemistry B* **2010**, *114*, 4984-4997.

(5) Borodin, O.; Gorecki, W.; Smith, G. D.; Armand, M. Molecular Dynamics Simulation and Pulsed-Field Gradient NMR Studies of Bis(fluorosulfonyl)imide (FSI) and Bis[(trifluoromethyl)sulfonyl]imide (TFSI)-Based Ionic Liquids. *Journal of Physical Chemistry B* **2010**, *114*, 6786-6798.

(6) Youngs, T. G. A.; Hardacre, C. Application of Static Charge Transfer within an Ionic-Liquid Force Field and Its Effect on Structure and Dynamics. *ChemPhysChem* **2008**, *9*, 1548-1558.

(7) Zhong, X.; Liu, Z.; Cao, D. Improved Classical United-Atom Force Field for Imidazolium-Based Ionic Liquids: Tetrafluoroborate, Hexafluorophosphate, Methylsulfate, Trifluoromethylsulfonate, Acetate, Trifluoroacetate, and Bis(trifluoromethylsulfonyl)amide. *The Journal of Physical Chemistry B* **2011**, *115*, 10027-10040.

(8) Hunt, P. A.; Ashworth, C. R.; Matthews, R. P. Hydrogen bonding in ionic liquids. *Chemical Society Reviews* **2015**, *44*, 1257-1288.

(9) Urahata, S. M.; Ribeiro, M. C. C. Structure of ionic liquids of 1-alkyl-3-methylimidazolium cations: A systematic computer simulation study. *The Journal of Chemical Physics* **2004**, *120*, 1855-1863.

(10) Mondal, A.; Balasubramanian, S. Quantitative Prediction of Physical Properties of Imidazolium Based Room Temperature Ionic Liquids through Determination of Condensed Phase Site Charges: A Refined Force Field. *The Journal of Physical Chemistry B* **2014**.

(11) Chaban, V. V.; Prezhdo, O. V. A new force field model of 1-butyl-3-methylimidazolium tetrafluoroborate ionic liquid and acetonitrile mixtures. *Physical Chemistry Chemical Physics* **2011**, *13*, 19345-19354.

(12) Ramya, K. R.; Kumar, P.; Venkatnathan, A. Molecular Simulations of Anion and Temperature Dependence on Structure and Dynamics of 1-Hexyl-3-methylimidazolium Ionic Liquids. *J. Phys. Chem. B* **2015**, *119*, 14800-14806.

(13) Mondal, A.; Balasubramanian, S. Quantitative Prediction of Physical Properties of Imidazolium Based Room Temperature Ionic Liquids through Determination of Condensed Phase Site Charges: A Refined Force Field. *J. Phys. Chem. B* **2014**, *118*, 3409-3422.

(14) Bowron, D. T.; D'Agostino, C.; Gladden, L. F.; Hardacre, C.; Holbrey, J. D.; Lagunas, M. C.; McGregor, J.; Mantle, M. D.; Mullan, C. L.; Youngs, T. G. A. Structure and Dynamics of 1-Ethyl-3-methylimidazolium Acetate via Molecular Dynamics and Neutron Diffraction. *J. Phys. Chem. B* **2010**, *114*, 7760-7768.

(15) Kohagen, M.; Brehm, M.; Thar, J.; Zhao, W.; Müller-Plathe, F.; Kirchner, B. Performance of Quantum Chemically Derived Charges and Persistence of Ion Cages in Ionic Liquids. A Molecular Dynamics Simulations Study of 1-*n*-Butyl-3-methylimidazolium Bromide. *J. Phys. Chem. B* **2011**, *115*, 693-702.

(16) Brehm, M.; Weber, H.; Pensado Alfonso, S.; Stark, A.; Kirchner, B. Liquid Structure and Cluster Formation in Ionic Liquid/Water Mixtures – An Extensive ab initio Molecular Dynamics Study on 1-Ethyl-3-Methylimidazolium Acetate/Water Mixtures – Part 2. *Z. Phys. Chem.* **2013**, *227*, 177-203.

(17) Matthews, R. P.; Villar Garcia, I. J.; Weber, C. C.; Griffith, J. A.; Cameron, F.; Hallett, J.; Hunt, P.; Welton, T. A structural investigation of ionic liquid mixtures. *Phys. Chem. Chem. Phys.* **2016**.

Conclusions and perspectives

This thesis presents a molecular dynamics description of the local structure in the mixtures of imidazolium-based ionic liquids (ILs) with perfluorinated anions on one side and dipolar aprotic solvents on the other side. These mixtures possess have advantageous properties for electrochemical applications (*e.g.*, high ionic conductivity, thermal and electrochemical stability, low environmental hazardness) and they can be fine-tuned due to their full miscibility. Understanding the nature of the interactions between the constituents and their behavior as a function of mixture composition is of crucial importance for their successful use in such applications.

Indeed, in this thesis, the mixtures of four imidazolium-based ILs with three dipolar aprotic molecular solvents have been investigated. The ILs contain a common cation 1-*n*-butyl-3-methlylimidazolium (C_4mim^+). It is combined with perfluorinated anions of different size, shape, symmetry, and electronic structure, namely, tetrafluoroborate (BF_4^-), hexafluorophosphate (PF_6^-), trifluoromethylsulfonate (TFO^-), and bis(trifluoromethanesulfonyl)imide ($TFSI^-$). Polar aprotic molecular solvents employed in this thesis are those common in electrochemistry of electrolyte solutions: acetonitrile (AN), γ-butyrolactone (GBL), and propylene carbonate (PC), which differ in terms of their polarity, donicity, viscosity, molecular shape and volume.

As a first step, the local structure in the neat ILs and molecular solvents has been analyzed. For the set of ILs it was established that H-bonding interactions at the H^2 site is strongly enhanced compared to the H^{4-5} sites in the case of asymmetric and/or strongly basic anions like TFO^- or $TFSI^-$. The results of orientational anlysis suggest that position of anion with respect to the imidazolium ring plane of cation is strongly anion-dependent, especially at the $C–H^2$ site. Namely, all the anions strongly prefer to occupy the on-top arrangement. The corresponding distribution at the $C–H^{4–5}$ sites is much more diffuse. Multiple H-bonding (bi- and even tri-dentate, where possible) with the nearest neighboring anion was observed to prevail at the $H^{4–5}$ sites compared to the H^2 one in all the considered ILs. Finally, cation-cation contacts via the aggregation of the butyl chains is much stronger and less anion-dependent than the π^+-π^+ stacking of the imidazolium rings. The latter, however, can occur simultaneously with the alkyl chain aggregation.

For the pure solvent our results show that although the dominant dipole-dipole orientation between a reference molecule and first neighbor is the antiparallel one, the parallel one has an effect on the outcome of the Kirkwood correlation factor. For the subsequent neighbors the antiparallel orientation is gradually weakened in favor of the parallel one. More distant neighbors tend to be parallel to the reference molecule. Some of the solvents molecules located at intermediate distances are arranged in T-shaped orientation. Furthermore, for the cyclic solvents GBL and PC the above/below and the stacking arrangements between a reference molecules and it first neighbor, are present in both liquids. Based on the nearest neighbor approach our results show that it is necessary to take in account the 4~6 nearest neighbor in the calculation of g_K in order to reproduce the experimental values. Finally, the analysis of the distance, H···Y, between the reference H atom and the neighbor H-bond accepting atom and the angle $\angle$C–H^i···Y indicates that they are compatible with a weak hydrogen bonding.

For the mixtures of imidazolium-based ILs the results show that in all the studied IL/molecular solvent mixtures, the distribution of the anion around the cation is not drastically affected in the range of x_{IL} between 1 and 0.3 and noticeable changes distance characteristics describing the cation and anion hydrogen bonding interactions, occur. These changes are associated with the expected weakening of the cation and anion interactions. This weakening is more important in PC and GBL in comparison to that in AN and the most affected cation···anion interaction are those in C_4mimTFSI and in C_4mimPF_6 and the least affected are those in C_4mimBF_4 and in C_4mimTFO. For the three solvents, the weakest interactions between the solvent and the cation are observed in the case of C_4mimTFO (the values of the distances characteristics describing the cation···solvent are small), while the strongest ones are observed in AN and GBL for C_4mimTFSI and for C_4mimPF_6 in PC. For the anion···solvent interactions, the three solvent have the weakest interactions with TFSI$^-$, AN and PC solvent have the strongest interaction with BF_4^-, while GBL interacts strongly with PF_6^-.

We have also analyzed the effect of two charge distribution models on the local structure on the model system C_4mimPF_6/AN, in the first one the charge distribution on the IL was independent of the ionic mole fraction and in the second one the charge distribution was scaled using a dependent mole fraction scaling factor. The effect of the charge model distribution on the H-bonding and on the stacking interactions between the cations is analyzed. To this end two distances characteristic of the hydrogen bond between the donor moiety and it close neighbor acceptor one are introduced. Furthermore, a coordinate system that defines unambiguously and stacking orientation between a reference cation and its close neighbor is introduced. It is shown that the scaling charges model introduce an artificial large extent of the aggregation of the studied IL, than in the case of the unscaled charge mode.

Taken together, the results of the present thesis work contribute to the general idea of structure-composition-property relationship in mixtures of ionic liquids with molecular solvent and will serve a good comprehensive basis for the following further developments in the field:

- The methodology used for the developing new potential models for the set of solvents used in this work may be applied for more complex and prospective systems. Thus, the new potential models for the organic dye molecules may be developed that may be applied in ternary systems containing IL-molecular solvent mixtures and dye molecules as electrolytes for dye-sensitized solar cells. The microscopic environment, in terms of its polarity, viscosity and possible specific intermolecular interactions, can significantly alter the photodynamics of the dye molecule which is, in turn, reflected in the performance of the entire device.
- Improvement of the potential models for classical MD simulations of IL/molecular solvent mixtures. The information about the primary and

secondary interaction sites and their behavior over entire range of the mixture compositions established in this work will be used for thorough testing and fine tuning of the new generation of potential models which include polarization effects.

- The MD simulation of the dissolution process of polysaccharides in ionic liquids (ILs) poses an environmentally acceptable alternative to prevalent cellulose processing methods. Efficient dissolution of cellulose containing materials in order to render them more accessible for hydrolyzing enzymes is key to an economical and sustainable biofuel production process.